Novel Catalyst Systems For DeNOx

Mcclymont, David

Award date:
2014

Awarding institution:
University of Bath

NOVEL CATALYST SYSTEMS FOR DENO$_x$

David William John McClymont

A thesis submitted for the degree of Doctor of Philosophy

University of Bath

Department of Chemical Engineering

January 2014

COPYRIGHT

Table of Contents

Acknowledgements

I have been touched by a huge number of positive influences throughout this project and I would like to extend my sincerest thanks to the following people:

In particular I am exceptionally grateful to my lead supervisor, Professor Stan Kolaczkowski, for his support, guidance, knowledge and dedication to the project which has shaped it into what it is today. He constantly encouraged me to broaden my experiences and has been central to my conversion from a chemist to a chemical engineer.

I would also like to extend my thanks to my co–supervisors; Professor Kieran Molloy and Dr Serpil Awdry for their help and advice.

I am indebted to the management of the Centre for Sustainable Chemical Technologies; in particular Professor Matthew Davidson, Dr Janet Scott and Dr Tim Mays, for providing me with the opportunity to study in Bath and the support afforded a member of the Doctoral Training Centre; including financial assistance for travel to conferences and on placements.

I am thankful to past and present members of the Kolaczkowski group, in particular Ben Firth, Dr Chien Dinh Le and Dr Frank Zhang, as well as the other student members of the Doctoral Training Centre, for the sharing of their experience, assistance and friendship.

I thank Dr *hab* Joanna Łojewska of the Jagiellonian University, Krakow and members of her research group; Joanna Kryca, Dr Przemysław Jodłowski and Dr Arkadiusz Knapik, for the opportunity to work in their group for two months and their continued friendship.

The technical support staff at the university including Robert Brain, John Bishop, Paul Frith, Phil Jones, Dr Marianne Harkins, Dr Dan Lou–Hing, Suzanne Barkley and Fernando Acosta provided exceptional assistance and services during the course of this project, and I am extremely appreciative of their enthusiasm and industry.

I am also grateful to Professor Stephen Myers, Mr Denny Hall and Professor Prabir Dutta of the Ohio State University, who in their own ways ensured I spent a thoroughly enjoyable and productive three months in Columbus, Ohio.

Finally, huge thanks go to my family and friends for their continual encouragement and support over the last few years.

Dissemination

Some of the results presented within this thesis have already been disseminated through posters, oral presentations and peer reviewed publications. A selection of such dissemination is presented below.

Poster Presentations

Silver catalysts for NO_x storage and reduction using hydrogen
D. W. J. McClymont, S. T. Kolaczkowski, K. C. Molloy & S. Awdry.
IChemE Sustainable and Environmental Catalysis Meeting, University of Bath, 25th–26th September 2013.

Silver catalysts for NO_x storage and reduction using hydrogen
D. W. J. McClymont, S. T. Kolaczkowski, K. C. Molloy & S. Awdry.
ChemEngDayUK 2013, Imperial College London, 25th–26th March 2013.

Novel catalyst systems for deNO_x
D. W. J. McClymont, S. T. Kolaczkowski, K. C. Molloy & S. Awdry.
DTC Symposium Series – Sustainable Industrial Catalysis, University of Bath, 29th January 2013.

Novel catalyst systems for deNOx
D. W. J. McClymont, S. T. Kolaczkowski, K. C. Molloy & S. Awdry.
IChemE Catalysis for Energy Meeting, University of Birmingham, 11th December 2012.

Novel catalyst systems for deNOx
D. W. J. McClymont, S. T. Kolaczkowski, K. C. Molloy & S. Awdry.
DTC Summer Showcase 2012, University of Bath, 9th–13th July 2012.

Multi–Step TPSR/QMS Technique to Study the Kinetics of NH_3–SCR
D. W. J. McClymont, J. Ochońska, S. T. Kolaczkowski & J. Łojewska
International Symposium on Nitrogen Oxides' Emission Abatement 2011, Zakopane, Poland, 4th–8th September 2011.

Copper exchanged zeolites for ammonia reduction of NO_x from biogas gas engines
D. W. J. McClymont, S. T. Kolaczkowski, J. Łojewska, K. C. Molloy & S. Awdry.
DTC Summer Showcase 2011, University of Bath, 11th–13th July 2011.

Oral Presentations

Novel catalyst systems for deNO_x
D. W. J. McClymont
DTC Summer Showcase 2013, University of Bath, 16th–18th September 2013.

Novel catalyst systems for deNO_x
D. W. J. McClymont
Department of Chemistry, Jagiellonian University, Krakow, Poland, 21st June 2011. (Invited Speaker)

Contribution to Publications

Copper exchanged ultrastable zeolite Y – A catalyst for NH_3–SCR of NO_x from stationary biogas engines
J. Ochońska, D. W. J. McClymont, P. J. Jodłowski, A. Knapik, B. Gil, W. Makowski, W. Łasocha, A. Kołodziej, S. T. Kolaczkowski & J. Łojewska.
In: Catalysis Today. 191, 1, pp. 6–11, **2012**.

Using a quadrupole mass spectrometer for on–line gas analysis – gasification of biomass and refuse derived fuel
C. D. Le, S. T. Kolaczkowski & D. W. J. McClymont.
2013 (*under review).*

Abstract

Although different approaches for the reduction of NO_x species have been widely investigated in the literature, there are a number of drawbacks to the current industrial processes. In addition, increasingly stringent legislation ensures continued interest in improving these methods. An opportunity to utilise the H_2 produced during biomass gasification to treat the subsequent exhaust emissions was identified and a number of novel catalyst systems were prepared and explored in a variety of different deNO_x processes, and their performance compared to typical 'standard' catalysts.

Measurements conducted on a pilot scale gasifier confirmed the presence of between 10 – 17 % H_2, depending on the conditions in the gasifier, and validated the approach of this work. An experimental set–up consisting of a 15 mm i.d. stainless steel reactor housed within an electric furnace was constructed and commissioned, and an analytical method for the detection of eight potential deNO_x reaction species was developed utilising a Quadrupole Mass Spectrometer (QMS).

All of the catalysts explored in this study (o.d. = 14 mm, length = 10 mm) were prepared through impregnation of supplied samples of cordierite substrate monoliths coated with a γ–Al_2O_3 washcoat. Results of catalytic studies make up the bulk of this thesis, and two such processes were explored:

(a) Selective Catalytic Reduction (SCR) – Pt/Al_2O_3 has already been widely explored for this process and Ag/Al_2O_3 was also prepared as a potential novel material. Although the Ag/Al_2O_3 catalyst displayed some conversion of NO at higher temperatures (e.g. 17 – 21 % at $\geq$ 350 ^oC), apparent selectivity to the formation of N_2 was poor (e.g. 40 – 41 %).

(b) NO_x Storage and Reduction (NSR) – $Ba/Pt/Al_2O_3$ is considered the standard catalyst for this process and was compared to two novel materials: $Ba/Ag/Al_2O_3$ and $K/Ag/Al_2O_3$. With respect to the standard catalyst, the novel systems demonstrated comparable, and in some cases improved performance depending on the NSR conditions at 400 ^oC. $Ba/Ag/Al_2O_3$ demonstrated a capacity to store 11 – 15 % of the supplied NO and subsequently reduce 6 – 77 % of the stored species to N_2. $K/Ag/Al_2O_3$ demonstrated a capacity to store 23 – 72 % of the supplied NO and subsequently reduce 60 – 92 % of the stored species to N_2.

Nomenclature

a_s	Specific surface area	$m^2\ g^{-1}$
a_m	Molecular cross sectional area of adsorbate molecule	nm^2
C	BET parameter	
$C_{i\,j}$	Ratio of partial pressure of species i at *m/z* j to that of species i at its associated 'main' peak, used in QMS calibration.	
C_i^{Inlet}	Inlet concentration of species i	ppm or %
C_i^{Outlet}	Outlet concentration of species i	ppm or %
h	Planck's constant	6.626×10^{-34} J s
ΔH^{298}	Enthalpy change of reaction at 298 K	J mol^{-1}
J	Photolysis rate coefficient	s^{-1}
K	Reaction rate coefficient	Various units
L	Avogadros constant	$6.022 \times 10^{23}\ mol^{-1}$
m/z	Mass–to–charge ratio	
n_m	Monolayer capacity	$cm^3\ g^{-1}$
ø	Diameter	mm or cm
P	Pressure	bar or Torr
P_i	Corrected partial pressure of species i	Torr
$P_{m/z\,j}$	Raw partial pressure of *m/z* j	Torr
P_0/P	Relative Pressure	
r	Radius	cm
RS_i	Relative Sensitivity value of species i, used in QMS calibration.	
t	Time	s, min or h
T	Temperature	°C
T_{MAX}	Temperature of reported maximum NO_x conversion	°C
ν	Frequency	Hz
V_a	Volume of gas adsorbed	$cm^3\ g^{-1}$
x_i	Concentration of species i, used in QMS calibration.	ppm or %
X_i	Total conversion of species i	%

Greek Symbols

α	Denotes a phase of Al_2O_3 formed above 1200 ^oC	
β	Relates to the accuracy of the gas mixtures supplied by BOC; ± 2 % with respect to the certification	
γ	Denotes a phase of Al_2O_3 formed above 300 ^oC	
δ	Denotes a phase of Al_2O_3 formed above 850 ^oC	
θ	Denotes a phase of Al_2O_3 formed above 1100 ^oC	
π	Constant, pi.	3.14

Abbreviations

BET	Brunauer Emmett Teller
BJH	Barrett Joyner Halenda
BOC	British Oxygen Company
CHP	Combined Heat and Power
CSI	Cells per Square Inch
CSP	Concentrated Solar Power
DC	Direct Current
$DeNO_x$	Removal of NO_x
DME	Dimethyl Ether
DOC	Diesel Oxidation Catalyst
DPF	Diesel Particulate Filter
DRIFTs	Diffuse Reflectance Infrared Fourier Transform spectroscope
EC	European Community
EI	Electron Ionization
ELV	Emission Limit Value
EREC	European Renewable Energy Council
EU	European Union
FG	Feedgas
FID	Flame Ionization Detector
FT	Fischer–Tropsch
FT–IR	Fourier Transform – Infrared

GC	Gas Chromatography
GC–MS	Gas Chromatography – Mass Spectrometer
HC	Hydrocarbon
HESS	High Efficiency Water Scrubber
IED	Industrial Emissions Directive
IGCC	Integrated Gasification Combined Cycle
IR	Infrared
IUPAC	International Union of Pure and Applied Chemistry
KK	Kolaczkowski–Kim
LAN	Local Area Network
LNT	Lean NO_x Trap
LPG	Liquefied Petroleum Gas
MB	Midbed
MCM	Mobil Crystalline Material
MFI	Mordenite Framework Inverted
MS	Mass Spectrometer
NDIR	Nondispersive Infrared
NO_x	Nitrogen Oxides
NSR	NO_x Storage and Reduction
PC	Personal Computer
PM	Particulate Matter
PPB	Parts Per Billion
PPM	Parts Per Million
PPMV	Parts Per Million by Volume
PSA	Pressure Swing Adsorption
PV	Photovoltaic
QIC	Quartz Inert Capillary
QMS	Quadrupole Mass Spectrometer
RC	Radio Communication
RES	Renewable Energy Source
RF	Radio Frequency
RGA	Residual Gas Analysis
ROG	Refinery Off–Gas
RS	Relative Sensitivity

SCR	Selective Catalytic Reduction
SEM	Secondary Electron Multiplier
SMROG	Steam–Methane Reformer Off–Gas
SNG	Synthetic Natural Gas
SSITKA	Steady–state Isotopic Transient Kinetic Analysis
STOS	Short Time–on–stream
TGA	Thermogravimetric Analysis
TOC	Total Organic Carbon
TP	Tailpipe
TPD	Temperature Programmed Desorption
TPSR	Temperature Programmed Surface Reaction
TWC	Three Way Catalyst
USY	Ultra Stabilised zeolite Y
UHV	Ultra High Vacuum
UV	Ultraviolet
VST	Vertical Split Tube furnace
WGS	Water Gas Shift
WID	Waste Incineration Directive
ZSM	Zeolite Socony Mobil

Units

Throughout this report, the SI system of units has been typically utilised and the base SI units of relevance to this project are displayed below:

Length	metre	m
Mass	kilogram	kg
Time	second	s
Electric current	ampere	A
Temperature	kelvin	K
Amount of substance	mole	mol

However, in some cases units derived from those above have also been utilised, and these are displayed below, in addition to some non–standard SI terms which are also generally accepted units:

Length	1 metre (m) = 10^2 cm = 10^3mm = 10^6 μm = 10^9 nm
Mass	1 kilogram (kg) = 1000 g = 6.02214 x 10^{26} atomic mass units (amu)
Electric current	1 ampere (A) = 10^6 μA
Temperature	kelvin (K) = Celsius (^{o}C) + 273.15 K
Volume	1 litre (L) = 1000 mL = 1 dm^3 = 1000 cm^3
Energy	1 joule (J) = 1 kg m^2 s^{-1}
Power	1 watt (W) = 1 J s^{-1}
Pressure	1 bar (bar) = 750.06 Torr
Voltage	1 volt (V) = 1 kg m^2 s^{-3} A^{-10}

Electronvolt (eV)	= 1.6021746565 x 10^{-19} J
Mass fraction (ω_i)	= Mass of substance i/mass of total mixture = (m_i/m_{tot})
Weight percent (wt%)	= Mass fraction (ω_i) x 100

CHAPTER 1
Introduction

1.1 Background

1.1.1 Biomass

As fossil fuel stocks diminish, alternative renewable resources are required as feedstocks for future energy and chemical supplies.

Higman *et al.* (2008) describe the term biomass as covering a broad range of materials that offer themselves as fuels or raw materials and which have in common that they are all derived from recently living organisms. In this definition they exclude traditional fossil fuels since, although they also derive from plant (coal) or animal (oil and gas) life, it has taken millions of years to convert them to their current form.

Higman *et al.* (2008) also go on to explain that there is still a potential overlap between what is classified as waste and what as biomass.

In terms of chemical composition, Raspolli Galletti *et al.* (2012) state that biomass predominantly consists of three polymeric components: cellulose, hemicellulose, and lignin. Cellulose is a long–chain polysaccharide formed by D–glucose units, linked by β–1, 4 glycosidic bonds. Hemicellulose is a complex, branched, and heterogeneous polymeric network based on pentoses, hexoses and sugar acids. Lignin is an amorphous polymer made by different phenolic compounds.

However, the exact proportions of these components, and the presence of other species, will differ depending on the source of biomass. Separation and subsequent processing of these fractions enables utilisation of biomass in a variety of applications to form various products.

In general, it is considered that biomass will make significant contributions to both the future energy and chemical industries. The European Renewable Energy Council (EREC) has predicted that a substantial portion of future European Union (EU) power will be generated from biomass technologies (Table 1.1).

Table 1.1 Expected installed renewable power capacities in the European Union (EU), adapted from EREC (2010).

Renewable Energy Source (RES)	Year			
	2007	2020	2030	2050
Wind	56	180	288.5	462
Hydro*	102	120	148	194
Photovoltaics (PV)	4.9	150	397	962
Biomass	**20.5**	**50**	**58**	**100**
Geothermal	1.4	4	21.7	77
Concentrated Solar Power (CSP)	0.011	15	43.4	96
Ocean	–	2.5	8.6	65
Total RES–E Capacity (GW)	185	521.5	965.2	1,956

*The capacity of pumped storage plants is not included.

Biomass is also regarded as important for the future production of both speciality and commodity chemicals; indeed biomass is already involved in the production of many chemical products. Klass (1998) states that biomass is utilised worldwide as a source of many naturally occurring and some synthetic specialty chemicals and cellulosic and starchy polymers. High value, low–volume products, including many flavourings, drugs, fragrances, dyes, oils, waxes, tannins, resins, gums, rubbers, pesticides, and specialty polymers, are commercially extracted from or produced by conversion of biomass feedstocks.

Thus technologies which process or utilise biomass are becoming increasingly common and important. However, the nature of the biomass will influence the most effective method of achieving the desired transformations.

1.1.2 Gasification

Gasification is a thermal process through which fuels and feedstocks, including biomass, can be converted to higher value resources. As described by Knoef (2005):

> Gasification adds value to low– or negative–value feedstock by converting them to marketable fuels and products. The process of biomass gasification is quite complex, and includes a number of steps:
>
> a) thermal decomposition to gas, condensable vapours and char (pyrolysis);
>
> b) subsequent thermal cracking of vapours to gas and char;
>
> c) gasification of char by steam or carbon dioxide;
>
> d) partial oxidation of combustible gas, vapours and char.

Panopoulos *et al.* (2012) express the typical composition of biomass as having the general formula $CH_{1.4}O_{0.6}$ and specify that cellulose and lignin have typical formulas of $CH_{1.4}O_{0.8}$ and $CH_{1.4}O_{0.4}$ respectively. As a result the fuel typically produced is rich in CO and H_2, although the composition of the produced gas is also dependent on the type of gasification process, the gasification agent and the gasification temperature (Figure 1.1). The gas produced may be classified as 'product' ('producer') gas or 'biosyngas' ('syngas'), depending on the process of its formation and its composition. Producer gas has a lower H_2 and CO content than syngas although it can be transformed to syngas through thermal treatment (at which point the H_2 and CO content is increased).

The gaseous fuel formed through biomass gasification can be used to provide energy through a number of different applications including gas engines, gas turbines and fuel cells. The application of interest in this study is that of a gas engine, where the gaseous product is burnt to provide combined heat and power (CHP) at a local level. In a similar manner to other energy providing processes, the emissions from this application, in which NO_x species are included, are heavy regulated.

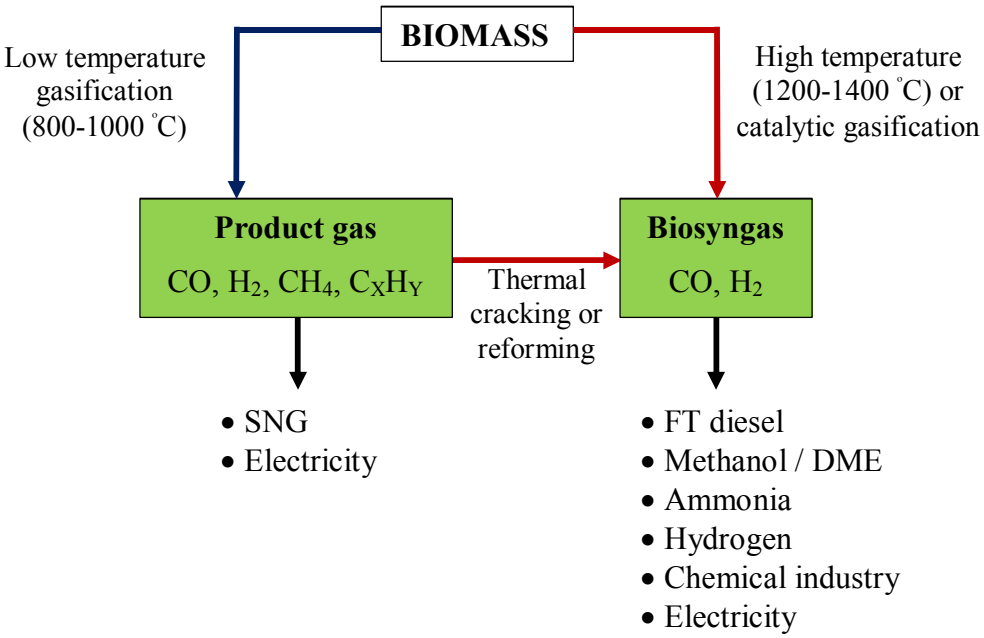

Figure 1.1 Difference of 'product gas' and 'biosyngas' and their typical applications, adapted from Boerrigter *et al.* (2005).

1.1.3 Legislation

The emissions of NO_x represent a major environmental issue, and to combat such pollution, legislation has been introduced throughout the industrialized world. In Europe, the waste incineration directive, or WID (Directive 2000/76/EC), regulates the emission limits of certain pollutants released to water or air, by waste incineration or co–incineration processes. This directive was recently incorporated, along with six other directives, into the industrial emissions directive, or IED (Directive 2010/75/EU). This directive applies to all new installations in the UK from 7 January 2013 and will apply to all existing installations from 7 January 2014.

NO_x are amongst the regulated species from waste incineration processes, and plants will need to adhere to both daily average emissions values (Table 1.2) and half–hourly average values (Table 1.3); where either no half–hourly average values exceeds any of the emission limit values set out in Column A of Table 1.3 or, where relevant, 97 % of the half–hourly average values over the year do not exceed any of the emission limit values set out in Column B of Table 1.3.

As such, systems to control the release of emissions from incineration and related processes are being developed to enable continued adherence to these regulations.

Table 1.2 Daily average emission limit values (ELVs) for waste incineration plants as specified in the IED (all values are quoted in mg Nm^{-3}).

Total dust	10
Gaseous and vaporous organic substances, expressed as total organic carbon (TOC)	10
Hydrogen chloride (HCl)	10
Hydrogen fluoride (HF)	1
Sulphur dioxide (SO_2)	50
Nitrogen monoxide (NO) and nitrogen dioxide (NO_2), expressed as NO_2 for existing waste incineration plants with a nominal capacity exceeding 6 tonnes per hour or new waste incineration plants	200
Nitrogen monoxide (NO) and nitrogen dioxide (NO_2), expressed as NO_2 for existing waste incineration plants with a nominal capacity of 6 tonnes per hour or less	400

Note: Reference conditions for these ELVs are as follows: dry gas, temperature of 273.15 K, pressure of 101.3 kPa and O_2 content of 11 % (3 % O_2 if mineral waste oil is being incinerated).

Table 1.3 Half–hourly average ELVs for waste incineration plants as specified in the IED (all values are quoted in mg Nm^{-3}).

	(100 %) A	(97 %) B
Total dust	30	10
Gaseous and vaporous organic substances, expressed as total organic carbon (TOC)	20	10
Hydrogen chloride (HCl)	60	10
Hydrogen fluoride (HF)	4	2
Sulphur dioxide (SO_2)	200	50
Nitrogen monoxide (NO) and nitrogen dioxide (NO_2), expressed as NO_2 for existing waste incineration plants with a nominal capacity exceeding 6 tonnes per hour or new waste incineration plants	400	200

1.1.4 Emission Control

1.1.4.1 NH_3/urea–SCR

The selective catalytic reduction of NO_x by ammonia (NH_3–SCR) is the current industrial practice for NO_x control from stationary sources, and urea–SCR is also a well–established method for removal of NO_x from mobile applications *i.e.* automotive diesel engines. These processes involve injecting the reductant into the exhaust stream from the system, where they selectively react with NO_x over a catalyst to form water and nitrogen (Reactions 1.4, 1.5 and 1.6). Note that in cases where urea is used, it is in the role of an ammonia carrier and this is formed *in situ* at the elevated temperatures of the process. The reactions involved are described in detail by Koebel *et al.* (2000), on which the following is based:

Urea is usually applied in a urea–SCR process as an aqueous solution. This solution is atomized into the hot exhaust gas stream, and the first step involves the evaporation of water from the droplets, thus leading to solid or molten urea:

$$\mathrm{NH_2 - CO - NH_{2(aqueous)}} \rightarrow \mathrm{NH_2 - CO - NH_{2(solid)}} + x\mathrm{H_2O} \qquad (1.1)$$

Pure urea will then heat up and decompose thermally according to:

$$\mathrm{NH_2 - CO - NH_{2(solid)}} \rightarrow \mathrm{NH_{3(gas)}} + \mathrm{HNCO}_{(gas)}, \quad \Delta H^{298} = 186\ kJ\ mol^{-1} \qquad (1.2)$$

Equimolar amounts of ammonia and isocyanic acid are thus formed. Isocyanic acid is very stable in the gas phase, but hydrolyses easily on many solid oxides with water vapour originating from the combustion process:

$$\mathrm{HNCO}_{(gas)} + \mathrm{H_2O}_{(gas)} \rightarrow \mathrm{NH_{3(gas)}} + \mathrm{CO_{2(gas)}}, \quad \Delta H^{298} = -96\ \mathrm{kJ}\ mol^{-1} \qquad (1.3)$$

It should also be noted that ammonia is manufactured from hydrocarbon starting materials which are finite natural resources. Urea is subsequently produced through the reaction of ammonia and carbon dioxide. Thus the use of either chemical may be considered as detrimental to both our efforts to reduce dependence on fossil fuels and the pledge to alleviate the associated issues of global warming and climate change.

Once the ammonia has formed it reacts with the NO_x present. Forzatti (2001) details the main reactions of SCR using ammonia:

$$4NH_3 + 4NO + O_2 \rightarrow 4N_2 + 6H_2O \quad (1.4)$$

$$2NH_3 + NO + NO_2 \rightarrow 2N_2 + 3H_2O \quad (1.5)$$

$$8NH_3 + 6NO_2 \rightarrow 7N_2 + 12H_2O \quad (1.6)$$

Ammonia is known as a 'selective' reductant as it has the ability to react solely with NO_x and not with other species present. This is another advantage which is not observed with other simple reagents such as carbon monoxide. However, oxidation can still occur at higher temperatures (Reaction 1.7) and this limits the maximum NO_x conversion possible:

$$4NH_3 + 5O_2 \rightarrow 4NO + 6H_2O \quad (1.7)$$

There are also operating issues at lower temperatures, in particular for mobile applications. Forzatti *et al.* (2009) emphasise that:

> "One problem of SCR systems for vehicles, however, is poor activity at low temperatures where most of the NO_x is produced, for example, during cold start–up and on travelling short distances."

In addition there is an intrinsic safety issue when utilising ammonia and urea in this application; both chemicals are highly toxic and the applications demand an additional tank of the nitrogenous reductant. This tank must be carefully considered when designing these systems as it presents further operating risks. Additionally, not all the ammonia is reacted over the catalyst and as a result 'slip' occurs; this requires an extra catalyst to convert the toxic NH_3 to N_2 and H_2O. An example of the type of NH_3/urea–SCR system which may be fitted to the exhaust from a biomass gasification CHP process is shown in Figure 1.2(A).

Another consideration, in relation to the mobile applications, is that a urea infrastructure is required to enable the reductant tank to be refilled at regular intervals. This would be costly to implement, although it is already in place over parts of Europe, and is a serious barrier to widespread urea–SCR use.

1.1.4.2 H_2–SCR

Recently it has been shown that hydrogen can be used to successfully reduce NO_x emissions to N_2 and H_2O:

$$2NO + 2H_2 \rightarrow 2H_2O + N_2 \quad (1.8)$$

$$2NO_2 + 2H_2 \rightarrow 4H_2O + N_2 \quad (1.9)$$

Although not yet a widespread technique, this approach has great implications as it may be possible to utilise the hydrogen formed in the application *e.g.* in the syngas from the biomass gasification process, to reduce the NO_x. This would negate the need for the additional tanks of reductant which would obviously save on the volume and costs of the system, as well as removing the safety risks and potentially harmful effects associated with the extra chemicals.

As can clearly be seen from the schematic in Figure 1.2(B); the H_2–SCR process would also reduce the necessary size of the exhaust treatment system, as a further oxidation catalyst to treat reductant slip is not required.

This approach to NO_x reduction may also have implications for automotive applications, where H_2 can be generated *in situ*. An excellent example of such an application can be found in a patent filed by Bartley *et al.* (2006), where H_2 generated from the diesel fuel is subsequently used in a H_2–SCR process to treat the emissions of the engine. This application is discussed further in Chapter 2.

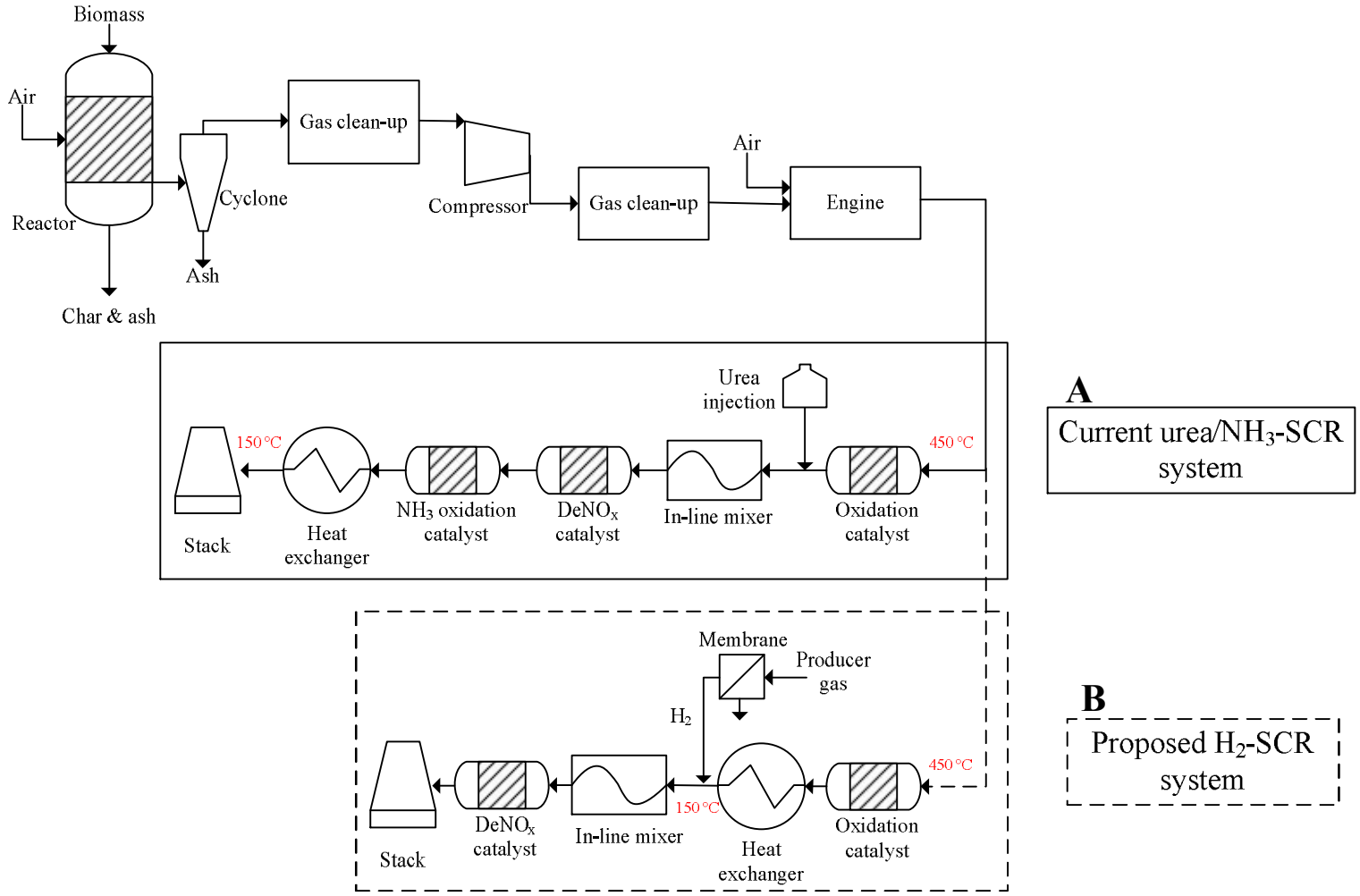

Figure 1.2 Schematic of a biomass CHP plant showing; (A) how existing technology could be applied and (B) the application of the proposed NO_x removal strategy.

1.1.5 Separation of H_2

To confirm the proposed approach it is important to give some thought to the method through which the hydrogen would be sequestered and subsequently utilised. Three main processes for hydrogen separation and purification exist:

- Pressure swing adsorption (PSA)
- Fractional/cryogenic distillation
- Use of membranes

Each approach has both advantages and disadvantages and thus all are suited to different applications. The techniques are briefly discussed here by way of introduction and to provide an example of how it is possible to obtain H_2 for the reduction process. They are not explored further within this study.

1.1.5.1 Pressure Swing Adsorption

PSA has become increasingly investigated over the past few decades and several key commercial processes exist. Sircar (2002) describes the basic concept as follows:

a) Certain components of a gas mixture are selectively adsorbed on a microporous–mesoporous solid adsorbent at a relatively high pressure by contacting the gas with the solid in a packed column of the adsorbent in order to produce a gas stream enriched in the less strongly adsorbed components of the feed gas.

b) The adsorbed components are then desorbed from the solid by lowering their superincumbent gas–phase partial pressures inside the column so that the adsorbent can be reused.

c) The desorbed gases are enriched in the more strongly adsorbed components of the feed gas.

d) No external heat is generally used for desorption.

Interestingly, Sircar *et al.* (2000) state that:

a) Production of pure hydrogen from a gas mixture containing 60–90 mol% hydrogen by using pressure swing adsorption (PSA) processes has become the state–of–the–art technology in the chemical and petrochemical industries.

b) The two most common gas streams used for this application are (a) the steam–methane reformer off–gas (SMROG) after it has been further treated in a water–gas shift reactor, and (b) the refinery off–gas (ROG) from various sources.

1.1.5.2 Fractional/Cryogenic Distillation

Cryogenic distillation is used for the separation of low molecular weight materials, however it is an energy intensive process; it utilises very low temperatures and high pressures to separate mixture of components based on their boiling points. Although reviewing hydrogen membrane separation techniques; Adhikari *et al.* (2006) explain that whilst it is possible to separate H_2 from other gas species using cryogenic distillation, it is perhaps not the ideal solution as:

a) The cryogenic process is a low–temperature separation process which uses the difference in boiling temperatures of the feed components to effect the separation.

b) Hydrogen has a high relative volatility compared to hydrocarbons.

c) If the feed contains significant amounts of carbon monoxide (CO) and carbon dioxide (CO_2), a methane wash column is required to reduce the levels of these gases.

d) Higher hydrogen recovery at moderate hydrogen purities (95 % or less) is possible with a cryogenic system; however, very high hydrogen purity is not practical.

It appears that the complex nature of the feed stream may restrict the use of this approach in the application of interest; CO would also be present in the feed stream and thus the additional methane wash column would also be required.

1.1.5.3 Membrane Separation

Membrane technology for the separation of hydrogen from gas mixtures has been prevalent on an industrial scale since 1980 when Permea (now part of Air Products) introduced their PRISM® membrane. There are many types of membranes; again each has different properties and limitations (Table 1.4), including different separation mechanisms, and thus each is suitable for different applications.

Kluiters (2004) describes the concept of a membrane as a barrier that permits selective mass transport between two phases. It is selective because some components can pass through the membrane more easily than others.

Specifically considering the extraction of a small quantity of H_2 from the gas produced in a biomass gasification process; the membrane chosen will depend on the position in the process where the H_2 is recovered. Removing H_2 after the cyclone, but before the gas clean–up, the temperature would be 300 – 400 ^oC. If H_2 was recovered just before the gas engine, the temperature would only be 20 – 30 ^oC. The presence of potential poisoning species, especially H_2S, would also be a major factor in deciding both which type of membrane and its location in the process.

Table 1.4 Selected properties of H_2 separation membranes, based on information in Kluiters (2004) and Ockwig *et al.* (2007).

	Dense Polymer	Ceramic		Metallic	Carbon
		Porous	Dense		
Temperature Range (°C)	<100	200 – 600	600 – 900	300 – 600	500 – 900
H_2 Selectivity	low	5 – 139	>1000	>1000	4 – 20
H_2 Flux ($\times 10^{-3}$ mol m^{-2} s^{-1})	low	60 – 300	6 – 80	60 – 300	10 – 200
Mechanical Issues	Swelling, compaction, mechanical strength	Brittle	Brittle	Phase transitions	Very brittle
Poisoning Issues	Degraded by H_2S, HCl, SO_x, CO_2	Stability in H_2O	Stability in CO_2, H_2S	Poisoned by H_2S, HCl, SO_x, CO_2	Oxidised and susceptible to strong adsorbing organic vapours
Materials	Polyesters, ethers, imides, urethanes, etc	Silica, alumina, zirconia, titania, zeolites	Proton conducting ceramics (mainly $SrCeO_{3-\delta}$, $BaCeO_{3-\delta}$)	Pd, Ta, V, Nb, and alloys	Porous carbons, single–wall carbon nanotubes
Transport Mechanism	Solution/diffusion	Molecular sieving	Solution/diffusion (proton conduction)	Solution/diffusion	Surface diffusion; molecular sieving

1.2 Motivation for Present Work

In this thesis, a process which can effectively reduce NO_x emissions from gas engines running on producer gas formed from biomass gasification, and which utilises H_2 formed from the gasification process to do so is of particular interest.

As NO_x is considered a very harmful and greatly polluting material, any action which aims to reduce emissions of NO_x, and subsequently its environmental impact can be considered as contributing to sustainable development. Several approaches have been developed but the removal of NO_x gases from many practical applications still represents a major problem for industry. This project places emphasis on the use of H_2 (already present in the system), to create a more sustainable and efficient processes with less waste. It also removes the dependence on vast quantities of additional, toxic materials which in themselves are manufactured from finite natural resources and contribute to global warming and climate change through their production.

A further interest in this work was the development of an analytical method enabling real–time measurements of the products of the studied deNO_x reactions using a Quadrupole Mass Spectrometer (QMS). Whilst there are many different analytical techniques for such analyses, various shortcomings include a limit on the number of species which can be accurately identified by each technique. The result is that it is often necessary to operate multiple techniques in tandem to measure all the potential species of interest. Given that the presence of particular species, although not detected, may impact on the measurement of others, using a single technique to identify all species would provide assurance of the accuracy of the obtained results.

1.3 Structure of the Thesis

The structure of this thesis is as follows:

Chapter 2 discusses the formation of NO_x and includes a brief literature review of the potential and previous uses of hydrogen in deNO_x applications. Studies which also confirmed the presence of H_2 in the gasification application, and work on the current industrial standard NH_3–SCR process, will also be presented. Finally, current analysis techniques for related deNO_x applications will be reviewed.

Chapter 3 describes catalyst preparation and characterization details, including justification of the chosen materials and methods, as well as some expected reaction mechanisms with relation to the H_2–SCR process. Procedures undertaken in the design and commissioning of the continuous flow fixed bed reactor utilised to investigate the reactions, in addition to preliminary and final H_2–SCR experimental results, are also described.

Chapter 4 in a similar manner to Chapter 3, the catalyst preparation procedures, justification of the chosen materials, expected reaction mechanisms with relation to the H_2–NSR process and preliminary and final results of the H_2–NSR reaction investigations are presented.

Chapter 5 summarises and draws conclusions on the results discussed in Chapters 3 and 4. Possible future approaches in order to continue the project are also proposed.

The appendices provide additional useful information such as the use of the Quadrupole Mass Spectrometer (QMS) for on–line gas analysis, and catalyst preparation procedures. A summary of the links between some of the chapters described here is presented in Figure 1.3.

As the author of this thesis I was responsible for the design and construction of the experimental reactors, the development of the analytical method that enabled the measurements to be performed as well as the performance of all the experimental measurements described. No other student was involved in the gathering of the data described in Figure 1.3.

In addition I gained invaluable experience through a number of case studies and placements including:

- Time spent with a colleague taking measurements on site at a biomass gasification plant in Chester, UK in order to assess the operation and subsequent performance of the technology.

- Two month placement working within a collaborating research group of the Jagiellonian University in Krakow, Poland on the related topic of NH_3–SCR. This provided an opportunity to experience research at another institution and to develop an understanding of the current industrial process for control of NO_x.

- Three month placement with the Ohio Bioproduct Innovation Center (OBIC) (part of the Ohio State University, Columbus, Ohio, USA), a commercialisation company operating in the bioeconomy sector, providing a real life insight to the development of waste to energy (and value added products) technologies, including those of interest in this project.

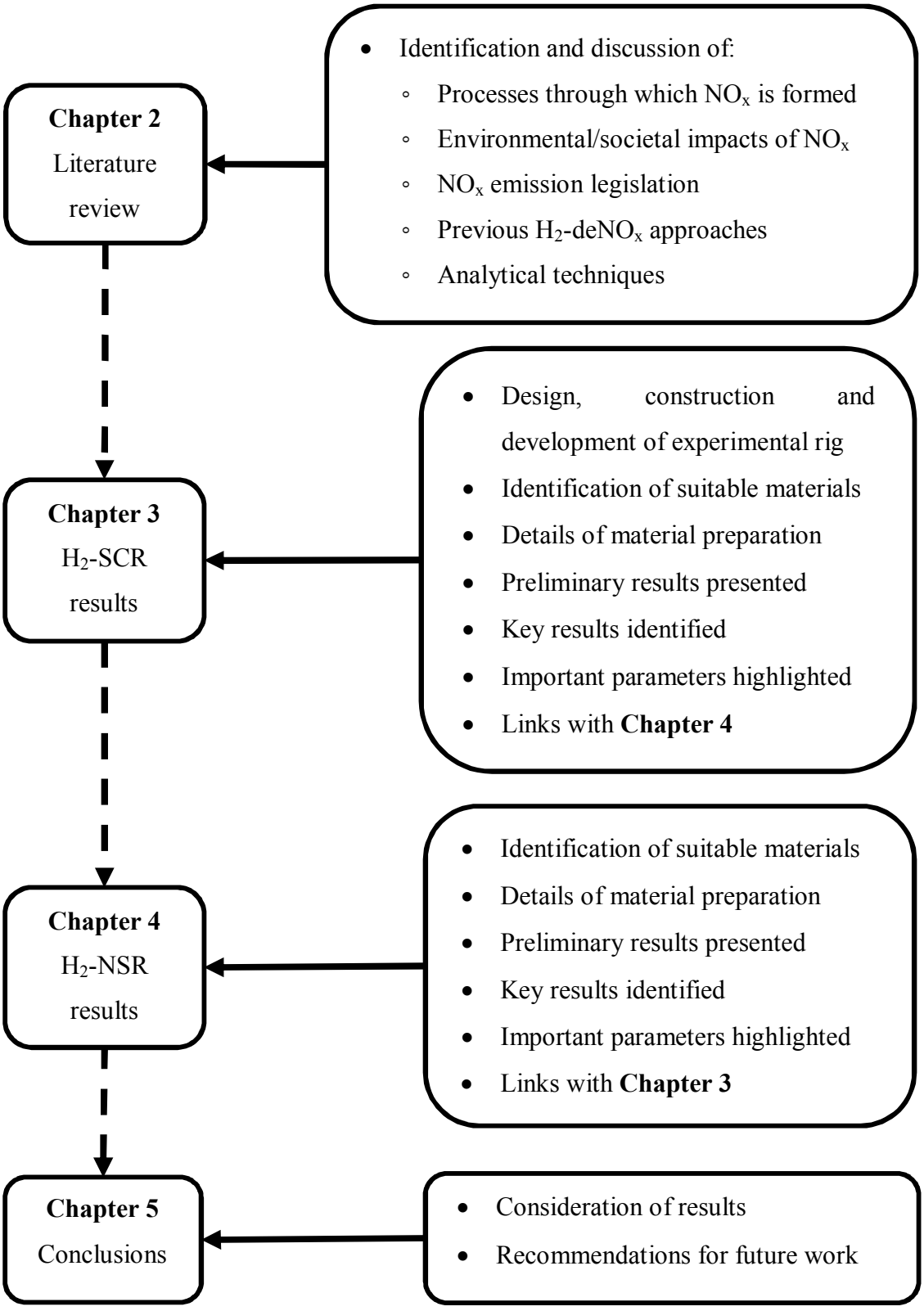

Figure 1.3 Diagram depicting the links between the different research activities discussed within this thesis and their associated chapters.

REFERENCES

Adhikari, S. and Fernando, S. (2006). Hydrogen Membrane Separation Techniques. Industrial & Engineering Chemistry Research, Vol. 45, No. 3, pp. 875–881.

Bartley, G. J. J. and Sharp, C. A. (2006). NO_x Reduction System for Diesel Engines, Using Hydrogen Selective Catalytic Reduction. US Patent, No. US 7135153 B2.

Boerrigter, H. and Rauch, R. (2005). Syngas Production and Utilization. In Handbook Biomass Gasification. H. Knoef, Ed., BTG Biomass Technology Group, pp. 211–230.

Directive 2000/76/EC of the European Parliament and of the Council of 4 December 2000 on the Incineration of Waste, Official Journal of the European Communities.

Directive 2010/75/EU of the European Parliament and of the Council of 24 November 2010 on Industrial Emissions (Integrated Pollution Prevention and Control), Official Journal of the European Union.

EREC, European Renewable Energy Council, RE–thinking 2050 – A 100 % Renewable Energy Vision for the European Union, Report (2010).

Forzatti, P. (2001). Present Status and Perspectives in De–NO_x SCR Catalysis. Applied Catalysis A: General, Vol. 222, No. 1–2, pp. 221–236.

Forzatti, P., Nova, I., et al. (2009). Enhanced NH_3 Selective Catalytic Reduction for NO_x Abatement. Angewandte Chemie International Edition, Vol. 48, No. 44, pp. 8366–8368.

Higman, C. and Van Der Burgt, M. (2008). Gasification. 2nd Edition, Elsevier. p. 75.

Klass, D. L. (1998). Biomass for Renewable Energy, Fuels, and Chemicals. Elsevier. p. 495.

Kluiters, S. C. A., Energy Research Centre of the Netherlands, Status Review on Membrane Systems for Hydrogen Separation, Report (2004).

Knoef, H. (2005). Practical Aspects of Biomass Gasification. In Handbook Biomass Gasification. H. Knoef, Ed., BTG Biomass Technology Group, p. 13.

Koebel, M., Elsener, M., et al. (2000). Urea–SCR: a Promising Technique to Reduce NO_x Emissions from Automotive Diesel Engines. Catalysis Today, Vol. 59, No. 3–4, pp. 335–345.

Ockwig, N. W. and Nenoff, T. M. (2007). Membranes for Hydrogen Separation. Chemical Reviews, Vol. 107, No. 10, pp. 4078–4110.

Panopoulos, K. D., Christodoulou, C., et al. (2012). Biomass Gasification: Gas Production and Cleaning for Diverse Applications – CHP and Chemical Syntheses. In Biorefinery: from Biomass to Chemicals and Fuels. M. Aresta, A. Dibenedetto and F. Dumeignil, Eds., Walter de Gruyter, p. 298.

Raspolli Galletti, A. M. and Antonetti, C. (2012). Biomass Pretreatment: Separation of Cellulose, Hemicellulose, and Lignin – Existing Technologies and Perspectives. In Biorefinery: from Biomass to Chemicals and Fuels. M. Aresta, A. Dibenedetto and F. Dumeignil, Eds., Walter de Gruyter, pp. 101–102.

Sircar, S. (2002). Pressure Swing Adsorption. Industrial & Engineering Chemistry Research, Vol. 41, No. 6, pp. 1389–1392.

Sircar, S. and Golden, T. C. (2000). Purification of Hydrogen by Pressure Swing Adsorption. Separation Science and Technology, Vol. 35, No. 5, pp. 667–687.

CHAPTER 2

Literature Review & Associated Experiences

In this chapter, a literature review is provided to describe in detail the:

- Processes which form NO_x, with respect to the application of interest;
- Environmental and societal impacts of NO_x;
- Legislation in place to combat NO_x emissions;
- Previous work where H_2 has been used as the reductant for deNO_x applications; and
- Various analysis techniques previously utilised for related deNO_x investigations.

In addition, a number of case studies will be encompassed within the chapter, to demonstrate the author's understanding of both the application of interest and current industrial approaches to the issue, as well as to verify the proposed solution.

2.1 Nitrogen Oxides

The term NO_x refers to a group of highly reactive gases which are known air pollutants, and Harrison (2001) states that by far the major proportion of emitted NO_x is in the form of NO. The chemistry of these oxides, and other reactive inorganic nitrogen species, is central to various atmospheric issues including; the formation of photochemical smog, the depletion of stratospheric ozone and the production of acid rain. Nitric oxide is a colourless, odourless gas and nitrogen dioxide is a reddish–brown gas, soluble in water, and with a pungent odour.

2.1.1 Sources and Formation of NO_x

NO_x gases are produced from both natural and pollutant sources. They are formed from various biological processes, and are also formed as a product of the combustion of fossil fuels. The environmental impact of these gases ensures there is great interest and debate about their emission levels from both mobile and stationary sources. Based on information in Manahan (2009):

a) Estimates of the quantities of NO_x entering the atmosphere vary widely, but generally range from a few tens of millions of metric tons per year to somewhat more than 100 million.

b) The biggest share of anthropogenic NO_x amounting to around 20 million metric tons per year enters the atmosphere from combustion of fossil fuels in both stationary and mobile sources.

c) A similar amount of NO_x is emitted from soil, much of it from the action of microorganisms on nitrogen fertilizer.

d) Other natural sources are biomass burning, lightning and to a lesser extent, atmospheric oxidation of NH_3.

In terms of NO_x formation from fossil fuel combustion; at very high temperatures nitrogen and oxygen will react to form nitric oxide:

$$N_2 + O_2 \rightarrow 2NO \qquad (2.1)$$

However, this process occurs at temperatures mainly above 1480 ^oC and thus is unlikely to contribute to NO_x formation in the application of interest. Once nitric oxide is formed it slowly reacts with oxygen in the air to form nitrogen dioxide:

$$2NO + O_2 \rightarrow 2NO_2 \qquad (2.2)$$

Formation of NO_x species within the application of interest will be discussed further in Section 2.1.1.1.1.

2.1.1.1 Down–draft Gasification Process

As already alluded to, the application of interest for this project is that of a biomass gasification CHP process. During the course of this project time was spent at Refgas Ltd, who have a pilot–scale gasification plant at Sandycroft (near Chester, UK) (Figure 2.2). A simplified schematic of the Refgas process is provided in Figure 2.1. This gives an indication of the type of technology which is currently being developed throughout the UK and the rest of the world. It is important to stress that this image represents a pilot–scale plant; the configuration of which may vary considerably for a commercial process. Additionally there are a number of different types of gasifier technology, which will not be discussed further here, and this schematic represents only one type of approach.

As can be seen from the schematic there are a number of stages involved in the process of gasifying a biomass material into a suitable fuel:

- The fuel (in this case waste wood) is fed into the top of the reactor.
- Combustion and partial oxidation reactions occur within the gasifier, forming a 'dirty' gas mixture.
- The gas leaves the reactor from the base at a temperature of ~550 ^{o}C.
- Char also leaves the reactor from the base and is collected in a suitable container.
- The gas passes through cyclones used to trap additional char fines and ash.
- The 'dirty' gas is now quenched with water and then passes through a high efficiency water scrubber known as a HESS unit.
- Additional residues/tars are now collected through use of a chiller unit.
- The 'clean' gas is supplied, under positive pressure, through filters to the storage tank.
- The gas can be directed to flare and/or a gas engine to be used to produce electrical energy.

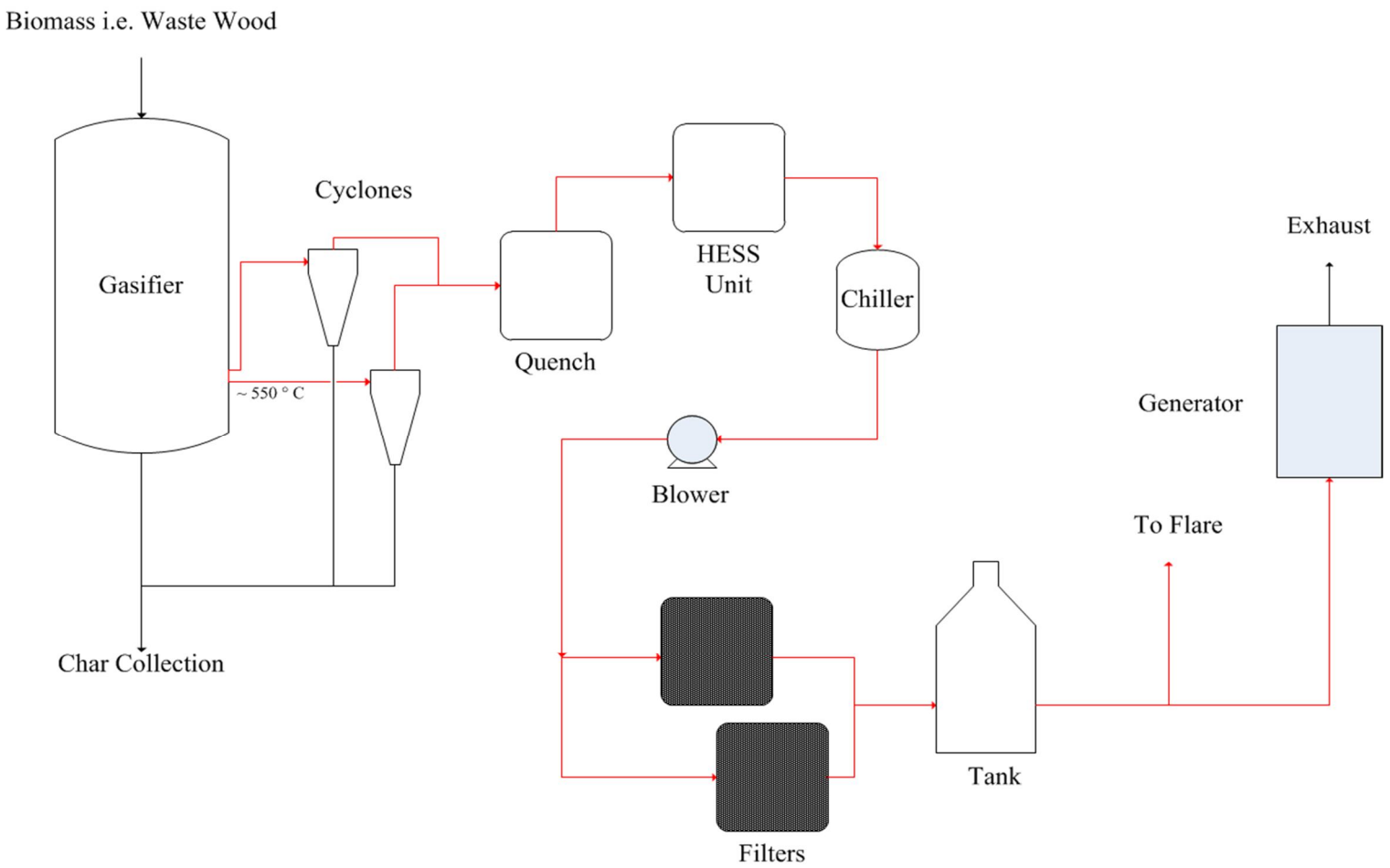

Figure 2.1 Simplified schematic of Refgas gasification process.

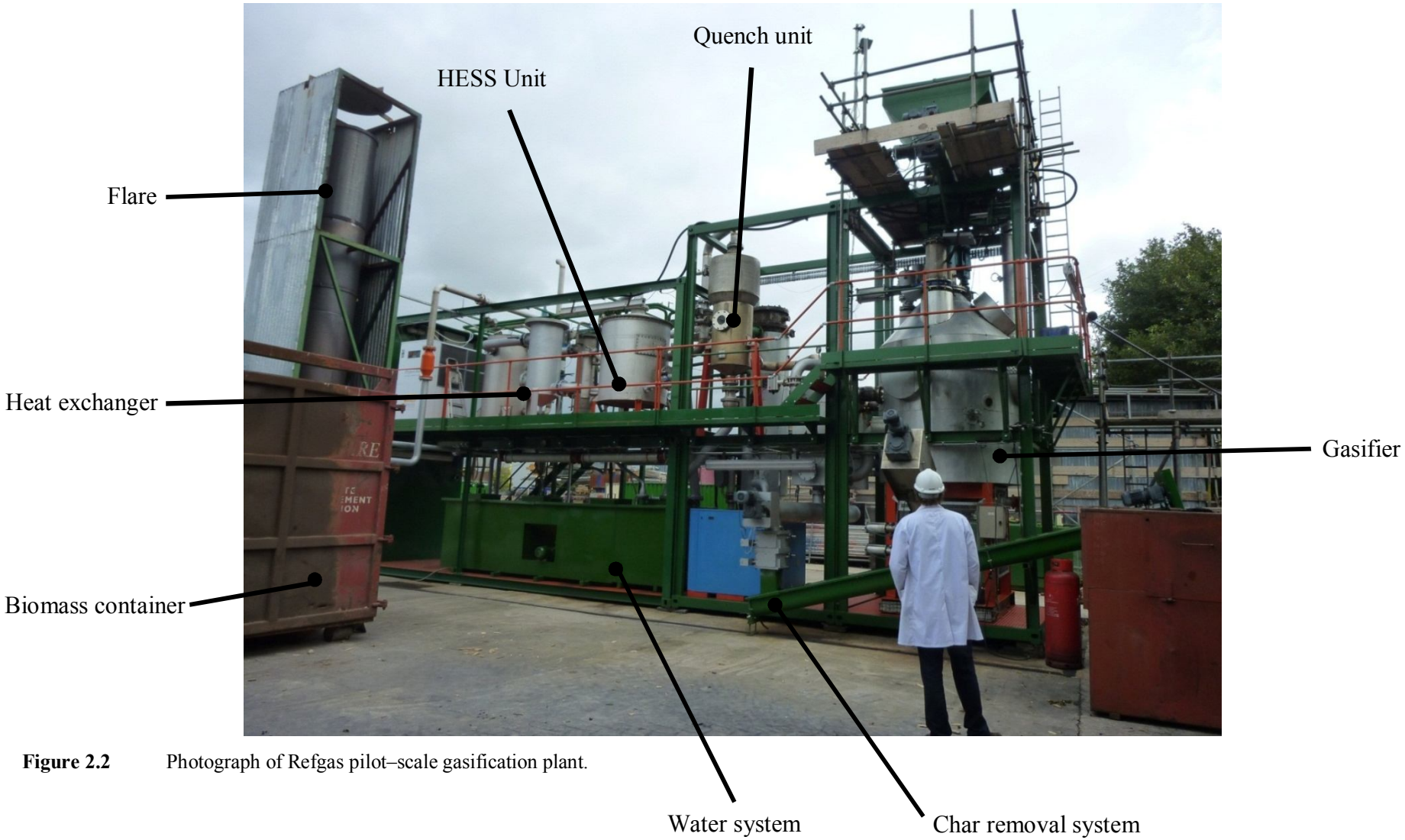

Figure 2.2 Photograph of Refgas pilot–scale gasification plant.

2.1.1.1.1 Formation of NO_x Species

Although gas clean–up units are in place at various points in the gasification process, their operation is intended only for certain species. Other species may be unaffected by the clean–up technology or formed as a result of undesired reactions which occur within these units.

Torres *et al.* (2007) summarise the source of NO_x formation in biomass gasification CHP processes. They state that biomass contains nitrogen as a part of proteins, DNA, RNA, chlorophyll, alkaloids and porphyrins. In biomass gasification, most of the nitrogen ends up as ammonia (NH_3) and N_2 with lower concentrations of hydrogen cyanide (HCN), isocyanic acid (HNCO), and nitrogen oxides (NO_x). The nitrogen containing species are undesirable because they can serve as precursors for NO_x in downstream burners, gas engines, or gas turbines.

Higman *et al.* (2008) describe the difficulties in removing NH_3 from syngas, stating that ammonia has a very high solubility in water (two orders of magnitude higher than CO_2). Hence it is seldom removed from the main wash or quench water circuit of carbon removal systems. The ammonia is therefore recycled in the scrubber wash water and partially stripped out by the syngas in the scrubber, such that the potential for full ammonia removal in the syngas water wash is seldom realised and an additional 'acid wash' is required for effective ammonia removal.

HCN can also rapidly decay to form amines (NH_i where i = 1, 2 or 3) which are then converted to NO_x. Figure 2.3 summarises some of the processes involved in NO_x formation that may occur within a biomass gasification CHP process:

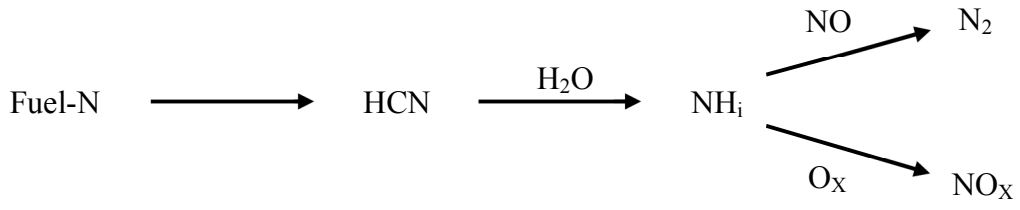

Figure 2.3 Typical mechanism for NO_x formation during a biomass gasification CHP process (i = 1, 2 or 3), adapted from Higman *et al.* (2008).

Miller *et al.* (2008) expand on this by detailing the complex reactions that HCN and NH_3 can undergo during combustion:

$$HCN + \frac{5}{4}O_2 \rightarrow NO + CO + \frac{1}{2}H_2O \quad (2.3)$$

$$HCN + \frac{3}{2}O_2 + NO \rightarrow N_2O + CO + \frac{1}{2}H_2O \quad (2.4)$$

$$HCN + \frac{3}{4}O_2 \rightarrow \frac{1}{2}NO + CO_2 + \frac{1}{2}H_2O \quad (2.5)$$

$$NH_3 + \frac{5}{4}O_2 \rightarrow NO + \frac{3}{2}H_2O \quad (2.6)$$

$$NH_3 + \frac{3}{4}O_2 \rightarrow \frac{1}{2}N_2 + \frac{3}{2}H_2O \quad (2.7)$$

Miller *et al.* (2008) go on to explain other factors which can influence the abundance of NO_x emissions in the exhaust stream from a combustion engine:

a) In general, NO and N_2O emissions increase with increasing nitrogen content in the fuel, whereas with increasing fuel volatile matter content, NO emissions usually increase but N_2O emissions decrease.

b) N_2O emissions are primarily dependent on the type of fuel (as well as combustion temperature, as discussed later), with low–rank fuels generating lower amounts of N_2O than higher rank fuels, i.e. N_2O emissions from lowest to highest – biomass, peat, oil shale, brown coal/lignite, bituminous coal. This is attributed to the amount of NH_3 released from the fuel as lower rank fuels (i.e. higher volatile matter fuels) release more NH_3 and their NH_3 to HCN ratio is greater than for higher rank fuels.

c) Oxidation of NH_3 results in NO formation, while HCN produces both NO and N_2O.

d) Combustion temperature has a significant effect on both NO and N_2O emissions. NO emissions increase, but N_2O emissions decrease.

2.1.1.1.2 Typical NO_x Emissions Levels

Although the exact level of NO_x emissions will vary through a number of factors already discussed i.e. type of gasification process and nature of biomass fuel, the technology in which the syngas produced is utilised will also play a part. Higman (2008) discuss the potential levels of NO_x which may be seen from different applications, including those already operational in industry, and state that:

> The high hydrogen content of syngas (which would be even higher in the carbon capture scenario) prohibits the use of current dry low NO_x burners as developed for natural gas. Instead, diffusion burners are used. Typically, one could achieve about 15 ppm (dry basis referred to 15 % O_2) in the exhaust of a gas turbine without SCR. In fact, some IGCCs such as the plant in Buggenum regularly achieve values under 10 ppmv without SCR.

Although the values reported here already appear to be relatively low (when compared to emissions of other species, including CO: 10 – 25 ppm), Higman (2008) go on to explain that improvement is still necessary, and say that:

> Some areas may, however, require SCR to achieve lower NO_x emission rates of 3 ppmv (dry basis referred to 15 % O_2) comparable with those for natural gas–fired turbines. In such a case, it is necessary to desulfurize the fuel gas further to about 15 ppmv so as to avoid formation of ammonium bisulfate from ammonia slip in the SCR, which can deposit on heat exchange surfaces downstream of the SCR.

2.2 Harmful Processes

The NO_x gases formed can then react with other chemicals present in the atmosphere, such as hydrocarbons and water, and contribute to atmospheric processes which are harmful to both the environment and human health.

2.2.1 Formation of Photochemical Smog

Hobbs (2000) summarises the role of these gases and their interactions in the formation of photochemical smog, stating that:

> The reactions start with the photolysis of NO_2:
>
> $$NO_2 + h\nu \xrightarrow{J} NO + O \qquad (2.8)$$
>
> ozone is then formed very quickly by:
>
> $$O + O_2 + M \xrightarrow{K_1} O_3 + M \qquad (2.9)$$
>
> where M is most likely N_2 or O_2. However, not much O_3 is formed directly by Reaction 2.9 since it is depleted by the rapid Reaction 2.10:
>
> $$O_3 + NO \xrightarrow{K_2} NO_2 + O_2 \qquad (2.10)$$
>
> which regenerates NO_2. If there were no other reactions, (2.8) – (2.10) would lead to a steady–state concentration of O_3 given by:
>
> $$[O_3] = \frac{J\,[NO_2]}{K_2\,[NO]} \qquad (2.11)$$
>
> where J is the photolysis rate coefficient.

The ozone and atomic oxygen formed are reactive species which then react with hydrocarbons to form aldehydes. These aldehydes do not vaporize as easily as hydrocarbons; tiny droplets are formed and the result is the 'haze' associated with photochemical smog.

2.2.2 Destruction of Stratospheric Ozone

Both nitric oxide and nitrogen dioxide also play a part in the destruction of stratospheric ozone. As described by Manahan (2009), the scheme begins with the depletion of ozone by nitric oxide:

$$O_3 + NO \rightarrow NO_2 + O_2 \qquad (2.10)$$

then the reaction of nitrogen dioxide with atomic oxygen formed from Reaction 2.8:

$$NO_2 + O \rightarrow NO + O_2 \qquad (2.12)$$

combining Reactions 2.10 and 2.12 results in a net reaction for the destruction of ozone:

$$O + O_3 \rightarrow O_2 + O_2 \qquad (2.13)$$

This destruction of stratospheric ozone can have huge implications for life on earth. For example Fahey *et al.* (2011) state that:

a) Stratospheric ozone is considered good for humans and other life forms because it absorbs ultraviolet–B (UV–B) radiation from the Sun. If not absorbed, UV–B radiation would reach Earth's surface in amounts that are harmful to a variety of life forms.

b) In humans, increased exposure to UV–B radiation increases the risks of skin cancer, cataracts, and a suppressed immune system.

c) UV–B radiation exposure before adulthood and cumulative exposure are both important health risk factors.

d) Excessive UV–B exposure also can damage terrestrial plant life, single–cell organisms, and aquatic ecosystems.

2.2.3 Health Effects

In addition to the impacts discussed in Section 2.2.2, NO_x species can also have significant detrimental effects on human health through direct exposure. For example, as discussed by Manahan (2009):

a) Just like carbon monoxide and nitrite, NO attaches to haemoglobin and reduces oxygen transport efficiency.

b) Acute exposure to NO_2 can be quite harmful to human health. For exposures ranging from several minutes to 1 h, a level of 50 – 100 ppm NO_2 causes inflammation of the lung tissue for a period of 6 – 8 weeks, after which time the subject normally recovers.

c) Exposure of the subject to 150 – 200 ppm NO_2 causes *bronchiolitis fibrosa obliterans*, a condition fatal within 3 – 5 weeks after exposure.

d) Death generally results within 2 – 10 days after exposure to 500 ppm or more of NO_2.

2.3 Legislation

As a result of the impact of these harmful processes; the emissions of nitrogen oxides represent a major environmental issue and hazard to health. In order to combat such pollution, various forms of legislation have been introduced throughout the industrialised world.

2.3.1 Industrial Emissions Directive

As previously mentioned in Chapter 1; the legislation applicable to the gasification of waste material to form a fuel subsequently utilised in a gas engine or turbine is the IED (Directive 2010/75/EU). With such legislation in place, and as these types of application processes are becoming more prevalent, it is becoming increasingly necessary to develop techniques to enable operation within the legal emissions limits and indeed this forms the basis for the justification of this work.

2.3.2 Euro Standards

In addition to the application of interest, the principle of NO_x reduction using hydrogen may be equally applied to other applications where both NO_x is formed and hydrogen may be generated *in situ*. As will be demonstrated in Section 2.4.2.2, techniques to produce hydrogen within a diesel engine have been developed and thus legislation for mobile applications may also be considered appropriate for discussion.

The European Union has introduced limits on pollution produced from motor vehicles; in particular nitrogen oxides and particulates. The emissions standards apply to all new vehicles sold in EU member states and the scheme imparts progressively stringent regulations. A plot of the specified emissions levels for carbon monoxide (CO), oxides of nitrogen (NO_x), total combined nitrogen oxides and hydrocarbons (NO_x + HC) and particulate matters (PM), for Euro Standards 2 through 6 is shown in Figure 2.4. The Euro 5 standard came into force on 1 September 2009 and the Euro 6 standard will come into force on 1 September 2014.

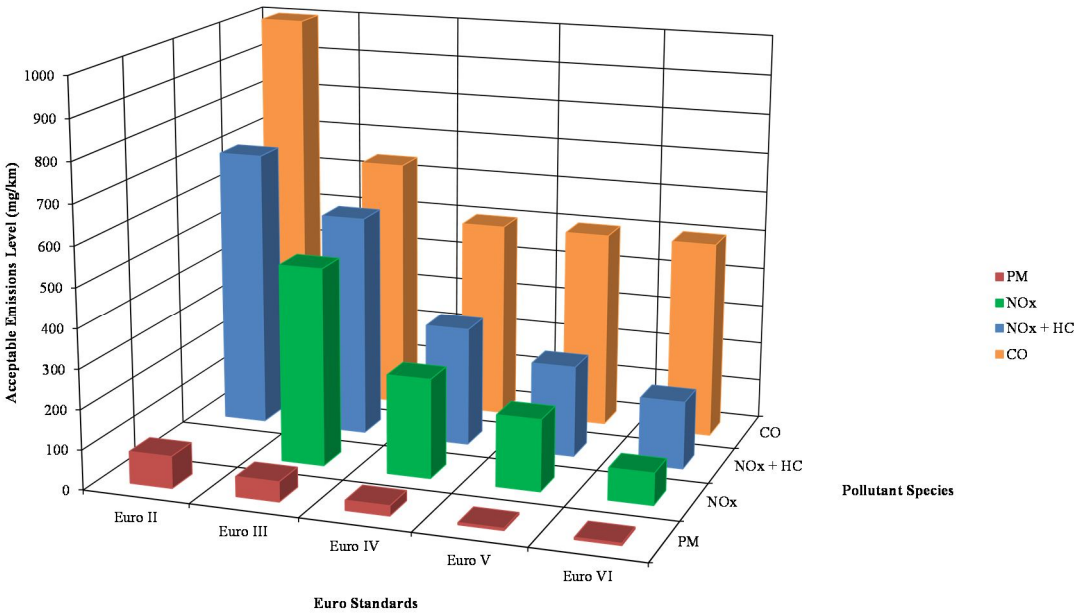

Figure 2.4 Plot of variation of acceptable emissions levels, for various pollutants from passenger cars with diesel engines, with the introduction of each Euro Standard. Data obtained from DieselNet (2012).

The European Union Regulation (EC) No 715/2007 details the acceptable emission levels from both diesel and petrol driven vehicles. It also provides details of the change in specified levels in relation to the previous standards as summarised:

a) **Euro 5 standard**

Emissions from diesel vehicles:

- nitrogen oxides (NO_x): 180 mg km^{-1} (20 % reduction of emissions in comparison to the Euro 4 standard);
- combined emissions of hydrocarbons and nitrogen oxides: 230 mg km^{-1};
- particulates: 5 mg km^{-1} (80 % reduction of emissions in comparison to the Euro 4 standard).

Emissions from petrol vehicles or those running on natural gas or LPG:

- nitrogen oxides (NO_x): 60 mg km^{-1} (25 % reduction of emissions in comparison to the Euro 4 standard);
- particulates (solely for lean burn direct – injection petrol vehicles): 5 mg km^{-1} (introduction of a limit that did not exist for the Euro 4 standard).

b) **Euro 6 standard**

Vehicles with a diesel engine will be required to substantially reduce their emissions of nitrogen oxides as soon as the Euro 6 standard enters into force. For example, emissions from vehicles used for transport will be capped at 80 mg km^{-1} (an additional reduction of more than 50 % compared to the Euro 5 standard). Combined emissions of hydrocarbons and nitrogen oxides from diesel vehicles will also be reduced. For example, these will be capped at 170 mg km^{-1} for cars and other vehicles used for transport.

As with the stationary applications, and although requirements will differ for different vehicles, continual development of emission treatment techniques is required to ensure continued adherence to the legislation.

2.4 NO_x Reduction Strategies

As with technological advancement in a bid to improve performance and efficiency, reduction in the levels of pollutant emissions will also continue to be pursued in order to reduce environmental impact. Strategies to minimise the production of NO_x emissions already exist and are continually being developed e.g. lean–burn engines or the use of fuels containing less N–species. However, additional exhaust treatment processes are often also required in order to meet the stringent regulations presented in Section 2.3.

There are already well established procedures for reducing NO_x emissions in some applications. For example; a three–way–catalyst (TWC) successfully converts NO_x, as well as carbon monoxide and hydrocarbon (HC) species, in the exhausts of petrol driven engines. However, this particular approach is not suitable for other applications with greater quantities of oxygen present i.e. diesel or biogas driven engines, the technology of interest for this study.

2.4.1 NH_3–SCR

Many approaches for the reduction of NO_x emissions exist and are in development. These techniques include (and are by no means limited to); direct NO_x decomposition (adsorption and subsequent dissociation on a metal surface), direct reduction using e.g. CO, HCs or ethanol, and NO_x storage and reduction (NSR), where NO_x species are 'trapped' and subsequently reduced through alternate lean and rich burn cycles. However, as already alluded to in Chapter 1; NH_3–SCR and urea–SCR are considered the standard approaches for stationary and mobile applications respectively. Although NH_3–SCR will be briefly discussed here, and with the exception of the NSR processes which will be explored in detail later in this chapter and the project, the other deNO_x approaches (which do not concern the use of H_2) will not be considered in any depth.

During the course of this project, two months was spent on placement working with a collaborator; Dr Joanna Łojewska of the Faculty of Chemistry at the Jagiellonian University, Krakow, Poland. Dr Łojewska's research group are also interested in deNO_x approaches, specifically NH_3–SCR to treat the exhausts of biogas fuelled gas engines, with a view to improving the performance of current installations by addressing several important problems typical of biogas exhaust treatment processes. These problems include the size of the cleaning installation, ammonia slip, thermal deactivation through the formation of hot spots, and the cost of noble metals catalysts. Their proposed solution to these issues is the use of so called structured reactors, based on metallic short channel structures, which demonstrate enhanced mass and heat transport properties as reported by Kolodziej *et al.* (2009). Theoretically this enables the reactor length to be considerably shortened, but the application of such structures is dependent on the development of new, highly–active catalysts with an improved conversion adjusted to the high transport properties, and also on the methods of catalyst deposition on the metallic surfaces of these structures. The materials they have investigated for these applications are typically zeolites.

This collaboration provided an exciting opportunity to develop a practical understanding of the NH_3–SCR process and experience first–hand related research in this field. Primary roles involved catalyst preparation and testing, and it was found that prepared copper exchanged ultrastable zeolite Y (Cu–USY) catalysts demonstrated high deNO_x activity at low temperatures with good hydrothermal resistance, in comparison with Cu–Y and Cu–ZSM 5 catalysts. The results of the work completed during the placement contributed to a publication, Ochońska *et al.* (2012).

2.4.2 Hydrogen as a Reducing Agent for DeNO$_x$

The main aim of this project is to investigate the use of hydrogen as a reductant to reduce NO_x to N_2 and H_2O through varying both the catalytic material and type of reducing process. It is important to consider the aspects of the final application and this will include the significant presence of O_2 which would also be found in the exhaust stream of such processes.

2.4.2.1 Hydrogen Presence in Biomass Gasification Process

The work conducted at Refgas Ltd (Section 2.1.1.1) included analysis of the composition of the 'clean' gaseous fuel produced from the complete gasification process. Using the QMS that will also be used for reaction gas analysis in this project, it was found that, depending on the conditions in the gasifier (Figure 2.5(A)), the composition of the clean syngas consisted of between 10 – 17 % hydrogen (Figure 2.5(B)). The measured data has been presented in order to highlight the variation in hydrogen production with gasifier conditions; through start–up in segment 1 and subsequent variation of gas flow rate and thus temperature in segments 2, 3 and 4. The confirmation of the presence of hydrogen in significant quantities validates the approach of this work.

At this point it is important to consider the levels of hydrogen ultimately required in the NO_x treatment process, with relation to the typical levels of NO_x produced from a gas turbine running on syngas reported in Section 2.1.1.1.2; >15 ppm NO_x. Even estimating a necessary hydrogen content of ten times that of NO_x, only 150 ppm (or 0.015 %) hydrogen would be required. Thus the hydrogen content of 10 – 17 % measured and displayed in Figure 2.5(B) would be more than sufficient, and the composition of the syngas supplied to the turbine would not be greatly altered.

The work at Refgas also presented a valuable opportunity to witness the type of application for which this research is being conducted, as well as gaining experience of being 'on site' at an operational plant. The measurements taken during this visit also contributed to the preparation of a paper, *Dinh Le et al (2013)*, regarding the novel use of the QMS to conduct on–line analysis of the syngas.

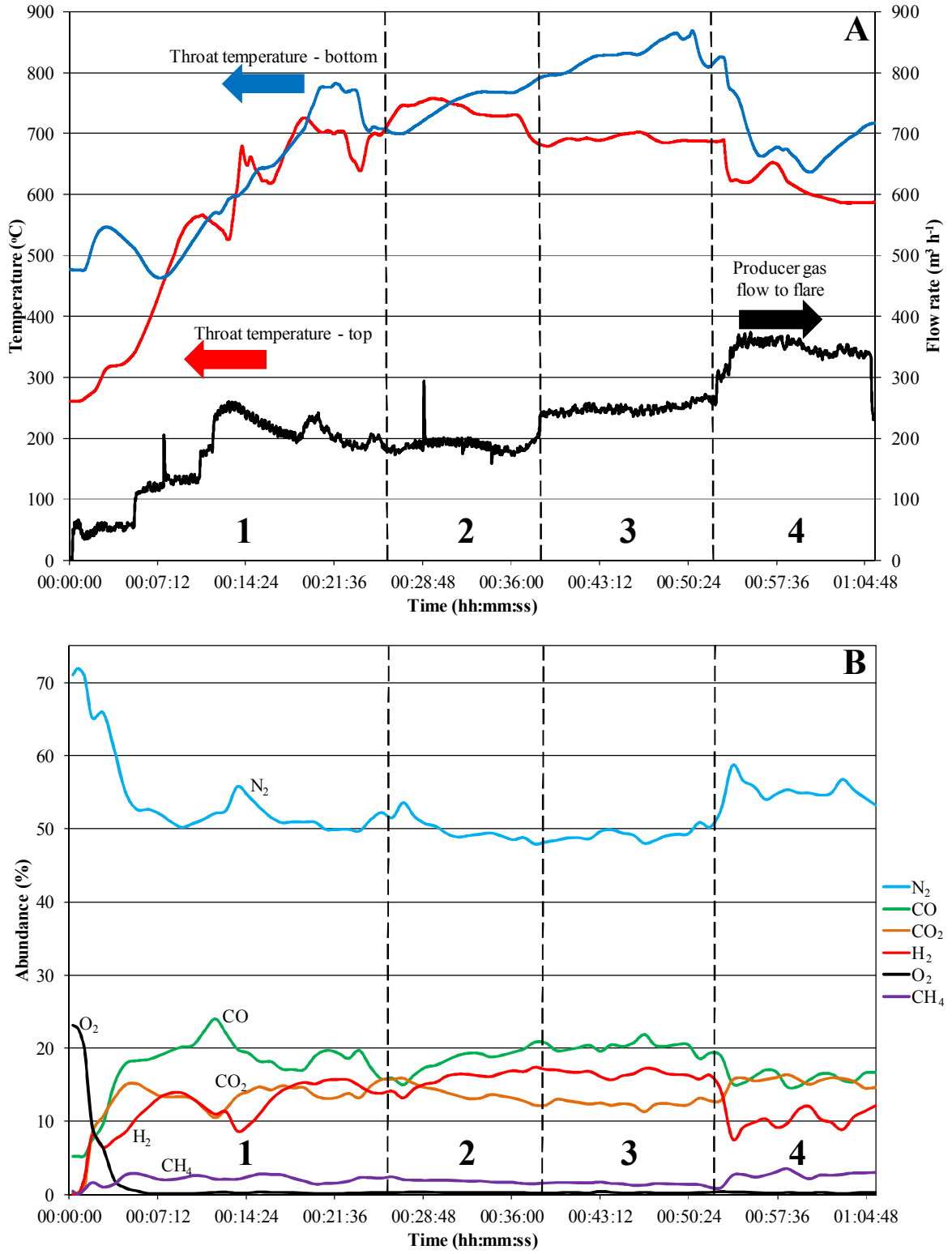

Figure 2.5 Measurements made during operation of the Refgas pilot–scale gasification facility: (A) – Conditions within the gasifier; temperatures and gas flow rate. (B) – Composition of clean gas. The dotted lines are included to create different segments, highlighting the impact of different operating conditions on the level of hydrogen (and other syngas components) produced during gasification of biomass.

2.4.2.2 Hydrogen Generation in Diesel Engine Exhausts

As already discussed, the production of hydrogen in the gasification process, and subsequent use in emissions reduction, can save on the costs associated with the use of additional reductants. However, hydrogen has also been considered for use as a reductant in other applications where it may already be present or can be easily generated. The abstract of a patent by Bartley *et al.* (2006) describes the nature of a process in which hydrogen is generated from diesel fuel *in situ*, before its subsequent use in a H_2–SCR unit to treat the NO_x emissions of a diesel engine:

> "An emission control system for reducing NO_x in the exhaust of a diesel engine. A partial oxidation system receives diesel fuel from the engine's fuel tank and partially oxidises the diesel fuel into hydrogen. The hydrogen is then introduced into the main exhaust line and the hydrogen–enhanced exhaust is delivered to a hydrogen selective catalytic reduction unit, which uses the hydrogen to convert the NO_x to nitrogen."

As is described in the patent, the SCR unit is combined with a partial oxidation unit, which provides the hydrogen necessary to reduce the emitted NO_x. Figure 2.6 is the schematic of the system, which also incorporates an optional water gas shift (WGS) catalyst to generate additional hydrogen through the following Reaction (2.14):

$$CO + H_2O \rightarrow H_2 + CO_2 \qquad (2.14)$$

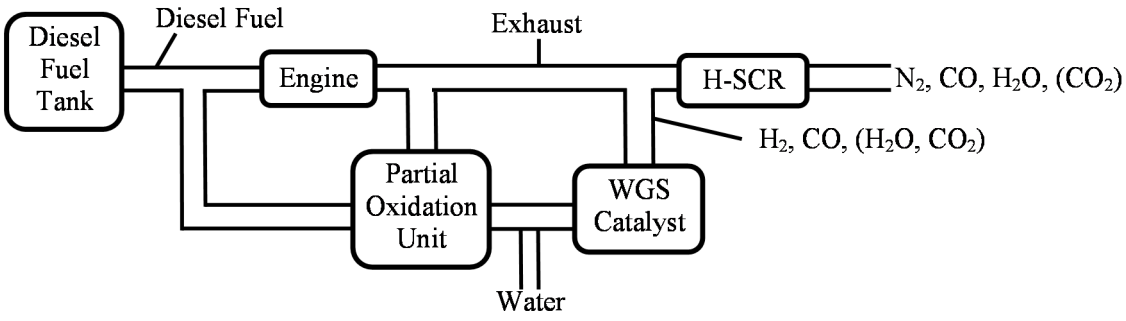

Figure 2.6 Schematic of proposed diesel engine NO_x emission control system, adapted from Bartley *et al.* (2006).

2.4.3 Previously Reported Work

Although not currently a commercial process, hydrogen for use as a reductant in $deNO_x$ applications has been studied in various capacities. A review of recent literature was conducted to investigate progress in the use of hydrogen to treat NO_x emissions, with a view to identifying a potential catalyst system and process which could be developed within this project. A schematic summarising the various H_2–$deNO_x$ processes considered in this literature review is presented in Figure 2.7. In some cases, particular catalyst systems and potential mechanisms have been further explored.

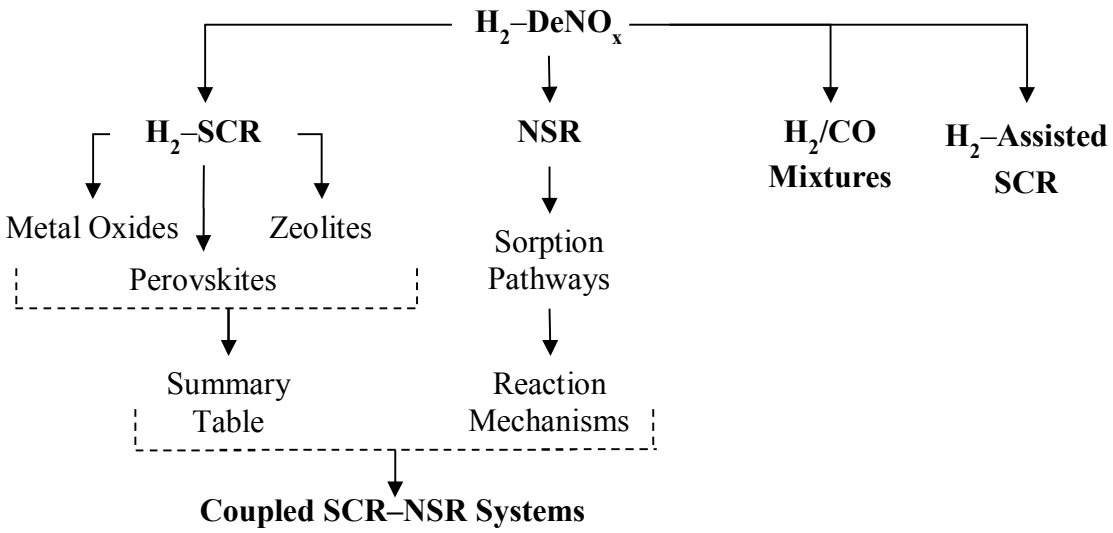

Figure 2.7 Schematic of various H_2–$deNO_x$ processes considered in this literature review. Note that the bold text represents section headings.

As such, the preparation methods, activities, selectivities and suitability to the specific application being considered were of most interest, and indeed influenced both the materials explored and the experimental conditions under which they were tested. Consideration was also given to the experience within the research group in terms of the types of materials explored for other, related exhaust treatment applications.

2.4.3.1 H_2–SCR

There has been greater interest in the use of hydrogen as a supplement in other SCR reactions (Section 2.4.3.2) than in direct H_2–SCR, however, as will be presented, a number of different catalyst systems have demonstrated activity towards NO_x reduction using only hydrogen. The key features of each system will be discussed before being directly compared in tabular form (Section 2.4.3.1.4). Note that the data presented in the table has often been interpreted from a figure presented within the stated reference and thus represents approximate, not necessarily absolute values, for an indication only.

In a recent review article Liu *et al.* (2012b) discussed the possible reactions that could occur during H_2–SCR with NO:

$$2NO + 4H_2 + O_2 \rightarrow N_2 + 4H_2O \quad (2.15)$$

$$2NO + 3H_2 + O_2 \rightarrow N_2O + 3H_2O \quad (2.16)$$

$$2NO + H_2 \rightarrow N_2O + H_2O \quad (2.17)$$

$$NO + \frac{5}{2}H_2 \rightarrow NH_3 + H_2O \quad (2.18)$$

$$NO + \frac{1}{2}O_2 \rightarrow NO_2 \quad (2.19)$$

$$H_2 + \frac{1}{2}O_2 \rightarrow H_2O \quad (2.20)$$

It is interesting to note the role oxygen plays in the above reactions. Whilst it appears necessary for successful reduction of NO to N_2 and H_2O (Reaction (2.15)), it is also involved in the formation of undesired side products NO_2 (Reaction (2.19)) and the direct reaction of H_2 to form H_2O (Reaction (2.20)).

Utilising the same approach, the desired reaction involving NO_2 during H_2–SCR of NO_x can also be predicted:

$$2NO_2 + 6H_2 + O_2 \rightarrow N_2 + 6H_2O \quad (2.21)$$

Liu *et al.* (2012b) goes on to describe the roles of each reaction in the overall process:

a) Reaction (2.15) is the most desirable reaction because the products are N_2 and H_2O.

b) N_2O, which is a greenhouse gas, can be formed as a byproduct during both reaction (2.16) and (2.17).

c) NH_3 could be produced by Reaction (2.18), although the presence of oxygen can inhibit its formation over some catalyst.

d) The formation of NO_2 via Reaction (2.19) may play an important role for the NO_x reduction to proceed due to its higher activity than NO.

e) Reaction (2.20) is the combustion reaction of H_2, which competes with Reaction (2.15) and leads to the low utilization of reducing agent for NO_x removal.

2.4.3.1.1 Noble Metal and Metal Oxide Based Catalysts

Noble metal and metal oxide based catalysts are typical heterogeneous catalyst systems considered for SCR and related processes for a number of decades (Nova *et al.* (2006)):

a) Different types of catalytic systems have been considered for use in the SCR reaction, including noble metals, metal oxides, and zeolites. Among these categories, metal–oxide based catalysts are the most commonly utilised SCR systems at present.

b) Supported noble metal catalysts, which were developed as automotive exhaust catalysts in the early 1970s, were first considered for the SCR of NO_x. These catalysts are very active in the SCR reaction but they also effectively oxidise both ammonia and sulfur dioxide. Besides, they are less tolerant to poisoning. For these reasons, noble metal catalysts were soon replaced by metal–oxide based catalysts.

c) Metal oxide catalysts, based on chromium, copper, iron, vanadium, and other oxides either unsupported or supported on alumina, silica, and titania have been investigated as candidates for NO_x reduction by ammonia since the mid–1960s.

The preparation of these materials is described in Spencer (1989), who stated that most industrial catalysts are made either by precipitation, when active phase and support are made together, or by the impregnation of an active phase on to a preformed support. In this instance typical support structures may include high surface area pellets, rings or monoliths.

2.4.3.1.1.1 Pd/Al_2O_3 Catalysts

Pd/Al_2O_3 materials have been widely explored as potential catalysts for the reduction of NO_x with H_2, as well as in other applications. Indeed this catalyst was initially chosen to be explored in a previous study, preceding this project, due to the experience within the research group of preparing and handling similar materials i.e. diesel oxidation catalysts (DOCs), which are typically Pd/Al_2O_3 or Pt/Al_2O_3 systems.

It was found that although the direct reaction of H_2 and NO to form H_2O was promoted in the absence of O_2, when a significant O_2 concentration was introduced the H_2 reacted directly with the O_2 and the NO was left unreacted. This was summarised in the conclusions of the aforementioned preliminary study by McClymont (2010), in which it was confirmed that Pd/Al_2O_3 catalysts:

- In the absence of O_2, can effectively reduce NO_x using H_2, however,
- Strongly promote the reaction between H_2 and O_2, even at low temperatures.

These observations agreed with the literature results for experimental conditions which mimicked the application environment (i.e. a high oxygen concentration) and a summary of the 'best' experimental performances for a number of these studies are presented in Table 2.1 along with the performance of selected other systems described in Section 2.4.3.1. The reported results are typically the maximum reported NO conversion, subsequent N_2 selectivity, S_{N2}, and relevant reaction temperature, enabling direct comparison of the various investigated systems.

It can be seen that in the presented examples, a maximum NO conversion of only ~40 % was achieved, reported by Marques *et al.* (2008), with a maximum selectivity of ~40 % reported by Macleod *et al.* (2002), who also concluded: in agreement with previous studies it was observed that pure H_2 is a poor reductant for NO_x reduction under lean burn conditions when employing Pd/Al_2O_3 as the catalysts.

It should also be noted that the limited activity observed in these studies was often achieved with H_2 in significant excess; H_2:NO ratios of at least 3:1, and up to a maximum of 10:1 were utilised. Whilst this may not be inconceivable from a practical perspective (as demonstrated in Sections 2.1.1.1.2 and 2.4.2.1 there will be relatively little NO and significant levels of H_2 present in the system), it does suggest that it is incredibly difficult to achieve the desired reaction with this catalyst.

In addition, the catalysts discussed in the references mentioned here were all prepared through impregnation methods, with Marques *et al.* (2008) additionally investigating the impact of the type of metal precursor on catalyst performance. This technique is widely used to prepare materials in the field of heterogeneous catalysis and such conditions may be easily replicated. Finally, the catalyst testing in these references was conducted on powder catalysts and not supported catalyst structures.

2.4.3.1.1.2 Pt/Al_2O_3 Catalysts

Pt/Al_2O_3 catalysts have also been extensively investigated for H_2–SCR processes, and with greater success than the Pd/Al_2O_3 system. Macleod *et al.* (2002) also explored a Pt/Al_2O_3 catalyst (in addition to their experiments on a Pd/Al_2O_3 system) and obtained significantly improved results in comparison (Table 2.1), concluding that:

> In agreement with previous studies, the $H_2/NO/O_2$ reaction under lean–burn conditions over platinum based catalysts was found to deliver high NO_x conversion efficiency (up to 80 % NO_x conversion) at relatively low temperature (~100 – 200 ^oC).

This result was subsequently matched by Itoh *et al.* (2010) (Table 2.1) in their study which directly compared the performance of catalysts prepared through two different preparation methods. They state:

> The solvothermal preparation is favourable to obtain the uniformly large spherical nanoparticles with high crystallinity, and the resultant catalyst possesses better deNO_x activity (NO conversion: 80 %, N_2 yield: 60 %) than that prepared by the impregnation method.

This result suggests that a 'solvothermal' preparation method; typically involving the use of an autoclave to subject the synthesis materials to high pressures and temperatures for a prolonged period of time, creates better performing catalysts than the more traditional impregnation method. This result will be considered again when reviewing the implications of this literature review for the project.

The demonstrated NO conversion and N_2 selectivity for the Pt/Al_2O_3 catalysts, although a significant improvement upon the Pd/Al_2O_3 systems, may still not be sufficient for the applications of interest. Indeed, the TWCs for related automotive emission control applications typically operate at almost complete conversion of the pollutant species. This is summarised by Twigg *et al.* (2006):

> "Once the catalyst is at operating temperature, the reactions are mass transfer controlled and conversions between 95 and 100 % are normal."

2.4.3.1.1.3 Additional Catalyst Systems

There have been many more metal/support combinations investigated for use in H_2–SCR reactions, albeit not as thoroughly explored as those discussed above. This may be explained by their relative lack of activity in comparison to the Pd and Pt catalysts and this is reflected in the typical reported experimental conditions; which are often relatively high in H_2 and low in both NO and O_2. As a result it is not necessary to discuss in detail any examples here, although a number of examples are presented in Table 2.1 for completeness.

2.4.3.1.2 Perovskites

A class of materials known as perovskites is one of the largest structural families in materials chemistry. Schwartz (2002) describes the basic perovskite structure:

> From the viewpoint of crystal structure, the ABO_3 type structure (Figure 2.8), in which the cation A usually has valence 2+ and the cation B has valence 4+, is the fundamental perovskite. The perovskite family is created by doping other types of cations into the stoichiometry and/or introducing anion deficiency.

Schwartz (2002) also describes current uses for the perovskite family of materials, stating that perovskite–structured materials have important applications in ferroelectricity, piezoelectricity, ferromagnetism, magnetoresistance, superconductivity, ionic conductivity, and dielectricity.

Perovskites typically consist of two or more mixed metal oxides and have also demonstrated significant activity in the reduction of NO_x using H_2. Costa *et al.* (2001) described the performance of their $Pt/La_{0.5}Ce_{0.5}MnO_3$ system, stating:

> In addition, the N_2 selectivity value of 88 % obtained on $Pt/La_{0.5}Ce_{0.5}MnO_3$, to our knowledge, is the highest value ever reported at the temperature at which maximum activity is observed for the $NO/H_2/O_2$ reaction with 5 % H_2O in the feed stream in the 100 – 200 ^oC low–temperature range.

Coupled with a reported NO conversion of 79 % (Table 2.1), the performance of this material exceeds that of Pt/Al_2O_3.

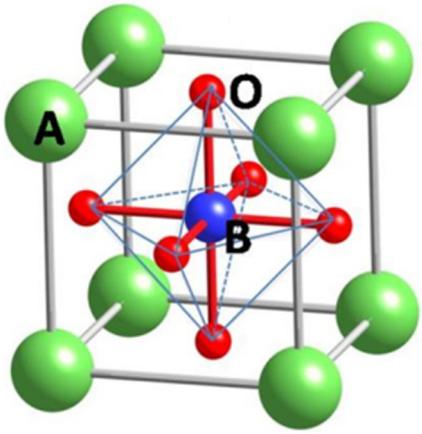

Figure 2.8 ABO_3 perovskite structure presented in Fu *et al.* (2011).

Chiarello *et al.* (2007a) subsequently achieved complete NO conversion with their $Pd/LaCoO_3$ system at 150 ^oC, with a comparable N_2 selectivity of 78 % (Table 2.1). This study investigated the performance of catalysts synthesised through a flame–spray pyrolysis method. The features of the synthesis procedure were identified in a related publication by Chiarello *et al.* (2007b):

a) $La(CH_3COO)_3 \cdot xH_2O$ (Aldrich, purity >99.9 %, H_2O 7.5 wt%, determined by TGA) and $Co(CH_3COO)_2 \cdot 4H_2O$ (Merck, purum) were dissolved in a mixture of propionic acid, n–propanol, and water (5:4:1 vol%) under vigorous stirring at 60 ^oC, to obtain a 1:1 metal–ion ratio and a 0.15 M overall metal concentration (sample LCO).

b) The desired amount of $Pd(CH_3COO)_2$ (Fluka, purum) was added when preparing the Pd–containing sample (PdLCO).

c) The liquid solution was fed at a rate of 4 mL/min by a microannular gear pump (HNP Mikrosysteme model mzr 2905) at the center of a vertical nozzle, together with 5 L/min of O_2 (1 bar pressure drop across the nozzle).

d) The obtained spray was ignited, and the flame was supported by a premixed methane/oxygen (1.0 L/min O_2 and 0.5 L/min CH_4) annular flame (12 mm diameter, 0.15 mm thick) surrounding the nozzle.

e) The powder thus produced was collected on a glass fiber filter (Whatman GF/D, 25.7 cm diameter) connected to a vacuum pump (Busch Seco SV 1040C).

Although the perovskite materials discussed here have shown very promising performance in the reduction of NO_x using H_2, it has also been demonstrated that they are often prepared through complex methods requiring numerous chemicals and synthesis steps, as well as intricate equipment.

2.4.3.1.3 Zeolites

As described by Maesen *et al.* (2001):

a) A zeolite is a crystalline aluminosilicate with a three–dimensional framework structure that forms uniformly sized pores of molecular dimensions. As the pores preferentially adsorb molecules that fit snugly inside the pores and exclude molecules that are too large, they act as sieves on a molecular scale.

b) Zeolites consist of robust, crystalline silica (SiO_2) frameworks. At some places in the framework Al^{3+} has replaced Si^{4+} and the framework carries a negative charge. Loosely held cations that sit within the cavities preserve the electroneutrality of the zeolite. Some of those cations are amenable to cation exchange and are able to reversibly interact with polar molecules.

A crystal structure of a typical zeolite is presented in Figure 2.9. Note the various channels, of different sizes, which may accommodate different sized molecules.

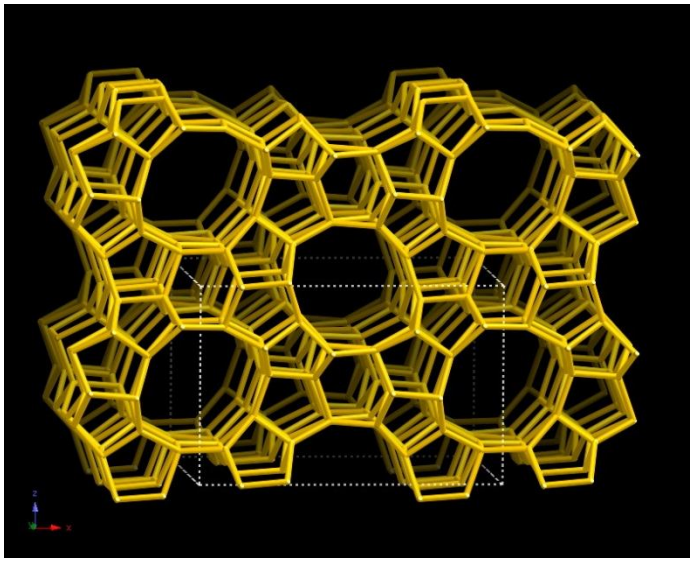

Figure 2.9 Crystal structure of ZSM–5/MFI type zeolite presented in Framework Type MFI (2007).

Zeolites are prepared under hydrothermal conditions, usually between 60 °C and 300 °C in a pressure vessel, over the course of a number of minutes, hours or days dependent on the synthesis mixture. Often, zeolite synthesis relies on the presence of a template, within the reaction mixture, that does not participate in the reaction but around which the structure is assembled.

Zeolites have long been known to demonstrate deNO_x activity both through direct decomposition (Iwamoto *et al.* (1991)) or in SCR reactions (Sato *et al.* (1991)). Zeolites were also the active component of the NH_3–SCR study conducted in Krakow, Poland as part of this project, which was previously discussed in Section 2.4.1 (Ochońska *et al.* (2012)). In addition, the structure of one of the types of zeolites explored in that study is presented in Figure 2.9.

Shibata *et al.* (2004) investigated H_2–SCR for a variety of platinum supported catalysts materials, including several zeolite supports. A Pt/MFI (Mordenite Framework Inverted) catalyst demonstrated both excellent NO conversion and N_2 selectivity (Table 2.1) however the temperature of operation was particularly low, ~100 °C, and NO_x conversion decreased at higher temperatures. A similar trend was observed for the other catalysts:

> "For all the catalysts, the NO_x conversion increased with the reaction temperature, reached a maximum at 373–423 K, and then decreased without any further increase in the temperature."

Li *et al.* (2010) investigated platinum supported on Ti–containing MCM–41 (Mobil Crystalline Material) catalysts and also observed excellent activity at lower temperatures. For Pt/Ti–MCM–41, a high N_2 selectivity of ca. 79 % was achieved at 140 °C when maximal NO_x conversion (ca. 89 %) was obtained. The investigated catalysts also showed some tolerance to the presence of small amounts of SO_2 and CO. The Pt/Ti–MCM–41 was tolerant to SO_2 at low concentration (~20 ppm) and the deactivation by SO_2 at higher concentration (~50 ppm) was reversible to a great extent. A more serious negative effect was observed at a higher concentration of CO in the range of 100–1000 ppm. Fortunately, the deactivation by CO was also found to be reversible and the NO_x conversion was easily recovered after removing CO from the inlet.

2.4.3.1.4 Summary Table

Table 2.1 Selected catalyst, reaction and performance characteristics of various references reporting H_2–SCR data.

Reference	Catalyst			Feed Composition (%)				Performance			Notes
	Metal	Loading (wt%)	Support	NO_x	H_2	O_2	Balance	Conversion of NO_x (%)	Selectivity to N_2, S_{N2} (%)	Temperature, T_{MAX} (°C)	
Macleod *et al.* (2002)	Pd	0.5	Al_2O_3	0.05	0.4	5.0	He	~10	~40	135	S_{N2} reported with respect to total reaction of NO, not only reduction reactions
Marques *et al.* (2008)	Pd	0.5	Al_2O_3	0.015	0.15	7.0	Ar	~40	–	250	–
Macleod *et al.* (2002)	Pt	0.5	Al_2O_3	0.05	0.4	5.0	He	~80	~50	145	S_{N2} reported with respect to the formation of N_2 and N_2O
Itoh *et al.* (2010)	Pt	1.0	Al_2O_3	0.1	0.4	2.0	N_2	~80	~60	120	–
Nanba *et al.* (2003)	Rh	3.0	Al_2O_3	0.1	1.0	2.0	He	70	–	252	Selectivity not reported
	Ir	1.0						70	–	177	
Costa *et al.* (2001)	Pt	0.1	$La_{0.5}Ce_{0.5}MnO_3$	0.25	1.0	5.0	He	79	88	140	Reaction mixture included 5 % H_2O
Chiarello *et al.* (2007a)	Pd	0.5	$LaCoO_3$	0.25	1.0	5	He	100	78	150	–
Shibata *et al.* (2004)	Pt	0.8	ZSM–5	0.1	0.5	6.7	He	~95	~70	~100	–
Li *et al.* (2010)	Pt	1.0	Ti–MCM–41	0.1	0.5	6.7	He	89	79	140	Performance in the presence of 20 ppm of SO_2 and CO also investigated

Note: Reminder of the stoichiometries of the proposed $H_2/NO_x/O_2$ reactions – 4:2:1 $H_2/NO/O_2$ and 6:2:1 $H_2/NO_2/O_2$. T_{MAX} is the reaction temperature at which maximum NO conversion is observed.

2.4.3.2 H_2–assisted SCR

As already alluded to, the use of H_2 has been explored in tandem with other reductants; typically hydrocarbons but also NH_3 and ethanol, in what is commonly referred to as H_2–assisted SCR.

Satokawa (2000) first reported the promotional effect of H_2 addition on hydrocarbon–SCR of NO over a Ag/Al_2O_3 catalyst. Subsequent studies on other silver catalysts have also reported enhanced activity by including H_2 in the reductant stream.

Burch *et al.* (2004) found that on addition of H_2 to their octane–SCR experiments (conducted over Ag/Al_2O_3 catalysts), greatly improved performance was achieved both in terms of NO_x conversion and the temperature window of operation. With octane alone, the activity first started to increase at a temperature of around 350 ^oC and reached a broad maximum around 500 ^oC before declining again. However, when 0.72 % H_2 was introduced, the NO_x reduction was seen to commence even at 100 ^oC and reached a maximum at around 200 ^oC. The conversion ranged from 100 % NO_x conversion (in the presence of hydrogen) to roughly 10 % conversion (when hydrogen was absent).

Burch *et al.* (2004) also identified the role H_2 played in the enhanced activity, stating that hydrogen has the effect of activating octane at lower temperatures and it also promotes the oxidation of NO to NO_2 in the absence of hydrocarbon.

Richter *et al.* (2004) explored a H_2/NH_3 mixture for a variety of silver catalysts although only the Ag/Al_2O_3 catalysts demonstrated significantly improved activity. They found that catalyst samples on γ–Al_2O_3 or mesoporous Al_2O_3 (sol–gel) supports responded in a pronounced way to co–fed H_2. The activity was boosted from values less than 10 % to 100 % at 300 ^oC, even in the presence of 7 % H_2O, with N_2 selectivities always higher than 95 %.

Breen *et al.* (2009) also reported a transient NO_x storage affect over a Ag/Al_2O_3 catalyst during H_2–assisted HC–SCR, which may have implications for NSR applications (Section 2.4.3.4).

2.4.3.3 H_2/CO Mixture

Another approach which may be of interest is the use of a mixture of both H_2 and CO to treat NO_x emissions. This is particularly relevant for this application; as can be seen from Figure 2.5(A) there is a significant CO presence (even greater than H_2) in the clean syngas, and thus theoretically both species may be used in NO_x reduction.

However, there may be practical issues with separation of *both* H_2 and CO together from the syngas mixture, as discussed in Chapter 1 some of described technologies would not be appropriate. In addition, this technique is also not applicable for some previously explored materials, as Macleod *et al.* (2002) state that the reduction of NO_x by hydrogen under lean burn conditions over Pt/Al_2O_3 is strongly poisoned by carbon monoxide.

However, some of the catalyst systems previously described demonstrated excellent deNO_x performance when using both H_2 and CO as reductants. Lee *et al.* (2004) found that the Pd/Al_2O_3 catalyst gave NO_x conversions up to 95.2 % at 150 ^oC, with complete CO and H_2 oxidation occurring between 150 and 200 ^oC.

Lee *et al.* (2004) explained the observed activity due to the presence of both reductants and as a result of the catalyst preparation method. They said that the synergistic effects of having both CO and H_2 in the feed as well as using $PdCl_2$ as the precursor with the alumina support enhance NO_x reduction to N_2 at low temperatures.

There is also interest in using H_2/CO mixtures to reduce stored NO_x species in NSR processes (Section 2.4.3.4). Dujardin *et al.* (2013) explained the reasoning behind investigating their catalyst performance with a H_2/CO reducing mixture, saying that:

a) The supply of hydrogen can be obtained using on–board fuel reformer.

b) However, the impact of CO has to be taken into account since fuel reforming leads to a gas mixture composed of H_2 and CO as main products.

However, the catalyst demonstrated poor activity at lower temperatures due to the extensive formation of carbonate species. It appears that at the very least CO will be present in the exhaust mixture and must be considered as a catalyst poison if it is not to be utilised in the reduction reactions.

2.4.3.4 NO_x Storage and Reduction (NSR)

Takahashi *et al.* (1996) first reported a novel technique for the treatment of NO_x emissions known as NO_x Storage and Reduction or NSR. In the study, a variety of catalysts were prepared and generally consisted of a noble metal and 'storage component' (alkaline earth metal) supported on alumina. Operating through alternating lean and rich conditions, the NO_x is initially 'stored' on the catalyst surface before subsequent reduction to form N_2. Alternatively, these types of catalysts are known as 'Lean NO_x Traps' (LNT) and both terms are used interchangeably throughout this thesis.

2.4.3.4.1 Three Proposed Pathways for NO_x Sorption

$Ba/Pt/Al_2O_3$ is considered the 'standard' NSR catalyst and has been extensively studied for this process since the original publication by Takahashi *et al.* (1996). As such, potential chemical processes involved during NSR cycles are well documented.

The following potential pathways Figure 2.10(A)–(C), have been recreated from Epling *et al.* (2004) and depict the routes through which NO_x species can be stored on the catalyst surface. The figures are included here as they represent both the desired and undesired NO_x storage pathways and aid understanding of the roles of the catalyst components and what would also be required of a novel material.

Note that in all cases the solid and dashed black arrows represent adsorption/desorption pathways from and to the gas phase, and the block arrows represent surface diffusion pathways. The overall chemical equations occurring at each site are also displayed.

In pathway A, Figure 2.10(A), the following steps occur:

1. Close proximity of Pt/Ba sites result in the rapid uptake of NO_x at these locations.
2. Ba sorbate sites further away from Pt sites have a slower uptake.
3. Ba sites not in contact with Pt sites trap NO_2 exclusively from the gas phase using the NO_2 disproportionation mechanism.

Nitrites and nitrates are formed at the Pt/Ba sites and use O_2 and NO_2 as oxygen sources for the further oxidation of nitrites to nitrates.

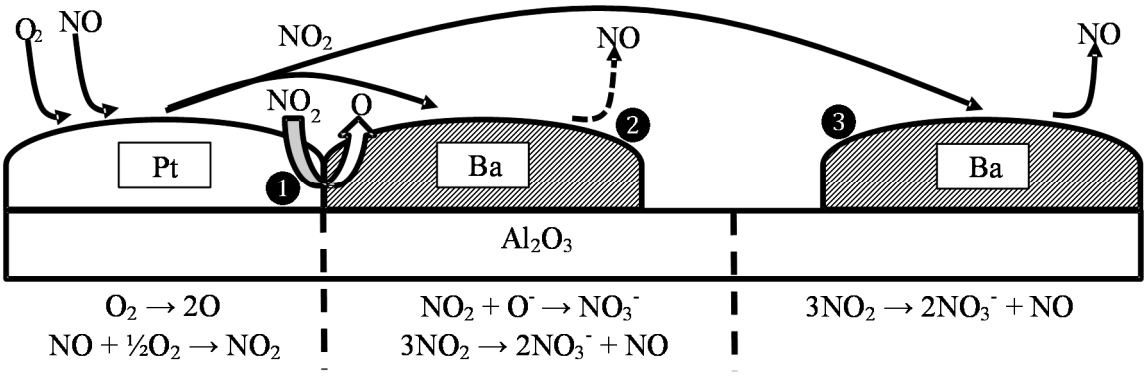

Figure 2.10(A) NO_x storage on $Ba/Pt/Al_2O_3$ – Pathway A.

In pathway B, Figure 2.10(B), a nitrate "spill over" type mechanism is seen. The sorbate sites near Pt are saturated rapidly due to the availability of adsorbed NO_2 and oxygen atoms. Although the trapping rate slows due to the increasing diffusion resistance as the N–species build up around the Pt particles, migration of the nitrate species away from the Pt sites occurs.

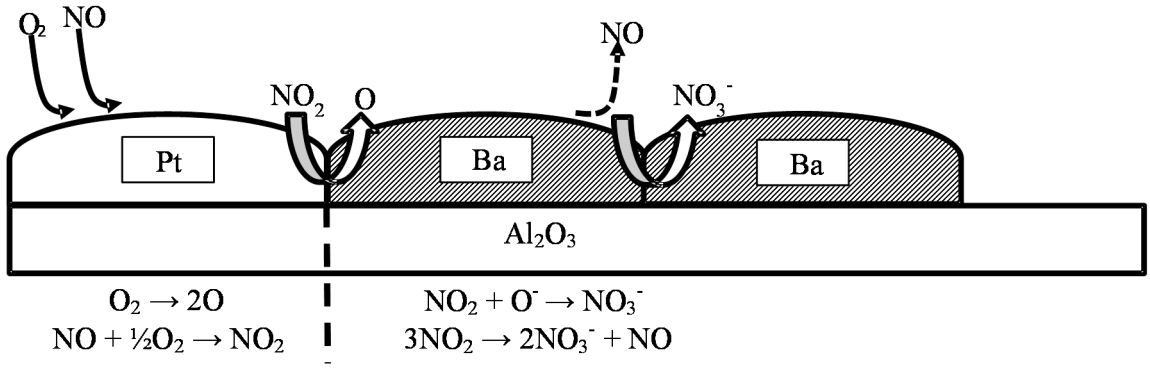

Figure 2.10(B) NO_x storage on $Ba/Pt/Al_2O_3$ – Pathway B: Nitrate "spill over" type mechanism.

In Pathway C, Figure 2.10(C), the lone Pt site, which is not adjacent to a Ba site, is only involved in the oxidation of NO to NO_2 and does not play a role in the storage of NO_2 on the Ba sites.

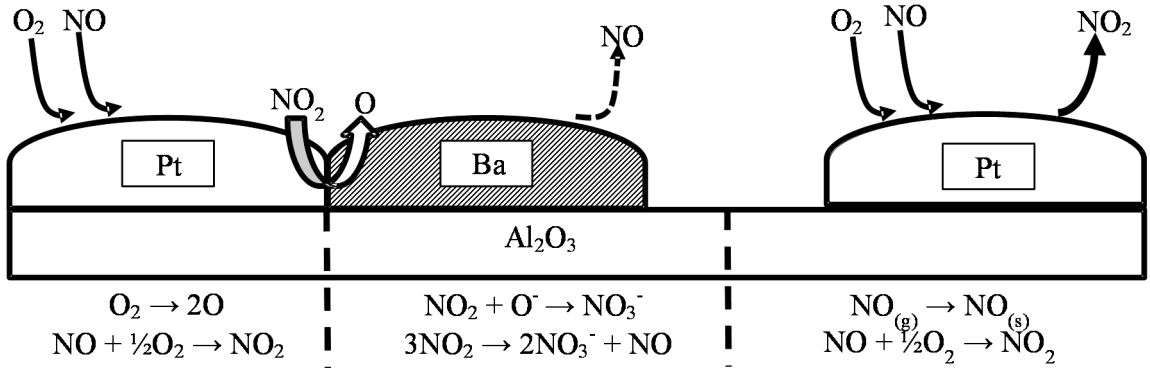

Figure 2.10(C) NO_x storage on $Ba/Pt/Al_2O_3$ – Pathway C.

Epling *et al.* (2004) then categorize the pathways displayed previously (Reactions (2.22)–(2.28) and provide the following explanation:

> A mixture of BaO, $Ba(OH)_2$ and $BaCO_3$ is present on the catalyst and each has different relative stabilities in comparison to the nitrate. The BaO is replaced first, followed by the replacement of $Ba(OH)_2$, then $BaCO_3$. These species are displaced to form the nitrites and nitrates.

NO sorbs *via*:

$$BaO + 2NO + O^* \rightarrow Ba(NO_2)_2 \quad (2.22)$$

$$BaO + 2NO + 3O^* \rightarrow Ba(NO_3)_2 \quad (2.23)$$

NO_2 sorbs *via*:

$$BaO + 2NO_2 + O^* \rightarrow Ba(NO_3)_2 \quad (2.24)$$

$$BaO + 2NO_2 \rightarrow Ba(NO_2)_2 + O^* \quad (2.25)$$

$$2BaO + 4NO_2 \rightarrow Ba(NO_2)_2 + Ba(NO_3)_2 \quad (2.26)$$

As shown, these typically result in nitrite or nitrate formation using O*. The O* originates from NO_2 or O_2:

$$BaO + 3NO_2 \rightarrow Ba(NO_3)_2 + NO \quad (2.27)$$

$$BaO + 2NO_2 + \frac{1}{2}O_2 \rightarrow Ba(NO_3)_2 \quad (2.28)$$

where the O_2 is dissociated on Pt.

2.4.3.4.2 Possible NSR Reactions

Once the NO_x has been adsorbed and stored on the catalyst surface in the form of nitrates and nitrites, there are a number of potential reactions that can subsequently occur. Figure 2.11(A)–(C) have been recreated from Balcon *et al.* (1999). Once again, inclusion of these figures aids understanding of the necessary processes for a successful NSR catalyst. Note that a subscript (g) denotes NO_2 in the gas phase, and a subscript (s) denotes stored NO_2. In these cases the use of NO_2 is not necessarily indicative of actual NO_2 molecules; it is a representation of both the nitrates and nitrites that are stored on the catalyst surface. Reaction A, Figure 2.11(A), depicts the release of stored NO_2 entities during rich phases.

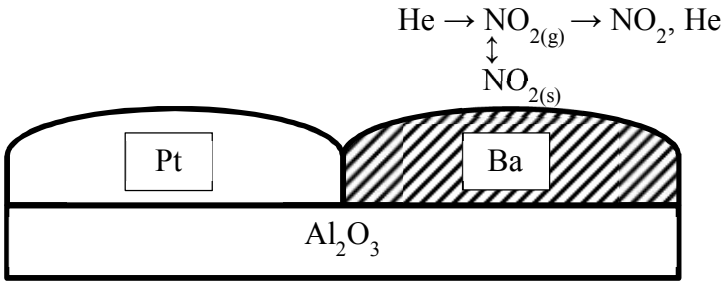

Figure 2.11(A) Reaction A: NO_2 release from Ba compounds in rich conditions (He carrier gas).

Reaction B, Figure 2.11(B), demonstrates the competitive effect of CO_2 on NSR processes. CO_2 can be introduced to interact with the same Ba storage sites as $NO_{2(g)}$, promoting the rapid release of stored NO_x molecules.

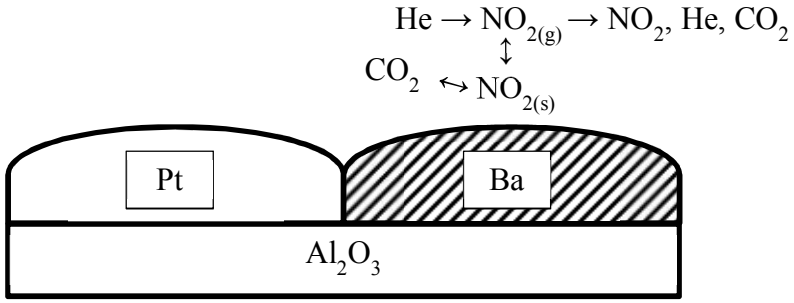

Figure 2.11(B) Reaction B: Competitive effect of CO_2 on NO storage and release (Ba–carbonates formed).

Reaction C, Figure 2.11(C), exhibits the process through which stored NO_x is first released by a reductant, in a similar fashion to Reaction A, before diffusion of $NO_{2(g)}$ towards the metallic sites. Subsequent reduction of NO_x by a reductant dissociated on these sites produces nitrogen and water. This is the desired process for this study.

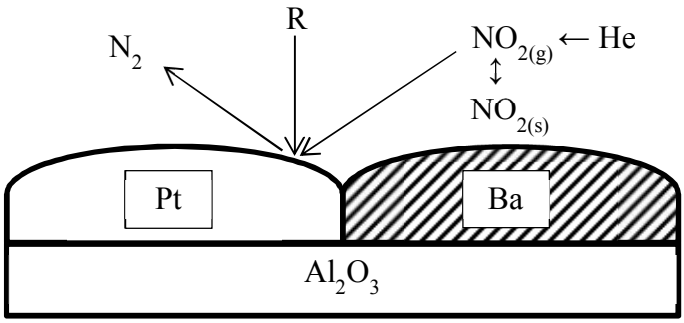

Figure 2.11(C) NO_2 release and reduction in the presence of a reducing agent, R = H_2 or CO or HCs.

2.4.3.4.3 H_2 use in NSR Experiments

Like the aforementioned SCR processes, many different reductants have been investigated for use in NSR cycles e.g. Fridell *et al.* (1999) and Abdulhamid *et al.* (2004) both trialled H_2, CO, C_3H_6 and C_3H_8 as reductants.

It is, however, widely considered that H_2 is the best reductant for NSR processes over a $Pt/Ba/Al_2O_3$ catalyst. For example, according to Poulston *et al.* (2003), H_2 was found to be more effective at regenerating the NO_x storage activity especially at lower temperature, but more importantly over the entire temperature window after catalyst ageing.

This view was shared by Liu *et al.* (2004), who stated that the order of efficiency in terms of conversion of stored NO_x to N_2 was H_2 > CO > propene. Additionally the use of hydrogen led to the lowest NO_2:NO ratio.

In terms of a possible mechanism, from results reported by Cumaranatunge *et al.* (2007) it was hypothesised that when using H_2 as the reductant; following initial reaction of H_2 and NO, NH_3 is formed as an intermediate which subsequently reduces more NO species. They stated that:

a) As the NO_x (NO + NO_2) is released from the trapping sites (the exact mechanism of release is not known), it reacts with H_2 over Pt to form NH_3, N_2 and N_2O as the N–containing species

b) The NH_3 formed will further react with more NO_x to give either N_2 or N_2O.

It must be noted here that these studies were often conducted with a view to using H_2 generated from means other than those proposed in this study. For example, Lietti *et al.* (2001) proposed that hydrogen is generated at the site with a small reformer that uses natural gas and steam as input streams.

2.4.3.5 Coupled SCR and NSR Systems

Finally, a few recent studies have investigated systems where both SCR and NSR processes are combined to provide NO_x reduction. Building upon the mechanism proposed by Cumaranatunge *et al.* (2007) above, Can *et al.* (2012) describe the following process:

a) Ammonia may be produced during the regeneration step of an NSR catalyst, by the direct reaction (NO_x + H_2) or/and the isocyanate route.

b) They state that recent literature highlights that the ammonia production rate is higher than the ammonia reaction rate with the remaining NO_x in order to form N_2.

c) They proposed that in order to optimize the use of the in situ produced ammonia, a catalyst dedicated to the NO_x–SCR by NH_3 could be added.

A representation of what this process may look like is depicted in Figure 2.12, which has been recreated from Xu *et al.* (2012), and represents the experimental set–up used to investigate a coupled LNT/SCR system to treat the emissions from a diesel powered engine.

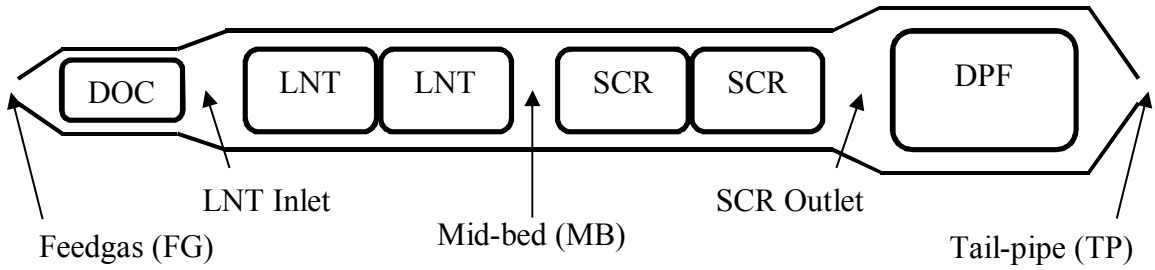

Figure 2.12 Example schematic of coupled LNT/SCR process applied to a diesel engine exhaust. Recreated from Xu *et al.* (2012). LNT: Lean NO_x Trap; DOC: Diesel Oxidation Catalyst; DPF: Diesel Particulate Filter.

The approach has been found to be quite successful for a variety of performance related factors. Wang *et al.* (2012) found that the formation of N_2O was greatly reduced using the coupled system with H_2 as the reductant, and they stated:

a) As expected, H_2 is the best NO_x reductant at all temperatures, while the benefit of the SCR catalyst is again apparent with respect to system NO_x conversion and the abatement of N_2O emissions.

b) N_2O selectivity is shown in Fig. 3 and is very low, peaking at a value of 8 % at 165 ^oC and then attaining a second maximum of 10 % at 250 ^oC.

From a practical perspective the coupled system also offers more advantages than a single LNT approach, in addition to greater NO_x conversion, highlighted by Xu *et al.* (2012):

- Higher NO_x conversions and a wider operating temperature window,
- improved durability of both the LNT and SCR catalyst (including an ability of the SCR catalyst to compensate for activity losses by the LNT), and
- benefits of the SCR catalyst in converting not only NO_x released from the LNT but also hydrocarbons that break through the LNT under purge conditions.

However, this sort of 'hybrid' approach provides many opportunities for other novel solutions for treating NO_x emissions. For example; Liu *et al.* (2012a) explored the performance of a "dual–layer monolithic catalyst" where a zeolite SCR catalyst was deposited directly on the surface of a NSR catalyst and Castoldi *et al.* (2011) explored a system where "the LNT and the SCR catalyst particles are physically mixed".

2.5 Analysis Techniques

Another novel aspect of this work relates to the real time analysis of the species produced in the reactions of interest. Whilst there have been many investigations of related catalytic systems and reaction conditions, there are also many different methods and types of equipment used for analysis. A review of the most common techniques for the analysis of related gas phase reactions is presented here.

Table 2.2 summarises the main analytical techniques utilised in the analysis of $deNO_x$ reaction products from the references discussed in this chapter, in addition to some from groups who are well–known in the field of $deNO_x$ (30 references sampled in total). Table 2.3 details specifically what techniques and combination of techniques were used within each investigation. Note that the various catalyst characterization techniques utilised throughout these studies are not discussed here.

It can be seen that from the sample taken, there are at least seven different analysis techniques commonly employed to measure the outlet gas composition from various $deNO_x$ reactions. An important point to note is that in most cases two or more detection techniques are often used in parallel to ensure measurement of a wide range of species and it does not appear there is a technique capable of solely identifying all the reaction components of interest (when a single technique is used, only select species are measured). Whilst it is not appropriate to discuss all the identified techniques in detail here, the main features of the most popular techniques will be highlighted.

Table 2.2 Summary of analysis techniques use in sample of 30 $deNO_x$ investigations.

Analytical Technique	Reported use (no. of references from sample)
Chemiluminescence NO_x analyser	14
MS	14
FTIR	12
GC	10
NDIR	5
IR	4
FID	3

Table 2.3 Details of specific analysis techniques used in sample of 30 $deNO_x$ investigations.

Reference	$DeNO_x$ Process*	$DeNO_x$ Reaction Analysis Equipment/Techniques
Macleod et al. (2002)	H_2 or CO–SCR	Chemiluminescence NO_x analyser, NDIR detectors, QMS
Marques et al. (2008)	H_2–SCR	Chemiluminescence NO_x analyser, IR analyser, FID detector
Itoh et al. (2010)	H_2–SCR	FTIR spectrometer,
Nanba *et al.* (2003)	H_2–SCR	GC, FTIR
Costa et al. (2001)	H_2–SCR	GC–MS, QMS
Chiarello et al. (2007a)	H_2–SCR	GC, QMS
Shibata et al. (2004)	H_2–SCR	GC, chemiluminescence NO_x analyser
Li *et al.* (2010)	H_2–SCR	GC, chemiluminescence NO_x analyser
Satokawa (2000)	H_2/HC–SCR	GC, chemiluminescence NO_x analyser
Burch et al. (2004)	H_2/HC–SCR	Chemiluminescence NO_x analyser, QMS
Richter et al. (2004)	H_2/NH_3–SCR	GC, NDIR
Breen et al. (2009)	H_2/HC–SCR	QMS
Lee et al. (2004)	H_2/CO–SCR	GC, chemiluminescence NO_x analyser
Dujardin et al. (2013)	H_2/CO–NSR	IR analyser, QMS, FTIR
Takahashi et al. (1996)	HC–NSR	Chemiluminescence NO_x analyser, QMS, FTIR
Fridell *et al.* (1999)	NSR	FID, IR, Chemiluminescence NO_x analyser
Abdulhamid *et al.* (2004)	NSR	Chemiluminescence NO_x analyser, IR, FTIR
Poulston *et al.* (2003)	H_2–NSR	QMS
Liu *et al.* (2004)	NSR	Chemiluminescence NO_x analyser, QMS
Cumaranatunge *et al.* (2007)	H_2–NSR	FTIR, QMS
Xu *et al.* (2012)	LNT/SCR	Chemical Ionization MS, FTIR, NDIR, Chemiluminescence NO_x analyser, Combined Flame Ionization/Magneto–pneumatic analyser
Wang *et al.* (2012)	LNT/SCR	Multi–gas analyser
Liu *et al.* (2012a)	H_2–LNT/SCR	FTIR, QMS
Castoldi *et al.* (2011)	H_2–LNT/SCR	QMS
Doronkin *et al.* (2012)	H_2/NH_3–SCR	FTIR
Lindholm *et al.* (2009)	H_2–NSR	Chemiluminescence NO_x analyser, NDIR, FTIR
Abu–Jrai *et al.* (2007)	HC–SCR	Chemiluminescence NO_x analyser, NDIR, FID, GC
Dhainaut *et al.* (2007)	H_2–SCR	MS, GC
Kim *et al.* (2013)	H_2/HC–SCR	FTIR
Kannisto *et al.* (2011)	HC–SCR	FTIR

*Note: where no reductant is specified in the $DeNO_x$ process description, several different reductants are investigated within that study.

2.5.1 Chemiluminescence NO_x Analysers

Atkins (2009) describes the process through which chemiluminescence NO_x analysers operate, from which the following key features are taken:

a) NO_x (chemiluminescence) analyzers measure NO by detecting the light emitted when NO is reacted with ozone (O_3).

b) The intensity of the light is proportional to the amount of NO in the sample gas and the intensity is measured and converted to an electrical signal

c) Other oxides of nitrogen are measured by passing them through a converter located before the reaction chamber. The converter changes any NO_2, NO_3, and so forth present in the sample gas into NO.

d) The converter can be bypassed so that either the total NO_x or NO alone can be measured.

The technique actually utilises the destructive chemistry of NO_x in the stratosphere, as already described in Section 2.2.2:

$$O_3 + NO \rightarrow NO_2 + O_2 \qquad (2.10)$$

Where the excited NO_2 which has formed through the reaction of NO and O_3 emits a photon (light), and the intensity is used to identify the quantities present.

Whilst this is an established and accurate technique, as the name suggests this equipment is only capable of measuring NO, NO_2 and overall NO_x levels and thus needs to be used in parallel with other techniques capable of measuring the other species of interest.

2.5.2 Mass Spectrometry

From the results of the sample of papers reviewed (see Tables 2.2 and 2.3) it can be seen that mass spectrometry is also a very common analysis technique and indeed it is utilised within this project for reaction analysis. Mass spectrometry separates chemical species through the differing mass–to–charge ratios (m/z) of ionized molecules. There are several different types of mass spectrometer, each utilising a different method of ionization to produce the ionized species. Each species has a distinct fragment pattern and thus this technique may be used to separate out mixtures of various chemicals. More detailed information on the theory and operation of mass spectrometry is provided in Appendix I.

It can be seen from Table 2.3 that mass spectrometry is not often used as an analysis technique in isolation; additional techniques are used in parallel. From this information it may be suggested that this technique is not suitable to measure all the species of interest. Closer inspection of the relevant references presented in Table 2.3 confirms this viewpoint and also raises questions about the use of MS in these studies; in the references discussed below there is no thorough explanation provided of how the MS was calibrated, and from personal experience this is a significant task (QMS calibration is discussed in Appendix I).

In addition, most references utilised an MS to follow the abundance of only a few (1 – 3) species or else do not discuss its use in detail. Only those which detail use of a QMS to separate a significant mixture of species will be discussed here.

Costa *et al.* (2001) described their use of a QMS to measure the abundance of six species:

> The gaseous responses obtained by mass spectrometry were calibrated against standard mixtures. The mass numbers (m/z) 15, 28, 30, 32, 44, and 46 were used for NH_3, N_2, NO, O_2, N_2O, and NO_2, respectively.

Although some level of calibration is undertaken, note that they are not measuring for H_2O (which is predominantly detected at m/z 18). In addition they are using m/z 15 to measure NH_3, presumably to avoid clashes with H_2O at m/z 17.

Chiarello *et al.* (2007a) monitored the abundance of nine species using a QMS for analysis and state that:

a) The m/z mass fragments 2, 12, 14, 18, 28, 30, 32, 44, and 46, corresponding to H_2, C, N, H_2O, N_2, NO, O_2, N_2O, and NO_2, were monitored.

b) In particular, N_2 and N_2O were distinguished from CO and CO_2 by the trend of m/z = 12. Indeed, the fact that the latter signal remained unperturbed during the experiment indicates that no C–containing species were formed or consumed.

Note whilst all the other species of interest were monitored here, there was no measure of NH_3 abundance.

Breen *et al.* (2007) provided a detailed description of the analysis used in Breen *et al.* (2009) as follows:

a) For most of the experiments, the following mass–to–charge (m/z) ratios were monitored as a function of time: 2 (H_2), 31 (^{15}NO), 30 ($^{15}N_2$), 46 ($^{15}N_2O$), 47 ($^{15}NO_2$), 57 (n–C_8H_{18}), and 82 (Kr).

b) For the experiments with ^{14}NO, a m/z ratio of 30 (^{14}NO) was monitored.

c) For both the ^{14}NO and ^{15}NO experiments, various other m/z ratios were also logged to pick up traces of some of the other gases, such as NH_3, CH_3CN, and HCN, that also can be formed under SCR conditions.

Although not all species of interest were considered here, it is interesting to note the use of isotopes, i.e. ^{15}NO gas, and their associated fragment patterns to separate gas mixtures.

Castoldi *et al.* (2004) provided a detailed description of the analysis used in Castoldi *et al.* (2011) as follows. It should be acknowledged that in this case some calibration was completed prior to analysis (although the NH_3 levels were not recorded):

a) The following mass–to–charge (m/z) ratios were used to monitor the concentration of products and reactants: 18 (H_2O), 28 (N_2 or CO), 30 (NO), 32 (O_2), 44 (N_2O or CO_2), and 46 (NO_2).

b) The mass spectrometer data were quantitatively analysed using the fragmentation patterns and the response factors determined experimentally from calibration gases.

2.5.3 FTIR

Infrared spectroscopy, like any optical spectroscopy, identifies a sample through its interaction with (infrared) light. Hof (2003) specifies the reasons for IR's popularity as an analysis technique, stating that:

a) The method is rapid, sensitive, easy to handle and provides many different sampling techniques for gases, liquids and solids.

b) Important aspects are the convenient qualitative and quantitative evaluation of the spectra.

FTIR is a type of mid–infrared technique, operating in the 2.5 – 25 μm (4000 to 400 cm^{-1}) range. Sablinskas (2003) describes the specific benefits of using an FTIR spectrometer, stating that:

a) The most significant advantage of FT spectrometers is that radiation from all wavelengths is measured simultaneously, whereas in dispersive spectrometers all wavelengths are measured consecutively.

b) Therefore, a FT spectrometer is much faster and more sensitive.

2.5.4 Gas Chromatography

As described by McNair *et al.* (1998), according to the International Union of Pure and Applied Chemistry (IUPAC), the definition of chromatography is such:

a) Chromatography is a physical method of separation in which the components to be separated are distributed between two phases, one of which is stationary (stationary phase) while the other (the mobile phase) moves in a definite direction.

b) Elution chromatography is a procedure in which the mobile phase is continuously passed through or along the chromatographic bed and the sample is fed into the system as a finite slug.

Thus in gas chromatography the mobile phase is a gas and as such it is a very common method for used for reaction gas analysis; through careful calibration and use of the correct column (stationary phase) it is possible to separate out complex gas mixtures.

However, the greatest drawback of a GC (which is not coupled to an MS) is that they are not connected 'on–line' and thus sampling of the reaction outlet and subsequent analysis is necessary. This creates a number of issues including reaction within the sample during the period from sampling to analysis, and poor understanding of the time frames/responses involved with the reaction of interest.

2.5.5 Other Techniques

As observed in Tables 2.2 and 2.3 there are additional techniques for measuring the presence of deNO_x species although they will not be discussed her. There are also some groups who utilise more specialised approaches for analysis; Steady–state Isotopic Transient Kinetic Analysis (SSITKA) involves replacing one of the reactants of a gas mixture with a stable isotope (in a similar manner to Breen *et al.* (2007) above) and recording the response. Savva *et al.* (2008) employed a SSITKA–DRIFTS approach whilst Chansai *et al.* (2011) further enhanced this method with their short time–on–stream (STOS) technique.

2.6 Conclusions Which Impact Upon the Work in this Thesis

Despite the vast quantities of literature information detailing various treatments of NO_x emissions with hydrogen, improvements in performance are required in order to make this a viable commercial process which competes with the current standard NH_3/urea practices.

With reference to what has been previously discussed in this chapter, the following conclusions can be drawn and their influence on this project highlighted:

2.6.1 Process

H_2–SCR and H_2–NSR have both been investigated with some success, although evidently the reported performances are not satisfactory enough to warrant commercialisation. Both processes are potentially applicable to the application of interest, and so both should be explored. In addition, the cyclic nature of NSR processes perhaps gives more scope for novel engineering solutions e.g. through dual stream exhausts.

It is recognised that the presence of catalyst poisons e.g. CO, H_2O or SO_2, and their impact on catalyst performance may have played a role in the scarce development of H_2 deNO_x catalysts. Thus catalyst poisoning is regarded as a very important topic. However, as will be described in later chapters; a 'clean' reaction gas mixture provided enough complications in terms of analysis and so whilst this issue is recognised as significant, it will not be addressed further in this thesis.

2.6.2 Catalysts

2.6.2.1 Materials

To summarise individually, the different materials reviewed for H_2–SCR:

- As a result of the conclusions previously obtained from the viability study, and that the application of interest involves significant amounts of O_2, Pd/Al_2O_3 was not considered to be explored further within the scope of this project.
- Pt/Al_2O_3 catalysts will be explored in this study as a material for confirming the experimental approach; by comparing obtained experimental results with those reported in the literature, the experimental set–up and conditions can be verified.
- Perovskites and Zeolites – as this study has a dual focus of investigation of both potential catalysts and processes, and is not solely concerned with intricate catalyst formation, these materials were deemed unsuitable for this particular project and thus have been discussed here only for completeness.

With respect to the reviewed literature and as a result of the conclusions above, it was decided that silver based catalysts would be explored for their $deNO_x$ activity in both SCR and NSR processes:

- Although they have demonstrated promising activity in H_2–assisted SCR and HC–SCR, their performance in direct H_2–SCR has not been reported.
- Silver catalysts have a long history of demonstrating both the reduction and oxidation chemistry deemed necessary for successful NSR reactions.
- Silver is abundant and cheaper than the metals used in current exhaust treatment applications.
- The proposed temperature window of operation for this application can be as high as ~450 ^oC (although it may be significantly lowered) and silver catalysts have demonstrated good activity at these temperatures for related processes.

Gamma alumina (γ–Al_2O_3) is a typical high surface area catalyst support material and is widely used in related applications (TWCs, DOCs etc). It has also been previously used within the research group. Due to its history and familiarity, it was chosen as the catalyst support material within this project.

In terms of storage components for the NSR catalysts; whilst other storage components have also been considered, Ba and K have demonstrated the best reported performance and will be explored with the combination of the active components discussed above.

2.6.2.2 Preparation Method

The preparation methods presented were generally similar; impregnation of metal oxides using a metallic solution. These are typically straightforward techniques and preparation conditions can be easily recreated. Other preparation techniques discussed such as solvothermal synthesis or flame–spray pyrolysis require additional, expensive apparatus and will not be pursued. Again, although it is recognised that the catalyst preparation method can have a significant impact on the catalyst performance, as this project involved both the process and the materials, significant emphasis was not placed on preparation techniques and the impact they may have.

2.6.2.3 Support

Although most of the reported literature work focusses on powder catalysts, this project will utilise catalysts supported on honeycomb monolith structures. These structures are typical of autocatalysts, and their advantages are well documented (Twigg *et al.* (2006)). Using monolithic structures also offers a more realistic indication of conditions and performance in the end application.

2.6.3 Analysis

A Quadrupole Mass Spectrometer (QMS) was utilised for reaction analysis within this project. The main advantage this provides is that of on–line, real time analysis as opposed to intermittent sampling and its associated issues. Although use of this instrumentation has been previously reported, it does not appear that a quantitative method for identifying *all* the potential reaction mixture species has been developed. The development of a suitable technique is described in Appendix I.

REFERENCES

Abdulhamid, H., Fridell, E., et al. (2004). Influence of the Type of Reducing Agent (H_2, CO, C_3H_6 and C_3H_8) on the Reduction of Stored NO_x in a $Pt/BaO/Al_2O_3$ Model Catalyst. Topics in Catalysis, Vol. 30–31, pp. 161–168.

Abu–Jrai, A. and Tsolakis, A. (2007). The Effect of H_2 and CO on the Selective Catalytic Reduction of NO_x Under Real Diesel Engine Exhaust Conditions Over Pt/Al_2O_3. International Journal of Hydrogen Energy, Vol. 32, No. 12, pp. 2073–2080.

Atkins, R. D. (2009). An Introduction to Engine Testing and Development. Society of Automotive Engineers, Inc. pp. 148–149.

Balcon, S., Potvin, C., et al. (1999). Influence of CO_2 on Storage and Release of NO_x on Barium–Containing Catalyst. Catalysis Letters, Vol. 60, No. 1–2, pp. 39–43.

Bartley, G. J. J. and Sharp, C. A. (2006). NO_x Reduction System for Diesel Engines, Using Hydrogen Selective Catalytic Reduction. US Patent, No. US 7135153 B2.

Breen, J. P., Burch, R., et al. (2007). A Fast Transient Kinetic Study of the Effect of H_2 on the Selective Catalytic Reduction of NO_x with Octane Using Isotopically Labelled ^{15}NO. Journal of Catalysis, Vol. 246, No. 1, pp. 1–9.

Breen, J. P., Burch, R., et al. (2009). NO_x Storage During H_2 Assisted Selective Catalytic Reduction of NO_x Reaction over a Ag/Al_2O_3 Catalyst. Catalysis Today, Vol. 145, No. 1–2, pp. 34–37.

Burch, R., Breen, J. P., et al. (2004). Exceptional Activity for NO_x Reduction at Low Temperatures Using Combinations of Hydrogen and Higher Hydrocarbons on Ag/Al_2O_3 Catalysts. Topics in Catalysis, Vol. 30/31, No. 1–4, pp. 19–25.

Can, F., Courtois, X., et al. (2012). An Overview of the Production and use of Ammonia in NSR plus SCR Coupled System for NO_x Reduction from Lean Exhaust Gas. Catalysis Today, Vol. 197, No. 1, pp. 144–154.

Castoldi, L., Bonzi, R., et al. (2011). Catalytic Behaviour of Hybrid LNT/SCR Systems: Reactivity and *In Situ* FTIR Study. Journal of Catalysis, Vol. 282, No. 1, pp. 128–144.

Castoldi, L., Nova, I., et al. (2004). Study of the effect of Ba loading for catalytic activity of Pt–Ba/Al_2O_3 model catalysts. Catalysis Today, Vol. 96, No. 1–2, pp. 43–52.

Chansai, S., Burch, R., et al. (2011). The use of Short Time–On–Stream *In Situ* Spectroscopic Transient Kinetic Isotope Techniques to Investigate the Mechanism of Hydrocarbon Selective Catalytic Reduction (HC–SCR) of NO_x at Low Temperatures. Journal of Catalysis, Vol. 281, No. 1, pp. 98–105.

Chiarello, G. L., Ferri, D., et al. (2007a). Flame–synthesized $LaCoO_3$–supported Pd: 2. Catalytic Behavior in the Reduction of NO by H_2 Under Lean Conditions. Journal of Catalysis, Vol. 252, No. 2, pp. 137–147.

Chiarello, G. L., Grunwaldt, J. –D., et al. (2007b). Flame–synthesized $LaCoO_3$–supported Pd: 1. Structure, Thermal Stability and Reducibility. Journal of Catalysis, Vol. 252, No. 2, pp. 127–136.

Costa, C. N., Stathopoulos, V. N., et al. (2001). An Investigation of the NO/H_2/O_2 (Lean–deNO_x) Reaction on a Highly Active and Selective Pt/$La_{0.5}Ce_{0.5}MnO_3$ Catalyst. Journal of Catalysis, Vol. 197, No. 2, pp. 350–364.

Cumaranatunge, L., Mulla, S. S., et al. (2007). Ammonia is a Hydrogen Carrier in the Regeneration of Pt/BaO/Al_2O_3 NO_x Traps with H_2. Journal of Catalysis, Vol. 246, No. 1, pp. 29–34.

Dhainaut, F., Pietrzyk, S., et al. (2007). NO + H_2 Reaction on Pd/Al_2O_3; Under Lean Conditions: Kinetic Study. Topics in Catalysis, Vol. 42–43, No. 1, pp. 135–141.

DieselNet (2012). European Union – Cars and Light Trucks. Emission Standards. Available from: http://www.dieselnet.com/standards/eu/ld.php [Accessed 19th May 2013].

Directive 2010/75/EU of the European Parliament and of the Council of 24 November 2010 on Industrial Emissions (Integrated Pollution Prevention and Control), Official Journal of the European Union.

Doronkin, D. E., Fogel, S., et al. (2012). Study of the "Fast SCR" – like Mechanism of H_2–assisted SCR of NO_x with Ammonia over Ag/Al_2O_3. Applied Catalysis B: Environmental, Vol. 113–114, No. 0, pp. 228–236.

Dujardin, C., Kouakou, A., et al. (2013). Advantages of Syngas for the Regeneration of NO_x Trap System Investigated with Operando IR Measurements. Catalysis Today, Vol. 205, pp. 10–15.

Epling, W. S., Campbell, L. E., et al. (2004). Overview of the Fundamental Reactions and Degradation Mechanisms of NO_x Storage/Reduction Catalysts. Catalysis reviews. Science and engineering, Vol. 46, No. 2, pp. 163–245.

Fahey, D. W. and Hegglin, M. I. (2011). Twenty Questions and Answers About the Ozone Layer: 2010 Update. Scientific Assessment of Ozone Depletion: 2010. Geneva, Switzerland, World Meteorological Organization. pp. 72. Available from: http://www.esrl.noaa.gov/csd/assessments/ozone/2010/ [Accessed 7th May 2013].

Framework Type MFI (2007). Database of Zeolite Structures. Structure Commission of the International Zeolite Association. Available from: http://izasc.ethz.ch/fmi/xsl/IZA-SC/ftc_fw.xsl?-db=Atlas_main&-lay=fw&-max=25&STC=MFI&-find [Accessed 6th June 2013].

Fridell, E., Skoglundh, M., et al. (1999). NO_x Storage in Barium–Containing Catalysts. Journal of Catalysis, Vol. 183, No. 2, pp. 196–209.

Fu, D. and Itoh, M. (2011). Ferroelectricity in Silver Perovskite Oxides. In Ferroelectrics – Material Aspects. M. Lallart, Ed., InTech, p. 2.

Harrison, R. M. (2001). Pollution: Causes, Effects and Control. 4th Edition. pp. 179–181.

Higman, C. (2008). Gasification. In Combustion Engineering Issues for Solid Fuel Systems. B. G. Miller and D. A. Tillman, Eds., Elsevier, p. 465.

Higman, C. and Van Der Burgt, M. (2008). Gasification. 2nd Edition, Elsevier. pp. 234–235.

Hobbs, P. V. (2000). Introduction to Atmospheric Chemistry. Cambridge University Press. pp. 158–160.

Hof, M. (2003). Basics of Optical Spectroscopy. In Handbook of Spectroscopy. G. Gauglitz and T. Vo–Dinh, Eds., Vol. 1, Wiley–VCH, pp. 39–47.

Itoh, M., Iwamoto, J., et al. (2010). $DeNO_x$ Catalytic Activity over Pt/Al_2O_3 Prepared by Solvothermal Method. Materials Chemistry and Physics, Vol. 124, No. 1, pp. 587–591.

Iwamoto, M., Yahiro, H., et al. (1991). Removal of Nitrogen Monoxide Through a Novel Catalytic Process. 1. Decomposition on Excessively Copper–Ion–Exchanged ZSM–5 Zeolites. The Journal of Physical Chemistry, Vol. 95, No. 9, pp. 3727–3730.

Kannisto, H., Karatzas, X., et al. (2011). Efficient Low Temperature Lean NO_x Reduction Over Ag/Al_2O_3–A System Approach. Applied Catalysis B: Environmental, Vol. 104, No. 1–2, pp. 74–83.

Kim, P. S., Kim, M. K., et al. (2013). Effect of H_2 on $DeNO_x$ Performance of HC–SCR over Ag/Al_2O_3: Morphological, Chemical, and Kinetic Changes. Journal of Catalysis, Vol. 301, No. 0, pp. 65–76.

Kolodziej, A. and Lojewska, J. (2009). Mass Transfer for Woven and Knitted Wire Gauze Substrates: Experiments and Modelling. Catalysis Today, Vol. 147, pp. S120–S124.

Lee, Y. –W. and Gulari, E. (2004). Improved Performance of NO_x Reduction by H_2 and CO over a Pd/Al_2O_3 Catalyst at Low Temperatures Under Lean–burn Conditions. Catalysis Communications, Vol. 5, No. 9, pp. 499–503.

Li, L., Wu, P., et al. (2010). Low Temperature H_2–SCR Over Platinum Catalysts Supported on Ti–containing MCM–41. Applied Catalysis B: Environmental, Vol. 94, No. 3–4, pp. 254–262.

Lietti, L., Forzatti, P., et al. (2001). NO_x Storage Reduction over Pt–Ba/γ–Al_2O_3 Catalyst. Journal of Catalysis, Vol. 204, No. 1, pp. 175–191.

Lindholm, A., Currier, N. W., et al. (2009). The Influence of the Preparation Procedure on the Storage and Regeneration Behavior of Pt and Ba Based NO_x Storage and Reduction Catalysts. Applied Catalysis B: Environmental, Vol. 88, No. 1–2, pp. 240–248.

Liu, Y., Harold, M. P., et al. (2012a). Coupled NO_x Storage and Reduction and Selective Catalytic Reduction Using Dual–layer Monolithic Catalysts. Applied Catalysis B–Environmental, Vol. 121, pp. 239–251.

Liu, Z. and Anderson, J. A. (2004). Influence of Reductant on the Thermal Stability of Stored NO_x in Pt/Ba/Al_2O_3 NO_x Storage and Reduction Traps. Journal of Catalysis, Vol. 224, No. 1, pp. 18–27.

Liu, Z., Li, J., et al. (2012b). Recent Advances in the Selective Catalytic Reduction of NO_x by Hydrogen in the Presence of Oxygen. Energy & Environmental Science, Vol. 5, No. 10, pp. 8799–8814.

Macleod, N. and Lambert, R. M. (2002). Lean NO_x Reduction with CO + H_2 Mixtures over Pt/Al_2O_3 and Pd/Al_2O_3 Catalysts. Applied Catalysis B: Environmental, Vol. 35, No. 4, pp. 269–279.

Maesen, T. and Marcus, B. (2001). Chapter 1 The Zeolite Scene – An Overview. In Studies in Surface Science and Catalysis. H. van Bekkum, E. M. Flanigen, P. A. Jacobs and J. C. Jansen, Eds., Vol. Volume 137, Elsevier, pp. 1–9.

Manahan, S. E. (2009). Environmental Chemistry. 9th Edition, CRC Press. pp. 293–297.

Marques, R., Mazri, L., et al. (2008). Selective Reduction of NO_x by Hydrogen and Methane in Natural Gas Stationary Sources over Alumina–Supported Pd, Co and Co/Pd catalysts: Part A. On the Effect of Palladium Precursors and Catalyst Pre–Treatment. Catalysis Today, Vol. 137, No. 2–4, pp. 179–184.

McClymont, D., Centre for Sustainable Chemical Technologies, Catalyst System Design for the Control of NO_x Using Hydrogen. MRes Project, Report (2010).

McNair, H. M. and Miller, J. M. (1998). Basic Gas Chromatography. Wiley.

Miller, B. G. and Miller, S. F. (2008). Fluidized–Bed Firing Systems. In Combustion Engineering Issues for Solid Fuel Systems. B. G. Miller and D. A. Tillman, Eds., Elsevier, pp. 295–297.

Nanba, T., Kohno, C., et al. (2003). Improvements in the N_2 Selectivity of Pt Catalysts in the NO–H_2–O_2 Reaction at Low Temperatures. Applied Catalysis B: Environmental, Vol. 46, No. 2, pp. 353–364.

Nova, I., Beretta, A., et al. (2006). Monolithic Catalysts for NO_x Removal from Stationary Sources. In Structured Catalysts and Reactors. A. Cybulski and J. A. Moulijn, Eds., 2nd Edition, CRC Press, p. 175.

Ochońska, J., McClymont, D., et al. (2012). Copper Exchanged Ultrastable Zeolite Y – A catalyst for NH_3–SCR of NO_x from Stationary Biogas Engines. Catalysis Today, Vol. 191, No. 1, pp. 6–11.

Poulston, S. and Rajaram, R. R. (2003). Regeneration of NO_x Trap Catalysts. Catalysis Today, Vol. 81, No. 4, pp. 603–610.

Regulation (EC) No 715/2007 of The European Parliament and of the Council of 20 June 2007 on Type Approval of Motor Vehicles with Respect to Emissions from Light Passenger and Commercial Vehicles (Euro 5 and Euro 6) and on Access to Vehicle Repair and Maintenance Information., Official Journal of the European Union.

Richter, M., Fricke, R., et al. (2004). Unusual Activity Enhancement of NO Conversion over Ag/Al_2O_3 by Using a Mixed NH_3/H_2 Reductant Under Lean Conditions. Catalysis Letters, Vol. 94, No. 1/2, pp. 115–118.

Sablinskas, V. (2003). Instrumentation. In Handbook of Spectroscopy. G. Gauglitz and T. Vo–Dinh, Eds., Vol. 1, Wiley–VCH, pp. 48–69.

Sato, S., Yu–u, Y., et al. (1991). Cu–ZSM–5 Zeolite as Highly Active Catalyst for Removal of Nitrogen Monoxide from Emission of Diesel Engines. Applied Catalysis, Vol. 70, No. 1, pp. L1–L5.

Satokawa, S. (2000). Enhancing the $NO/C_3H_8/O_2$ Reaction by Using H_2 over Ag/Al_2O_3 Catalysts Under Lean–exhaust Conditions. Chemistry Letters, No. 3, pp. 294–295.

Savva, P. G. and Efstathiou, A. M. (2008). The Influence of Reaction Temperature on the Chemical Structure and Surface Concentration of Active NO_x in H_2–SCR over $Pt/MgOCeO_2$: SSITKA–DRIFTS and Transient Mass Spectrometry Studies. Journal of Catalysis, Vol. 257, No. 2, pp. 324–333.

Schwartz, M. (2002). Encyclopedia of Smart Materials, Volumes 1–2. John Wiley & Sons. p. 992.

Shibata, J., Hashimoto, M., et al. (2004). Factors Controlling Activity and Selectivity for SCR of NO by Hydrogen over Supported Platinum Catalysts. The Journal of Physical Chemistry B, Vol. 108, No. 47, pp. 18327–18335.

Spencer, M. S. (1989). Fundamental principles. In Catalyst Handbook. M. V. Twigg, Ed., 2nd Edition, Wolfe, p. 37.

Takahashi, N., Shinjoh, H., et al. (1996). The New Concept 3–Way Catalyst for Automotive Lean–Burn Engine: NO_x Storage and Reduction Catalyst. Catalysis Today, Vol. 27, No. 1–2, pp. 63–69.

Torres, W., Pansare, S. S., et al. (2007). Hot Gas Removal of Tars, Ammonia, and Hydrogen Sulfide from Biomass Gasification Gas. Catalysis Reviews–Science and Engineering, Vol. 49, No. 4, pp. 407–456.

Twigg, M. V. and Wilkins, A. J. J. (2006). Autocatalysts: Past, Present, and Future. In Structured Catalysts and Reactors. A. Cybulski and J. A. Moulijn, Eds., 2nd Edition, CRC Press, p. 120.

Wang, J. and Crocker, M. (2012). N_2O Mitigation in a Coupled LNT–SCR System. Catalysis Letters, Vol. 142, No. 10, pp. 1167–1174.

Xu, L. and McCabe, R. W. (2012). LNT Plus *In Situ* SCR Catalyst System for Diesel Emissions Control. Catalysis Today, Vol. 184, No. 1, pp. 83–94.

CHAPTER 3

Experimental – Investigation of Reaction Mechanisms and Transient Behaviour of H_2–SCR Catalysts in a Continuous Flow Fixed Bed Reactor

The processes through which active materials for the H_2–SCR investigation were prepared and characterized will be discussed. The experimental set–up and procedures to be followed when investigating the activity of catalysts in treating NO_x emissions with hydrogen will also be explained. Finally, preliminary experimental results, obtained through commissioning of the experimental set–up and analysis technique, along with 'final' results of the chosen materials performance will be presented and discussed.

3.1 Catalyst Preparation

3.1.1 Summary

A summary flow diagram of the catalysts prepared in this project, and their associated $deNO_x$ process, is presented in Figure 3.1. Note that only the SCR catalysts (their makeup indicated with a *dotted* black line) are considered within this chapter. All of the catalysts consist of a cordierite substrate and an intermediate γ–Al_2O_3 layer and were prepared from samples supplied by a major catalyst manufacturer. The make–up of the catalysts then differs in the loading of additional components upon the γ–Al_2O_3 support, which determines which process the catalyst material is applicable to.

It should be noted that catalyst preparation does not form a major interest in this particular research project, and indeed catalysts were prepared in order to confirm the $deNO_x$ approach and not to investigate the impact of slight variations in preparation method, e.g. catalyst loading, calcination temperature etc. As such, preparation procedures for the catalysts prepared above were influenced by and adjusted from several literature sources (Table 3.1).

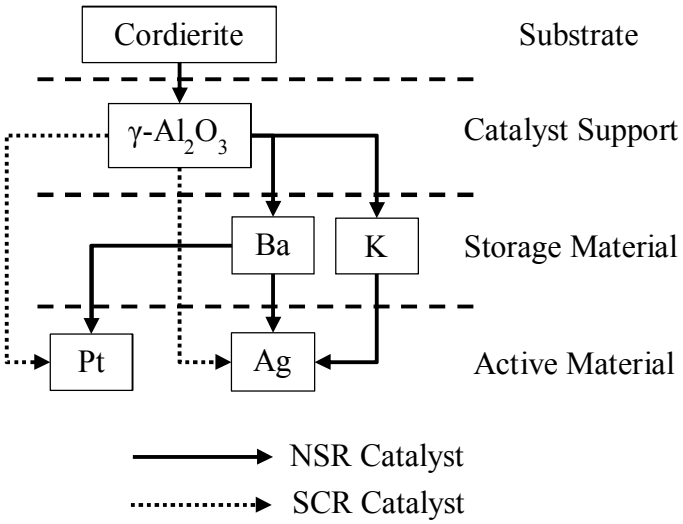

Figure 3.1 Schematic describing the make–up of catalyst materials prepared for investigation.

Table 3.1 Summary of selected references consulted during development of SCR catalyst preparation methods.

Catalyst	Reference
Pt	Klinghoffer *et al.* (1998)
Ag	Doronkin *et al.* (2012)

Although brief descriptions of the catalyst preparation methods are disclosed within this chapter, examples of detailed synthesis procedures can be found in Appendix II, where some indication of slight variations in the different batches of catalysts made can be gleaned. However, a typical catalyst preparation procedure involved:

- Preparation of a solution containing the desired metal species;
- Submersion of the sample(s) in the solution for a determined time period;
- Removal of excess solvent in the sample channels through a particular drying procedure;
- Removal of residual solvent and formation of desired active species through calcination at a particular temperature.

Figure 3.2 gives an indication of how the catalyst support structures are first prepared from the supplied monoliths and then how the washcoat and any active components are dispersed throughout the monoliths.

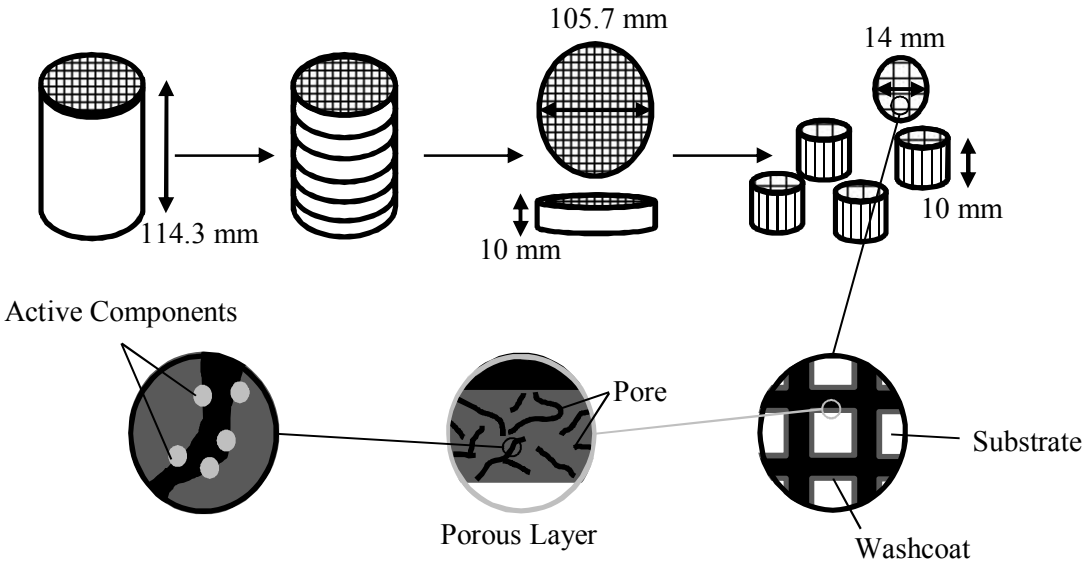

Figure 3.2 Overview of catalyst preparation method and dispersion of components in the prepared monoliths.

3.1.2 Catalyst Support Structure

Catalysts may be supported on a number of different materials and in different structures, dependent on their application. Common support structures include honeycomb monoliths and pellets and each have a number of different advantages. The catalysts prepared for this study will be supported on honeycomb monolithic structures; these are cylindrical in shape and consist of many parallel channels where the catalyst will have been deposited and through which the gas will flow. The channels may be circular or triangular, but are most often square in shape, and the structures typically exhibit a high cell density e.g. 400 CSI (cells per square inch).

The benefits of such a support, as discussed in Hayes *et al.* (1997) are:

a) The monolith configuration combines a high surface–to–volume ratio with low pressure drop.

b) The uniformity of the honeycomb matrix helps to ensure an even flow distribution across the bed with minimal 'channelling'.

c) If particulates are present in the gaseous stream these can pass easily through the reactor provided that the diameter of the channel is greater than that of the particles.

Monolithic structures are therefore of interest in this project, due to the advantages highlighted above. They can also be used in a modular system (Figure 3.3), which yields further advantages including ease of replacement should a unit fail.

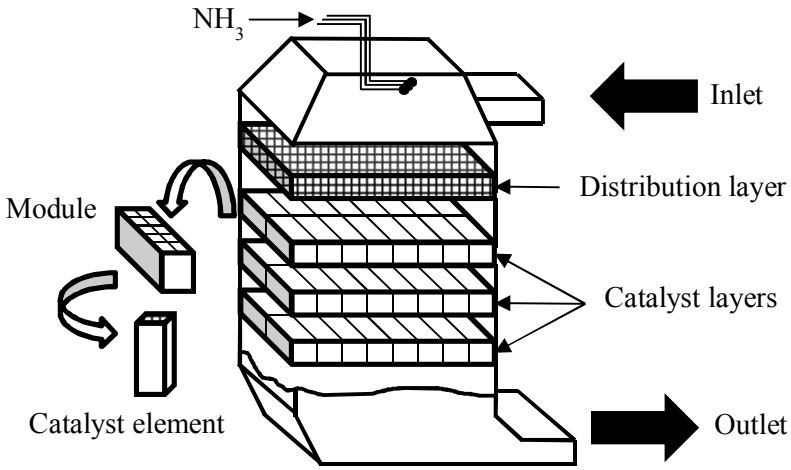

Figure 3.3 Example of monoliths used in a modular NH_3–SCR application, recreated from Forzatti (2001).

Monolith support structures with a cell density of 400 CSI for use in this project, were supplied by a major catalyst manufacturer. Initially supplied with an axial length of 114.3 mm and outer diameter of 105.7 mm (Figure 3.4), cross–sectional 'slices' of 10 mm height (e.g. Figure 3.6) were prepared using a band saw. Monolith 'samples' could then be obtained using a punch set with the desired diameter, to remove sections from the slices.

The particular monolith samples in use for catalytic investigations had an outer diameter of 14 mm and an axial length of 10 mm (e.g. Figure 3.5), with a volume of 0.00154 L. They contained approximately 80 channels, each with dimensions of 1 x 1 mm. Both uncoated and γ–Al_2O_3 coated cordierite substrates were supplied for use in this project.

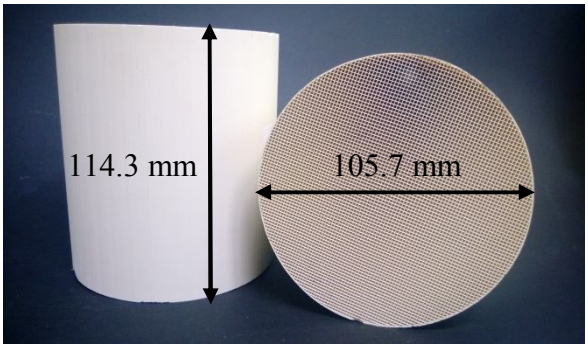

Figure 3.4 Photograph of unsliced monoliths, supplied by a major catalyst manufacturer.

3.1.3 Catalyst Support Materials

3.1.3.1 Cordierite Substrate

The substrate forms the core part of any monolithic catalyst as it produces the channel structure and surface upon which the active components are supported. Ceramic materials are generally preferred as substrates due to their relatively low manufacturing cost. Cordierite is a ceramic material typically consisting of $2MgO.2A1_2O_3.5SiO_2$ (Buschow *et al.* (2001)), which amounts to a weight percentage breakdown of: 13.78 % magnesia (MgO), 34.86 % alumina (Al_2O_3) and 51.36 % silica (SiO_2). It has a beige appearance (Figure 3.5). Cordierite is widely used in automotive catalytic converter technology, which of course is akin to the application of interest in this project. Cordierite offers a number of benefits to automotive applications, which are described by Lachman *et al.* (1992):

a) Their thermal shock resistance is low, due to a low thermal expansion coefficient.

b) Their porosity and pore size distribution is suitable for ease of washcoat application and good washcoat adherence.

c) There is sufficient refractoriness, because the melting point exceeds 1450 ^{o}C.

d) They have sufficient strength to survive in an exhaust environment.

e) They exhibit compatibility with washcoats and catalysts.

Therefore, cordierite could be equally applicable to the after treatment of biogas engines.

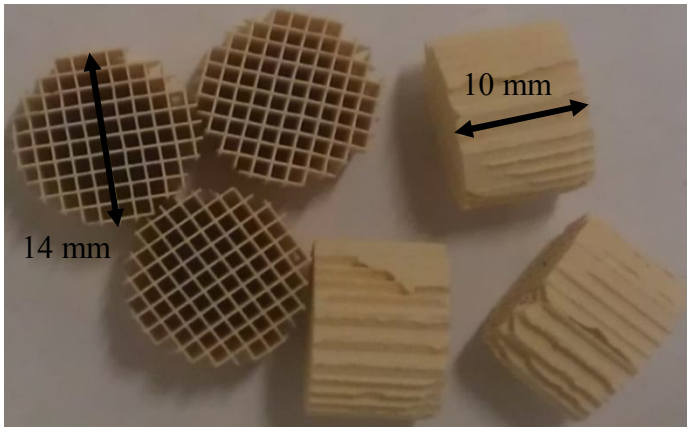

Figure 3.5 Photograph of bare cordierite monolith samples.

3.1.3.2 Alumina Washcoat

Although cordierite is the preferred choice of substrate, it has a relatively low surface area which in isolation renders it unsuitable as a catalyst support in the applications of interest. This issue is resolved by coating the cordierite with a porous material, known as a washcoat, which acts as an intermediate layer and provides the high surface area (100 – 200 $m^2\ g^{-1}$) required for the catalyst. In some cases, the washcoat can also play a role in the reaction of interest, although this is dependent on the nature of the coating and the reaction under investigation.

In this project, gamma alumina (γ–Al_2O_3) coated monoliths supplied by a major catalyst manufacturer are used as catalyst supports. As previously mentioned the investigation of catalyst preparation, and by extension washcoat adherence to the substrate, is not of specific interest in this project. Thus by utilising provided materials, difficulties that may be experienced in catalyst preparation such as washcoat integrity and inconsistencies in different batches, can hopefully be avoided.

That being said, variations in the thickness of γ–Al_2O_3 washcoating on the supplied monoliths has previously been identified by Kolaczkowski *et al.* (2012) (Figure 3.6), building upon similar work by Plummer *et al.* (1999). To combat this, γ–Al_2O_3 monolith samples (Figure 3.8) were only prepared from areas of cross–sectional slices which appeared to have a consistent coating thickness. This was determined by visual inspection only.

A further drawback to using provided γ–Al_2O_3 coated monoliths, is that the wt% loading of the γ–Al_2O_3 on the cordierite substrate cannot be definitely determined. However, by comparing the weight of both coated and uncoated samples, provided from the same supplier, the washcoat loading may be estimated (Table 3.2). The obtained value of 29.6 wt% Al_2O_3 compares favourably with that reported by Yap (2010) of 30.65 wt%, who studied these samples in great detail.

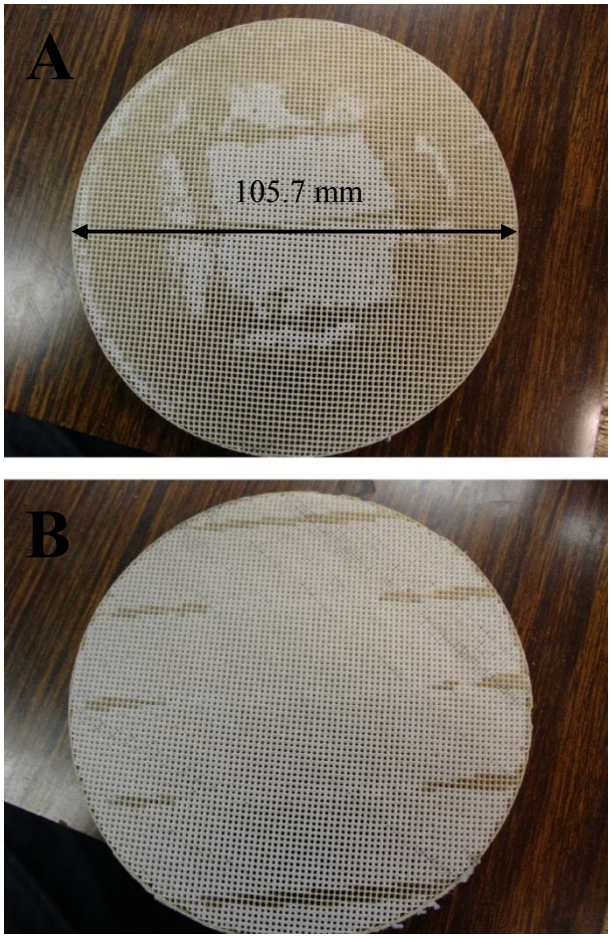

Figure 3.6 Examples of the inconsistencies in washcoat distribution (A and B) in two cross–sectional slices of a supplied γ–Al_2O_3 monolith, reported with permission from Kolaczkowski *et al.* (2012).

Table 3.2 Percentage weight of cordierite and γ–Al_2O_3 washcoat in γ–Al_2O_3 coated monolith samples.

Average Values*				
Weight of Cordierite Sample (g)	Weight of γ–Al_2O_3 Coated Sample (g)	Weight of γ–Al_2O_3 Coating (g)	Cordierite Loading (%)	γ–Al_2O_3 Washcoat Loading (%)
0.5775 ± 0.0216	0.8205 ± 0.0432	0.2430	70.4	29.6

*Cordierite samples measured = 96. γ–Al_2O_3 samples measured = 96.

It should be noted that it is possible to form several different phases of alumina depending on the preparation procedure, and in particular the heat treatment it is subject to (Figure 3.7). This is described by Brinker *et al.* (1990) who detail the temperatures necessary to achieve phase transformation of a boehmite (γ–AlO(OH)) xerogel:

$$\mathrm{AlOOH} \xrightarrow{300\ ^\circ\mathrm{C}} \gamma - \mathrm{Al_2O_3} \xrightarrow{850\ ^\circ\mathrm{C}} \delta - \mathrm{Al_2O_3} \xrightarrow{1100\ ^\circ\mathrm{C}} \theta - \mathrm{Al_2O_3} \xrightarrow{\geq 1200\ ^\circ\mathrm{C}} \alpha - \mathrm{Al_2O_3}$$

Figure 3.7 Phase transformations of Al_2O_3 and the associated temperatures.

The supplied samples had been calcined at 650 °C for 5 hours in order to produce the desired γ–Al_2O_3 phase.

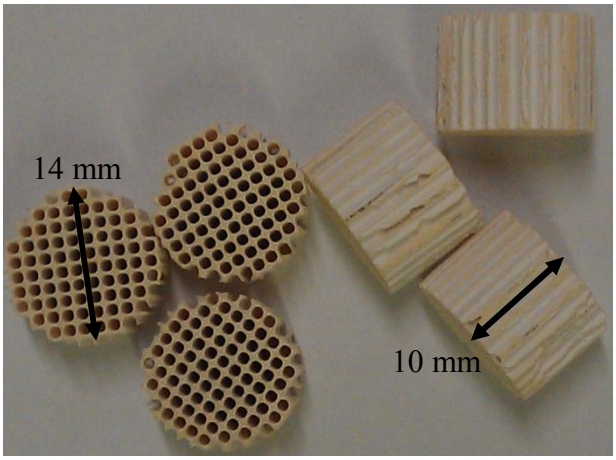

Figure 3.8 Photograph of γ–Al_2O_3 coated monolith samples.

3.1.4 Active Components

Having previously been explored for both SCR and NSR processes, the preparation of platinum catalysts in this study was with a view to comparing results to the literature and validating the experimental procedures. Silver catalysts, although they have been explored for related deNO_x processes e.g. H_2–assisted HC–SCR, have not been investigated in direct H_2–SCR.

3.1.4.1 Pt/Al_2O_3

With reference to the procedure described in Klinghoffer *et al.* (1998), a 1 wt% aqueous platinum solution was prepared using hexachloroplatinic acid. The monoliths were submerged in the solution for a total of 10 min, during which they were turned over once. Once removed from the solution the monoliths were placed in a ceramic dish and dried for 2 h at 120 ^oC before they were calcined at 500 ^oC in static air overnight (15 h). As can be seen from Figure 3.9, the monolith samples were now a deep black in colour. Specific details of an example platinum coating procedure is provided in Appendix II–A.

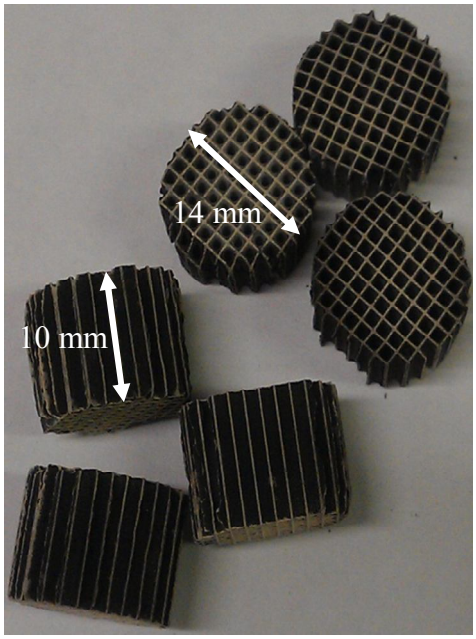

Figure 3.9 Photograph of 0.8 wt% Pt/Al_2O_3 coated monolith samples.

3.1.4.2 Ag/Al_2O_3

Silver was chosen as the active component due to its performance in related $deNO_x$ processes (e.g. H_2–assisted HC–SCR), and its history of redox chemistry, i.e. it is capable of facilitating both the reducing and oxidising reactions necessary in the NSR processes (Chapter 4).

With consultation of Doronkin *et al.* (2012), silver nitrate was dissolved in water in order to produce a solution of ~2 wt% silver. The monoliths were submerged in the solution for 2 h. Once removed from the solution the monoliths were placed in a ceramic dish and dried overnight (19 h) at room temperature before they were calcined at 550 °C for 4 h in static air. The monoliths were a grey colour. Specific details of an example silver coating procedure is provided in Appendix II–B.

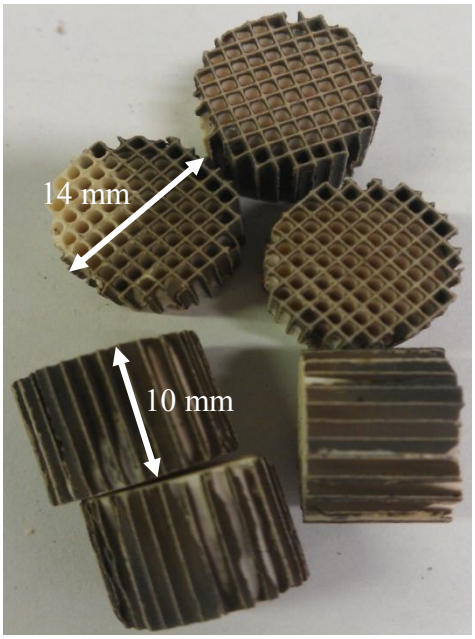

Figure 3.10 Photograph of 2.3 wt% Ag/Al_2O_3 coated monolith samples.

3.2 Catalyst Characterisation

The catalysts in this study were characterised through a variety of different methods:

a) Visual observations to identify coating uniformity.
b) Weight measurements to obtain information on washcoat and active component loading.
c) N_2 adsorption analysis to obtain catalyst surface area and porosity information.

3.2.1 Visual Observation

As may be observed from some of the photographs in Section 3.1, the catalyst preparation procedures, although conducted with the intention of producing consistent samples, sometimes resulted in non–uniform coatings. As a result, the prepared samples subsequently selected for experimental investigations were chosen by the apparent consistent coverage of the necessary components. Note that observations were made with the naked eye and there was no microscope use.

3.2.2 Weight Measurements

Washcoat loading, as described in Section 3.1.3.2, was determined through weighing samples of uncoated and γ–Al_2O_3 coated ceramic substrate. Active component loading was then determined by weighing the γ–Al_2O_3 coated monolith samples prior to deposition, followed by weighing after deposition and calcination. Although his technique results in an accurate measure of the average amount of active component present on the monolith samples, it fails to address issues such as the aforementioned uniformity of the coating.

It was assumed, for the purposes of this project, that the measured weight difference represented the amount of each metal loaded upon the monolith samples. However, it should be noted that due to the preparation procedures described in Section 3.1.4, realistically the specified loadings represent an active component species and not the pure metal i.e. it is known that PtO is formed through the procedure described in Section 3.1.4.1 above, and it is responsible for producing the black colour of the monolith samples.

Finally the specified loadings (Table 3.3) are reported with respect to the entirety of the catalyst makeup i.e. the combined weight of the substrate, washcoat and any active components present.

Table 3.3 Details of prepared H_2–SCR catalyst loadings.

Catalyst	Average Values	
	Washcoat Loading (%)	Metal Loading (%)
γ–Al_2O_3	29.6	–
Pt/Al_2O_3	29.4	0.8
Ag/Al_2O_3	28.9	2.3

3.2.3 Nitrogen Adsorption

Nitrogen adsorption measurements are a typical characterisation technique used to determine the surface area and pore size of porous materials. Adsorption can be described as the enrichment of one or more of the components in the region between two bulk phases, the interfacial layer, with one phase a solid and the other a fluid. Alternatively it can be described as the accumulation or adhesion of a chemical species onto the surface of a particle. It is not to be confused with absorption, which describes the penetration of a fluid into the solid phase. Adsorption occurs as a result of the interaction between the solid surface and the molecules in the fluid phase. There are two types of adsorption:

- Physisorption is adsorption without chemical bonding, van der Waals interactions are responsible.
- Chemisorption is adsorption that involves a chemical bond, a chemisorbed molecule undergoes a reaction or dissociation and cannot normally be recovered.

A schematic representation of physisorption is presented in Figure 3.11. The adsorptive is the species in the gas state. The build–up of this species on the adsorbent surface is known as the adsorbate.

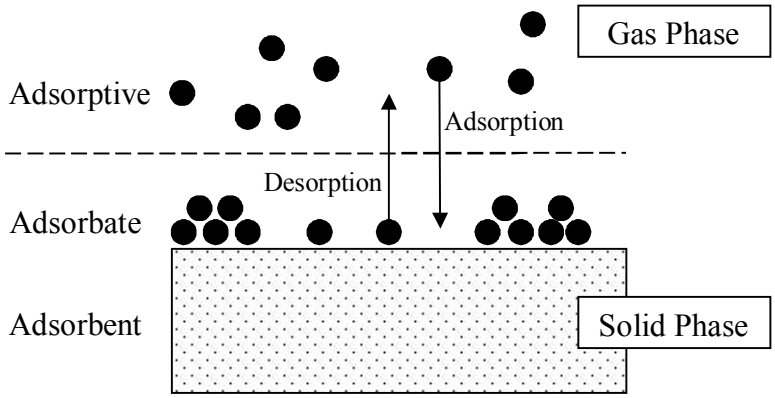

Figure 3.11 Schematic representation of the process of adsorption.

Nitrogen adsorption studies were conducted on a Quantachrome Instruments NOVA 2200e Surface Area and Pore Size Analyzer using a volumetric gas adsorption method (as opposed to a gravimetric method). Samples were degassed under vacuum at 200 ^{o}C for 1 h to remove all physisorbed species. Measurements were conducted on all samples discussed in Section 3.1, with the exception of the cordierite substrate which has been explored in previous studies and is known to demonstrate a very low surface area (<5 m^2 g^{-1}). Due to the resolution of the instrument it was necessary to ensure there was at least 10 m^2 of sample present to obtain an accurate measurement, and thus the samples were of sufficient abundance to reflect this.

Figure 3.12 Photograph of Quantachrome Instruments NOVA 2200e utilised within this project.

3.2.3.1 Adsorption–desorption Isotherm

This type of plot depicts the amount of adsorbate on the adsorbent as a function of pressure at constant temperature (in this case the temperature is 77.3 K). The isotherm is constructed point–by–point as a known amount of gas is admitted to a vessel of known volume and containing the adsorbent. The amount of gas adsorbed by the sample is calculated from the change in pressure. There are a number of different typical shapes of adsorption plots, Figure 3.13, depending on the nature of the material under investigation.

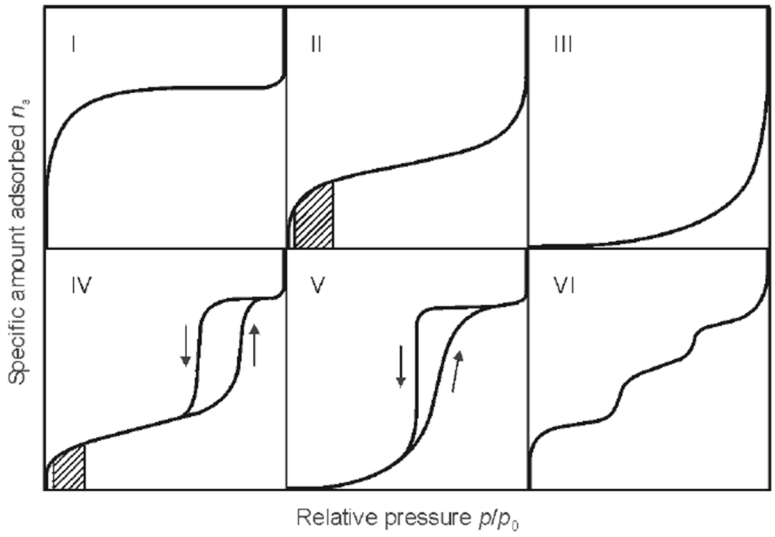

Figure 3.13 IUPAC classification of adsorption isotherms, type I–VI as specified by International Organization for Standardization (2008).

A typical nitrogen adsorption–desorption isotherm obtained for a γ–Al_2O_3 catalyst sample explored in this project, is displayed in Figure 3.14. The shape of the isotherm displayed in Figure 3.14 is typical of all the materials explored within this project, and with relation to the isotherm shapes presented in Figure 3.13 is a type IV isotherm (mesoporous solid) in accordance with IUPAC convention.

Hysteresis is a phenomenon which occurs when the rate of desorption differs from the rate of adsorption. Hysteresis occurred during the nitrogen adsorption–desorption measurement of all the samples investigated in this project and can be clearly seen in Figure 3.14. It may be explained by evaporation mechanisms or the pore structure of the material under investigation. The different shapes of hysteresis loops have also been classified and are presented in Figure 3.15.

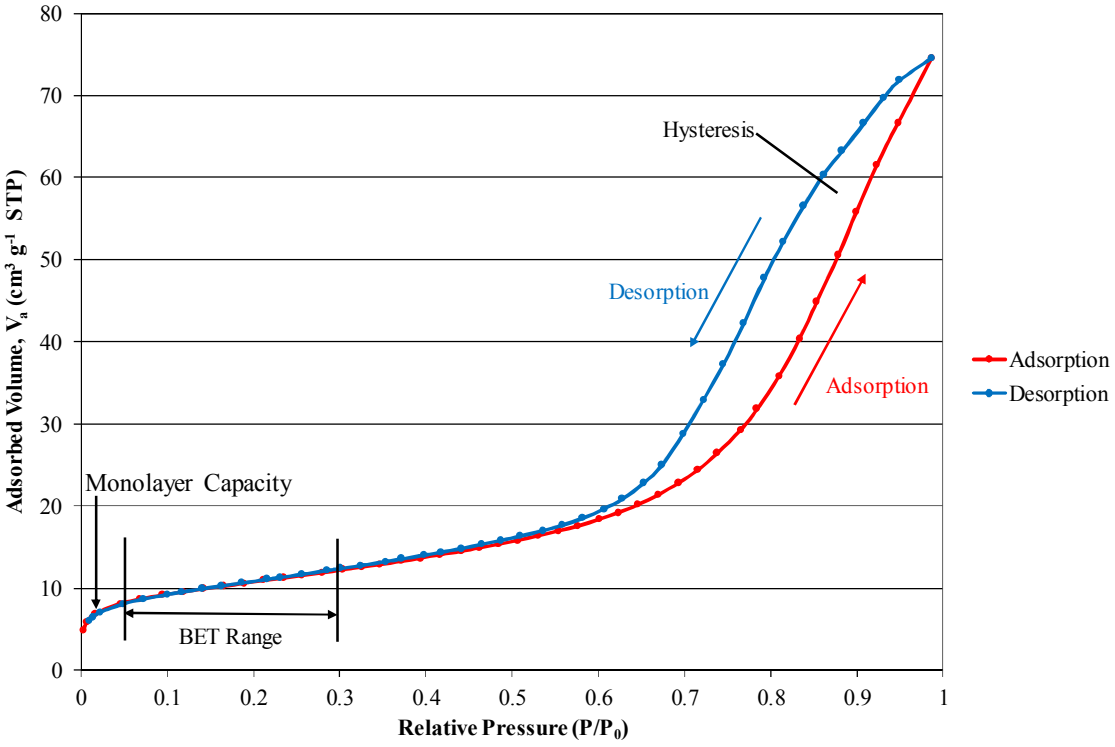

Figure 3.14 Nitrogen adsorption–desorption isotherm for γ–Al_2O_3 catalyst.

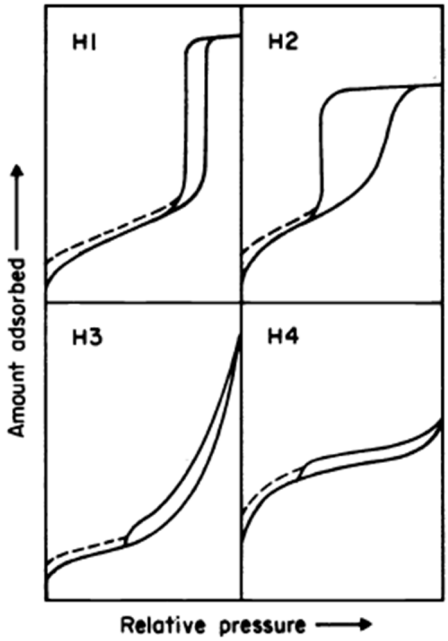

Figure 3.15 Types of hysteresis loop as specified by Sing *et al.* (1985).

3.2.3.2 Brunauer–Emmett–Teller (BET) Surface Area

Brunauer *et al.* (1938) reported a method for calculating the specific surface area of a porous solid by measuring the amount of physically adsorbed gas. Now known as the BET method, this approach has been widely adopted as a standard approach (International Organization for Standardization (2008)), and facilitates the direct comparison of porous materials, although is only applicable to those materials which demonstrate type II or type IV adsorption isotherms (Figure 3.13).

From the measurements the volume of gas adsorbed, V_a in $cm^3\ g^{-1}$, is calculated and plotted against the respective relative pressure, P/P_0, to give the adsorption isotherm (Figure 3.14). For the BET diagram, the volume of gas adsorbed, V_a in $cm^3\ g^{-1}$, is plotted against $1/[V_a((P_0/P)–1)]$ within the relative pressure range 0.05 to 0.3 (this range is depicted by the shaded areas in the type II and type IV isotherms displayed in Figure 3.13). The graph should take the form y = a + bx and the intercept, a, should be positive.

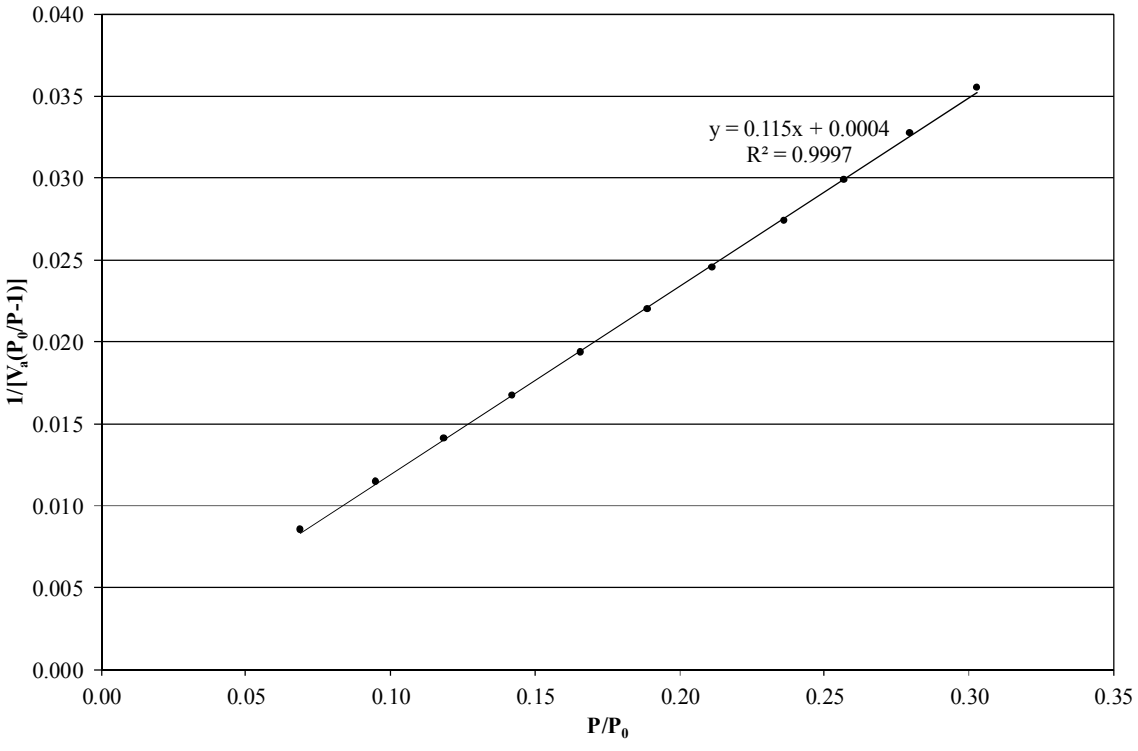

Figure 3.16 BET plot for γ–Al_2O_3 catalyst.

From this graph the monolayer capacity, n_m, the amount of adsorbate needed to occupy all sites of adsorption, can be calculated (and this point is also identified on Figure 3.14):

$$n_m = \frac{1}{a+b} \tag{3.1}$$

as can the BET parameter, *C*, which gives an indication of the strength of the adsorbent–adsorbate interaction although it cannot be used to calculate the adsorption enthalpy quantitatively:

$$C = \frac{b}{a} + 1 \tag{3.2}$$

The specific surface area, a_s, can then be calculated from the monolayer capacity by considering the average area occupied by an individual molecule in the complete monolayer:

$$a_s = n_m a_m L \tag{3.3}$$

where a_m = 0.162 nm^2, the molecular cross sectional area of N_2 at 77.3 K and L is Avogadros constant = 6.022 x 10^{23} mol^{-1}. Equation 3.3 now becomes:

$$a_s = 9.76 \times 10^4 n_m \tag{3.4}$$

a_s has units of m^2 g^{-1}. The measured surface areas of the H_2–SCR catalysts explored in this study are presented in Table 3.4.

As previously shown; the cordierite substrate demonstrates a very low surface area although accounts for most of the mass of the catalyst systems (>70 %). As such, it is possible to calculate for the apparent γ–Al_2O_3 component surface area by assuming that there is no surface area contribution from the cordierite and recalculating for the mass of the γ–Al_2O_3 component only. The results of these recalculations are also presented in Table 3.4.

3.2.3.3 Barrett–Joyner–Halenda (BJH) Porosity

The BJH method, developed by Barrett *et al.* (1951), is one of the most popular models for calculating pore size distribution and assumes the pores are cylindrical in shape.

$$\text{BJH adsorption average pore diameter} = \frac{4 \times \text{BJH cumulative pore volume}}{\text{BJH cumulative pore area}} \quad (3.5)$$

Although detailed description of the calculations is not appropriate here, the results of the BJH adsorption analysis for the H_2–SCR catalysts are presented in Table 3.4.

3.2.3.4 Summary

A summary of the N_2 adsorption analysis conducted on the H_2–SCR catalysts is presented in Table 3.4. From the obtained N_2 isotherms, the following observations can be made:

- All of the catalysts investigated demonstrate a Type IV isotherm according to IUPAC convention.
- In addition, all of the catalysts demonstrated a hybrid of Type H1 and H3 hysteresis.
    - Not pure H1 as the adsorption does not plateau at high P/P_0.
    - Not pure H3 as the hysteresis loop does not close with a distinct step.
- The presence of macropores is identified due to the lack of a plateau when P/P_0 approaches 1. It is assumed these are attributable to the cordierite substrate.
- Given that there is some estimation of the coating mass and assumption of no cordierite contribution within the surface area calculation; the measured attributable γ–Al_2O_3 BET surface area agrees well with the typical surface area for γ–Al_2O_3 of 100 – 200 $m^2\ g^{-1}$ as reported by Hayes *et al.* (1997).
- The reduction in catalyst surface area as components are loaded on the γ–Al_2O_3 washcoat may be explained by "partial plugging of supports by loading of other components", as reported by Kobayashi *et al.* (2006). This may also explain the observed increase in average pore diameter, as the smallest pores would be 'plugged' first.

Table 3.4 Calculated BET surface area and BJH average pore diameter of H_2–SCR catalyst samples.

Catalyst	Mass of Sample (g)	Attributable Coating Mass (g)	Reported BET Surface Area ($m^2\ g^{-1}$)	BET Surface Area based on Coating ($m^2\ g^{-1}$)	BJH Adsorption Average Pore Diameter (nm)
γ–Al_2O_3	0.4319	0.1279	37.74	127.41	9.4536
Pt/Al_2O_3	0.2991	0.0904	38.04	125.91	11.7794
Ag/Al_2O_3	0.4900	0.1532	37.26	119.18	10.5480

3.3 Design & Commissioning of the Continuous Flow Fixed Bed Reactor

In order to draw accurate conclusions it is important that each material, as far as possible, is subject to the same experimental conditions, thus allowing for fair comparisons. The ultimate purpose of the research should also be considered throughout, and the experimental conditions should somewhat resemble those expected in the end application. Throughout the planning and subsequent execution of the described experiments it is imperative to acknowledge why that particular experiment is being carried out and what is expected to be learnt from it.

3.3.1 Experimental Set–up

A schematic and photograph of the overall experimental set–up are shown in Figure 3.17(A) and Figure 3.17(B) respectively. Throughout design, development and commission of the apparatus slight adjustments were made, for various reasons, resulting in several iterations and configurations. However, within this thesis the rig is presented in its final form. The reaction gases were supplied from BOC, Bristol, UK and consisted of:

- 8102 ppm H_2 in N_2
- 4025 ppm NO (Total NO_x = 4050 ppm) in N_2
- Air
- 'Zero' N_2

'Zero' refers to the purity of the gases which in this instance is 99.998 % and thus there is a total impurity concentration of 20 ppm. The H_2 and NO mixtures were supplied with an accuracy of ± 5 % with respect to the certified values. The reactant gases were supplied, through flexible stainless steel hoses, to variable area flowmeters (Figure 3.18(A)) where the flow rate to the catalysts could be varied e.g. 30 to 300 cm^3 min^{-1}. The flowmeters were supplied by MPB Industries Ltd, Peckham, UK with customised ranges for the reaction gases operating under experimental conditions (inlet pressure: 1 bar, outlet pressure: atmospheric). The flowmeters are from the MPB '1200 Long' series and the have a flow tube length of 295 mm. Their specified operating ranges are shown in Table 3.5.

Table 3.5 Specified flow ranges for flowmeters and their relevant reaction gases.

Reaction Gas	Flow range (cm^3 min^{-1})
8000 ppm H_2/N_2	30 – 300
4000 ppm NO/N_2	30 – 300
Air	55 – 500
N_2	33 – 330

However, due to varying operating conditions it was necessary to calibrate the flow meters in–house. This involved using a 'soap bubble meter' of known volume, with varying volume indication levels, charged with a small amount of soap solution. The gas was then supplied to the bottom of the bubble meter, at a certain set point on the flow meter to be calibrated, and soap bubbles formed. These bubbles then travelled up the bubble meter and the time taken for them to pass between two marked points of known volume (1, 9 or 90 cm^3 dependent on the flowmeter set point) recorded. From this data, the flow rate of the gas at that particular set point could be calculated. This method was then repeated for a number of different set points and the obtained data was plotted. A line of best fit was applied to the plotted data and this relationship provided a flow rate for every set point on the rotameter. This process was repeated for each gas and flowmeter set, including reaction and calibration gases.

The gases were then fed, through ¼" (6.35 mm) stainless steel tubing, to a series of valves which could be adjusted in order to provide the desired mixture to the reactor. The inclusion of a solenoid valve (Figure 3.18(B)) enabled instantaneous switching between two reactant streams; a necessary technique for investigating the NSR process as will be discussed in Chapter 4.

The catalysts were encased in a cylindrical stainless steel reactor of length 100 mm and inner diameter of 15 mm (Figure 3.18(C)). The catalyst pieces were maintained in position using quartz wool wrapped around the outside of the monoliths, which prevented gas flow down the sides of the samples and directed it through the channels. The reactor was housed in the centre of a Carbolite (Hope, UK) VST 12/600 electric furnace (Figure 3.18(D)) fitted with a 3216P1 temperature controller. The furnace had a heated length of 600 mm and a maximum temperature of 1200 ^{o}C, however, given that the maximum explored operating temperature was 700 ^{o}C the power output was restricted to 40 % in order to provide greater control at lower temperatures. The configuration of the furnace was such that it was hinged; allowing it to be opened up, affording easy access to the reactor within, without requiring the reactor, reactor inlet and exhaust to be detached and removed each time a sample needed to be changed.

The reactor was connected to stainless steel tubes which act as an inlet and outlet for the gases and two K–type thermocouples were positioned both 5 mm before and 5 mm after the catalyst within. The K–type thermocouples, along with a third placed within the furnace although outside the reactor, were connected to a data logger and real time temperature measurements stored on a dedicated data acquisition PC. A measured change in temperature over the catalyst bed may indicate a reaction is occurring although the extent of the change will be determined by many factors including: the particular reaction or the flow rate and composition of the gases. It was also necessary to calibrate the thermocouples utilised within the reactor, this was achieved through use of an Isotech Jupiter 650S thermocouple calibration block. By comparing the set furnace temperature to that measured by the thermocouples, a linear relationship can be established and any variation accounted for during programming of the data acquisition software.

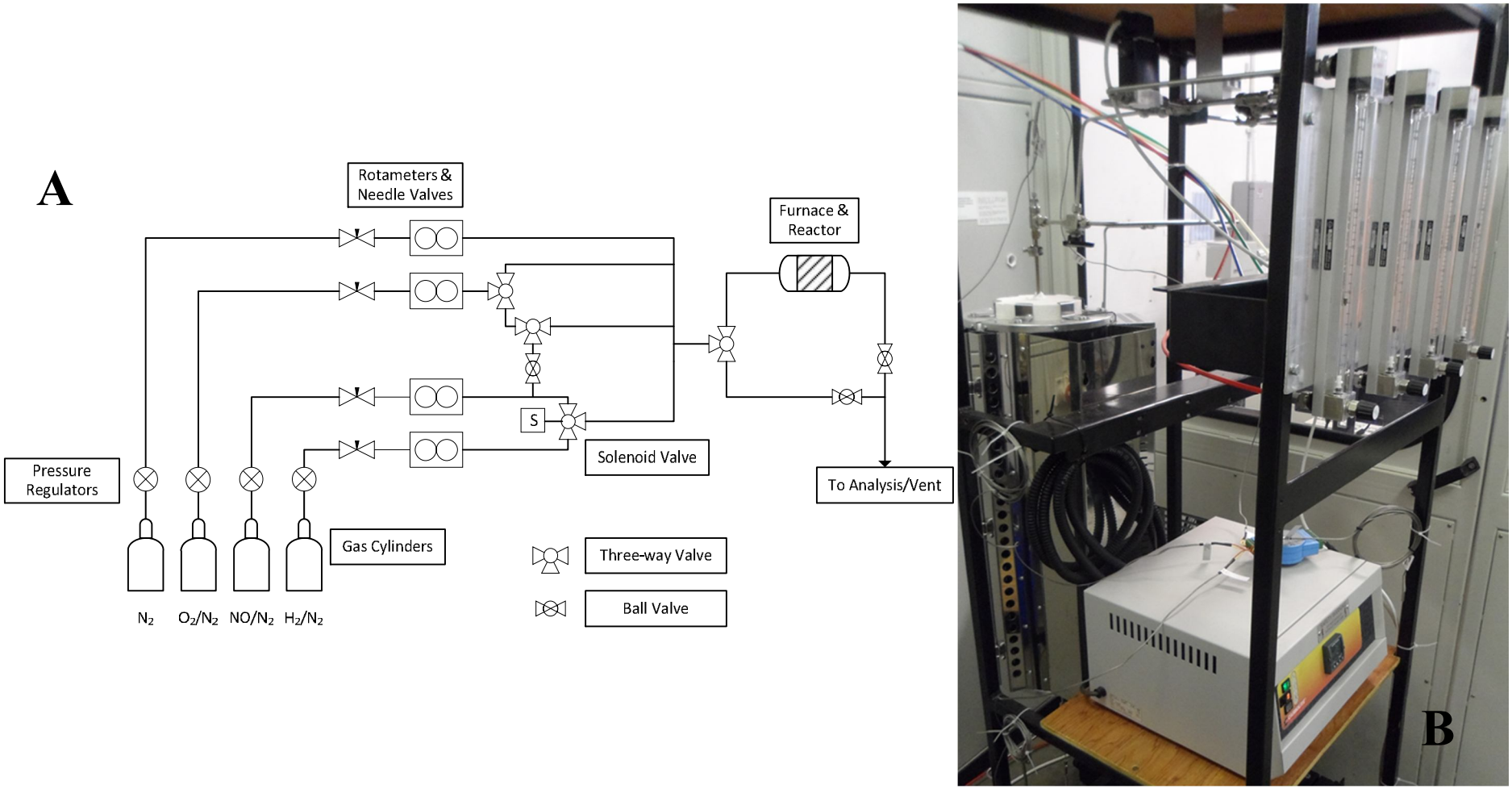

Figure 3.17 Experimental set–up constructed and utilised within this study: (A) – Schematic, (B) – Photograph.

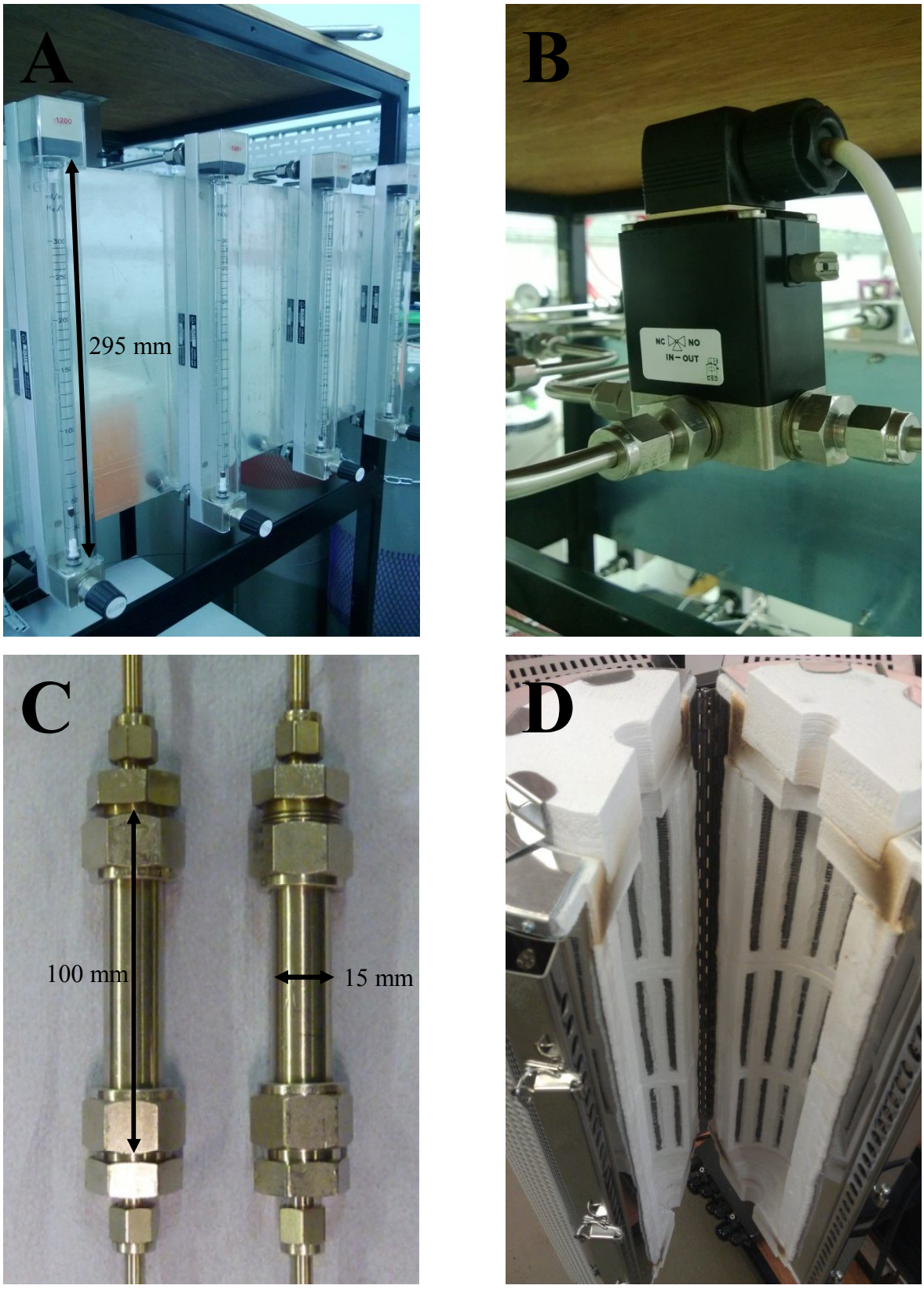

Figure 3.18 Photographs of (A) flowmeters, (B) solenoid valve, (C) reactors and (D) furnace used in the experimental set–up.

The outlet from the reactor was directed to the analysis equipment, a Hiden Analytical HPR–20 Quadrupole Mass Spectrometer (Figure 3.19). Using Hiden's MASsoft software, the activity and selectivity of the catalysts was recorded. In addition, the mass spectrometer operates through a sampling line and thus is not necessarily restricted by reaction flow rates, although if the flow rate is too great it may be difficult to identify subtle changes in the system.

Figure 3.19 Photograph of Hiden HPR–20 gas analysis system.

Full details of QMS calibration are described in Appendix I, although the main aspects of the approach will be summarised here:

a) Development of an experimental set–up which enabled delivery of the necessary gas species, and combination of gas species, to the QMS.

b) Optimisation of the QMS operating parameters to enable separation of overlapping species fragment patterns. Adjusted operating parameters included: vacuum pressure, electron energy, electron emission and SEM Detector voltage.

c) Refinement of the analysis method to improve accuracy in measurements by encompassing: background levels, pattern fragmentation and relative sensitivity values.

3.3.2 Flow Rate Considerations

When designing the experiments it was important to consider the flow rates with respect to the end application.

a) Based on data on exhaust treatment in Bennett (1990), the following was obtained and analysed:
Estimate of application exhaust flow rate: 900 dm^3 min^{-1}.

Diameter of autocatalyst exhaust: ø = 10 cm.

Cross sectional area of autocatalyst exhaust = $\pi r^2 = \pi (10/2)^2 = 78.54$ cm^2

Diameter of reactor utilised in the preliminary deNO_x study: ø = 1.5 cm.

Cross sectional area of preliminary study reactor = $\pi r^2 = \pi (1.5/2)^2 = 1.77$ cm^2

$Area_{Bennett}/area_{Prelim} = 78.54/1.77 = 44.37$

Thus to scale down the gas flow from 900 dm^3 min^{-1} to a reactor of diameter, ø = 1.5 cm: 900/44.37 = 20.28 dm^3 min^{-1} = <u>1216.8 dm^3 h^{-1}</u>

b) Next consideration was then given to the experimental conditions chosen by those known for their experimental laboratory scale work in the field of deNO_x (Castoldi *et al.* (2010)):

Reported reactor diameter, ø = 0.7 cm

Cross sectional area of reactor = $\pi r^2 = \pi (0.7/2)^2 = 0.38$ cm^2

Reported reactant mixture flow rate: 6 dm^3 h^{-1} = 0.1 dm^3 min^{-1}.

$Area_{Prelim}/area_{Castoldi} = 1.77/0.38 = 4.66$

Scaling up the flow rates to a reactor diameter, ø = 1.5 cm,

6 dm^3 h^{-1} x 4.66 = <u>27.96 dm^3 h^{-1}</u>

Although the gas flow rate in (a) is very much greater than in (b), it was decided to adopt the lower flow as the time–scale(s) of the transient response would be less prone to measurement errors. Thus, the preliminary experimental procedure (with a total flow rate of 28.20 $dm^3\ h^{-1}$ or 0.48 $dm^3\ min^{-1}$) was in the correct range and should be maintained.

3.3.3 Presentation of Results

Depending on the type of experiment undertaken, different measures of success will be employed. Beyond merely stating absolute values, these measures may include:

- Conversion of all reactants; NO, H_2 and O_2, and
- conversion of NO to both desired products and unwanted by–products.

NO conversion will be calculated as follows:

$$X_{\mathrm{NO}} = 1 - \frac{C_{\mathrm{NO}}^{\mathrm{Outlet}}}{C_{\mathrm{NO}}^{\mathrm{Inlet}}} \tag{3.6}$$

Where X_i denotes total conversion of species *i* and C_i^{Inlet} and C_i^{Outlet} are the concentrations of NO at the inlet and outlet of the reactor respectively. In a similar manner, H_2 conversion and O_2 conversion will be calculated as such:

$$X_{\mathrm{H_2}} = 1 - \frac{C_{\mathrm{H_2}}^{\mathrm{Outlet}}}{C_{\mathrm{H_2}}^{\mathrm{Inlet}}} \tag{3.7}$$

$$X_{\mathrm{O_2}} = 1 - \frac{C_{\mathrm{O_2}}^{\mathrm{Outlet}}}{C_{\mathrm{O_2}}^{\mathrm{Inlet}}} \tag{3.8}$$

NO conversion to NH_3, N_2O and NO_2 were calculated correspondingly:

$$X_{\mathrm{NO\rightarrow NH_3}} = \frac{C_{\mathrm{NH_3}}^{\mathrm{Outlet}}}{C_{\mathrm{NO}}^{\mathrm{Inlet}}} \tag{3.9}$$

$$X_{\mathrm{NO\rightarrow N_2O}} = \frac{2 \times C_{\mathrm{N_2O}}^{\mathrm{Outlet}}}{C_{\mathrm{NO}}^{\mathrm{Inlet}}} \tag{3.10}$$

$$X_{\mathrm{NO\rightarrow NO_2}} = \frac{C_{\mathrm{NO_2}}^{\mathrm{Outlet}}}{C_{\mathrm{NO}}^{\mathrm{Inlet}}} \tag{3.11}$$

Note that the previous conversions take in to account the stoichiometries of the expected reactions (Equation 2.15 – 2.19).

As all reactions are carried out with N_2 as the carrier gas and thus with N_2 in great excess (>94 %), it is difficult to measure the subtle concentration changes which result from NO reduction (and subsequent N_2 formation). Additionally, formation of H_2O through the oxidation of H_2 and O_2 means it is also difficult to attribute H_2O formation to NO reduction. However, by considering the formation of the other N–species it is possible to calculate an apparent N_2 formation which allows the complete NO conversion to be realised. As such, it is important to consider the potential reactions discussed by Liu *et al.* (2012) and presented in Chapter 2 (Section 2.4.3.1), in terms of the stoichiometry of the NO reactant and N–species formation:

$$2NO + 4H_2 + O_2 \rightarrow N_2 + 4H_2O \quad (2.15)$$

$$2NO + 3H_2 + O_2 \rightarrow N_2O + 3H_2O \quad (2.16)$$

$$2NO + H_2 \rightarrow N_2O + H_2O \quad (2.17)$$

$$NO + \frac{5}{2}H_2 \rightarrow NH_3 + H_2O \quad (2.18)$$

$$NO + \frac{1}{2}O_2 \rightarrow NO_2 \quad (2.19)$$

Taking into account the stoichiometries displayed in Reactions 2.15–2.19, the apparent N_2 formation and thus, conversion of NO to N_2, may be calculated as follows:

$$C_{N_2}^{Outlet} = C_{NO}^{Inlet} - C_{NO}^{Outlet} - C_{NH_3}^{Outlet} - C_{NO_2}^{Outlet} - 2 \times C_{N_2O}^{Outlet} \quad (3.12)$$

$$X_{NO \rightarrow N_2} = \frac{C_{N_2}^{Outlet}}{C_{NO}^{Inlet}} \quad (3.13)$$

3.4 H_2–SCR: A Preliminary Set of Experiments

In this section experiments are performed over selected initial parameters, in order to fully explore the different processes and identify potential limitations and exploitations. Utilising the equipment previously described in Section 3.3.1 the experiments generally consisted of the catalysts being heated at a set ramp rate, to defined intervals where the temperature would be held constant and the desired gas mixture being supplied, up to a maximum temperature. The samples were subject to a number of different sequences, depending on the type of investigation being undertaken e.g. SCR or TPD. Details of the different reaction sequences are provided before the results of each individual experiment.

Due to the nature of the equipment and the measurements, it was not practical to be able to supply a completely consistent reaction mixture to every catalyst and thus although the reaction mixture compositions are specified, this is generally for comparison purposes and in actuality there is an element of deviation from the quoted values depending on the experiment. This also holds true for specified temperatures, however, the measured values will be presented in plots and tables without adjustment. Indeed the raw measurements presented here subsequently influenced further calibration of the QMS as described in Appendix I. As such, the parameters described in Appendix I do not necessary correlate to those utilised to obtain measurements presented in this section. Individually presented data points were calculated by averaging the measured raw signal from the mass spectrometer over a period of 5 minutes (typically ~15 – 20 data points) unless stated, after the system had equilibrated at constant temperature. The data points are connected to give an indication of trends and the connections do not represent recorded data. Where appropriate, arrows are utilised to highlight inlet conditions and identify which species concentration corresponds to which axis.

Finally, these results are not considered absolute and a detailed breakdown and analysis of final results will be presented in Section 3.5. The purpose of these initial experiments was to identify any shortcomings and allow optimisation of the experimental procedure, as well as gain an indication of catalyst performance (which allowed for greater accuracy in QMS calibration). As a result there are subtle differences between the described procedures for experimentation and analysis and these are highlighted throughout the description of the results.

3.4.1 Aims and Objectives

SCR experiments will investigate the ability of the catalyst materials to reduce NO using H_2 (in the presence or absence of O_2) and report the results in terms of conversion of reactants and selectivity to desired and undesired products. The performance of the catalyst materials will initially be investigated only at temperatures up to 250 ^oC.

3.4.2 Predicted Outcomes

It is expected that the $deNO_x$ activity will generally improve as temperature is increased, although there may be little improvement (or indeed a drop in performance) above a particular temperature, and that selectivity to different products may also vary with temperature. It is known that with some materials the reaction between H_2 and O_2 to form H_2O is favourable and thus it is expected that $deNO_x$ activity in the absence of O_2 will be greater than in the presence of O_2. However, it may be that there is some optimum level of O_2 or indeed a certain tolerance within the system up to a particular O_2 concentration, although this will not be explored here.

3.4.3 Pt/Al_2O_3

The Pt/Al_2O_3 catalyst was studied as an example of a 'typical' or 'standard' H_2–SCR catalyst and to confirm the SCR experimental approach. The catalysts were prepared in–house by impregnating supplied alumina coated monoliths, with an aqueous platinum solution, full details can be found in Section 3.1.4.1. The catalysts had an average platinum loading of 0.8 wt% and an average γ–Al_2O_3 loading of 29.4 wt% with respect to the complete catalyst system.

3.4.3.1 Absence of O_2

The first studies investigated that the Pt/Al_2O_3 catalyst was capable of facilitating the H_2 deNO_x reaction and thus aimed to react H_2 and NO directly, in the absence of O_2. The following overall reaction is desired:

$$2NO + 2H_2 \rightarrow N_2 + 2H_2O \quad (3.14)$$

However, as explained in Chapter 2, Section 2.4.3.1, undesired side reactions may also occur:

$$2NO + H_2 \rightarrow N_2O + H_2O \quad (2.17)$$

$$NO + \frac{5}{2}H_2 \rightarrow NH_3 + H_2O \quad (2.18)$$

The reactor was loaded with three Pt/Al_2O_3 monolith pieces. First the Pt species on the catalyst were reduced to form the active metal species; the samples were heated to 350 °C at a rate of 10 °C min^{-1} and subject to 8000 ppm H_2 in N_2 at a flow rate of 300 cm^3 min^{-1} for 1 h before the reactor was then cooled to 100 °C.

During cooling the gas flow was directed through the reactor bypass and a gas composition consisting of 500 ppm NO and 2000 ppm H_2 with a N_2 balance and a total flow rate of ~440 cm^3 min^{-1} (26.50 dm^3 h^{-1}) was set (Table 3.6). In this instance the desired gas composition was set using the QMS and thus only an approximate total flow rate is provided.

Table 3.6 Approximate gas mixture flow rates and ultimate inlet composition utilised during preliminary H_2–SCR investigations in the absence of O_2 over 0.8 wt% Pt/Al_2O_3.

Gas Mixture	Flow Rate (dm^3 h^{-1})	Flow Rate (cm^3 min^{-1})	Composition
4000 ppm NO/N_2	3.29	55	500 ppm NO 2000 ppm H_2 balance N_2
8000 ppm H_2/N_2	6.54	109	
N_2	16.67	278	
Total	26.50	442	

Once the desired reactor temperature had been reached and was stabilised, the gas flow was directed through the reactor for 30 min whilst the temperature remained constant, before it was returned to the bypass. This process was repeated for each temperature (up to 250 °C at 50 °C intervals) and enabled the inlet and outlet of the reactor to be consecutively measured in order to identify any drift in the inlet composition which may occur from the rotameters. This in theory can enable slight changes to be made in the flow rates to produce somewhat constant inlet conditions between different temperatures, however this was *not* performed in this instance and the set flow rates were not altered throughout the experiment. This produced an initial data set as is shown in Figure 3.20, which is provided for discussion.

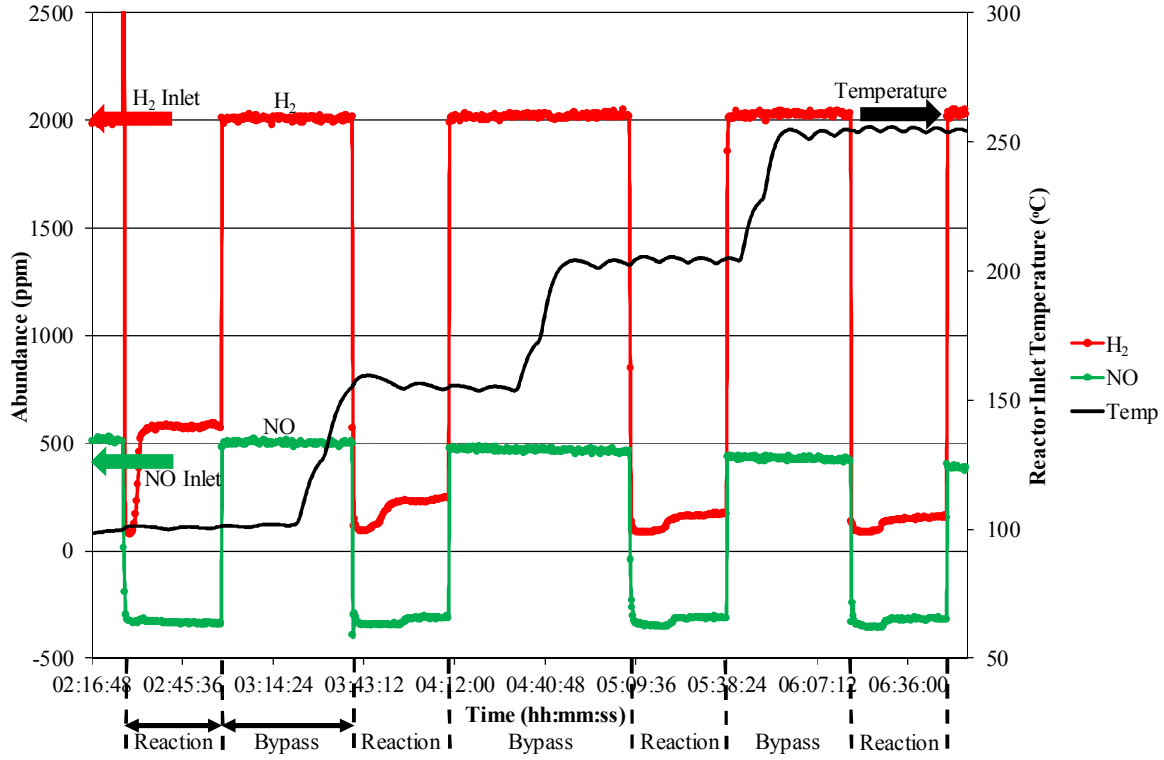

Figure 3.20 Example of typical plot from Pt/Al_2O_3 H_2–SCR study with no O_2 in the reactant mixture.

The plot presents a number of issues:

- From a technical perspective the manual switch between the reactor and the bypass generally works very well, enabling an almost instantaneous transfer between the two. Although the flow rates were not adjusted in this instance, the ability to measure and adjust the reactor inlet conditions is invaluable.

- As can be clearly seen; there is a drop in NO concentration over the period of measurement, which is accompanied by a very slight increase in the H_2 concentration. This may demonstrate some instability in the rotameters; however this can be countered by adjusting the flow rates. In any case the concentration change is not great over each measurement period and should not contribute a significant error to the results.

- Due to the furnace operation, small temperature fluctuations within the reactor can be seen.

- It is obvious that the NO concentration falls significantly below zero (up to –340 ppm) during the reaction. This can be accounted for by the calibration of the MS, which incorporated every single possible reaction species, desired products and by–products. As there is no O_2 in this particular reaction mixture, and the contribution of O_2 at 30 amu has been allowed for, there is an error in the NO reading. This highlights the potential need to produce different calibration methods for both different reaction inlet and possible outlet conditions, and this will be pursued further.

- In terms of the deNO_x reaction; a rise in both NO and H_2 levels can be seen immediately after switching to the reactor before equilibrium is reached.

The performance of the catalyst can now be considered, by comparing the concentration of different species at the different temperatures. The readings from the last five minutes of the 30 min period in which the reactants were supplied to the catalysts were averaged to provide the data points shown in Figure 3.20. A summary of the data is also provided in Table 3.7.

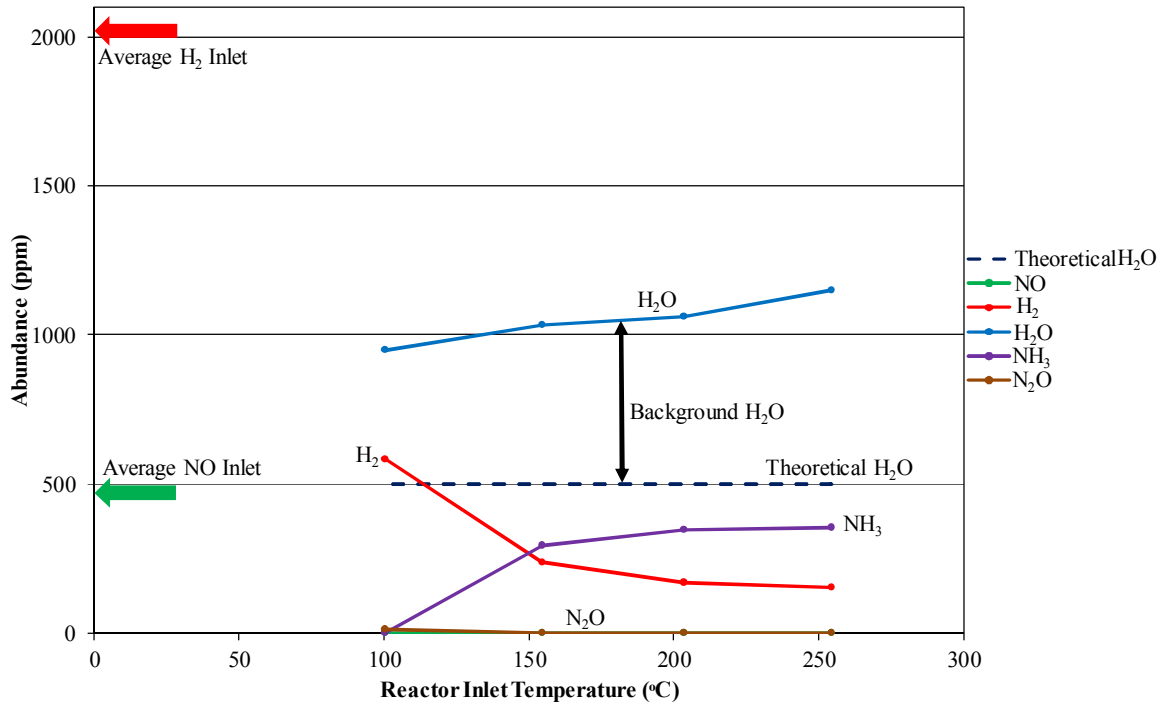

Figure 3.21 H_2–SCR, in the absence of oxygen, over 0.8 wt% Pt/Al_2O_3. Reaction conditions: 500 ppm NO, 2000 ppm H_2, balance N_2.

Table 3.7 Summary of absolute measured species abundance for H_2–SCR, in the absence of oxygen, over 0.8 wt% Pt/Al_2O_3.

Temperature (°C)	Measured Outlet Concentration ppm					%
	NO	H_2	H_2O	N_2O	NH_3	N_2
21.6	512	1999	1698*	–	–	99.52
100.5	0	584	949	13	1	99.64
155.0	0	237	1033	1	296	99.66
203.8	0	170	1061	1	347	99.66
254.4	0	153	1149	1	356	99.67

*Background level of H_2O measured

It should be noted that, as already alluded to, due to the operation of some items of equipment the exact composition of the reaction mixture supplied to the catalyst will differ at different temperatures. Nevertheless, the obtained data can give a strong indication of the performance of the catalyst if not comparable absolute values. As can be seen from the plot, at temperatures as low as 100 ^{o}C the NO is completely converted. There is also significant conversion of H_2; 70 % at 100 ^{o}C increasing to over 90 % at 200 ^{o}C and 250 ^{o}C. In the absence of O_2 it is clear that Pt/Al_2O_3 promotes a H_2 deNO_x reaction.

However, there are other points to note: there is a significant level of H_2O present in both the reaction and product mixtures. The reaction gas cylinders contain a certain amount of H_2O and the product values quoted here have been normalised to try and represent the amount of H_2O which has been produced from the reaction only i.e. the 'background' H_2O reading has been subtracted from the measured values. However, as can been seen from Figure 3.20 there is still an extra 500+ ppm H_2O in the system, above the theoretical H_2O level, although the origin of this additional H_2O is not clear. Furthermore, the method through which the QMS is calibrated for the reaction mixture only accounts for a significant level of H_2O (in excess of 0.6 %) and thus may be overly sensitive at lower levels of H_2O, leading to inaccurate results. That over 90 % of the H_2 is converted is also surprising given that it is in great excess, with comparison to the NO, and in the absence of O_2 there should be no other species for it to react with.

There is also some demonstration of selectivity in the deNO_x reaction: undesired by–products N_2O and NH_3 are produced in varying concentrations over a range of temperatures. A very small concentration, only 13 ppm, of N_2O is found at 100 ^{o}C whilst there is almost no formation at temperatures above that. The abundance of NH_3 increases significantly to 296 ppm at 150 ^{o}C and up to 356 ppm at 250 ^{o}C. Again this value of NH_3 identifies a shortcoming in the calibration procedure, as the measured levels are greater than the value at which the method was developed (100 – 150 ppm) and so perhaps at these greater values the measurements are not as accurate. Thus the need for a more robust method, enabling measurement of different species over wide concentration ranges, or indeed different methods for different reaction conditions, is again highlighted.

By directly comparing the data obtained during reaction over the catalyst at different temperatures, trends can be identified. In Figures 3.22(A)–(D) the raw data has been plotted which, as previously discussed, may not provide accurate absolute values but gives an indication of any patterns. What is immediately clear is that there is a period of stabilisation immediately after introducing the gas mixture to the catalyst where both NO and H_2 levels are initially constant. However, after a 5 – 15 min period, depending on the reaction temperature, the levels of these species gradually increase and stabilise at a slightly higher concentration. Additionally, the difference in the initial and final stable concentrations decreases with increasing temperature. Given that during the desired deNO_x reaction H_2O would be formed, it may be reasonably expected that the H_2O levels should decrease when the H_2 and NO levels increase. Indeed there is some indication of this pattern at temperatures above 100 ºC but due to the difficulties in accurately measuring the H_2O it is not possible to definitely confirm.

Furthermore, when NH_3 begins to be formed its abundance follows the same trend as both the NO and H_2 abundance although not in the same time frame; after 10 – 12 min under reaction conditions NH_3 levels increase to a higher stable concentration. This is surprising as it is thought that an increase in NH_3 would be accompanied by a decrease in H_2 and NO as it may be formed either through Reaction 2.18 displayed previously, or Reaction 3.15, the hydrogenation of adsorbed nitrogen (formed from dissociated NO) as discussed by Li *et al.* (2012):

$$3H_{ads} + N_{ads} \rightarrow NH_3 \qquad (3.15)$$

On closer inspection it also appears that the H_2O and NH_3 abundances are linked: the H_2O concentration drops as the NH_3 concentration increases. Due to the method of measurement, where both species are responsible for contributing to QMS peaks at 17 and 18 amu, it may be that there is still overlap in the results and further development of the method is required to enable complete separation of the peaks.

It should also be noted that there was no NO_2 detected at any point during the experiment, which given the lack of O_2 present in the reaction mixture, is not surprising.

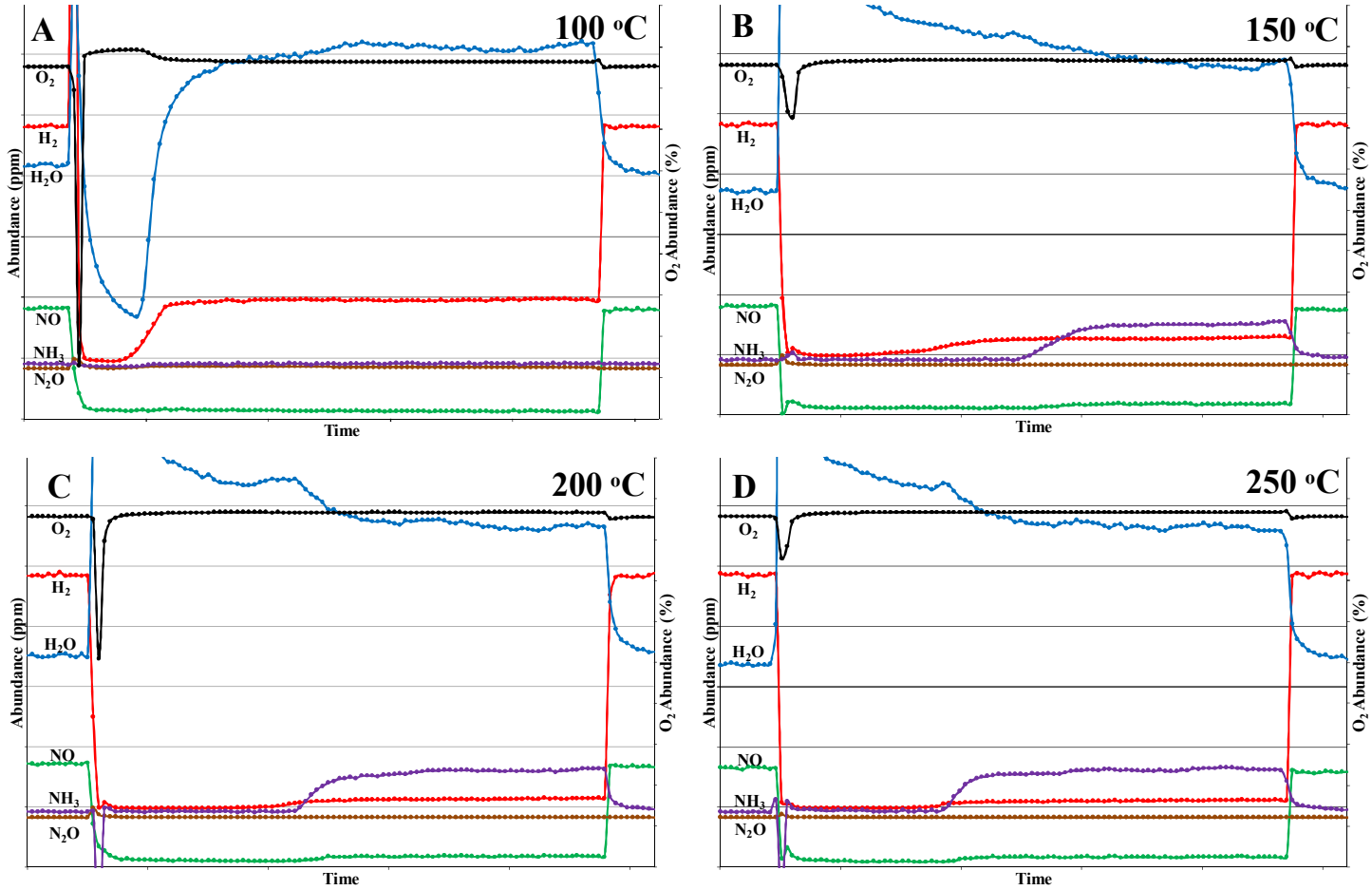

Figures 3.22(A)–(D) Plots of species abundance during H_2 SCR, in the absence of O_2, over 0.8 wt% Pt/Al_2O_3 at different temperatures (A – 100 °C, B – 150 °C, C – 200 °C and D – 250 °C). Key: O_2 – black, H_2O – blue, H_2 – red, NO – green, NH_3 – purple and N_2O – brown.

Further information may be learned from the temperature measurements at the reactor inlet and outlet, Figure 3.23. However, although care was taken to position the thermocouples as close to the catalysts as possible, and from the QMS measurements it appears a reaction is occurring, there is no measured increase in temperature over the length of the reactor. In fact it appears that there is a slight decrease during the periods of reaction, indeed this may account for the apparent change in stabilised concentrations witnessed in Figures 3.22(A)–(D). It may be that the experimental set–up is not capable of measuring such subtle changes in temperature across the catalyst bed although improving the resolution of temperature measurements may be explored.

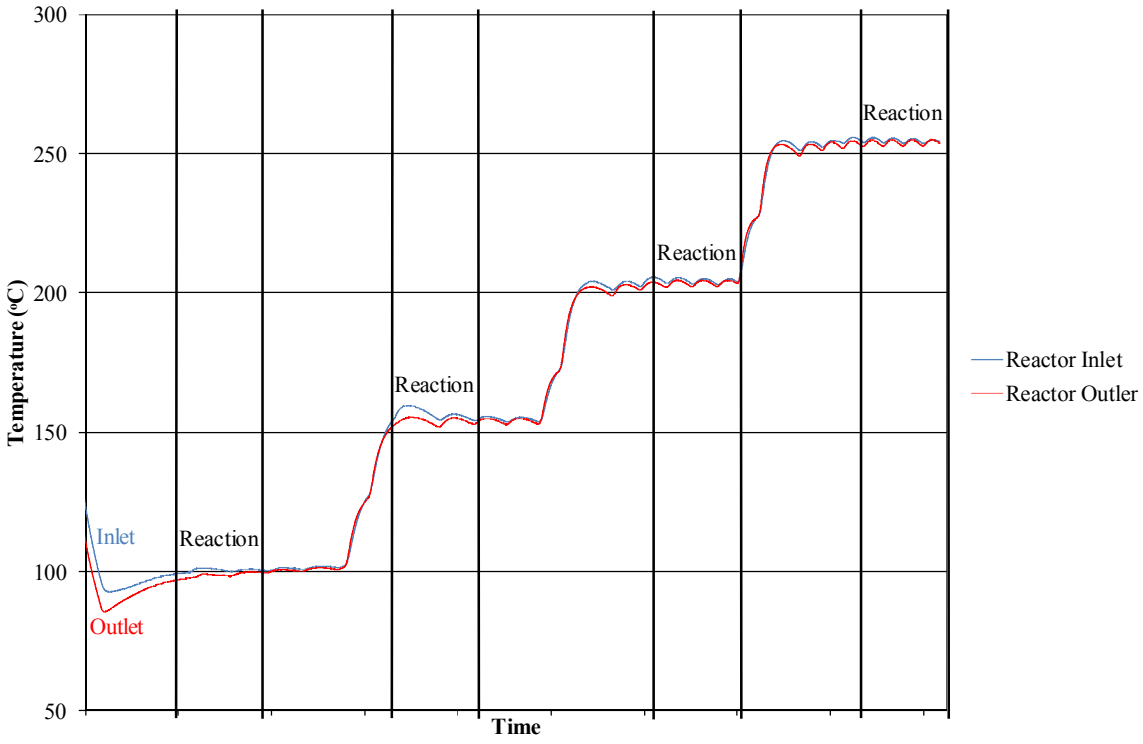

Figure 3.23 Reactor inlet and outlet temperatures over the course of H_2–SCR, in the absence of oxygen, over 0.8 wt% Pt/Al_2O_3.

Further issues which also need to be considered are the huge initial H_2O peaks which occur when the gas flow is switched back to the reactor, an indication of which can be gleaned from Figures 3.22(A)–(D). A similar phenomenon occurs with both NO and NH_3 peaks although in these instances the peaks are negative.

3.4.3.2 Presence of O_2

The experiment was repeated in the presence of O_2 to provide more realistic conditions with respect to the end application. As a reminder, as explained in Chapter 2, Section 2.4.3.1, in the presence of O_2 the following reactions are now expected:

$$2NO + 4H_2 + O_2 \rightarrow N_2 + 4H_2O \quad (2.15)$$

$$2NO + 3H_2 + O_2 \rightarrow N_2O + 3H_2O \quad (2.16)$$

$$2NO + H_2 \rightarrow N_2O + H_2O \quad (2.17)$$

$$NO + \frac{5}{2}H_2 \rightarrow NH_3 + H_2O \quad (2.18)$$

$$NO + \frac{1}{2}O_2 \rightarrow NO_2 \quad (2.19)$$

$$H_2 + \frac{1}{2}O_2 \rightarrow H_2O \quad (2.20)$$

In this instance there was no pre–treatment of the catalyst. The catalysts were heated at a rate of 2 ^{o}C min^{-1} to 50 ^{o}C and subject to a 1 h dwell. The catalysts were then heated at a rate of 5 ^{o}C min^{-1} up to 250 ^{o}C with a 1 h dwell at each 50 ^{o}C interval.

A gas composition consisting of 500 ppm NO, 2000 ppm H_2 and 5 % O_2 with a N_2 balance and a total flow rate of ~440 cm^3 min^{-1} (26.50 dm^3 h^{-1}) was set (Table 3.8). In this instance the flow rates were adjusted between each reaction, if required, in order to obtain more consistent inlet conditions between each temperature (Table 3.9). In general the inlet conditions were very close to the desired values; the greatest recorded variation being within 2.6 % of the specified concentration, this level of error is acceptable and this procedure should be adopted for future experiments.

Table 3.8 Approximate gas mixture flow rates and ultimate inlet composition utilised during preliminary H_2–SCR investigations over 0.8 wt% Pt/Al_2O_3.

Gas Mixture	Flow Rate ($dm^3\ h^{-1}$)	Flow Rate ($cm^3\ min^{-1}$)	Composition
4000 ppm NO/N_2	3.29	55	500 ppm NO
8000 ppm H_2/N_2	6.54	109	2000 ppm H_2
Air	6.31	105	5.0 % O_2
N_2	10.36	173	balance N_2
Total	26.5	442	

Table 3.9 Summary table of inlet conditions for deNO_x reaction over 0.8 wt% Pt/Al_2O_3 at different temperatures.

Temperature (°C)	Inlet Conditions			
	NO (ppm)	H_2 (ppm)	O_2 (%)	N_2 (%)
53.0	489	2027	4.93	94.54
97.7	487	2023	4.97	94.54
147.5	512	2000	5.00	94.53
202.4	499	1992	4.98	94.56
253.6	498	1976	4.99	94.57

As can be seen from Figure 3.24(A), Figure 3.24(B) and Figure 3.25 the Pt/Al_2O_3 catalyst successfully promotes the H_2 $deNO_x$ reaction in the presence of O_2, with comparable performance to the previous experiment.

At a temperature of 50 °C, both NO and H_2 are almost completely converted, with 98 % and 95 % conversion respectively. There is also some conversion of O_2; 2.3 % at 50 °C, which given the concentration of O_2 in the reaction mixture, is a significant amount. However, at higher temperatures different trends for each species are observed; whilst H_2 reaches a maximum conversion of 97 % at 100 °C it maintains this level of conversion throughout the higher temperatures. In contrast, the NO conversion drops to a minimum of 27 % at 150 °C before recovering to a conversion of 63 % at 250 °C. The O_2 conversion also follows a different trend, although it is perhaps difficult to see due to presentation of the data; there is a general increase in conversion with temperature, although with a small drop from 100 °C to 150 °C, before a maximum conversion of 2.8 % is reached at 250 °C.

There also appears to be some obvious temperature selectivity of the reaction. At 50 °C the majority of the NO has been reacted with H_2 to form N_2 and H_2O, although there is also a small amount, ~60 ppm, of N_2O formed (Figure 3.24(B)), most likely from the reaction of NO and O_2. The excess H_2 is likely reacted with O_2 to form more H_2O. When the temperature is increased to 100 °C, although a decrease in NO conversion, and subsequently a decrease in N_2O formation (to ~30 ppm), is detected, there is more reaction between H_2 and O_2 and the H_2O level increases (remaining constant as the temperature is increased further). At 150 °C a further decrease in NO conversion and some formation of NO_2 (~195 ppm), from reaction of NO and O_2, is observed. The formation of NO_2 increases at higher temperatures, accompanied by an increase in conversion of both NO and O_2. The maximum measured value of NO_2 is in excess of 1300 ppm which, given the inlet concentration of NO should only be 500 ppm, does not appear accurate. Much like the NH_3 reading in the previous experiment, the calibration method allowed for much lower (trace) concentrations of NO_2 and thus the higher levels which appear to have been formed here are exaggerated. Additionally there was no NH_3 detected throughout this reaction.

To summarise it appears that the most suitable temperature for H_2 $deNO_x$ with Pt/Al_2O_3 is 50 °C, although this is not ideal as there is a significant level of N_2O formed, which in itself is a potent greenhouse gas. Generally, as temperature continues to increase; first NO conversion drops and then NO_2 formation dramatically rises.

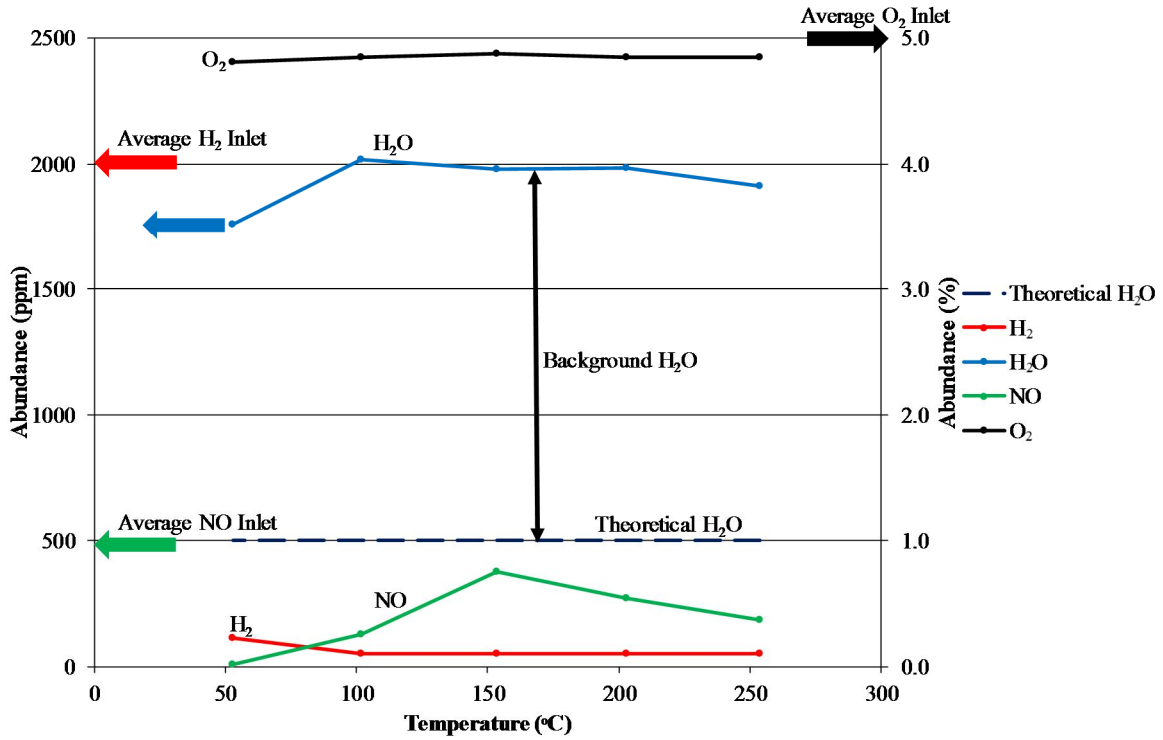

Figure 3.24(A) H_2–SCR (main species) over 0.8 wt% Pt/Al_2O. Reaction conditions: 500 ppm NO, 2000 ppm H_2, 5 % O_2, balance N_2.

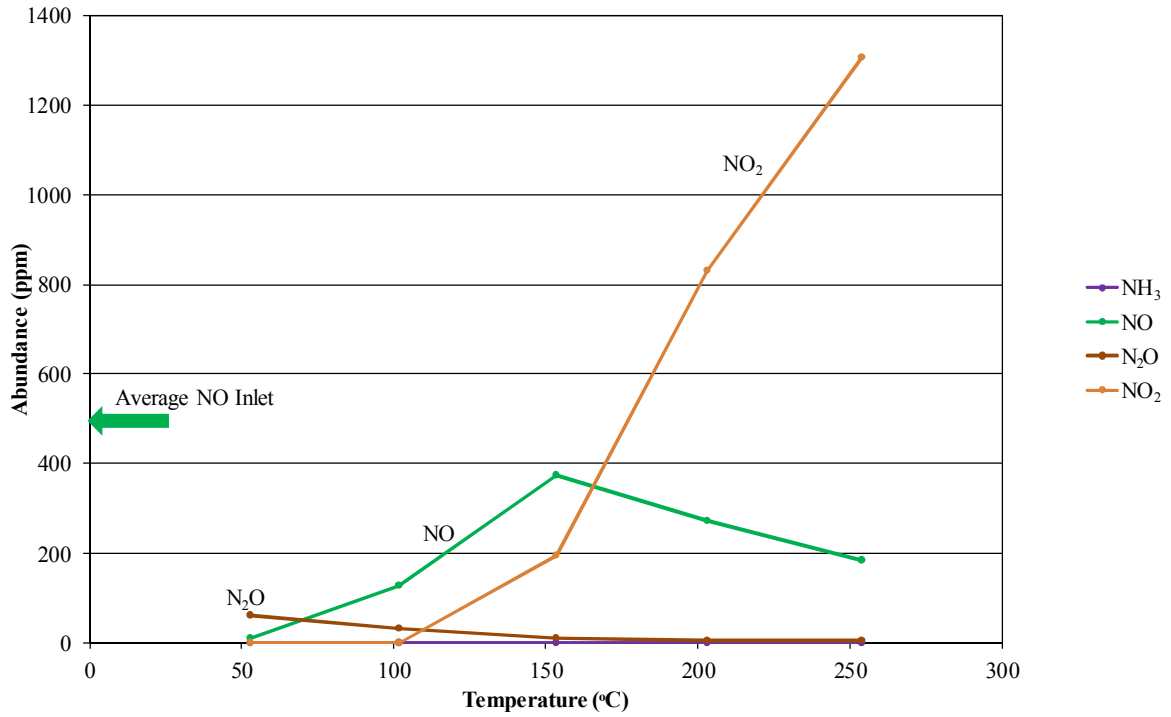

Figure 3.24(B) H_2–SCR (trace species) over 0.8 wt% Pt/Al_2O_3. Reaction conditions: 500 ppm NO, 2000 ppm H_2, 5 % O_2, balance N_2.

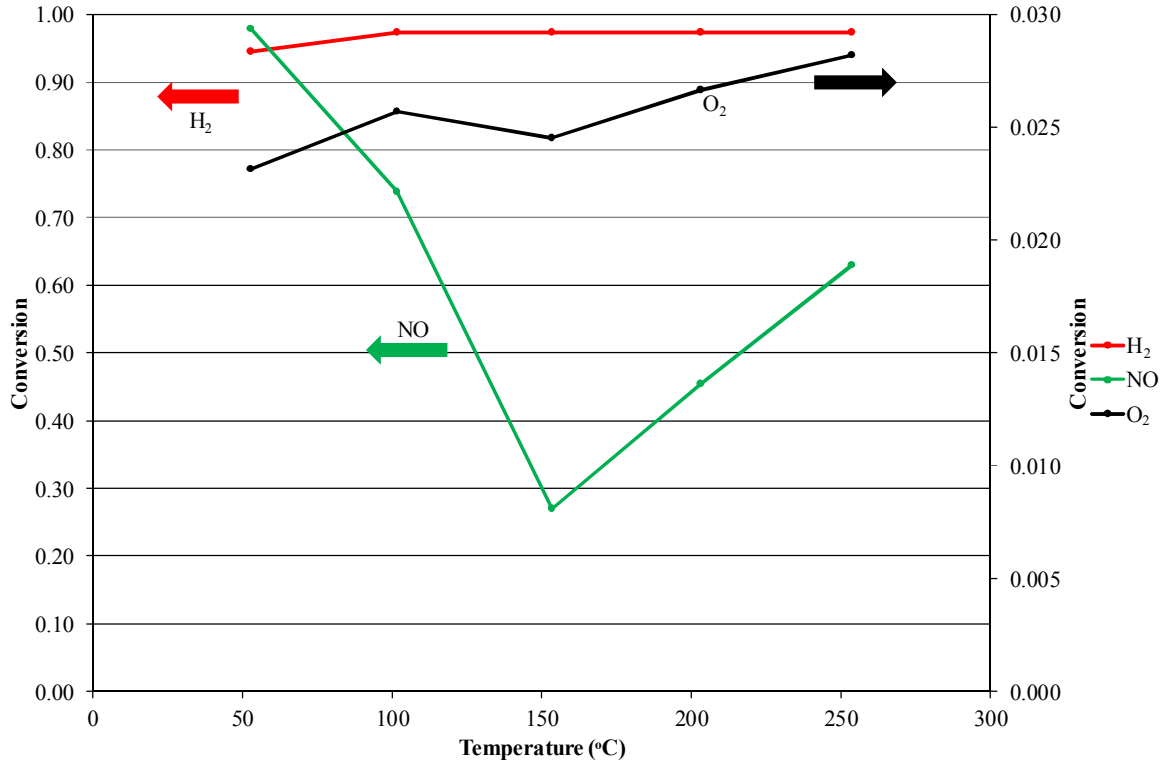

Figure 3.25 H_2–SCR (conversion) over 0.8 wt% Pt/Al_2O_3 catalyst. Reaction conditions: 500 ppm NO, 2000 ppm H_2, 5 % O_2, balance N_2.

3.4.4 Ag/Al_2O_3

The previous experiments were repeated with a previously unexplored material, Ag/Al_2O_3, as a potential novel H_2–SCR catalyst. The catalysts were prepared in–house by impregnating alumina coated monoliths with an aqueous silver solution, full details can be found in Section 3.1.4.2. The catalysts had an average silver loading of 2.3 wt% and an average γ–Al_2O_3 loading of 28.9 wt% with respect to the complete catalyst system.

3.4.4.1 Absence of O_2

As a reminder, in the absence of O_2, the following reactions are now expected. Desired overall reaction:

$$2NO + 2H_2 \rightarrow N_2 + 2H_2O \qquad (3.14)$$

Undesired side reactions as explained in Chapter 2, Section 2.4.3.1:

$$2NO + H_2 \rightarrow N_2O + H_2O \qquad (2.17)$$

$$NO + \frac{5}{2}H_2 \rightarrow NH_3 + H_2O \qquad (2.18)$$

The reactor was loaded with three Ag/Al_2O_3 monolith pieces. The following flow rates were set and unaltered for the duration of the experiment (Table 3.10).

Table 3.10 Approximate gas mixture flow rates and ultimate inlet composition utilised during preliminary H_2–SCR investigations in the absence of O_2 over 2.3 wt% Ag/Al_2O_3.

Gas Mixture	Flow Rate ($dm^3\ h^{-1}$)	Flow Rate ($cm^3\ min^{-1}$)	Composition
4000 ppm NO/N_2	3.29	55	500 ppm NO 2000 ppm H_2 balance N_2
8000 ppm H_2/N_2	6.54	109	
N_2	16.67	278	
Total	26.50	442	

The catalysts were then heated at a rate of 5 $^oC\ min^{-1}$ up to 250 ^oC with a 1 h dwell at each 50 ^oC interval.

It appears that the experiment was started prematurely and the supplied species concentrations were not stable. This is most easily seen in the measured abundance of H_2, which initially increases from 20 °C to 150 °C, before a slight decrease is seen. However, some information of catalyst performance can be gleaned: the catalyst does not appear particularly active although there is some slight conversion of NO at higher temperatures. This is accompanied by a slight decrease in H_2 abundance and perhaps a slight increase in H_2O (H_2O has not been normalised, thus the presented values are not accurate and are included for completion). There also appears to be some formation of NH_3 at temperatures of 100 °C and above.

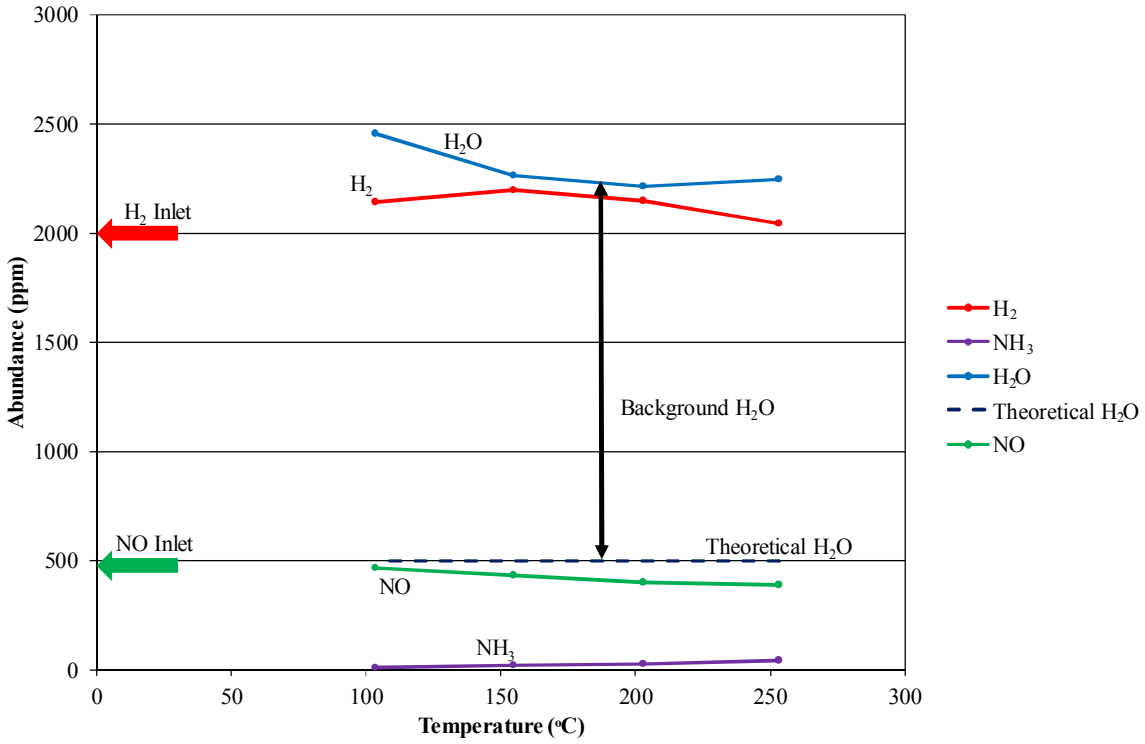

Figure 3.26 H_2–SCR, in the absence of oxygen, over 2.3 wt% Ag/Al_2O_3. Reaction conditions: 500 ppm NO, 2000 ppm H_2, balance N_2.

This experiment should be repeated, with the previously described process ensuring that the inlet concentration is adjusted at each temperature, enabling more accurate measurements.

3.4.4.2 Presence of O_2

As a reminder, as explained in Chapter 2, Section 2.4.3.1, in the presence of O_2 the following reactions are now expected:

$$2NO + 4H_2 + O_2 \rightarrow N_2 + 4H_2O \quad (2.15)$$

$$2NO + 3H_2 + O_2 \rightarrow N_2O + 3H_2O \quad (2.16)$$

$$2NO + H_2 \rightarrow N_2O + H_2O \quad (2.17)$$

$$NO + \frac{5}{2}H_2 \rightarrow NH_3 + H_2O \quad (2.18)$$

$$NO + \frac{1}{2}O_2 \rightarrow NO_2 \quad (2.19)$$

$$H_2 + \frac{1}{2}O_2 \rightarrow H_2O \quad (2.20)$$

The following flow rates were set and unaltered for the duration of the experiment (Table 3.11).

Table 3.11 Approximate gas mixture flow rates and ultimate inlet composition utilised during preliminary H_2–SCR investigations over 2.3 wt% Ag/Al_2O_3.

Gas Mixture	Flow Rate ($dm^3\ h^{-1}$)	Flow Rate ($cm^3\ min^{-1}$)	Composition
4000 ppm NO/N_2	3.29	55	500 ppm NO 2000 ppm H_2 5.0 % O_2 balance N_2
8000 ppm H_2/N_2	6.54	109	
Air	6.31	105	
N_2	10.36	173	
Total	26.5	442	

The catalysts were then heated at a rate of 5 $^oC\ min^{-1}$ up to 250 ^oC with a 1 h dwell at each 50 ^oC interval. Again, however the flow rates were set at the beginning of the experiment and not altered throughout. As has already been seen this may lead to drift and the alternative procedure, where the flow rates are adjusted if need be at each temperature, should be adopted in repeat experiments.

There are some trends which can be identified, even if absolute values may not be trusted:

- There is very little, if any change, in NO concentration throughout.
- At temperatures above 100 °C both H_2 and O_2 levels decrease. This is accompanied by an apparent increase in H_2O concentration, suggesting these two species are merely reacting together.
- There is little evidence of trace species although this may be a result of the experimental measurement procedure.

Perhaps Ag/Al_2O_3 is not a suitable material for this reaction, although it may be that the catalyst loading is not sufficient for the reaction conditions or that the investigated temperature window is too narrow. This will be explored in further experiments.

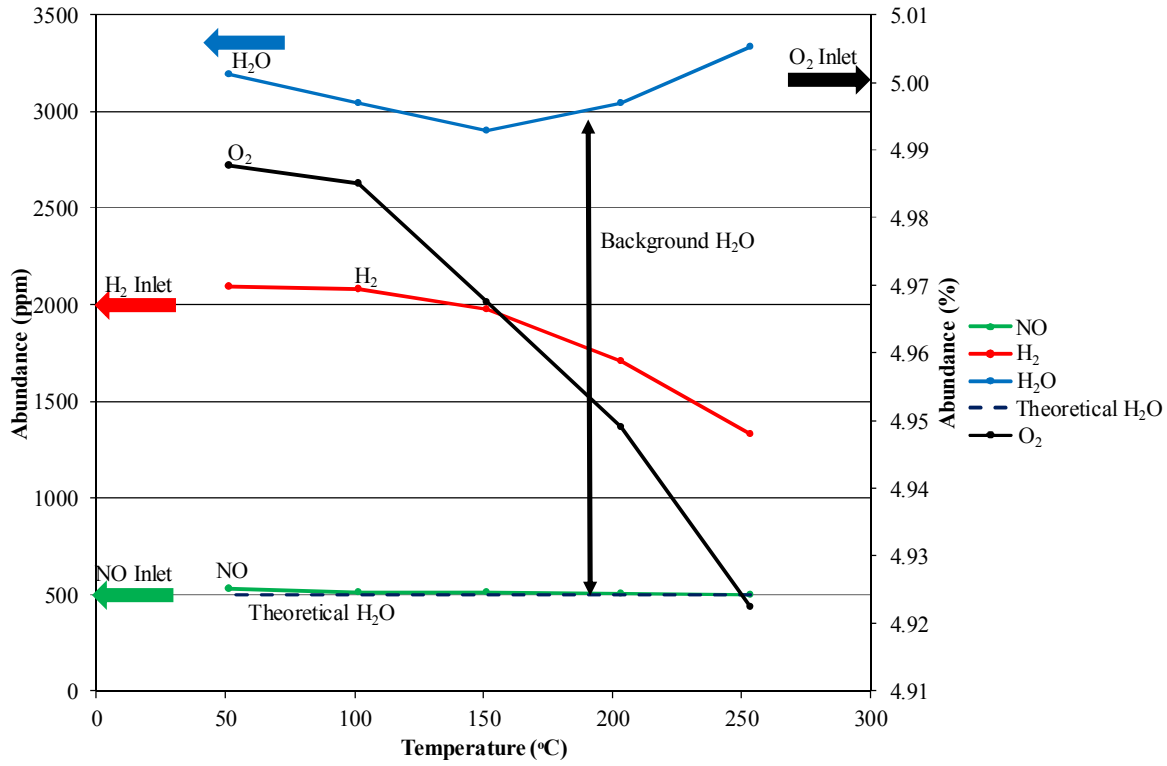

Figure 3.27 H_2–SCR over 2.3 wt% Ag/Al_2O_3 catalysts. Reaction conditions: 500 ppm NO, 2000 ppm H_2, 5 % O_2, balance N_2.

3.4.5 Identified Issues and Limitations

There are a number of issues with both the experimental procedure and experimental results, from both catalysts, which will need to be addressed in the future:

- Apparent presence of large amounts of H_2O in the reaction mixture – what impact is this having on the reaction and subsequent measurements? Given that it is a desired product of the H_2–SCR reaction, a large background reading could be masking the production of H_2O seen from the reaction and distorting the results.

- Apparent sensitivity of QMS procedure to trace species i.e. NO_2 and to a lesser extent NH_3.

3.4.6 Conclusions and Subsequent Actions Taken

These preliminary trials were very important to:

- Establish viable operation envelopes;

- Identify potential experimental problems and thereby find solutions so as to improve the experimental technique.

As a result of what has been discussed previously, a number of steps were implemented to improve the overall experimental method:

- Refinement of the method of calibrating the QMS in order to improve the accuracy in detecting NO_2 and NH_3.

- Investigation of possible methods of removing/reducing background H_2O levels.

3.5 H_2–SCR: Final Results

In this section the results of H_2–SCR experiments, performed over selected parameters identified through the preliminary experiments described in Section 3.4, are presented. The experimental set–up and general procedures explained in Section 3.3.1 remained the same whilst specific details of the different reaction sequences are provided before the results of each investigation.

Once again, although the reaction mixture compositions are specified, due to the nature of the equipment and the measurements it was not practical to consistently obtain these exact conditions and so they are provided as a guideline only. This also holds true for specified temperatures.

The challenges of producing a robust analytical method are well documented in Appendix I. Although every effort was made to produce a reliable and robust method; in some instances gentle manipulation of the data was required to negate erroneous 'background' readings and present a true reflection of species abundance, however, all results were processed in exactly the same fashion. Individually presented data points were calculated by averaging the measured raw signal from the mass spectrometer over a period of 5 minutes (typically ~6 – 8 data points) unless stated, after the system had equilibrated at constant temperature. The data points are connected to give an indication of trends and the connections do not represent recorded data. Where appropriate, arrows are utilised to highlight inlet conditions and identify which species correspond to which axis.

The catalysts were subject to the following standardised procedures. These first involved pre–treatment with the intention of removing any undesired surface species, before the catalysts were subject to the desired reaction mixtures and processes. The justifications for the procedures are provided within each description.

3.5.1 H_2–SCR

The reactor was loaded with three monolith pieces of the catalyst under investigation. First the samples were heated to 350 °C at a rate of 10 °C min^{-1} and subject to 8000 ppm H_2 in N_2 at a flow rate of 300 cm^3 min^{-1} for 1 h, before the reactor was then cooled to 50 °C. During cooling the gas flow was directed through the reactor bypass and an approximate gas composition consisting of 500 ppm NO, 2000 ppm H_2 and 5 % O_2 with a N_2 balance and a total flow rate of ~440 cm^3 min^{-1} (26.50 dm^3 h^{-1}) was set (Table 3.12). In this instance the desired gas composition was set using the QMS and thus only an approximate total flow rate is provided. Note that the reaction composition consisted of a smaller H_2:NO ratio (4:1) and/or a greater O_2 concentration than many of the examples discussed in Chapter 2. In addition, it was decided that as the composition of the exhaust fume in the final application would include a significant concentration of O_2, there was no benefit to exploring the H_2–SCR reaction in the absence of O_2.

Once the desired reactor temperature had been reached it was maintained for 1 h and the gas flow was directed through the reactor for 30 min before it was returned to the bypass. The temperature was then increased at a rate of 5 °C min^{-1} to a maximum temperature of 450 °C, and the procedure repeated at each 100 °C interval. This enabled the inlet and outlet of the reactor to be consecutively measured which in turn led to the identification and resolution of any drift in the inlet composition, producing somewhat constant inlet conditions at different temperatures. The maximum explored temperature was increased to 450 °C as in the preliminary experiments (Section 3.4) the Ag/Al_2O_3 catalyst demonstrated very little, if any, performance in the 50 – 250 °C range. Additionally, the operational exhaust temperature of the application of interest is around 450 °C and thus catalyst performance at this temperature is directly of interest.

Table 3.12 Approximate gas mixture flow rates and ultimate inlet composition utilised during final H_2–SCR investigations.

Gas Mixture	Flow Rate ($dm^3\ h^{-1}$)	Flow Rate ($cm^3\ min^{-1}$)	Composition
4000 ppm NO/N_2	3.29	55	500 ppm NO
8000 ppm H_2/N_2	6.54	109	2000 ppm H_2
Air	6.31	105	5.0 % O_2
N_2	10.36	173	balance N_2
Total	26.5	442	

3.5.1.1 Catalyst Substrate and Support

In order to correctly account for activity in terms of the components of the catalyst, it is important to first identify the behaviour of the substrate and support layers under SCR experimental conditions. As little activity is evident, these results will merely be summarised in an effort to minimise the number of graphs presented throughout this thesis.

3.5.1.1.1 Cordierite

The cordierite samples demonstrated no substantial reaction under SCR conditions up to a temperature of 450 ^{o}C; the supplied inlet conditions remained apparently unchanged although there was some detection of very low levels of N_2O ($\leq$10 ppm) and H_2O ($\leq$20 ppm) at temperatures of 200 ^{o}C and greater. There was also some formation of NO_2 ($\leq$ 5 ppm) at temperatures of 350 ^{o}C and greater.

3.5.1.1.2 γ–Al_2O_3

The γ–Al_2O_3 samples had an average loading of 29.6 wt% with respect to the complete catalyst system. They demonstrated no deNO_x reaction (consumption of NO) at temperatures up to 450 ^{o}C although there was consumption of H_2 and the formation of H_2O at temperatures of 200 ^{o}C and above. As there was no apparent reduction in the abundance of O_2 at these temperatures, it is postulated that the H_2 is reacting with surface O species. In addition there was no detection of trace species beyond very slight (~10 ppm) formation of N_2O at temperatures of 300 ^{o}C and above, although no apparent drop in NO levels.

3.5.1.2 Complete Catalyst Systems

3.5.1.2.1 Pt/Al_2O_3

As a reminder the Pt/Al_2O_3 catalyst was studied as an example of a typical H_2–SCR catalyst and preparation details can be found in Section 3.1.4.1. The catalysts had an average platinum loading of 0.8 wt% and an average γ–Al_2O_3 loading of 29.4 wt% with respect to the complete catalyst system. Finally, the potential reactions for H_2–SCR in the presence of O_2, first discussed in Chapter 2, Section 2.4.3.1, are as follows:

$$2NO + 4H_2 + O_2 \rightarrow N_2 + 4H_2O \quad (2.15)$$

$$2NO + 3H_2 + O_2 \rightarrow N_2O + 3H_2O \quad (2.16)$$

$$2NO + H_2 \rightarrow N_2O + H_2O \quad (2.17)$$

$$NO + \frac{5}{2}H_2 \rightarrow NH_3 + H_2O \quad (2.18)$$

$$NO + \frac{1}{2}O_2 \rightarrow NO_2 \quad (2.19)$$

$$H_2 + \frac{1}{2}O_2 \rightarrow H_2O \quad (2.20)$$

The measured abundances of both main and trace reactant species formed during H_2–SCR investigations over the Pt/Al_2O_3 catalyst are shown in Table 3.13, Figure 3.28(A) and Figure 3.28(B). Conversion of the supplied reactants is presented in Table 3.14 and Figure 3.29, whilst a breakdown of NO conversion to various N–species is presented in Table 3.15.

In general, a similar performance to the preliminary experiments on the same catalysts is observed (although following recalibration of the QMS the absolute values measured are more appropriate), demonstrating good repeatability between experiments. In addition, the results agree well with those reported for similar material and reaction condition combinations in the literature (e.g. Macleod *et al.* (2002)).

Table 3.13 Summary of measured species abundance in the outlet of H_2–SCR over 0.8 wt% Pt/Al_2O_3.

Temperature (°C)	Measured Outlet Concentration ppm							%
	NO	H_2	H_2O	NO_2	N_2O	NH_3	Apparent N_2	O_2
50.8	70	317	1541	0	83	2	166	5.3
155.2	341	0	1807	70	2	2	72	4.9
255.3	68	0	1638	257	0	2	98	4.8
355.2	178	0	1764	201	0	2	68	4.7
456.6	407	0	1864	71	0	2	24	4.9

Table 3.14 Summary of reactant conversion during H_2–SCR over 0.8 wt% Pt/Al_2O_3.

Temperature (°C)	Conversion (%)		
	NO	H_2	O_2
50.8	87.6	84.7	0.2
155.2	39.3	100.0	2.0
255.3	86.9	100.0	10.5
355.2	65.6	100.0	6.4
456.6	22.8	100.0	3.9

Table 3.15 Summary of NO conversion during H_2–SCR over 0.8 wt% Pt/Al_2O_3.

Temperature (°C)	Conversion of NO (%)				
	Overall	NO to NO_2 (oxidation)	NO to N_2O (reduction)	NO to NH_3 (reduction)	NO to N_2 (reduction)
50.8	87.6	0.0	29.0	0.4	58.3
155.2	39.3	12.5	0.7	0.4	25.7
255.3	86.9	49.2	0.0	0.4	37.3
355.2	65.6	38.9	0.0	0.4	26.3
456.6	22.8	13.5	0.0	0.3	8.9

The main observations of this investigation are summarised below:

- Two local 'maxima' of NO conversion (~87 %) were observed at 50 ^{o}C and 250 ^{o}C.

- Significant formation (+70 ppm) of NO_2 occurs at temperatures of 150 ^{o}C and higher, with a maximum of 257 ppm formed at 250 ^{o}C.

- N_2O was only produced (83 ppm) at 50 ^{o}C.

- The presence of O_2 in the reaction mixture inhibits NH_3 formation (in agreement with the preliminary results for this catalyst system), as stated by Liu *et al.* (2012). Although very small amounts of NH_3 are detected (2 ppm), these may be regarded as erroneous and attributed to the contribution of H_2O at 17 amu (as discussed in Appendix I) due to its presence in significant quantities.

- Complete conversion of H_2 occurs at temperatures above 50 ^{o}C. Whilst some of this is involved in NO_x reduction to N_2 and N_2O, the excess H_2 reacts with oxygen over the catalyst to form H_2O.

- In terms of selectivity towards NO reduction and oxidation, the NO conversion to reduction products (N_2, N_2O and NH_3) versus NO conversion to oxidation products (NO_2) data is presented in Table 3.15 and Figure 3.30. It can be clearly observed that NO reduction dominates at lower temperatures. However, as the temperature increases NO oxidation becomes increasingly significant, until it is more prevalent than NO reduction processes at temperatures of 250 ^{o}C and above.

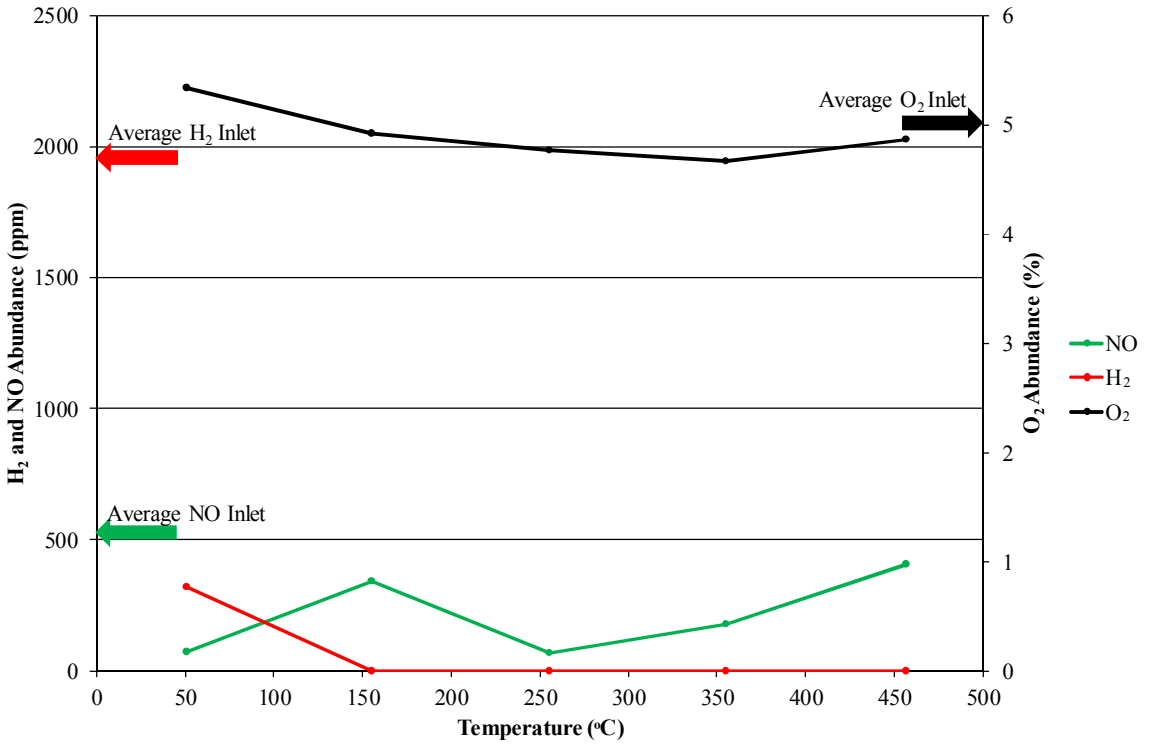

Figure 3.28(A) H_2–SCR (main species) over 0.8 wt% Pt/Al_2O_3. Reaction conditions: 500 ppm NO, 2000 ppm H_2, 5 % O_2, balance N_2.

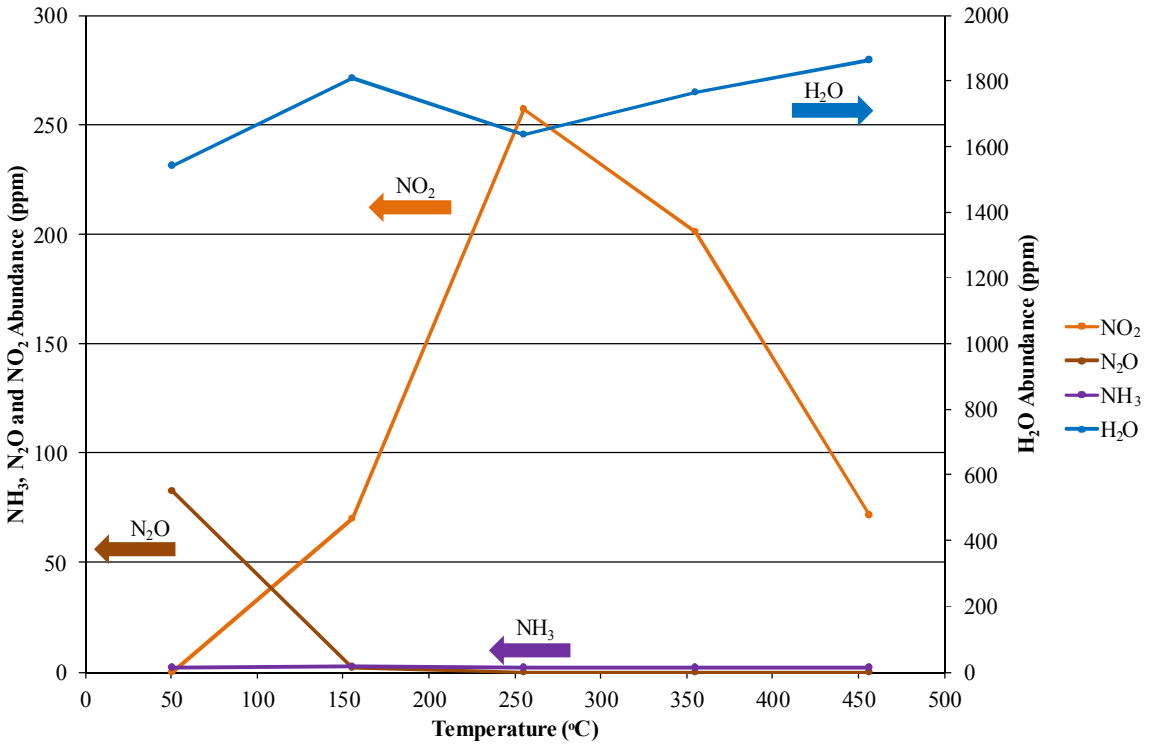

Figure 3.28(B) H_2–SCR (trace species) over 0.8 wt% Pt/Al_2O_3. Reaction conditions: 500 ppm NO, 2000 ppm H_2, 5 % O_2, balance N_2.

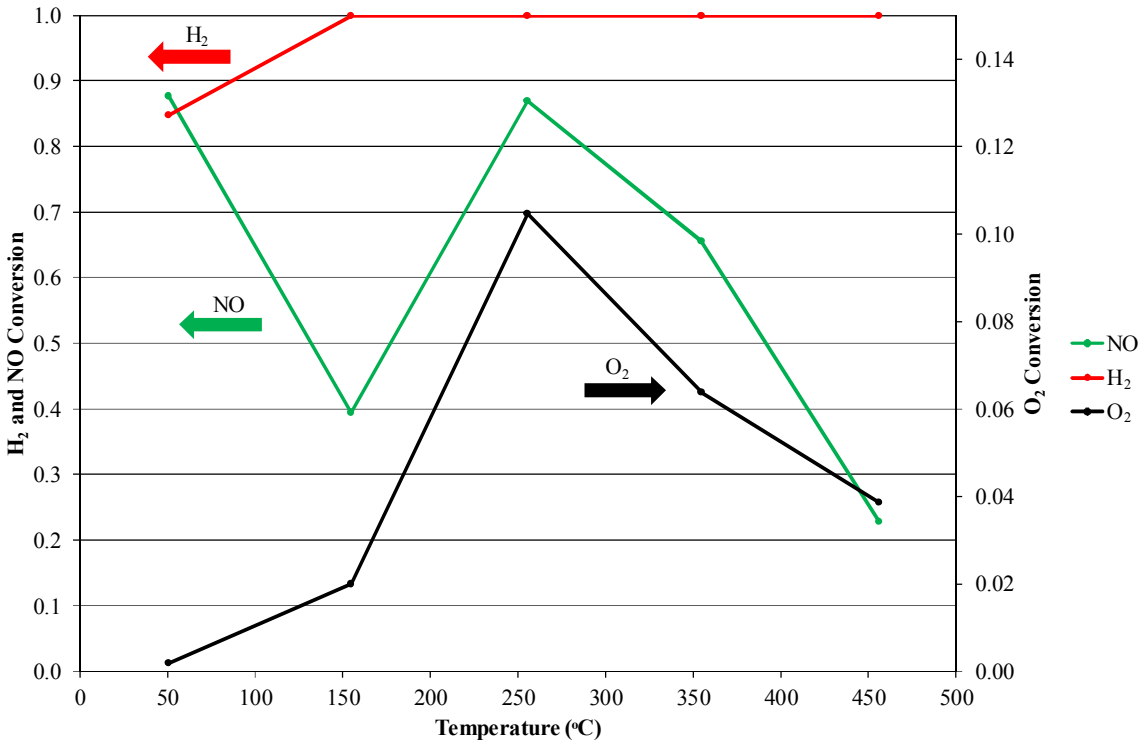

Figure 3.29 H_2–SCR (conversion) over 0.8 wt% Pt/Al_2O_3. Reaction conditions: 500 ppm NO, 2000 ppm H_2, 5 % O_2, balance N_2.

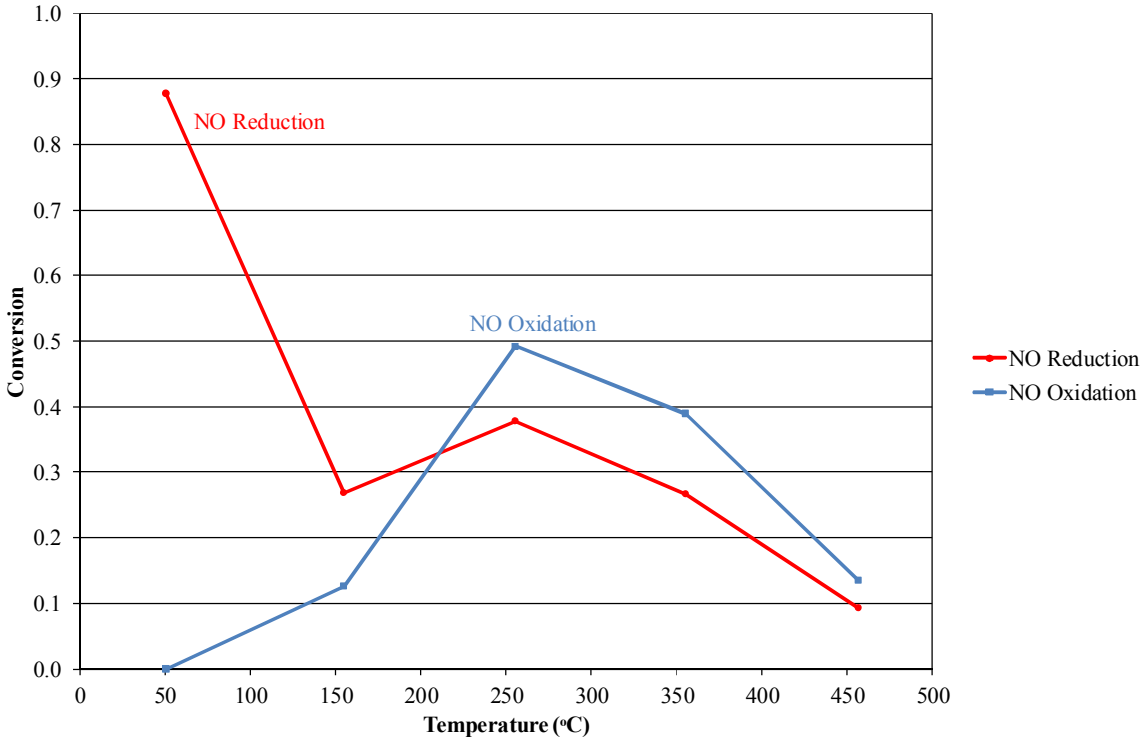

Figure 3.30 Temperature profiles for NO Reduction (●) and NO oxidation (■) over 0.8 wt% Pt/Al_2O_3. Reaction conditions: 500 ppm NO, 2000 ppm H_2, 5 % O_2, balance N_2.

3.5.1.2.2 Ag/Al_2O_3

As a reminder Ag/Al_2O_3 is being explored as a potential novel H_2–SCR catalyst. Full details of the catalyst preparation can be found in Section 3.1.4.2. The catalysts had an average silver loading of 2.3 wt% and an average γ–Al_2O_3 loading of 28.9 wt% with respect to the complete catalyst system. Once more, the potential reactions for H_2–SCR in the presence of O_2, first discussed in Chapter 2, Section 2.4.3.1, are as follows:

$$2NO + 4H_2 + O_2 \rightarrow N_2 + 4H_2O \quad (2.15)$$

$$2NO + 3H_2 + O_2 \rightarrow N_2O + 3H_2O \quad (2.16)$$

$$2NO + H_2 \rightarrow N_2O + H_2O \quad (2.17)$$

$$NO + \frac{5}{2}H_2 \rightarrow NH_3 + H_2O \quad (2.18)$$

$$NO + \frac{1}{2}O_2 \rightarrow NO_2 \quad (2.19)$$

$$H_2 + \frac{1}{2}O_2 \rightarrow H_2O \quad (2.20)$$

The measured abundance of both main and trace reactant species formed during H_2–SCR investigations over the 2.3 wt% Ag/Al_2O_3 are displayed in Table 3.16, Figure 3.31(A) and Figure 3.31(B). The measured conversions of the reactant species are displayed in Table 3.17 and Figure 3.32 and a breakdown of NO conversion to various N–species is displayed in Table 3.18. Once again the obtained results closely resemble those of the preliminary experiments and suggest good repeatability.

Table 3.16 Summary of measured species abundance in the outlet of H_2–SCR over 2.3 wt% Ag/Al_2O_3.

Temperature (°C)	Measured Outlet Concentration ppm							%
	NO	H_2	H_2O	NO_2	N_2O	NH_3	Apparent N_2	O_2
50.8	578	2111	0	0	2	0	0	5.3
155.2	562	1869	356	0	1	0	5	5.2
255.3	554	57	2091	7	2	1	0	4.9
355.2	397	0	2032	63	0	1	21	4.8
456.6	421	0	2051	52	0	1	18	4.9

Table 3.17 Summary of reactant conversion during H_2–SCR over 2.3 wt% Ag/Al_2O_3.

Temperature (°C)	Conversion (%)		
	NO	H_2	O_2
50.8	0.0	0.0	0.0
155.2	2.2	15.5	0.8
255.3	0.0	97.5	2.0
355.2	21.3	100.0	4.0
456.6	17.7	100.0	3.7

Table 3.18 Summary of NO conversion during H_2–SCR over 2.3 wt% Ag/Al_2O_3.

Temperature (°C)	Conversion of NO (%)				
	Overall	NO to NO_2 (oxidation)	NO to N_2O (reduction)	NO to NH_3 (reduction)	NO to N_2 (reduction)
50.8	0.0	0.0	0.6	0.0	0.0
155.2	2.2	0.0	0.4	0.0	1.8
255.3	0.0	1.2	0.6	0.3	0.0
355.2	21.3	12.6	0.0	0.3	8.5
456.6	17.7	10.2	0.0	0.3	7.2

The main observations of this investigation are summarised below:

- There is very little performance observed at temperatures up to 250 °C beyond H_2 and O_2 consumption and the accompanying formation of H_2O. Consumption of H_2 begins at 150 °C (15.5 % conversion), reaching 97.5 % conversion at 250 °C and 100 % by 350 °C.

- At lower temperatures (<350 °C) there is no obvious consumption of NO beyond very slight (2.2 %) conversion at 150 °C.

- At higher temperatures (≥350 °C) there is some consumption of NO (21.3 % at 350 °C, 17.7 % at 450 °C) although this is also accompanied by formation of NO_2 (63 ppm at 350 °C, 52 ppm at 450 °C).

- Again, although very small amounts of NH_3 are detected (1 ppm) at temperatures of 250 °C and higher, these may be regarded as erroneous and attributed to the contribution of H_2O at 17 amu (Appendix I).

- There is only very slight (1 – 2 ppm) apparent formation of N_2O at lower temperatures (≤250 °C) only.

- O_2 consumption generally increases as temperature increases and may be attributed to the increasing formation of both H_2O and NO_2.

- In a similar manner to the Pt/Al_2O_3 performance (although the relative conversions are a lot less in this instance) there is an indication that NO reduction is slightly favoured at lower temperatures, whereas NO oxidation is preferred at higher temperatures.

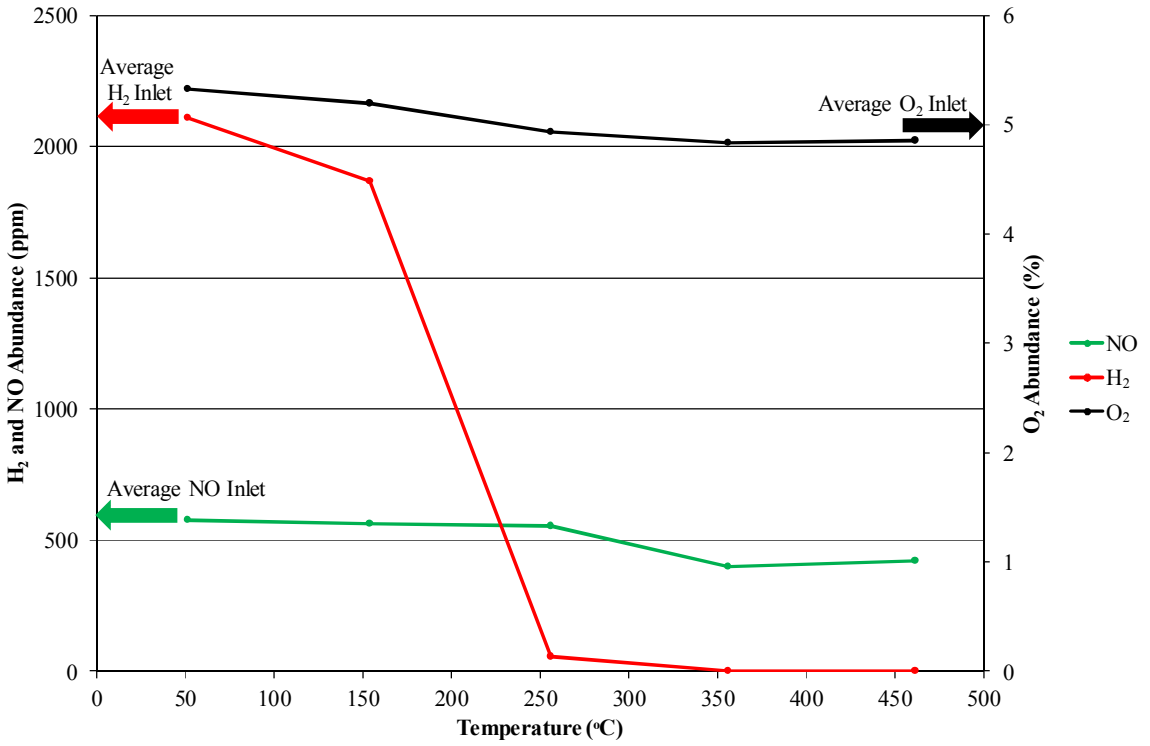

Figure 3.31(A) H_2–SCR (main species) over 2.3 wt% Ag/Al_2O_3. Reaction conditions: 500 ppm NO, 2000 ppm H_2, 5 % O_2, balance N_2.

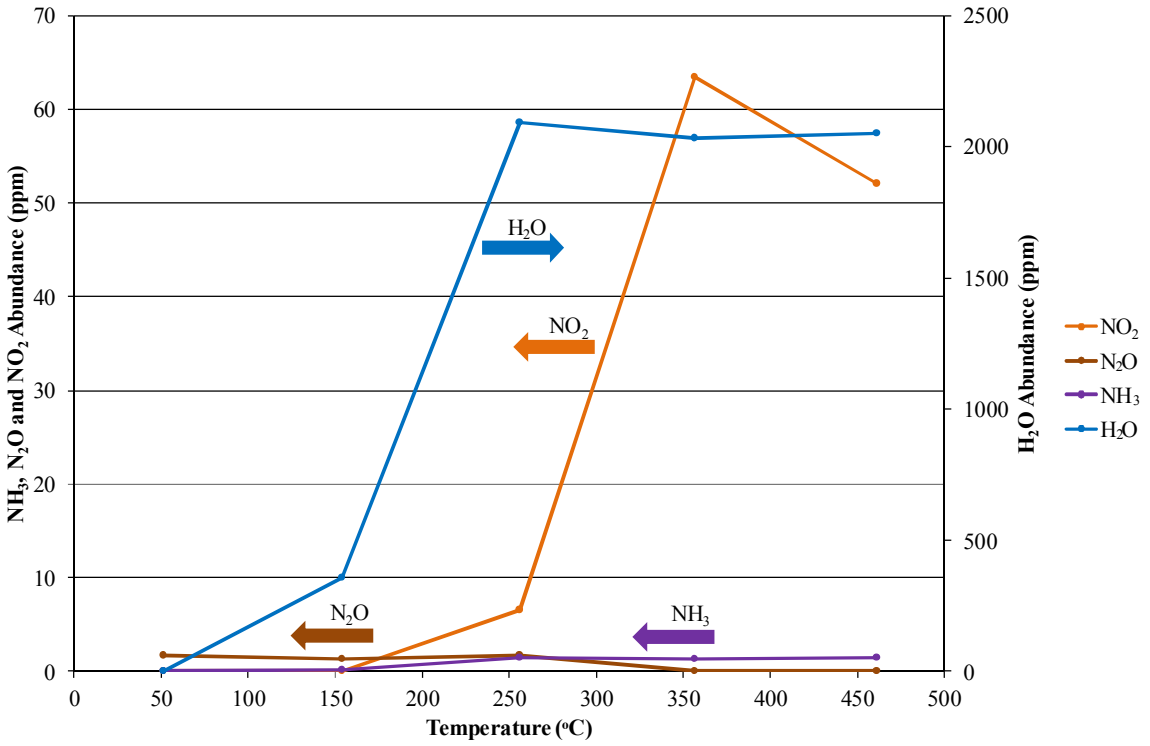

Figure 3.31(B) H_2–SCR (trace species) over 2.3 wt% Ag/Al_2O_3. Reaction conditions: 500 ppm NO, 2000 ppm H_2, 5 % O_2, balance N_2.

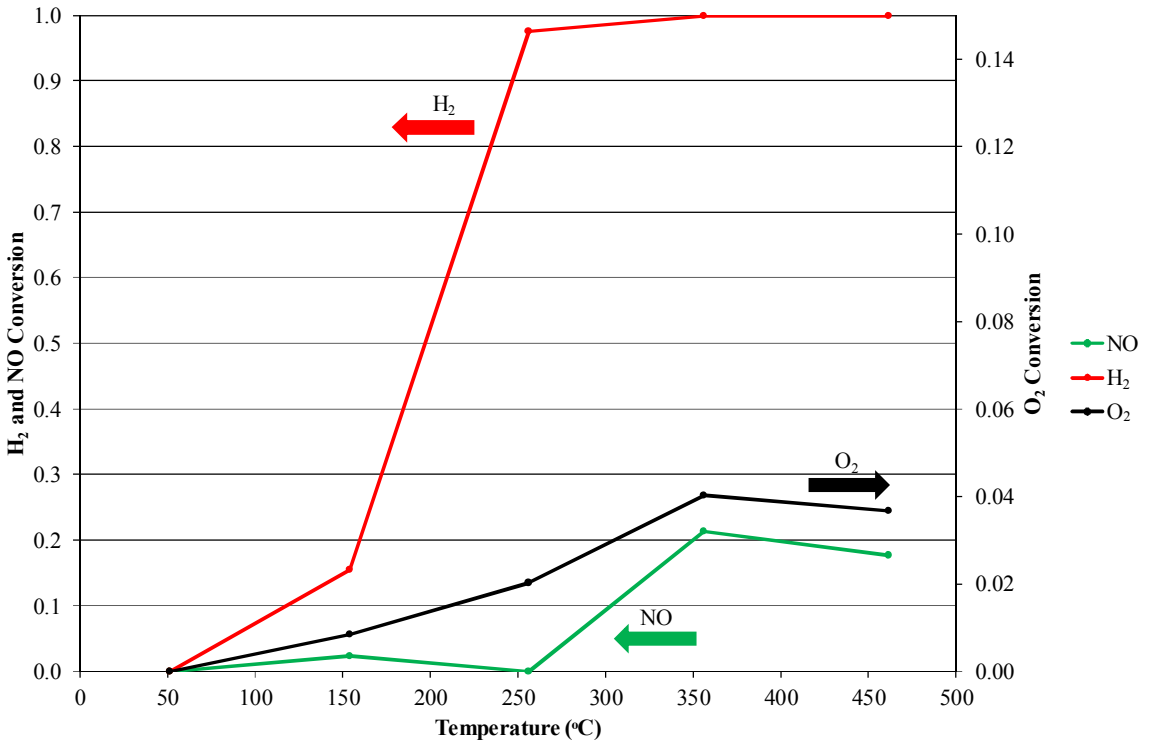

Figure 3.32 H_2–SCR (conversion) over 2.3 wt% Ag/Al_2O_3 catalysts. Reaction conditions: 500 ppm NO, 2000 ppm H_2, 5 % O_2, balance N_2.

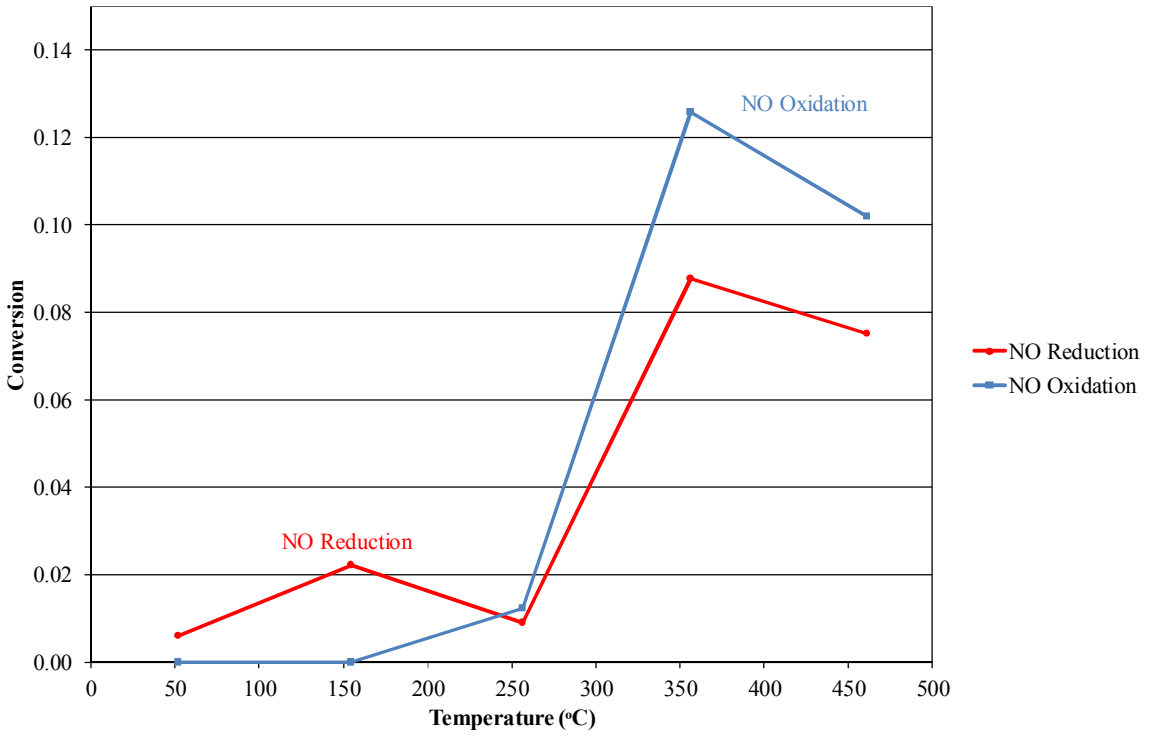

Figure 3.33 Temperature profiles for NO Reduction (●) and NO oxidation (■) over 2.3 wt% Ag/Al_2O_3. Reaction conditions: 500 ppm NO, 2000 ppm H_2, 5 % O_2, balance N_2.

3.5.1.3 H_2–SCR Conclusions

Although the obtained traces have been discussed in detail throughout presentation of the results, a number of overall conclusions can be made with regards to the SCR reaction investigations when considering the complete data sets. In addition, these conclusions do align with the results of the preliminary study:

- The cordierite substrate demonstrated no reaction.
- The γ–Al_2O_3 washcoat demonstrated no significant deNO_x reaction.
- 50 ^oC appears to be the most suitable temperature for direct NO_x reduction using H_2 over Pt/Al_2O_3, although there is a significant level of N_2O formed (itself a potent greenhouse gas) and at higher temperatures, formation of NO_2 dominates.
- It appears that Ag/Al_2O_3 is not a suitable material for direct reduction of NO_x using H_2. NO conversion was very limited throughout the explored temperature range and favoured oxidation to NO_2 as opposed to reduction to N_2.

Pt/Al_2O_3 is well known as an oxidation catalyst, even in the oxidation of NO as explored by Xue *et al.* (1996). The significant oxidation of NO at higher temperatures demonstrated here illustrates how it may be possible to utilise this process to produce an optimum ratio of NO and NO_2, which could then be exploited in a NO_x after treatment system. Indeed this approach is already practised in some exhaust after treatment processes and is proposed in Chapter 1 (Figure 1.2).

3.5.2 TPD

TPD measurements of adsorbed species were carried out in order to investigate the catalyst's abilities to adsorb different reactant species and identify any evidence of surface reactions at particular temperatures.

3.5.2.1 NO–TPD

The reactor was loaded with three monolith pieces of the catalyst under investigation. The reactor temperature was increased to 500 ^{o}C at a rate of 10 ^{o}C min^{-1} under a flow of N_2 at 300 cm^3 min^{-1}. Then 8000 ppm H_2 in N_2 was introduced at 300 cm^3 min^{-1} for 30 min, before the reactor was flushed with N_2 at 330 cm^3 min^{-1} for 15 min. The catalysts were then subject to 10 % O_2 at 600 cm^3 min^{-1} for 15 min before being cooled down in N_2 at 330 cm^3 min^{-1} to 150 ^{o}C. 1000 ppm NO in N_2 was then introduced at 400 cm^3 min^{-1} for 30 min. Finally the reactor was flushed with N_2 at 300 cm^3 min^{-1} for 15 min to remove any residual NO and the temperature increased to 700 ^{o}C at a rate of 10 ^{o}C min^{-1}. The desorbed species were subsequently measured.

3.5.2.1.1 Catalyst Substrate and Support

3.5.2.1.1.1 Cordierite

In light of the H_2–SCR results described in Section 3.5.1.1.1, TPD experiments were not performed on the cordierite substrate.

3.5.2.1.1.2 γ–Al_2O_3

In keeping with the results of the SCR experiment there was no apparent NO adsorption (and thus no desorption) witnessed during NO–TPD studies. It should be noted these early studies confirm that the quartz wool, utilised to prevent gas slip down the sides of the catalyst (as described in Section 3.3.1), plays no part in the investigated reactions.

3.5.2.1.2 Complete Catalyst Systems

3.5.2.1.2.1 Pt/Al_2O_3

The measured desorption species for NO–TPD over 0.8 wt% Pt/Al_2O_3 is presented in Figure 3.34. The main observations of this investigation are summarised below:

- The catalysts demonstrate some affinity for NO, as desorption of NO is apparent over the 175 – 350 ^oC temperature range.
- There is also some apparent formation of NO_2 at 150 ^oC, perhaps as a result of the reaction of surface O species with the supplied NO, and its subsequent desorption as temperature was increased to 350 ^oC.
- There was no N_2O formation observed.
- The apparent total abundance of the evolved N–species accounts for only 46.1 % of the adsorbed NO.

Table 3.19 details the selectivity in terms of the observed N–species which evolved during NO–TPD over 0.8 wt% Pt/Al_2O_3. The formation of NO_2 demonstrates some consistency with the H_2–SCR results presented in Figure 3.28(A) and Figure 3.28(B) (formation of NO_2 at 150 °C).

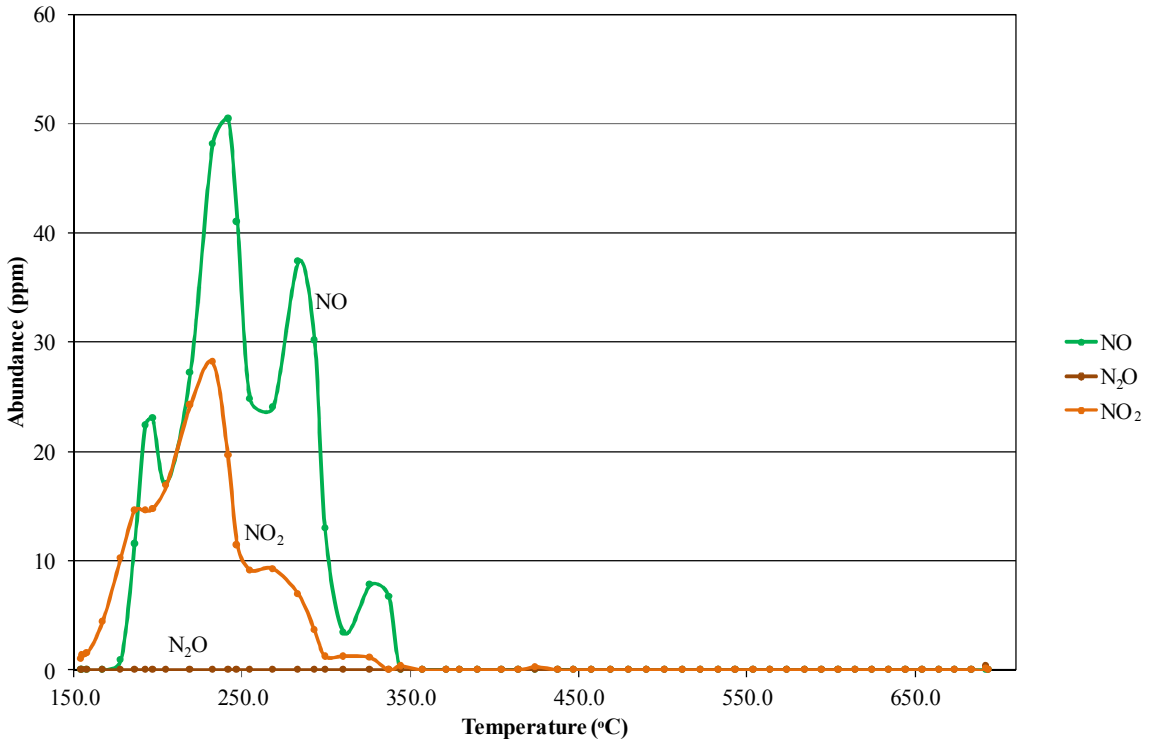

Figure 3.34 NO–TPD over 0.8 wt% Pt/Al_2O_3. Adsorption temperature = 150 °C.

Table 3.19 Proportion of the N–containing species desorbed during NO–TPD over 0.8 wt% Pt/Al_2O_3.

Species	% of desorption products
NO	66.5
NO_2	33.5

3.5.2.1.2.2 Ag/Al_2O_3

The measured desorption species for NO–TPD over 2.3 wt% Ag/Al_2O_3 is presented in Figure 3.35. The main observations of this investigation are summarised below:

- Overall, there is very little affinity demonstrated for NO although there is some desorption of NO at lower temperatures (reaching a maximum recorded concentration of 25 ppm at 200 ^oC).
- Again there is also some formation of NO_2, and subsequent desorption at lower temps, although it is of the order of 2 – 4 ppm.
- Interestingly there is some formation of N_2O and a consistent, very low desorption concentration (1 – 2 ppm) of N_2O from ~200 ^oC up to a maximum of 7 ppm at ~590 ^oC.
- The apparent total abundance of the evolved N–species accounts for only 32.9 % of the adsorbed NO.

Table 3.20 details the selectivity in terms of the observed N–species which evolved during NO–TPD over 0.8 wt% Pt/Al_2O_3.

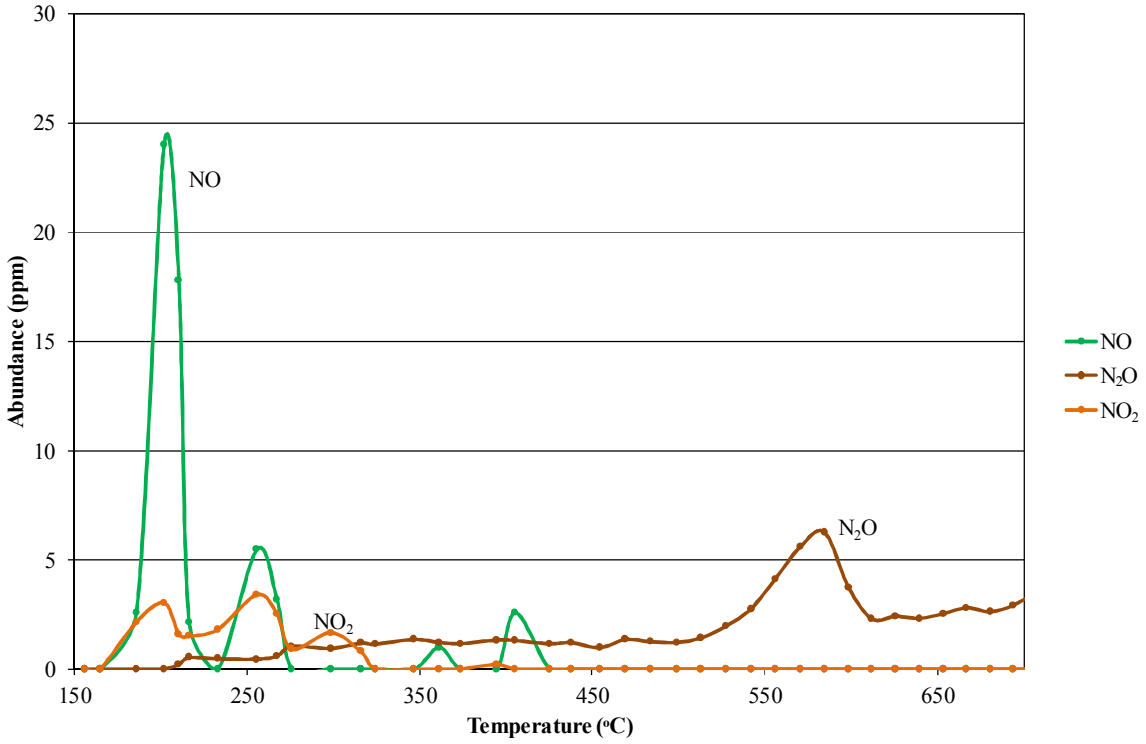

Figure 3.35 NO–TPD over 2.3 wt% Ag/Al_2O_3 catalysts. Adsorption temperature = 150 °C.

Table 3.20 Proportion of the N–containing species desorbed during NO–TPD over 2.3 wt% Ag/Al_2O_3.

Species	% of desorption products
NO	41
N_2O	45.1
NO_2	13.9

3.5.2.2 H_2–TPD

The reactor was loaded with three monolith pieces of the catalyst under investigation. The reactor temperature was increased to 500 ^oC at a rate of 10 ^oC min^{-1} under a flow of N_2 at 300 cm^3 min^{-1} and then cooled to 200 ^oC, the adsorption temperature. 2000 ppm H_2 in N_2 was introduced at 440 cm^3 min^{-1} for 5 min, before the reactor was flushed with N_2 at 330 cm^3 min^{-1} for 5 min. The temperature was then increased to 500 ^oC at a rate of 5 ^oC min^{-1} and then 700 ^oC at a rate of 10 ^oC min^{-1} and the desorbed species were subsequently measured. The slower temperature ramp rate to 500 ^oC was imposed in an effort to identify desorbed species.

However, although the preliminary investigated H_2–TPD procedure (Chapter 4) did provide some evidence of H_2 affinity for a $Ba/Pt/Al_2O_3$ catalysts, and the adsorption temperature was increased as a result, there was no apparent desorption observed for any the catalyst materials investigated in this Section and as a result, there will be no presentation of H_2–TPD results here.

3.5.2.3 TPD Conclusions

Although the obtained traces have been discussed in detail throughout the presentation of the results, a number of overall conclusions can be made with regards to the TPD reaction investigations when comparing the results obtained from both complete catalyst systems.

These conclusions relate to the NO–TPD summary information presented in Table 3.21 and Table 3.22:

- There was no affinity to NO demonstrated during TPD investigations with γ–Al_2O_3.
- The NO–TPD behaviour of both Pt/Al_2O_3 and Ag/Al_2O_3 catalyst at 150 ^oC appeared to align with the observed H_2–SCR results at the same reaction temperature in terms of the demonstrated affinity for NO.
- Pt/Al_2O_3 demonstrated the greatest affinity for NO at an adsorption temperature of 150 ^oC. However, adsorption levels appear low in comparison to supplied amounts; 2.8 – 4.1 %.
- In the absence of supplied O_2 during adsorption and desorption, both catalysts demonstrated some capacity for formation of other N–species; NO_2 formation in the case of Pt/Al_2O_3 and both N_2O and NO_2 formation in the case of Ag/Al_2O_3.

In terms of the H_2–TPD investigations, there may be a number of explanations for the absence of adsorption demonstrated:

- Incorrect adsorption temperature.
- The change in partial pressure once the H_2 inlet feed is stopped results in desorption of lightly adsorbed surface H_2 during flushing of the reactor.
- Possible surface reaction not observed through the experimental procedure i.e. formation of H_2O or NH_3.

Table 3.21 Summary table detailing the relative measured amounts of NO adsorbed and subsequently desorbed during NO–TPD investigations.

Catalyst	NO–TPD	
	Relative amount of NO adsorbed (%)	Relative amount of N–species desorbed (%)
Pt/Al_2O_3	4.1	46.1
Ag/Al_2O_3	2.8	32.9

Table 3.22 Summary table detailing the relative proportion of each N–species desorbed during NO–TPD investigations.

Catalyst	NO–TPD Proportion (%)		
	NO	N_2O	NO_2
Pt/Al_2O_3	66.5	–	33.5
Ag/Al_2O_3	41.0	45.1	13.9

3.5.3 Key Conclusions

In light of the results obtained for the explored materials in both SCR and TPD investigations, a number of key conclusions can be drawn which in turn influenced the next stage of the project:

- The developed methods for preparation of the investigated catalysts proved successful and may be applied to related systems.
- The constructed experimental set–up was successfully operated, providing the desired reaction conditions at a variety of temperatures.
- The catalyst systems were robust, demonstrating repeatable performance after multiple experimental runs during both preliminary and final investigations.
- Both Pt/Al_2O_3 and Ag/Al_2O_3 do not appear to be suitable catalyst systems for H_2–SCR of NO_x to N_2 within the explored temperature range; an alternative deNO_x approach is required.
- However, the ability to form NO_2 through the oxidation of NO was displayed by both catalyst systems at a variety of temperatures (although predominantly at the higher end of the explored temperature range), and in both investigated processes.
- Such oxidation behaviour is necessary for a successful NSR catalyst as described in Chapter 2 (Section 2.4.3.4). It is envisaged that the SCR materials explored here may form the basis for NSR catalysts, and by coupling with various ‘storage components’ their activity may be explored.

REFERENCES

Barrett, E. P., Joyner, L. G., et al. (1951). The Determination of Pore Volume and Area Distributions in Porous Substances. I. Computations from Nitrogen Isotherms. Journal of the American Chemical Society, Vol. 73, No. 1, pp. 373–380.

Bennett, C. (1990). Monolith Reactors for Automobile Catalysts. PhD Thesis, Department of Chemical Engineering, University of Bath, Bath.

Brinker, C. J. and Scherer, G. W. (1990). Sol–gel Science: The Physics and Chemistry of Sol–gel Processing. Academic Press. p. 600.

Brunauer, S., Emmett, P. H., et al. (1938). Adsorption of Gases in Multimolecular Layers. Journal of the American Chemical Society, Vol. 60, No. 2, pp. 309–319.

Buschow, K. H. J., Cahn, R. W., et al. (2001). Encyclopedia of Materials – Science and Technology. Elsevier. pp. 4673–4674.

Castoldi, L., Lietti, L., et al. (2010). The NO_x Storage–reduction on Pt–K/Al_2O_3 Lean NO_x Trap Catalyst. Journal of Catalysis, Vol. 276, No. 2, pp. 335–350.

British Standards Institution (2008) Determination of the Specific Surface Area of Solids by Gas Adsorption – BET Method.

Doronkin, D. E., Fogel, S., et al. (2012). Study of the "Fast SCR" – like Mechanism of H_2–assisted SCR of NO_x with Ammonia over Ag/Al_2O_3. Applied Catalysis B: Environmental, Vol. 113–114, No. 0, pp. 228–236.

Forzatti, P. (2001). Present Status and Perspectives in De–NO_x SCR Catalysis. Applied Catalysis A: General, Vol. 222, No. 1–2, pp. 221–236.

Hayes, R. E. and Kolaczkowski, S. T. (1997). Introduction to Catalytic Combustion. Gordon and Breach Science Publisher. pp. 30–38.

Klinghoffer, A. A., Cerro, R. L., et al. (1998). Catalytic Wet Oxidation of Acetic Acid Using Platinum on Alumina Monolith Catalyst. Catalysis Today, Vol. 40, No. 1, pp. 59–71.

Kobayashi, M. and Hagi, M. (2006). V_2O_5–WO_3/TiO_2–SiO_2–SO_4^{2-} Catalysts: Influence of Active Components and Supports on Activities in the Selective Catalytic Reduction of NO by NH_3 and in the Oxidation of SO_2. Applied Catalysis B–Environmental, Vol. 63, No. 1–2, pp. 104–113.

Kolaczkowski, S., Ye, S., et al. (2012). Transient Experiments on a Full–scale DOC – Methodology and Techniques to Support Modelling. Catalysis Today, Vol. 188, No. 1, pp. 53–61.

Lachman, I. M. and Williams, J. L. (1992). Extruded Monolithic Catalyst Supports. Catalysis Today, Vol. 14, No. 2, pp. 317–329.

Li, J., Wu, G. J., et al. (2012). NO Selective Reduction by Hydrogen Over Bimetallic Pd–Ir/TiO_2 Catalyst. Catalysis Communications, Vol. 24, pp. 38–43.

Liu, Z., Li, J., et al. (2012). Recent Advances in the Selective Catalytic Reduction of NO_x by Hydrogen in the Presence of Oxygen. Energy & Environmental Science, Vol. 5, No. 10, pp. 8799–8814.

Macleod, N. and Lambert, R. M. (2002). Lean NO_x Reduction with CO + H_2 Mixtures over Pt/Al_2O_3 and Pd/Al_2O_3 Catalysts. Applied Catalysis B: Environmental, Vol. 35, No. 4, pp. 269–279.

Plummer, H. K., Jr, R. J., et al. (1999). Measurement of Automotive Catalyst Washcoat Loading Parameters by Microscopy Techniques. Microscopy and Microanalysis, Vol. 5, No. 4, pp. 267–281.

Sing, K. S. W., Everett, D. H., et al. (1985). Reporting Physisorption Data for Gas Solid Systems with Special Reference to the Determination of Surface–area and Porosity (Recommendations 1984) Pure and Applied Chemistry, Vol. 57, No. 4, pp. 603–619.

Xue, E., Seshan, K., et al. (1996). Roles of Supports, Pt Loading and Pt Dispersion in the Oxidation of NO to NO_2 and of SO_2 to SO_3. Applied Catalysis B: Environmental, Vol. 11, No. 1, pp. 65–79.

Yap, Y. H. (2010). Characterisation of a Diesel Oxidation Catalyst. PhD Thesis, Department of Chemical Engineering, University of Bath, Bath.

CHAPTER 4

Experimental – Investigation of Reaction Mechanisms and Transient Behaviour of H_2–NSR Catalysts in a Continuous Flow Fixed Bed Reactor

In a similar manner to Chapter 3; the processes through which active materials for the H_2–NSR investigation were prepared and characterized will be detailed. Preliminary experimental results, obtained through commissioning of the experimental set–up and analysis technique, along with final results of the chosen materials performance will be presented and discussed.

4.1 Catalyst Preparation

4.1.1 Summary

A reminder of the summary flow diagram of the catalysts prepared in this project, and their associated deNO_x process, is presented in Figure 4.1. Note that only the NSR catalysts, indicated with a solid black line, are considered within this chapter.

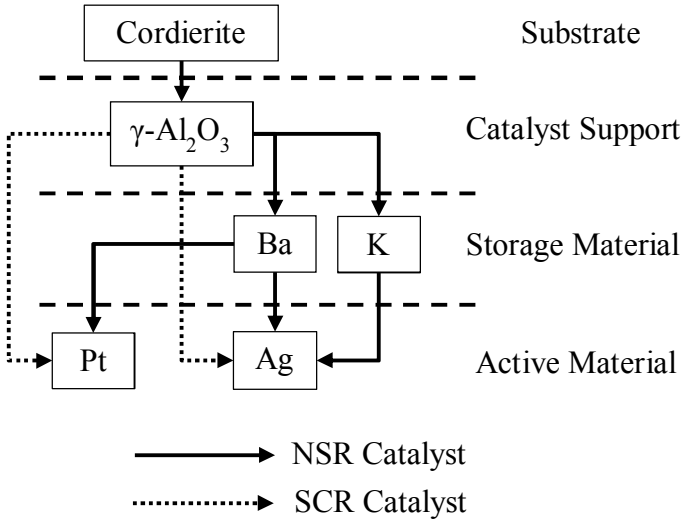

Figure 4.1 Schematic describing the make–up of catalyst materials prepared for investigation.

Table 4.1 Summary of selected references consulted during development of NSR catalyst preparation methods.

Catalyst	Reference(s)
Pt	Klinghoffer *et al.* (1998)
Ag	Doronkin *et al.* (2012)
Ba	Cant *et al.* (2002), Han *et al.* (2001)
K	Castoldi *et al.* (2010)

The NSR catalysts explored in this section were typically prepared in a similar manner to the SCR catalysts as described in Chapter 3, (Section 3.1) and some examples of detailed synthesis procedures can also be found in Appendix II. The references consulted when constructing the preparation methods are listed in Table 4.1.

4.1.2 Storage Components

As discussed in Chapter 2; an NSR catalyst requires a 'storage component' to facilitate temporary storage of the NO_x species during the 'lean period' before subsequent reduction on exposure to a H_2–rich feed. Ba and K are most commonly reported NSR storage components and thus were investigated here, although there are several other examples; Sakamoto *et al.* (2012) also investigated Na as a storage component, and Roy *et al.* (2009) reported that Mg, Ca, and Sr have also been explored.

In preparation of NSR catalysts, two separate steps are required to load both the storage component and the active component on to the γ–Al_2O_3 washcoat. It was found that the order of addition of components to the washcoated monoliths was significant. In cases where the 'storage' component was first loaded on to the sample; during the subsequent step, as the monoliths were submerged in the active component solutions, a reaction occurred, and it appeared that the storage component layer was removed from the catalyst. On such occasions a deposit was formed in the bottom of the beaker. This was confirmed through weighing of the catalyst samples.

Thus all NSR catalysts reported in the study were first coated with the active metal component i.e. Pt or Ag, calcined, and then coated with the storage component i.e. Ba or K. In these cases, the order in which the catalyst components are displayed denotes the order in which they were applied to the cordierite substrate i.e. Ba/Pt/Al_2O_3 reading from left to right indicates that the Ba component was last to be applied after the Pt component, and that the Al_2O_3 washcoat was applied first. This rule holds true for all multi–component catalysts reported in this study.

Whilst it is reported that a particular metal species e.g. Ba, is being supported on the catalysts it is likely in fact that it is a related species which is actually deposited. For example, in the case of the barium component, it is likely that BaO would be formed through the described experimental procedure. Further, on exposure to air these BaO species may undergo reaction to form $Ba(OH)_2$, or $BaCO_3$. The same can be said for the other metal components, although the exact nature of the species formed depends on the particular metal. In some cases it is known that these species participate in the reactions.

However, the experimental procedures, in particular the pre–treatment processes, are designed as such that only the surface species desired for reaction will be present during experimental trials and subsequently reported. For this reason the titles given to different catalysts in this study will detail the desired metal component only, and not any oxides or other related species.

4.1.2.1 Barium

With consideration of the catalyst preparation procedures detailed in Cant *et al.* (2002) and Han *et al.* (2001); barium nitrate was dissolved in water and the monoliths were submerged for 30 min. Once removed from the solution the monoliths were placed in a ceramic dish and dried at 120 ^{o}C overnight (18 h) before they were calcined at 550 ^{o}C for 4 h. This coating procedure was repeated twice to produce a mass loading considered adequate. The appearance of the monolith samples (Figure 4.2) was not vastly changed from that of the γ–Al_2O_3 monolith samples (detailed in Chapter 3), with perhaps a brighter white coating apparent in places. Specific details of an example barium coating procedure is provided in Appendix II–C.

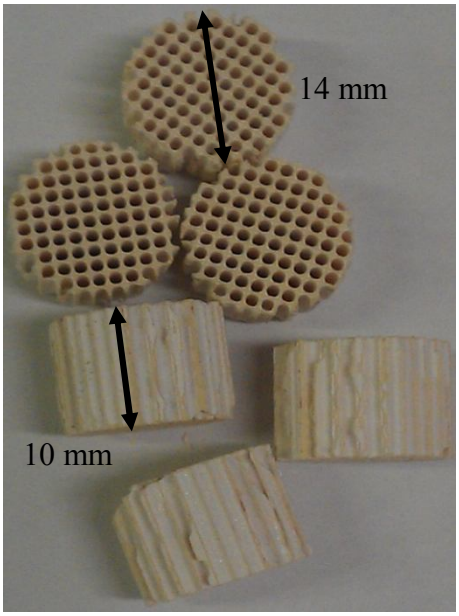

Figure 4.2 Photograph of 3.6 wt% Ba/Al_2O_3 coated monolith samples.

4.1.2.2 Potassium

With reference to the preparation procedure detailed in Castoldi *et al.* (2010); potassium acetate was dissolved in water. The monoliths were submerged in the solution for 30 min. Once removed from the solution the monoliths were placed in a ceramic dish and dried at 120 °C overnight (19 h) before they were calcined at 500 °C for 4 h. The monoliths generally now had a slight grey colour (Figure 4.3) although some parts appeared black – this may be explained by the samples close proximity to the furnace wall during calcination, or it could indicate poor dispersion of the potassium species. Specific details of an example potassium coating procedure is provided in Appendix II–D.

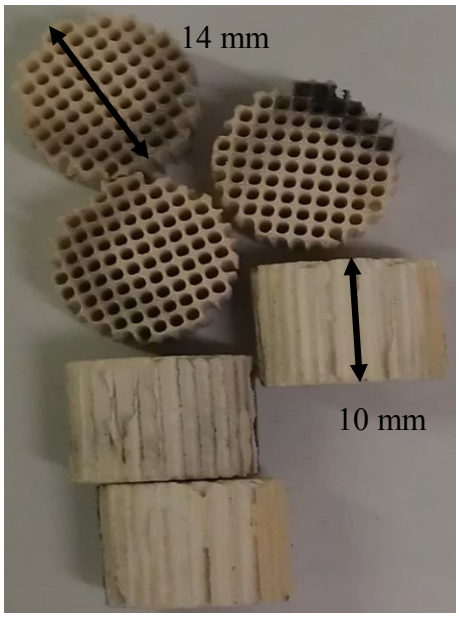

Figure 4.3 Photograph of 19.2 wt% K/Al_2O_3 coated monolith samples.

4.1.3 Active Components

As a reminder, the preparation of the platinum catalysts in this study was with a view to comparing results to the literature and validating the experimental procedures. Silver was chosen as an active component due to its performance in related deNO_x processes (e.g. H_2–assisted HC–SCR), and its history of redox chemistry, i.e. perhaps it is capable of facilitating both the reducing and oxidising reactions necessary in the NSR processes, although silver catalyst performance has not been reported for direct H_2–SCR, or H_2–NSR processes.

4.1.3.1 Ba/Pt/Al_2O_3

The platinum component was loaded on to the catalysts in the same manner as described in Chapter 3, Section 4.1.4.1 and with reference to the procedure detailed in Klinghoffer *et al.* (1998). Following addition of both platinum and then barium to the γ–Al_2O_3 samples, the catalysts were dark grey in colour (Figure 4.4). Specific details of an example platinum coating procedure is provided in Appendix II–A.

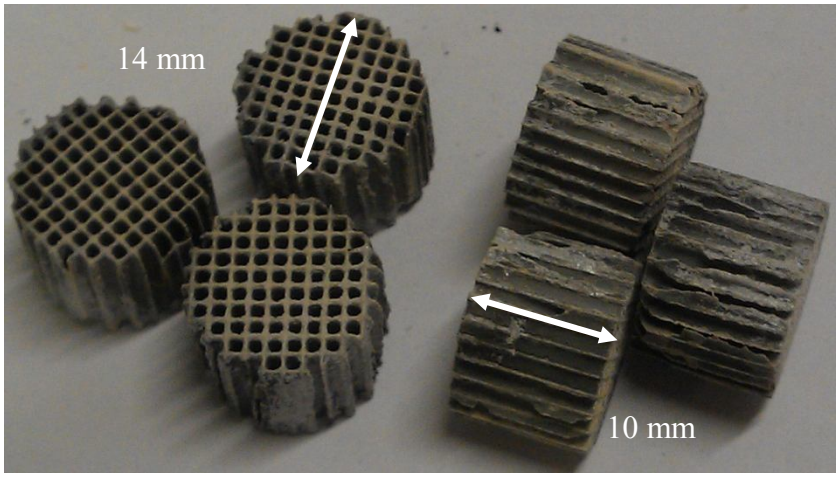

Figure 4.4 Photograph of Ba/Pt/Al_2O_3 coated monolith samples.

4.1.3.2 $Ba/Ag/Al_2O_3$ and $K/Ag/Al_2O_3$

The silver component was loaded on to the catalysts in the same manner as described in Chapter 3, Section 4.1.4.2 and with consultation of the procedure described in Doronkin *et al.* (2012). Silver nitrate was dissolved in water in order to produce a solution of ~2 wt% silver. The monoliths were submerged in the solution for 2 h. Once removed from the solution the monoliths were placed in a ceramic dish and dried overnight (19 h) at room temperature before they were calcined at 550 °C for 4 h. The prepared $Ba/Ag/Al_2O_3$ catalysts were grey whilst the prepared $K/Ag/Al_2O_3$ catalysts were a dark grey in colour (Figure 4.5). Specific details of an example silver coating procedure is provided in Appendix II–B.

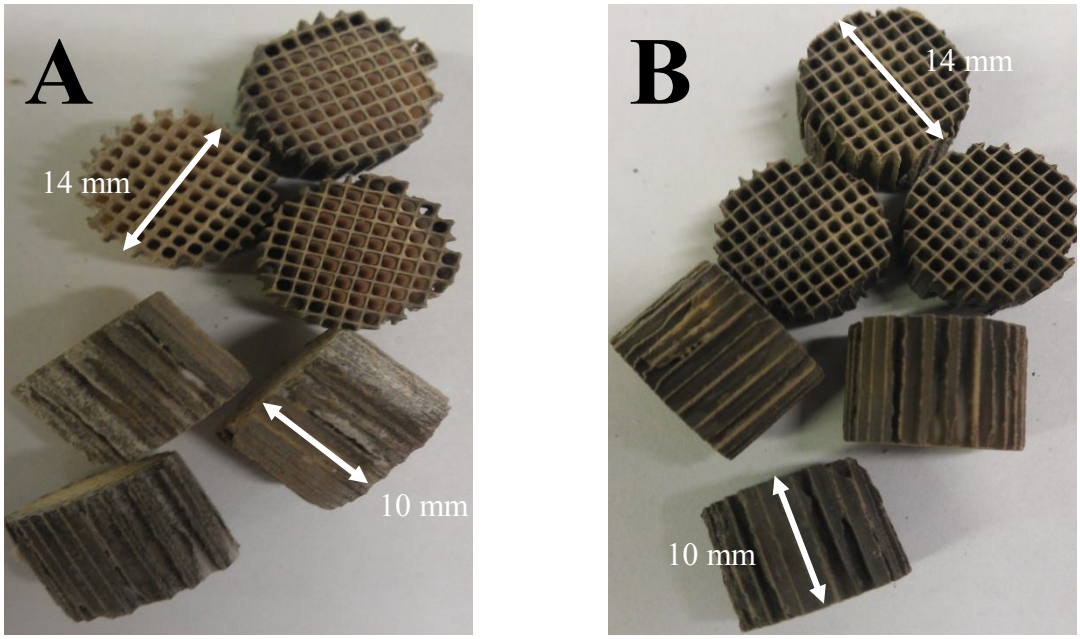

Figure 4.5 Photograph of (A) $Ba/Ag/Al_2O_3$ and (B) $K/Ag/Al_2O_3$ coated monolith samples.

4.2 Catalyst Characterisation

Details of catalyst characterisation procedures are presented in Chapter 3. Only the results of the NSR catalyst characterisation will be presented here.

4.2.1 Weight Measurements

The specified loadings in Table 4.2 are reported with respect to the entirety of the catalyst makeup i.e. the combined weight of the substrate, washcoat and any active components present.

Table 4.2 Details of prepared H_2–NSR catalyst loadings.

Catalyst	Average Values		
	Washcoat Loading (%)	Metal 1 Loading (%)	Metal 2 Loading (%)
γ–Al_2O_3	29.6	–	–
Ba/Al_2O_3	28.5	3.6	–
K/Al_2O_3	23.9	19.2	–
$Ba/Pt/Al_2O_3$	28.2	0.2 (Pt)	4.7 (Ba)
$Ba/Ag/Al_2O_3$	27.6	1.8 (Ag)	5.0 (Ba)
$K/Ag/Al_2O_3$	24.3	2.1 (Ag)	16.0 (K)

4.2.2 Nitrogen Adsorption Analysis

A summary of the N_2 adsorption analysis conducted on the H_2–NSR catalysts is presented in Table 4.3. In addition, the observations made for the SCR catalysts in terms of N_2 isotherm shape (Chapter 3, Section 1.2.3.4) also hold true for the NSR catalysts although they will not be discussed here.

Table 4.3 Calculated BET surface area and BJH average pore diameter of H_2–NSR catalyst samples.

Catalyst	Mass of Sample (g)	Attributable Coating Mass (g)	Reported BET Surface Area ($m^2\ g^{-1}$)	BET Surface Area based on Coating ($m^2\ g^{-1}$)	BJH Adsorption Average Pore Diameter (nm)
γ–Al_2O	0.4319	0.1279	37.74	127.41	9.4536
Ba/Al_2O_3	0.5128	0.1650	31.38	97.53	10.5480
K/Al_2O_3	0.5755	0.2482	20.20	46.85	11.7794
$Ba/Pt/Al_2O_3$	0.3901	0.1290	34.65	104.74	10.4184
$Ba/Ag/Al_2O_3$	0.4303	0.1479	32.72	95.23	11.8416
$K/Ag/Al_2O_3$	0.5706	0.2417	22.20	52.40	13.4750

4.3 H_2–NSR: A Preliminary Set of Experiments

In this section experiments are performed over selected initial parameters, in order to explore the different processes and identify potential limitations and exploitations. Utilising the equipment previously described in Chapter 3 (Section 3.3) the experiments generally consisted of the desired gas mixtures alternatively being supplied (through use of a solenoid valve) to the catalysts, whilst they were being held at a defined temperature. The samples were subject to a number of different sequences, depending on the type of investigation being undertaken e.g. NSR, TPD or TPSR. For the preliminary results details of the different reaction sequences are provided before the results of each individual experiment.

Once again, it should be acknowledged that the reaction mixture compositions and reaction temperatures specified during procedure or results descriptions are quoted to enable direct comparison between different catalyst samples and thus there will be an element of deviation from the quoted values depending on the experiment. However, the realised inlet compositions and reaction temperatures will be displayed in plots and tables without adjustment. In addition, the raw measurements presented here subsequently influenced further calibration of the QMS as described in Appendix I, and as such, the parameters detailed in Appendix I do not necessary correlate to those utilised to obtain measurements presented in this section.

Presented data points are connected to give an indication of trends and the connections do not represent recorded data. Where appropriate, arrows are utilised to highlight inlet conditions and identify which species concentration corresponds to which axis.

Finally, these results are not considered absolute and a detailed breakdown and analysis of final results will be presented in Section 4.4. The purpose of these initial experiments was to identify any shortcomings and allow optimisation of the experimental procedure, as well as gain an indication of catalyst performance (which allowed for greater accuracy in QMS calibration). As a result there are subtle differences between the detailed procedures for experimentation and analysis and these are highlighted throughout description of the results.

4.3.1 Aims and Objectives

NSR experiments will investigate the ability of the prepared catalyst materials to:

- Convert NO species to other N–containing species in the presence and absence of O_2 during the 'lean' phase and temporarily 'store' the created N–containing species.
- Provide a platform for the reduction of the stored N–containing species with H_2 during the 'rich' phase.
- Selectively form the desired products on reaction of the stored N–containing species with H_2.

Adsorption/desorption tests and TPD measurements of adsorbed species will be carried out in order to investigate the catalysts abilities to adsorb different species and identify any evidence of surface reactions at particular temperatures.

4.3.2 Predicted Outcomes

4.3.2.1 NSR Studies

Taking into account the sorption and reaction pathways previously discussed in Chapter 2 (Section 2.4.3.4) it is possible to make predictions in terms of the shape of the obtained NSR experimental plots (Figure 4.6):

Firstly, it may be expected that on switching to a particular 'phase' (rich or lean) there would be a delay seen before 'breakthrough' of the reactant species (NO or H_2). This would be due to NO_x storage and subsequent reduction respectively and eventually, in the absence of any further reaction, the outlet concentration of these species would reach the inlet concentration. Additionally a decrease in O_2 concentration may be expected during the initial stages of each lean phase and production of H_2O seen during initial stages of each rich phase. There may also be some production of other undesired species at various points e.g. NO_2 or N_2O during the lean phase and NH_3 during the rich phase, depending on the properties of the catalyst.

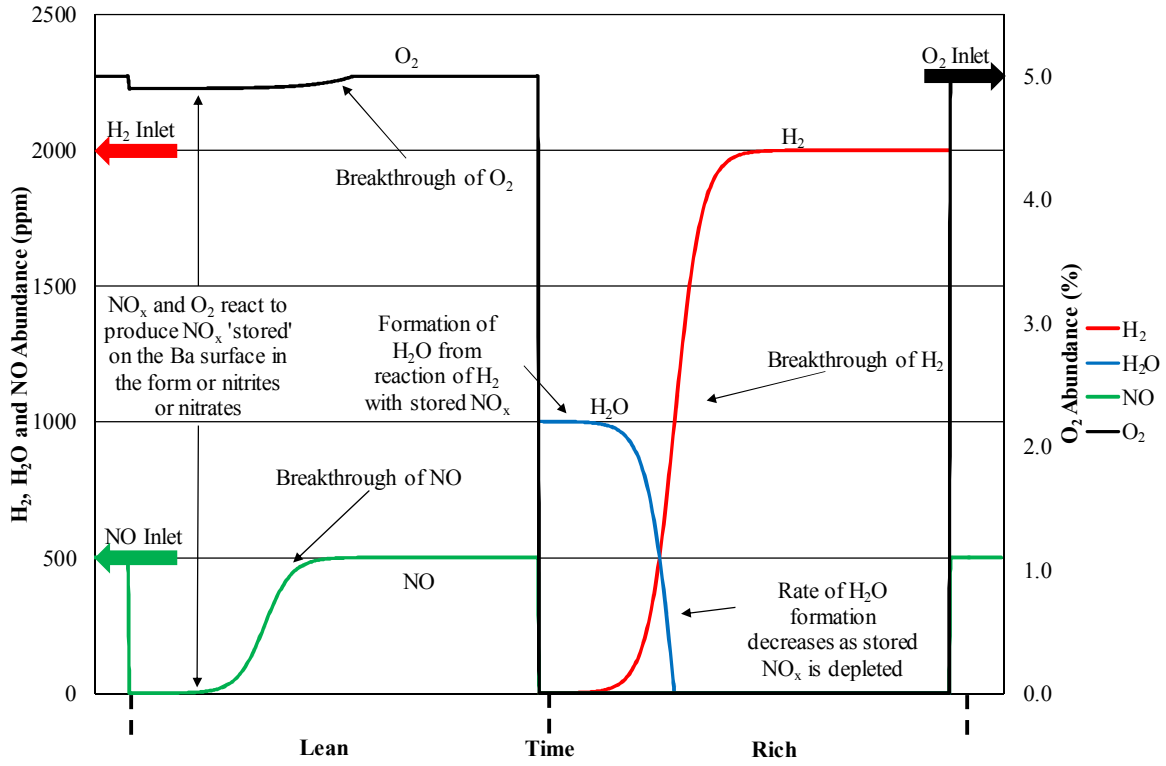

Figure 4.6 Expected shape of the NSR experimental plots.

The overall desired reactions for each period are described in the equations that follow, and the actual sorption and reduction mechanisms were already discussed earlier (Chapter 2, Section 2.4.3.4):

Lean periods:

$$BaO + 2NO + \frac{1}{2}O_2 \rightarrow Ba(NO_2)_2 \qquad (4.1)$$

$$BaO + 2NO + \frac{3}{2}O_2 \rightarrow Ba(NO_3)_2 \qquad (4.2)$$

Rich periods:

$$Ba(NO_2)_2 + 3H_2 \rightarrow BaO + N_2 + 3H_2O \qquad (4.3)$$

$$Ba(NO_3)_2 + 5H_2 \rightarrow BaO + N_2 + 5H_2O \qquad (4.4)$$

However, there are also potential undesired reactions that form unwanted by–products, such as those discussed in Roy *et al.* (2009):

$$Ba(NO_3)_2 + 3H_2 \rightarrow BaO + 2NO + 3H_2O \quad (4.5)$$

$$Ba(NO_3)_2 + 4H_2 \rightarrow BaO + N_2O + 4H_2O \quad (4.6)$$

$$Ba(NO_3)_2 + 8H_2 \rightarrow BaO + 2NH_3 + 5H_2O \quad (4.7)$$

It is also expected, as is reported in the literature, that the catalysts will require conditioning i.e. they must undergo several rich and lean cycles, before they produce a repeatable performance.

Finally, it is necessary to attempt to design the experiments such that any observed adsorption or desorption processes are associated with surface chemistry and not merely the change in bulk gas composition. This is discussed by Lietti *et al.* (2001) who state that the sequence of phases in their transient experiments was designed in an attempt to separate the effects associated with adsorption and desorption merely caused by changes in gas compositions, from those associated with surface chemical reactions.

4.3.2.2 TPD/TPSR Studies

It is expected that every material will have some affinity for each reactant. Due to the storage component of the NSR materials it is perhaps expected that they will demonstrate a greater affinity for NO than the SCR catalysts.

4.3.3 $Ba/Pt/Al_2O_3$

The $Ba/Pt/Al_2O_3$ catalyst was studied as an example of a typical NSR catalyst and to confirm the NSR experimental approach. The catalysts were prepared in house by impregnating supplied alumina coated monoliths, first with an aqueous platinum solution and secondly with an aqueous barium solution. Synthesis details can be found in Section 4.1. The catalysts had an average platinum loading of 0.2 wt%, an average barium loading of 4.7 wt% and an average γ–Al_2O_3 loading of 28.2 wt% with respect to the complete catalyst system.

4.3.3.1 NSR Studies

The reactor was loaded with three $Ba/Pt/Al_2O_3$ monolith pieces. The temperature was increased to 350 ^oC at 10 ^oC min^{-1} and the catalyst reduced under 8000 ppm H_2 in N_2 at a flow rate of ~300 cm^3 min^{-1} for 1 h. This initial reduction was conducted after reference to Nova *et al.* (2006), who found that because their experiments were performed in the absence of CO_2, and regeneration was carried out with H_2 or by heating, this led to the transformation of $BaCO_3$, which was originally present on the calcined samples (presumably as a result of the preparation process) into BaO and $Ba(OH)_2$. The temperature was maintained whilst the following compositions were approximately set using the reactor bypass (Table 4.4). They were unaltered for the duration of the experiment. The conditions were alternatively cycled, for periods of 25 min each and the raw data is presented in Figure 4.7.

Table 4.4 Approximate gas mixture flow rates and ultimate inlet compositions utilised during preliminary H_2–NSR investigations over $Ba/Pt/Al_2O_3$.

Sequence	Gas Mixture	Flow Rate ($dm^3\ h^{-1}$)	Flow Rate ($cm^3\ min^{-1}$)	Composition
Lean	4000 ppm NO/N_2	3.31	55	500 ppm NO 2.5 % O_2 balance N_2
	Air	3.32	55	
	N_2	19.88	331	
	Total	26.50	441	
Rich	8000 ppm H_2/N_2	6.62	110	2000 ppm H_2 balnce N_2
	N_2	19.88	331	
	Total	26.50	441	

There were a number of issues which arose from the above plot. Firstly, although three cycles have been undertaken there are still slight differences in the final two consecutive cycles and conceivably more lean/rich sequences are required to achieve consistent behaviour. It is also apparent that during the reaction both NO and H_2 abundances do not reach their inlet values (maximum NO outlet: 195 ppm and maximum H_2 outlet: 1648 ppm during the last cycle) and thus surface reactions must be occurring to account for this.

Addressing the 'lean' cycle; there is a short delay before breakthrough of NO and an initial drop in O_2 concentration. This may be considered the NO_x storage period (where NO_x is adsorbed and stored as nitrates and nitrites) before saturation of the catalyst surface is reached. However, the increase in NO is accompanied by formation, and sharp rise in abundance, of NO_2. Indeed the NO_2 levels reach in excess of 1000 ppm which given the inlet concentration of NO is only ~500 ppm, seems inaccurate. This phenomenon (formation of great quantities of NO_2) was also seen during the preliminary H_2–SCR trials over Pt/Al_2O_3 and again highlights the shortcomings of the preliminary analysis method. There was also some formation of N_2O observed during each 'lean' period.

A similar delay in breakthrough of H_2 is seen during 'rich' periods. Concurrently there is large formation of H_2O which drops off as the H_2 level increases. It may be postulated that the H_2 is reacting with stored NO_x species and forming H_2O (Equation 4.4) as there is no N–species observed during the 'lean' periods. However it is also known that Pt/Al_2O_3 promotes the direct reaction of H_2 and O_2 at this temperature (Chapter 3, Section 3.5.1) and although there is no O_2 supplied during the 'rich' period, the formation of H_2O may be a result of the reaction of H_2 with surface O–species. There is also a significant background reading of H_2O, as previously observed during the preliminary H_2–SCR trials and again this suggests the analysis method requires refinement. Additionally, in this experiment NH_3 was not measured (it was not included in the analysis method) but this may be a side product at this point and should be investigated in future experiments.

The formation of H_2O is also accompanied by an increase in temperature, as can be seen in Figure 4.8, which includes the raw data abundances of selected species and accompanying reactor inlet and outlet temperatures, and Table 4.5 which includes measured reactor temperatures averaged over a 60 s period. Throughout the experiment it appears that the reactor outlet temperature is greater than the reactor inlet and this is particularly true at the beginning of each period (where the data presented in the table is sampled from). This suggests exothermic reactions are taking place over the catalyst, thus providing the identified temperature difference. In addition, the reactor temperature is generally hotter during the rich periods. Note: the sinusoidal shape of the temperature plots may be attributed to the operation of the furnace which 'pulses' in order to maintain the set point temperature.

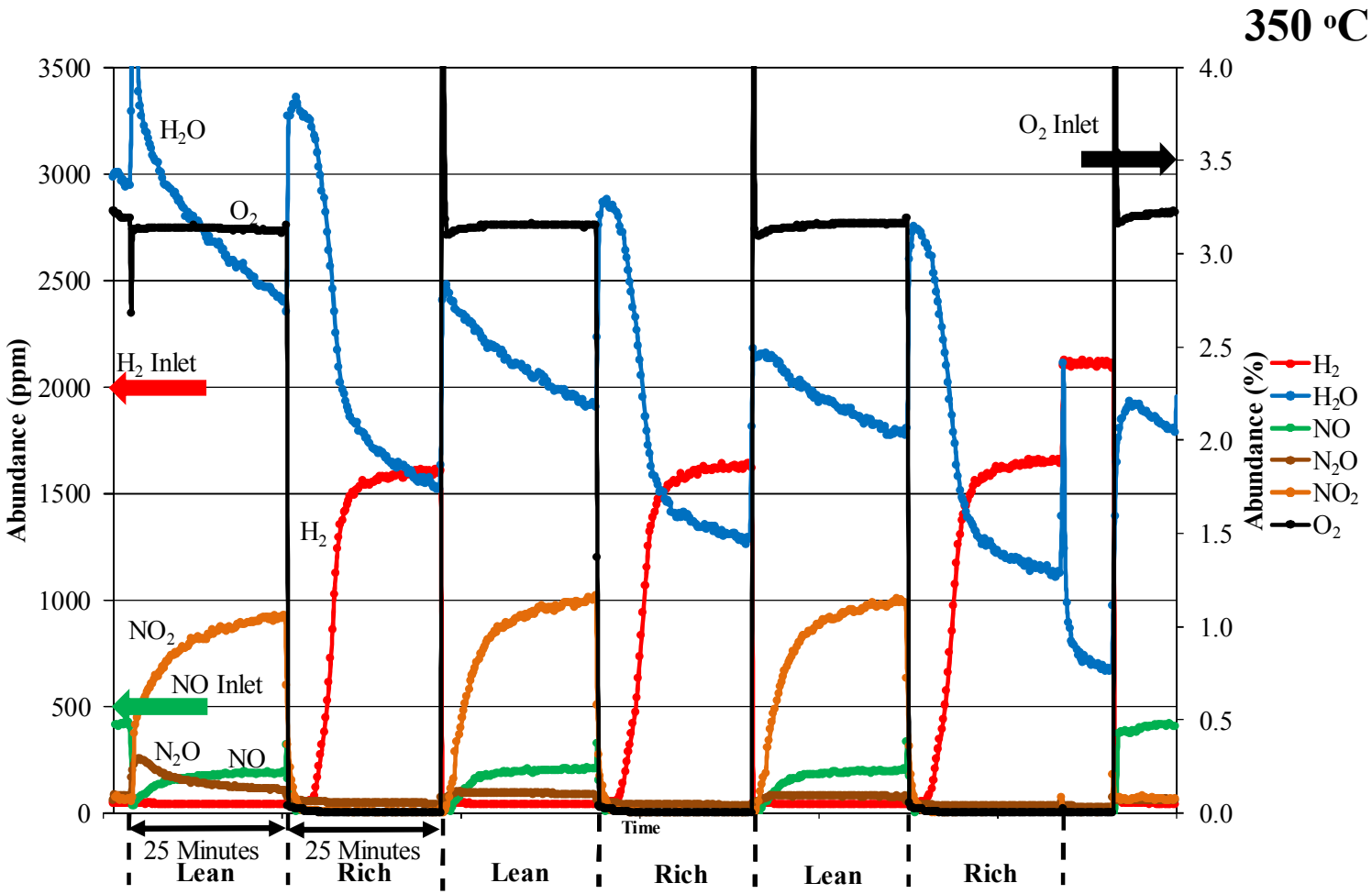

Figure 4.7 H_2–NSR over $Ba/Pt/Al_2O_3$ at 350 °C. Lean conditions: 500 ppm NO, 3.5 % O_2, balance N_2. Rich conditions: 2000 ppm H_2, balance N_2. Note that the secondary y–axis denotes O_2 abundance only.

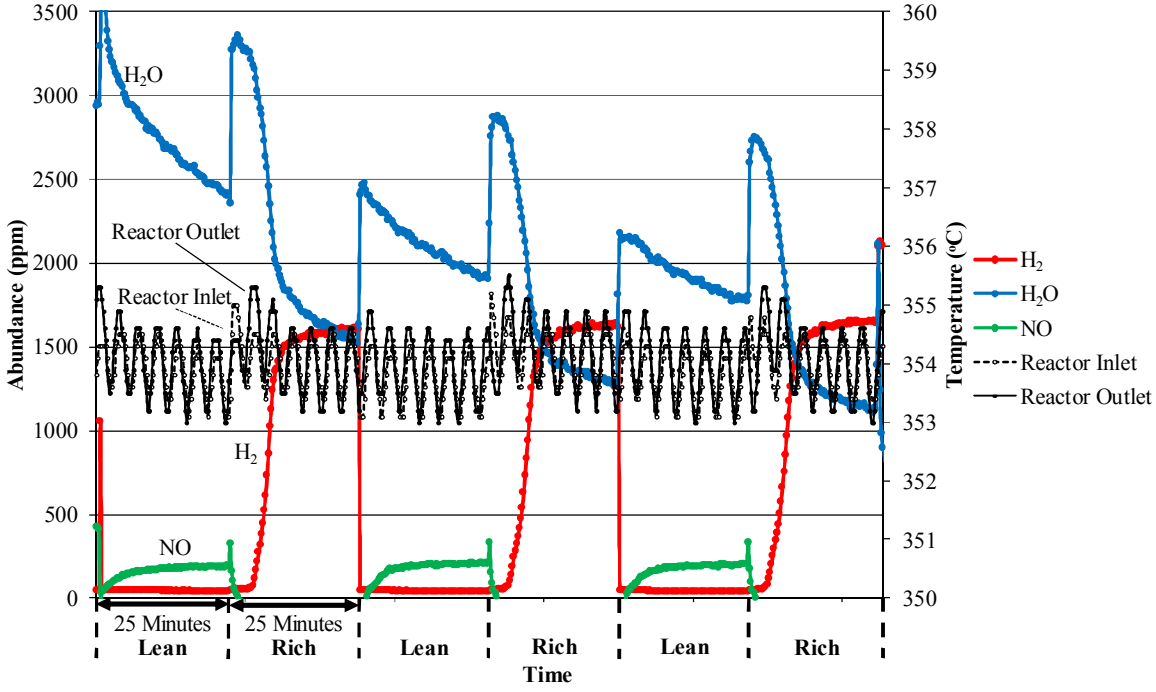

Figure 4.8 Measured abundance of selected reaction species during NSR cycles and measured reactor inlet and outlet temperatures.

Table 4.5 Measured reactor inlet and outlet temperatures at various stages in the NSR cycles.

Cycle	Temperature (°C)		
	Inlet	Outlet	Difference
Lean 1	354.1	355.2	1.1
Lean 2	354.2	354.8	0.6
Lean 3	354.2	354.8	0.6
Rich 1	354.5	355.3	0.9
Rich 2	354.7	355.4	0.6
Rich 3	354.6	355.3	0.7

4.3.3.2 TPD Studies

The reactor was loaded with three $Ba/Pt/Al_2O_3$ monolith pieces. The temperature was increased to 400 ^oC at 10 ^oC min^{-1}, under a N_2 flow rate of ~330 cm^3 min^{-1}, and dwelled for 1 h. The reactor was then cooled to ~35 ^oC and the catalysts subject to 2000 ppm H_2 in N_2 at a flow rate of 441 cm^3 min^{-1} for 0.5 h. The feed was then switched to N_2 for 0.5 h, at a flow rate of ~330 cm^3 min^{-1}, before the temperature was again increased to 400 ^oC at 10 ^oC min^{-1} and the desorbed species measured.

As can be seen from Figure 4.9, after the switch to H_2 for the adsorption period there is a small delay before the inlet conditions are reached. This indicates adsorption of H_2 species onto the surface of the catalyst and indeed this is verified when a very broad and slight peak is observed soon after the reactor temperature is increased (during desorption) from around 03:25:00 until 03:40:00.

Further analysis of the areas of these peaks confirms that only 18.06 % of the adsorbed species are subsequently desorbed. This low value creates questions about the experimental procedure, the analysis and the nature of the material. In terms of procedure, the shape of the H_2 adsorption peak does not represent a classic breakthrough curve, indeed there is a steep jump from a lower concentration to the inlet concentration shortly after the H_2 has been introduced and so perhaps there is an error here. There may also be errors in calculating the area under the curve and projected area should there be no adsorption of the reactant species. Additionally it may be that a higher temperature is required to completely desorb all H_2 species.

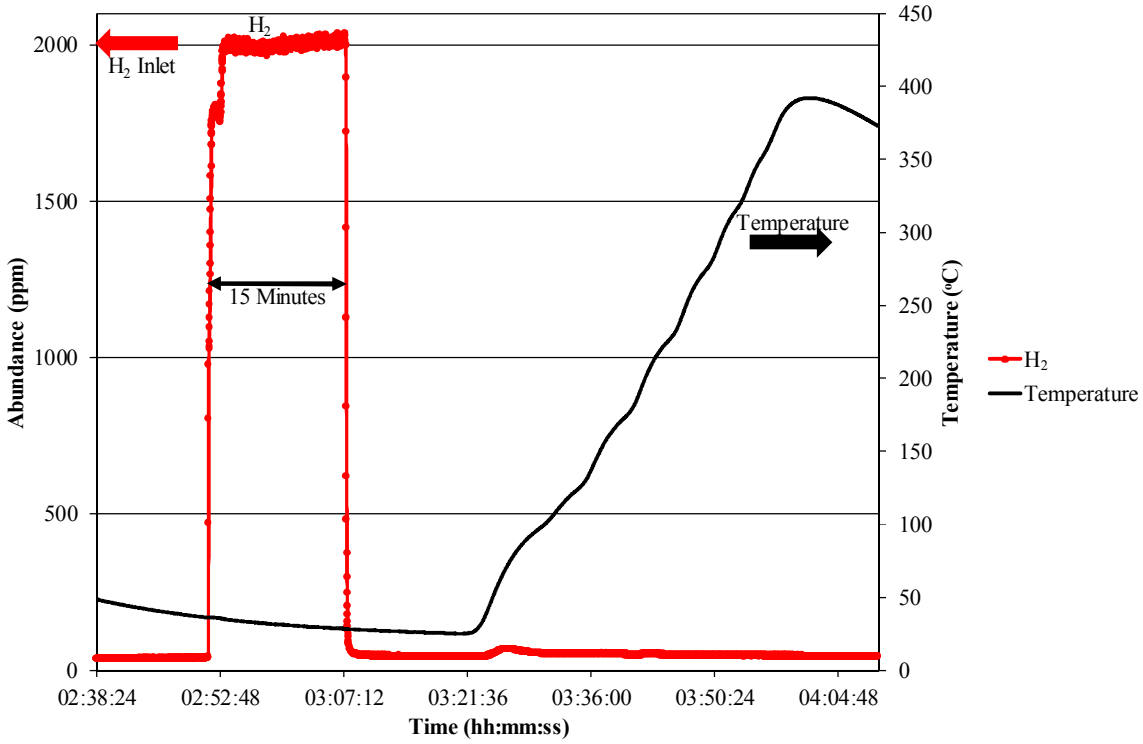

Figure 4.9 H_2–TPD over $Ba/Pt/Al_2O_3$.

4.3.4 $Ba/Ag/Al_2O_3$

The previous NSR experiments were repeated with an unexplored material, $Ba/Ag/Al_2O_3$, as a potential novel catalyst. The catalysts were prepared in house by impregnating alumina coated monoliths, first with an aqueous silver solution and secondly with an aqueous barium solution. Synthesis details can be found in Section 4.1. The catalysts had an average silver loading of 1.8 wt%, an average barium loading of 5.0 wt% and an average γ–Al_2O_3 loading of 27.6 wt% with respect to the complete catalyst system.

4.3.4.1 NSR Studies

The catalysts were explored in similar, although not identical, conditions to those described for the $Ba/Pt/Al_2O_3$ NSR experiment previously (Section 4.3.3.1). The reactor was first loaded with three $Ba/Ag/Al_2O_3$ monolith pieces. The temperature was increased to 350 ^oC at 10 ^oC min^{-1} and the catalyst reduced under 8000 ppm H_2 in N_2 at a flow rate of ~300 cm^3 min^{-1} for 1 h. The temperature was maintained whilst the following compositions were approximately set using the reactor bypass (Table 4.6). They were unaltered for the duration of the experiment:

Table 4.6 Approximate gas mixture flow rates and ultimate inlet compositions utilised during preliminary H_2–NSR investigations over $Ba/Ag/Al_2O_3$.

Sequence	Gas Mixture	Flow Rate (dm^3 h^{-1})	Flow Rate (cm^3 min^{-1})	Composition
Lean	4000 ppm NO/N_2	2.63	44	500 ppm NO 5.0 % O_2 balance N_2
	Air	5.53	92	
	N_2	15.64	261	
	Total	23.80	397	
Rich	8000 ppm H_2/N_2	5.05	84	2000 ppm H_2 balance N_2
	N_2	15.64	261	
	Total	20.69	345	

The conditions were alternatively cycled, for varying periods of time (Table 4.7) until the measured results were deemed repeatable between two consecutive cycles (Figure 4.10).

Table 4.7 Cycle times for $Ba/Ag/Al_2O_3$ H_2–NSR experiment.

Cycle No.	Period Length (min)	
	Lean	Rich
1	45	40
2	25	20
3	20	15
4	15	10
5	15	10

The following plot displays similar trends to that obtained for the $Ba/Pt/Al_2O_3$ catalyst. Five cycles were undertaken and the catalyst demonstrated repeatable behaviour between cycles four and five. Again, it is apparent that during the reaction both NO and H_2 abundances do not reach their inlet values (maximum NO outlet: 312 ppm and maximum H_2 outlet: 1014 ppm during the last cycle) and thus surface reactions must be occurring to account for the difference.

Addressing the 'lean' cycle; once more there is a short delay before breakthrough of NO, and an initial drop in O_2 concentration. These changes can be attributed to the NO_x storage period before saturation of the catalyst surface is reached. Again, the increase in NO is accompanied by formation, and sharp rise in abundance of NO_2 (reaching a maximum concentration in excess of 600 ppm). Additionally, there was no apparent formation of N_2O in this instance.

A delay in breakthrough of H_2 is seen during 'rich' periods and again there is large formation of H_2O which drops off as the H_2 level increases (there are also significant quantities of apparent background H_2O present). Once more it may be assumed that at least some of the H_2 is reacting with stored NO_x species and forming H_2O (Equation 4.4) as there are no N–species observed during the rich periods. Finally, as in the previous experiment NH_3 was not measured, but this may be a side product at this point and should be investigated in future experiments.

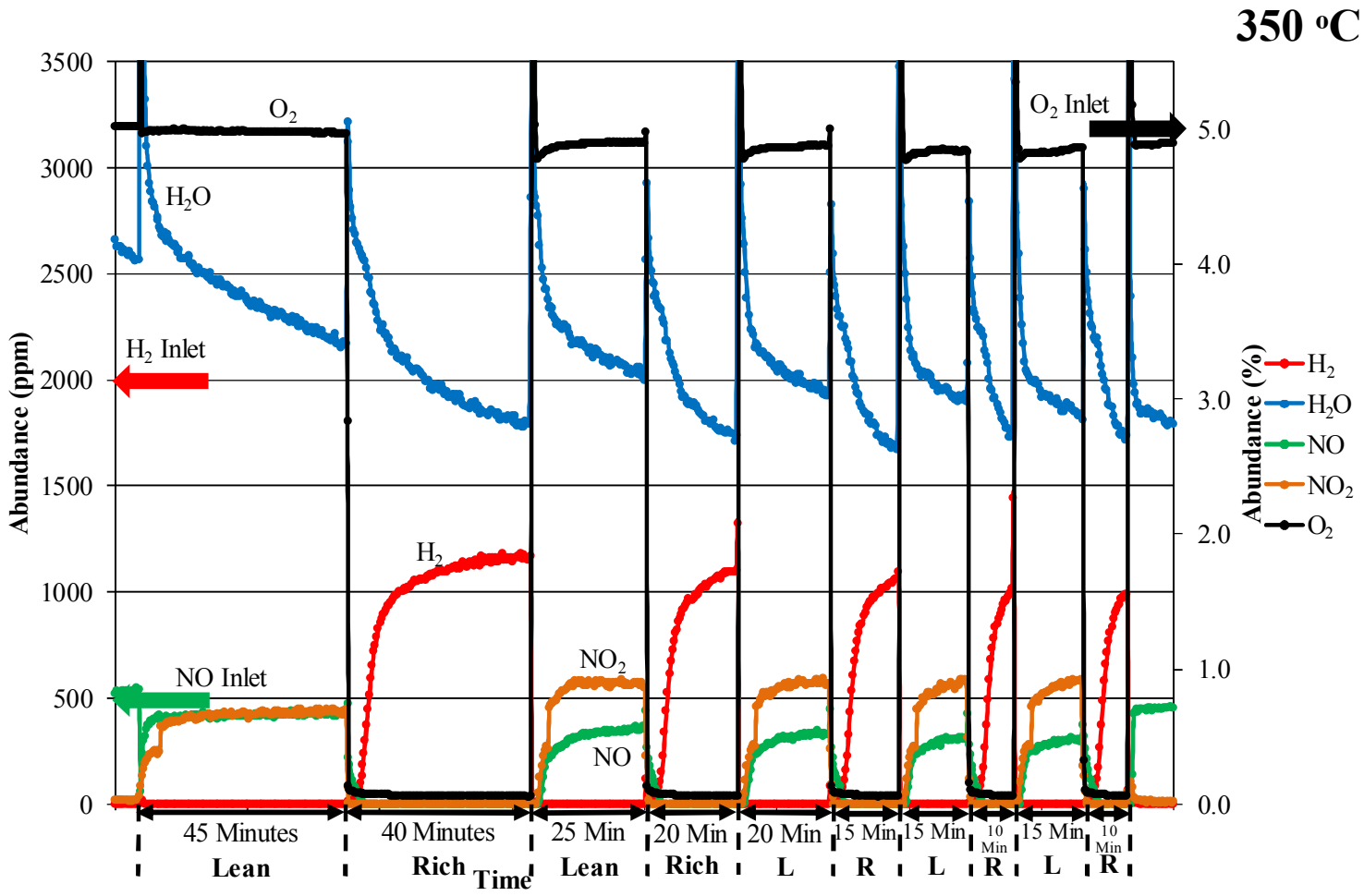

Figure 4.10 H_2–NSR over $Ba/Ag/Al_2O_3$ at 350 °C. Lean conditions: 500 ppm NO, 5 % O_2, balance N_2. Rich conditions: 2000 ppm H_2, balance N_2. Note that the secondary y–axis denotes O_2 abundance only. L = Lean cycle, R = Rich cycle.

4.3.5 Identified Issues and Limitations

Once again, there were a number of issues with both the experimental procedures and experimental results, from both catalysts, which required addressing:

- It was confirmed that several lean and rich cycles i.e. 3–4, are required before consistent results are achieved – this had to be built in to the final experimental procedure.

- The initial inlet conditions of each species were not reached at any time during the actual experimental trials; it appears there are surface reactions occurring between inlet species.

- Large spikes in the H_2O and O_2 levels were seen when switching between cycles. This may be expected for H_2O during the rich periods as it is a desired product of the reaction, although it is not expected for O_2.

- The apparent presence of large amounts of H_2O in the reaction mixture accompanied by a constantly drop in H_2O levels over the course of each cycle; was observed, perhaps there was contamination of the line?

- Again there appears to be an apparent sensitivity of the QMS procedure to NO_2, which is produced in high quantities in comparison to the inlet concentration of NO. The QMS method required refinement.

In terms of the TPD trials, the low % desorbed species value observed in this experiment may be the result of several issues:

- Error in the experimental procedure i.e. problem with the solenoid valve when switching to the adsorbent stream or insufficient temperature reached;

- Incorrect analysis.

It appears that the absolute value of H_2 adsorbed is also very small, although this may simply be due to the fact that the material has little affinity for the species as opposed to any experimental error.

4.3.6 Conclusions and Subsequent Actions taken

Again the 'general' predicted outcomes were mostly realised in the initial H_2–NSR experimental trials. The experimental procedure appeared appropriate and produced somewhat expected results; there was a delay at the beginning of each cycle before breakthrough of each reactant species was seen, attributable to periods of storage and reduction, and lower NO levels (than the supplied inlet concentration) and an apparent production of H_2O were also measured during the respective periods. Thus both tested catalysts appear to demonstrate some deNO_x activity in the H_2–NSR process.

However, there was a large amount of NO_2, in excess of 1000 ppm for the $Ba/Pt/Al_2O_3$ system and 600 ppm for the $Ba/Ag/Al_2O_3$ system, produced in both cases. Although, N_2O formation was only witnessed during the $Ba/Pt/Al_2O_3$ investigation.

In terms of the TPD measurement; once again the experimental approach appears appropriate with both adsorption and subsequent desorption apparent.

There are now a number of steps which were implemented to improve the overall experimental method and complete this section of study. Indeed some of these actions had already been considered in response to the shortcomings of the SCR experimental method:

- Refinement of the method of calibrating the QMS in order to improve the accuracy in detecting NO_2.
- Inclusion of NH_3 in the measurement method as it may be a by–product of the reaction of H_2 with stored NO_x species.
- Investigation of possible methods of removing/reducing background H_2O levels.

4.4 H_2–NSR: Final Results

In this section the results of H_2–NSR experiments, performed over selected parameters identified through the preliminary experiments described in Section 4.3, are presented. The experimental set–up and general procedures detailed in Chapter 3 remained the same whilst the specific details of the different reaction sequences are provided before each set of results.

Once again, although the reaction mixture compositions are specified, due to the nature of the equipment and the measurements it was not practical to consistently obtain these exact conditions and so they are provided as a guideline only. Again, although every effort was made to produce a reliable and robust method; in some instances gentle manipulation of the data was required to negate erroneous 'background' readings and present a true reflection of species abundance; however, all results were processed in exactly the same fashion.

The data points are presented as observed and are connected to give an indication of trends only, the connections do not represent recorded data. Where appropriate, arrows are utilised to highlight inlet conditions and identify which species correspond to which axis. In addition, for ease of display and analysis; only one lean/rich cycle (obtained once repeatable performance was observed) for each of the NSR investigations will be presented.

The catalysts were subject to the following standardised procedures. In some cases this first involved pre–treatment with the intention of removing any undesired surface species, before the catalysts were subject to the desired reaction mixtures and processes. In other cases (the NSR investigations), in the absence of pre–treatment the catalysts were subject to the lean/rich cycles until repeatable performance between cycles was observed. The justifications for the procedures are provided within each description.

4.4.1 H_2–NSR

It should be noted that in refining the experimental procedure from the preliminary investigations, it was decided that the catalyst performance should be explored in two different rich period conditions; one in the absence of O_2 and another in the presence of O_2. For the purposes of the straightforward reporting of results, the conditions under which the catalysts are investigated will be labelled as follows:

- Lean vs Rich 1.
- Lean vs Rich 2.

The experimental temperature of 400 ^oC was chosen in an effort to improve on the performance of the silver catalysts demonstrated at 350 ^oC in the preliminary experiments (Section 4.3.4) as was the O_2 concentration of 3.2 % (as opposed to 5 %); through reducing the production of NO_2.

4.4.1.1 Lean vs Rich 1

The reactor was loaded with three monolith pieces. The temperature was increased to 400 ^{o}C at 10 ^{o}C min^{-1} under N_2 at a flow rate of ~330 cm^3 min^{-1}. The temperature was maintained whilst the following flow rates and compositions were approximately set using the reactor bypass (Table 4.8). The inlet conditions were unaltered for the duration of each NSR experiment and alternatively cycled, for periods of 30 min each, until repeatable measurements between consecutive cycles were observed; it is for this reason that pre–treatment was deemed unnecessary.

Table 4.8 Approximate gas mixture flow rates and ultimate inlet compositions utilised during final H_2–NSR 'Lean vs Rich 1' investigations.

Sequence	Gas Mixture	Flow Rate (dm^3 h^{-1})	Flow Rate (cm^3 min^{-1})	Composition
Lean	4000 ppm NO/N_2	8.24	137	1000 ppm NO 3.2 % O_2 balance N_2
	N_2	19.88	331	
	Air	5.06	84	
	Total	33.18	553	
Rich 1	8000 ppm H_2/N_2	8.87	148	2500 ppm H_2 balance N_2
	N_2	19.88	331	
	Total	28.75	479	

It is apparent in Table 4.8 that there is some difference in the total flow rates between the different lean and rich periods; this is unavoidable due to the resources and experimental set–up, however the flow rates are not substantially different and for the purposes of this investigation the impact may be considered negligible.

4.4.1.1.1 Catalyst Substrate and Support

Through a similar approach to Chapter 3; in order to correctly account for activity in terms of the individual components of the catalyst, it is important to first identify the behaviour of only the substrate and support layers under NSR experimental conditions. As little activity is evident, the results from these materials will merely be summarised in an effort to minimise the number of graphs presented throughout this thesis. Note that the catalyst substrate and support materials were only investigated under a lean/rich cycle which utilised the 'Rich 1' conditions detailed in Table 4.8.

4.4.1.1.1.1 Cordierite

The cordierite samples demonstrated no substantial reaction under NSR conditions at a temperature of 400 ^{o}C. During the lean period the supplied inlet conditions remained apparently unchanged and there was only very slight detection of trace species formation; NO_2 (≤4 ppm) and N_2O (≤6 ppm). In switching to the rich period, there is also no suggestion of H_2 consumption, but there was apparent formation of trace levels of H_2O (≤32 ppm), N_2O (≤23 ppm) and NO_2 (≤10 ppm). These species concentrations peak immediately after switching to the rich period and then gradually decrease in concentration as the period progresses. This does suggest the cordierite has some affinity for NO and facilitates its reaction with H_2 or O–species to form the observed compounds.

4.4.1.1.1.2 γ–Al_2O_3

The γ–Al_2O_3 samples had an average loading of 29.6 wt% with respect to the complete catalyst system. Once more there was no substantial reaction observed under NSR conditions at a temperature of 400 ^oC. There was no apparent consumption of NO or O_2 during the lean period, although some formation of NO_2 ($\leq$ 10 ppm, presumably from the oxidation of NO) was observed. On switching to the rich phase, consumption of H_2 was observed although there were no trace species detected beyond formation of H_2O; initially in a concentration of 1980 ppm before a gradual decrease to 121 ppm over the course of the rich period. By combining the observed concentrations of H_2 and H_2O and comparing them to the inlet H_2 concentration (in this case 2139 ppm), the values are in strong agreement and in the absence of any trace species it may be assumed that the H_2 is reacting only with surface oxygen species to form the H_2O observed.

Assuming a consistent coating of γ–Al_2O_3 on the substrate samples, it may be assumed that one of the other oxides of which cordierite consists of i.e. MgO or SiO, is responsible for the apparent and slight storage and reduction behaviour (formation of N_2O in the rich period) described in Section 4.4.1.1.1.1.

4.4.1.1.2 Storage Components

As a reminder, Ba and K are included in the NSR catalysts as 'storage components' to facilitate temporary storage of the NO_x species during the lean period before subsequent reduction on exposure to the rich period. It was also deemed important to explore the behaviour of the storage components in the absence of the noble metal component, under NSR conditions, with a view to possibly gleaning information on the mechanism of the storage. Once again, the results from these materials will merely be summarised in an effort to minimise the number of graphs presented throughout this thesis.

4.4.1.1.2.1 Ba/Al_2O_3

The investigated samples had an average barium loading of 3.6 wt% and an average γ–Al_2O_3 loading of 28.5 wt% with respect to the complete catalyst system. Preparation details can be found in Section 4.1.

The Ba/Al_2O_3 system demonstrated some level of both NO and O_2 consumption during the initial stages of the lean phase. This was accompanied by NO_2 formation, which peaked at 47 ppm immediately after switching to the lean conditions and then levelled out at 23 ppm as the period progressed. There was also some slight N_2O formation which only occurred after 15 min in to the lean phase and gradually increased to 5 ppm by the end of the phase. Upon switching to the rich phase there is some indication of H_2 consumption accompanied by formation of H_2O (in similar manner to γ–Al_2O_3 above: initially 212pm which gradually decreases to 117 ppm) in addition to N_2O (23 ppm) and NO_2 (10 ppm) (in these cases initial concentration is greatest and then gradually decreases). There is also some measurement of NO (89 ppm), the concentration of which gradually decreases over the course of the period. It may be that NO is loosely adsorbed on to the surface of the catalyst, without undergoing a chemical reaction, and when the bulk gas composition changes from the lean phase to the rich phase, the result is the desorption of the NO species.

4.4.1.1.2.2 K/Al_2O_3

The investigated samples had an average potassium loading of 19.2 wt% and an average γ–Al_2O_3 loading of 23.9 wt% with respect to the complete catalyst system. Preparation details can be found in Section 4.1.

On introducing the lean phase there is a strong indication of NO storage through consumption of NO and O_2 without the accompanying formation of NO_2. Indeed there is no NO_2 observed throughout the lean period and formation of N_2O occurs only after 600 s of the period, at which point it gradually increases until an outlet value of 30 ppm is reached.

On switching to the rich phase an increase in formation of N_2O to 64 ppm is observed before it gradual decreases to 17 ppm over the course of the period. Additionally, there is some formation of NO_2 (9 ppm) also observed, although it decreases to 0 ppm over the course of the period, and apparent desorption of NO (94 ppm) which again gradually decreases to 21 ppm over the course of the rich phase. In terms of H_2 consumption, conversion of 6.7 % is observed at the end of the rich phase whilst formation of H_2O gradually decreases from a peak of 157 ppm to 138 ppm.

4.4.1.1.3 Complete Catalyst Systems

4.4.1.1.3.1 $Ba/Pt/Al_2O_3$

As a reminder, the $Ba/Pt/Al_2O_3$ catalyst was studied as an example of a typical NSR catalyst and to confirm the NSR experimental approach. The catalysts had an average platinum loading of 0.2 wt%, an average barium loading of 4.7 wt% and an average γ–Al_2O_3 loading of 28.2 wt% with respect to the complete catalyst system. Preparation details can be found in Section 4.1.

The $Ba/Pt/Al_2O_3$ catalyst demonstrated a similar performance to preliminary experiments (albeit at a different reaction temperature) when subject to the final H_2–NSR experimental conditions. However, due to recalibration of the QMS the measured species concentrations are more appropriate, and indeed where applicable the mass balances are realised. In addition, the performance strongly resembles that of similar investigations of this catalyst material in the literature described previously in Chapter 2 i.e. Lietti *et al.* (2001), Cumaranatunge *et al.* (2007) and Abdulhamid *et al.* (2004), validating the experimental approach and analysis methods.

The overall measured abundances of both main and trace reactant species formed during H_2–NSR investigations over the $Ba/Pt/Al_2O_3$ catalyst under 'Lean vs Rich 1' conditions are shown in Figure 4.11. In addition, the species formed during the lean phase only are presented in Figure 4.12 and similarly during the rich phase only in Figure 4.13 (main species) and Figure 4.14 (trace species).

It can be observed from the overall plot of both the lean and rich cycle in Figure 4.11 that on exposure to the lean phase there is clear evidence of NO_x storage occurring due to the breakthrough curves of both NO and O_2. This is accompanied by the evolution of H_2O (initially in a concentration of 380 ppm), a phenomena described in Lietti *et al.* (2001) and which suggests NO_x storage is also occurring on $Ba(OH)_2$ sites. NO_2 is also formed and its concentration increases to 283 ppm over time. By considering Figure 4.12 it can be seen that the NO_x^{Outlet}(= NO^{Outlet} + NO_2^{Outlet}) approaches the NO^{Inlet} concentration, and the area apparent between the NO_x^{Outlet} and NO^{Inlet} plots represents the amount of NO_x stored on the catalyst. Through calculation this area relates to **18.8 %** of the supplied NO during the lean phase.

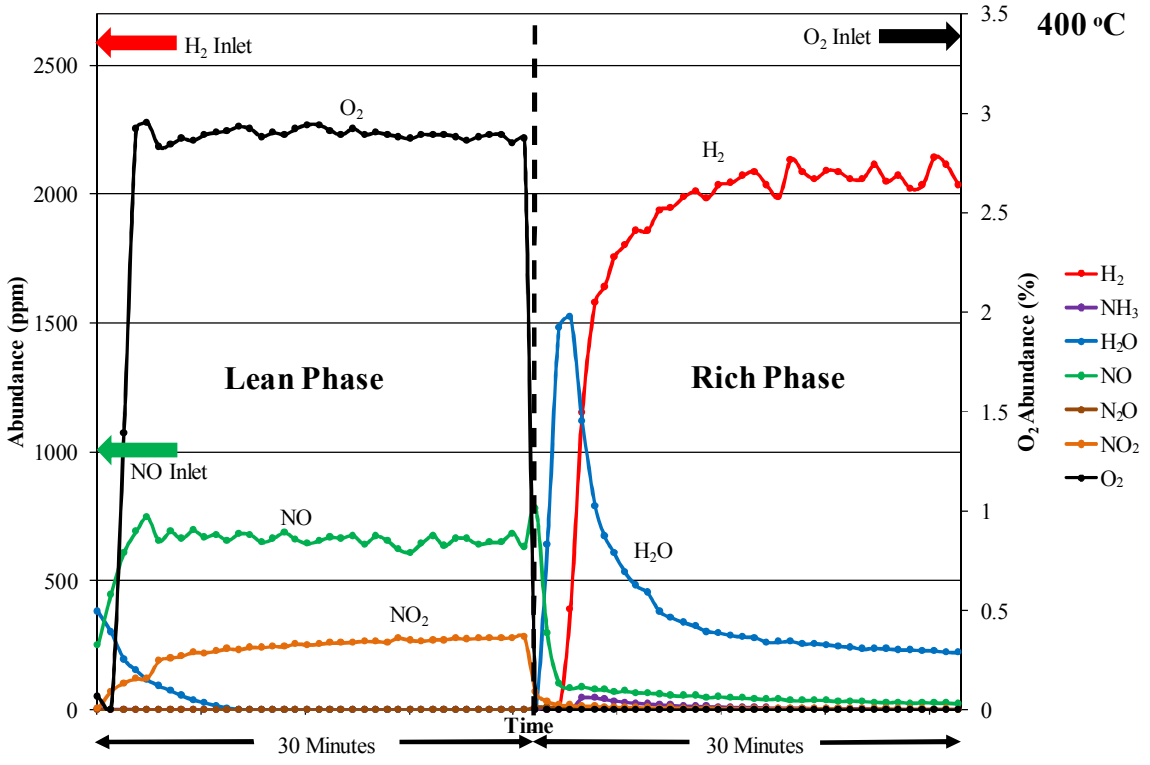

Figure 4.11 H_2–NSR over $Ba/Pt/Al_2O_3$ under 'Lean vs Rich 1' conditions at 400 °C. Lean conditions: 1000 ppm NO, 3.2 % O_2, balance N_2. Rich conditions: 2500 ppm H_2, balance N_2. Note that the secondary y–axis denotes O_2 abundance only.

It should be noted here that the significant formation of NO_2 observed in this experiment appears to result in a reduction in the accuracy of the measured O_2 concentration. This is a consequence of the limitations of the equipment utilised within the QMS method, which did not allow the contributions of NO_2 at secondary peaks to be accurately measured when NO_2 is present in high concentrations. As a result the calculated contribution of NO_2 at 32 amu is significantly greater than in reality, which results in an apparent lower measured concentration of O_2. However, the O_2 present is in great excess with respect to the other reactants and it is still possible to identify trends in the O_2 trace. Therefore, although this highlights a shortcoming in the QMS method, and indeed it applies to each experiment detailed in this section, it was not deemed to significantly affect the performance level indicators utilised in this project.

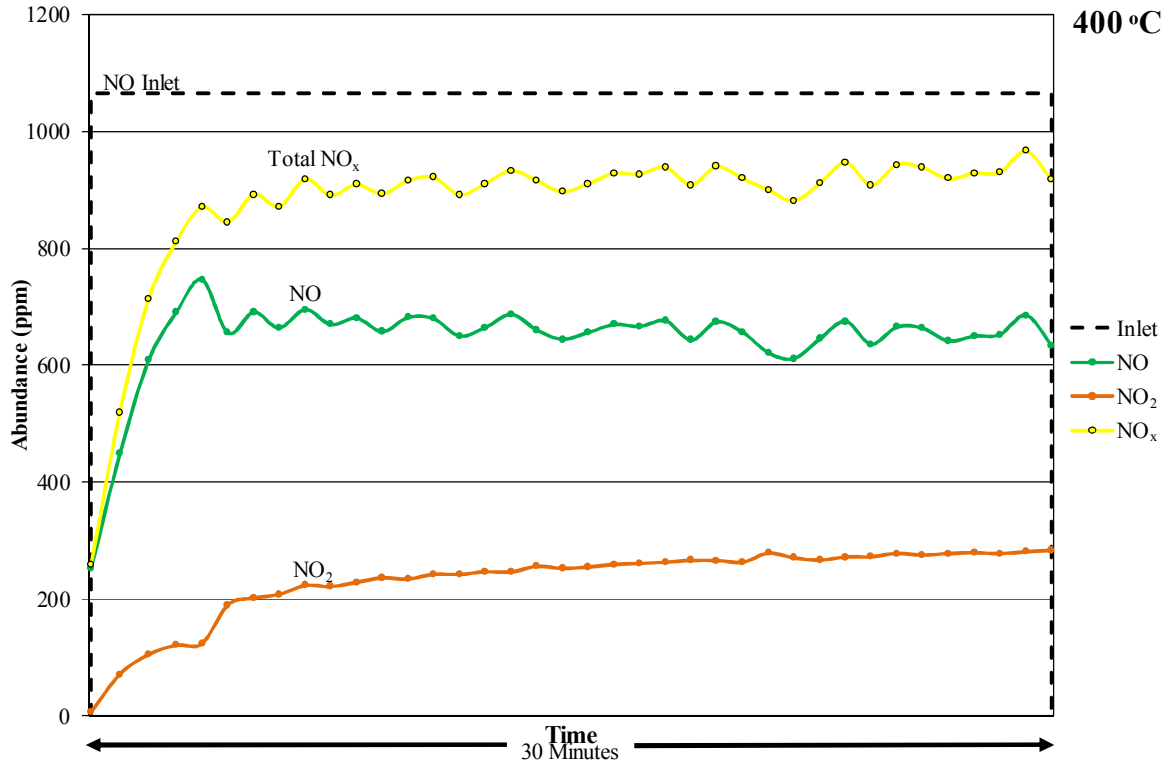

Figure 4.12 Species observed during the lean phase of H_2–NSR over $Ba/Pt/Al_2O_3$ under 'Lean vs Rich 1' conditions at 400 °C. Lean conditions: 1000 ppm NO, 3.2 % O_2, balance N_2.

On switching to the rich phase (Figure 4.13) initial formation of H_2O is oberved after 95 s, which peaks at 1522 ppm and then gradually decreases to 222 ppm as time progresses. This is closely followed by the breakthrough of H_2 after 190 s, which reaches 2036 ppm, corresponding to a conversion of 20.4 %, at the end of the rich phase. These traces (formation of H_2O before breakthrough of H_2) indicate the reduction of stored NO_x, perhaps through Equation 4.4 detailed previously.

Whilst it may be desirable to combine the H_2 and H_2O outlet values and compare the total to the H_2 inlet value, in a similar manner to the NO_x species above, it is not advisable due to the production of species such as NH_3 through Equation 4.7 detailed previously:

$$Ba(NO_3)_2 + 8H_2 \rightarrow BaO + 2NH_3 + 5H_2O \qquad (4.7)$$

The stoichiometry of the reaction is such that the ratio of H_2^{Inlet}:H_2O^{Outlet} does not equal 1, and any presumption as such may lead to inaccurate results. Although it may be argued that by consideration of the other species formed it may be possible to account for the stoichiometry of the reaction, through the analytical technique and methods under use it is impossible to definitively assign the reaction mechanisms. In addition undesired surface reactions may also be occurring, such as that shown below:

$$BaO + H_2O \rightarrow Ba(OH)_2 \qquad (4.8)$$

However, the trace of the H_2^{Inlet} will be included on the plots in order to provide a relative indication of the catalyst performances. As can be seen from Figure 4.13, without further manipulation the combination of H_2 and H_2O outlet concentrations corresponds to greater than 90 % of the inlet H_2 concentration at the end of the rich phase. Thus it may be stated that the QMS method is well calibrated, certainly with respect to the method utilised in the preliminary NSR experiments (Section 4.3).

Now considering the trace species observed during the rich phase (Figure 4.14); a significant quantity of NO (782 ppm) is immediately apparent (even greater than the final NO outlet concentration measured in the lean phase) although this rapidly decreases to 25 ppm by the end of the lean period. In addition to the apparent reduction of stored NO_x species, this measured NO may be accounted for in a number of ways:

- It is weakly adsorbed surface NO (not incorporated into $Ba(NO_3)_2$ or $Ba(NO_2)_2$) which is desorbed on introduction of a different gas composition.
- It is the result of the reaction of H_2 with stored $Ba(NO_3)_2$ or $Ba(NO_2)_2$ (Equation 4.5).
- The rate of reaction of NO release is greater than the rate of reaction of NO reduction.

A similar trace is observed for NO_2 albeit in much smaller quantities (69 ppm down to 2 ppm). There is also some immediate formation of N_2O but again in very slight quantities: initially 12 ppm and then down to 0 after 660 s. Finally, NH_3 formation was also observed after 190 s and this peaked at 46 ppm before gradually reducing over the course of the period. As was discussed previously in Chapter 2, Section 2.4.3.4.3, it is thought that the mechanism of stored NO_x reduction with H_2 over $Ba/Pt/Al_2O_3$, beyond reaction between NO and H_2, involves the formation of NH_3 which subsequently reacts to reduce the NO_x species. Perhaps the breakthrough of NH_3, which closely matches that of H_2 breakthrough, indicates that the stored NO_x species have been reduced at this point and the NH_3 formed is unreactive towards the remaining species or the other species present.

Finally, by considering the apparent abundance of NO_x stored during the lean phase detailed above, and the total abundance of N–containg species produced in the rich phase; it is possible to calculate the apparent proportion of stored NO_x which is converted to the desired product, N_2. Ideally it would also be possible to directly measure the abundance of N_2 formed during the rich phase, but this is not possible whilst using N_2 as the carrier gas. As a result the calculated amount of stored NO_x which is converted to N_2 is **56.8 %.**

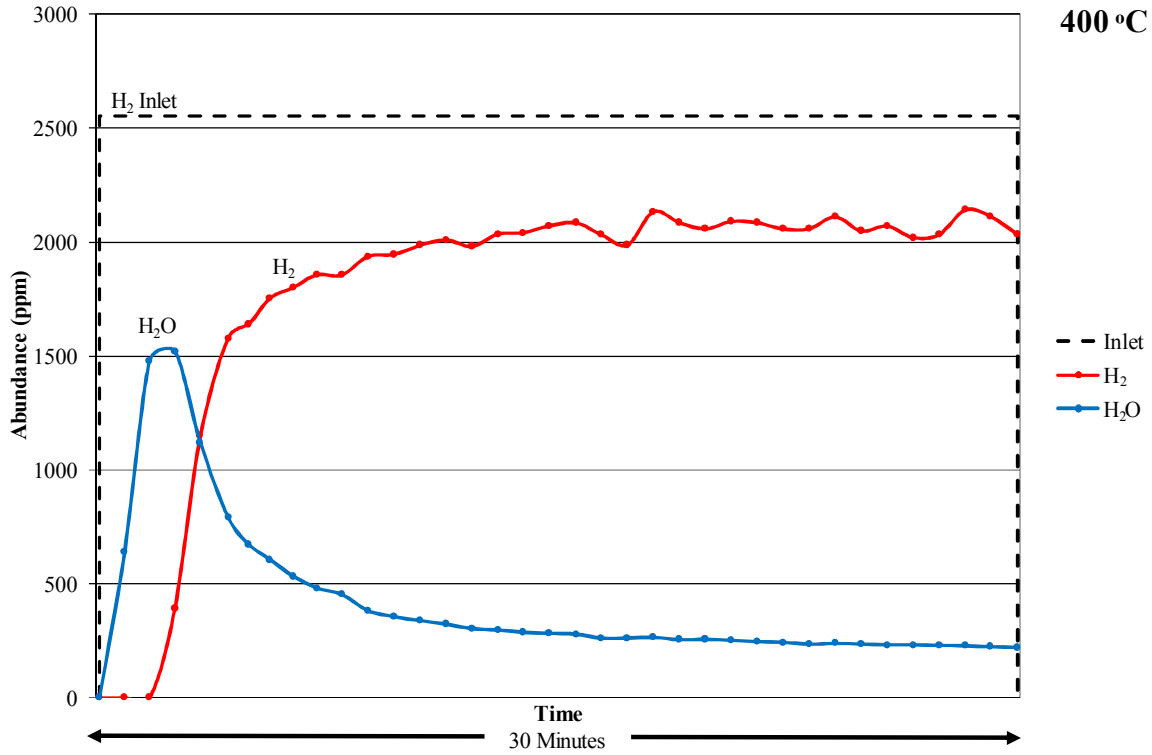

Figure 4.13 Main species observed during the rich phase of H_2–NSR over $Ba/Pt/Al_2O_3$ under 'Lean vs Rich 1' conditions at 400 °C. Rich conditions: 2500 ppm H_2, balance N_2.

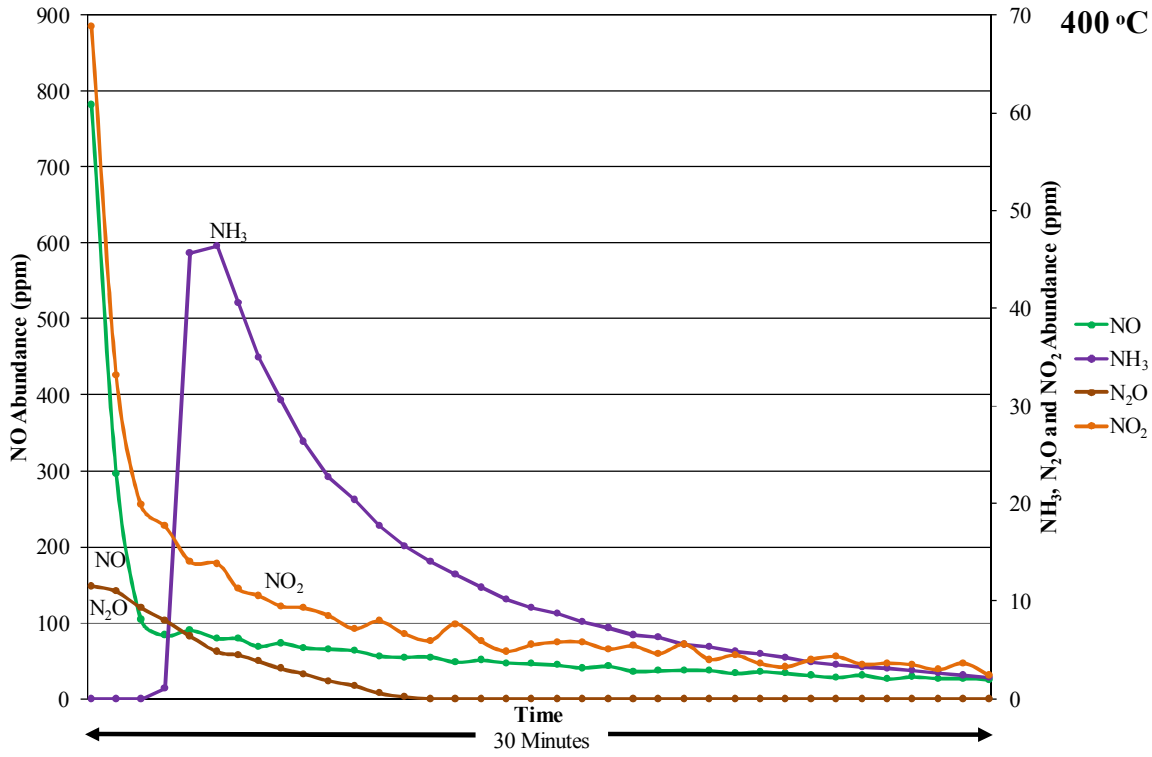

Figure 4.14 Trace species observed during the rich phase of H_2–NSR over $Ba/Pt/Al_2O_3$ under 'Lean vs Rich 1' conditions at 400 °C. Rich conditions: 2500 ppm H_2, balance N_2. Note the primary x–axis denotes NO concentration only.

4.4.1.1.3.2 $Ba/Ag/Al_2O_3$

$Ba/Ag/Al_2O_3$ was explored as a potential novel H_2–NSR catalyst. The catalysts had an average silver loading of 1.8 wt%, an average barium loading of 5.0 wt% and an average γ–Al_2O_3 loading of 27.6 wt% with respect to the complete catalyst system. Preparation details can be found in Section 4.1.

The overall measured abundances of both main and trace reactant species formed during H_2–NSR investigations over the $Ba/Ag/Al_2O_3$ catalyst under 'Lean vs Rich 1' conditions are shown in Figure 4.15. In addition, the species formed during the lean phase only are presented in Figure 4.16 and similarly during the rich phase only in Figure 4.17 (main species) and Figure 4.18 (trace species).

The $Ba/Ag/Al_2O_3$ catalyst, in some aspects, demonstrates very similar performance to the 'standard' $Ba/Pt/Al_2O_3$ catalyst (Figure 4.11 and Figure 4.12). Considering the overall plot in Figure 4.15 and lean phase plot in Figure 4.16;

- Initial consumption of both NO and O_2.
- Initial formation of H_2O (1212 ppm) gradually decreases to 0 ppm after 17 min.
- Formation of NO_2 increases to 253 ppm as the period progresses.
- $NO_x^{Outlet} \approx NO^{Inlet}$ by the end of the lean period; **10.5 %** of supplied NO stored during the lean period.

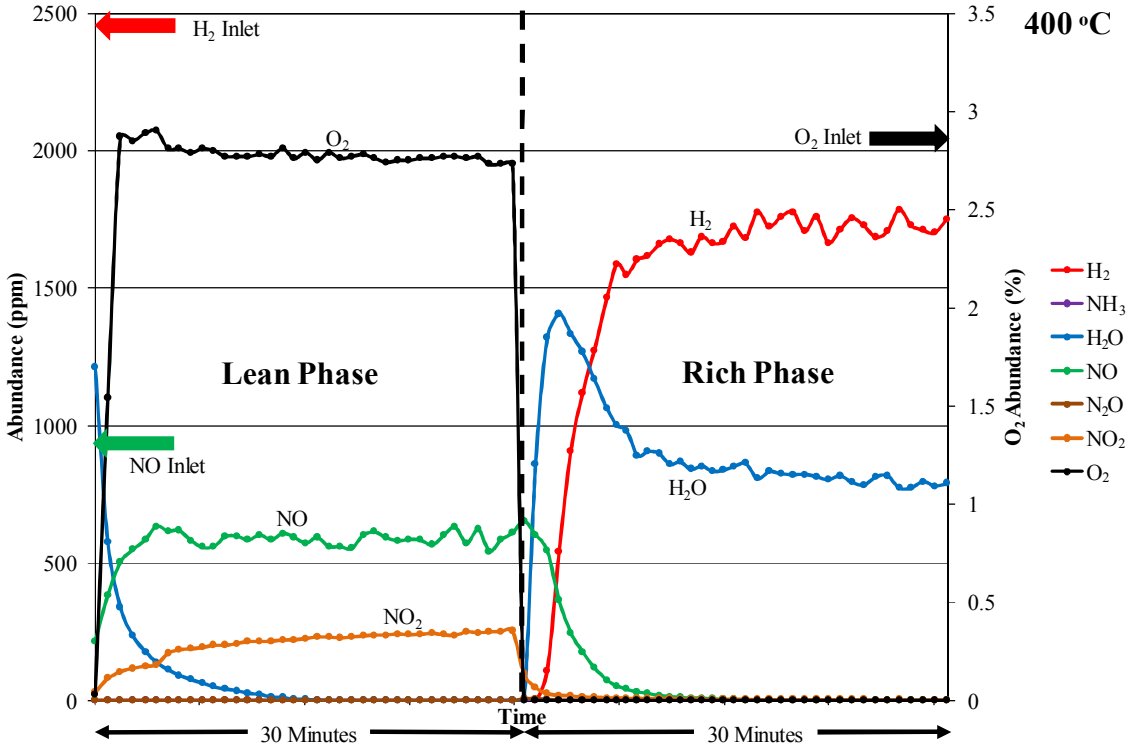

Figure 4.15 H_2–NSR over $Ba/Ag/Al_2O_3$ under 'Lean vs Rich 1' conditions at 400 °C. Lean conditions: 1000 ppm NO, 3.2 % O_2, balance N_2. Rich conditions: 2500 ppm H_2, balance N_2. Note that the secondary y–axis denotes O_2 abundance only.

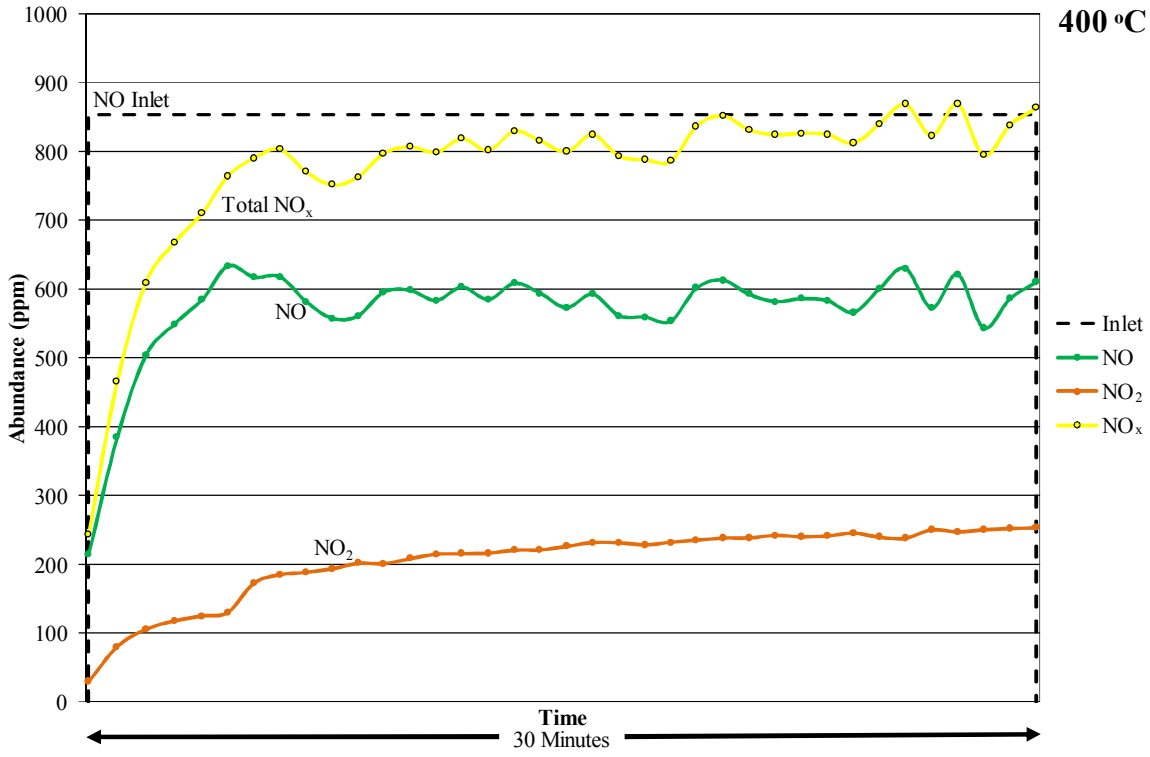

Figure 4.16 Species observed during the lean phase of H_2–NSR over $Ba/Ag/Al_2O_3$ under 'Lean vs Rich 1' conditions at 400 °C. Lean conditions: 1000 ppm NO, 3.2 % O_2, balance N_2.

On switching to the rich phase (Figure 4.17 and Figure 4.18) again similar performance to the $Ba/Pt/Al_2O_3$ catalyst (Figure 4.13 and Figure 4.14) is observed:

- Initial formation of H_2O (95 s) peaks at 1407 ppm and decreases to 790 ppm.
- Breakthrough of H_2 (140 s) reaches 1749 ppm, (= 30.4 % conversion at the end of the rich phase).
- Apparent reduction of stored NO_x in addition to significant levels of NO observed (653 ppm decreasing sharply to 0 ppm after 17.5 min).
- NO_2 abundance follows the NO trace albeit in much smaller quantities (89 ppm down to 3 ppm).
- Formation of N_2O occurs immediately in very slight quantities (initially 8 ppm decreasing to 0 after 240 s).
- $\leq$3 ppm NH_3 formation observed after 330 s and remained for the duration.
- As a result of the evolution of significant quantities of NO, in tandem with the formation of other N–containing species, the proportion of stored NO_x which is successfully converted to N_2 is only **5.6 %**.

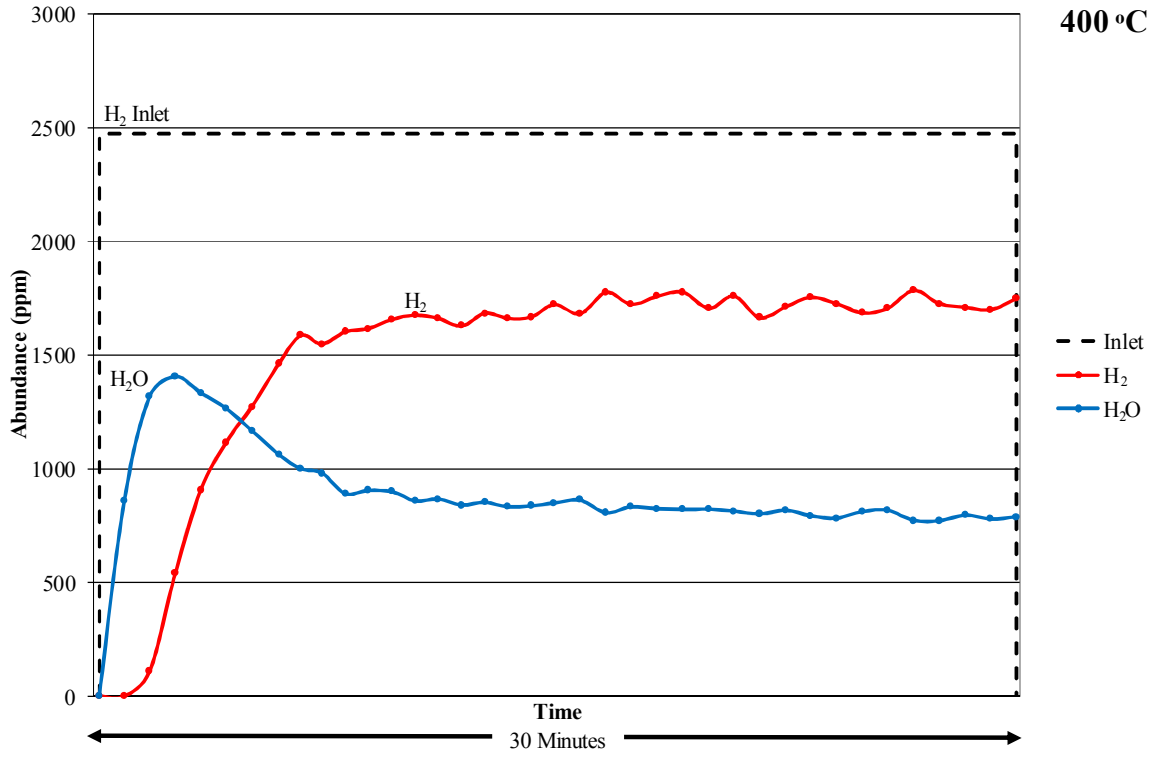

Figure 4.17 Main species observed during the rich phase of H_2–NSR over $Ba/Ag/Al_2O_3$ under 'Lean vs Rich 1' conditions at 400 °C. Rich conditions: 2500 ppm H_2, balance N_2.

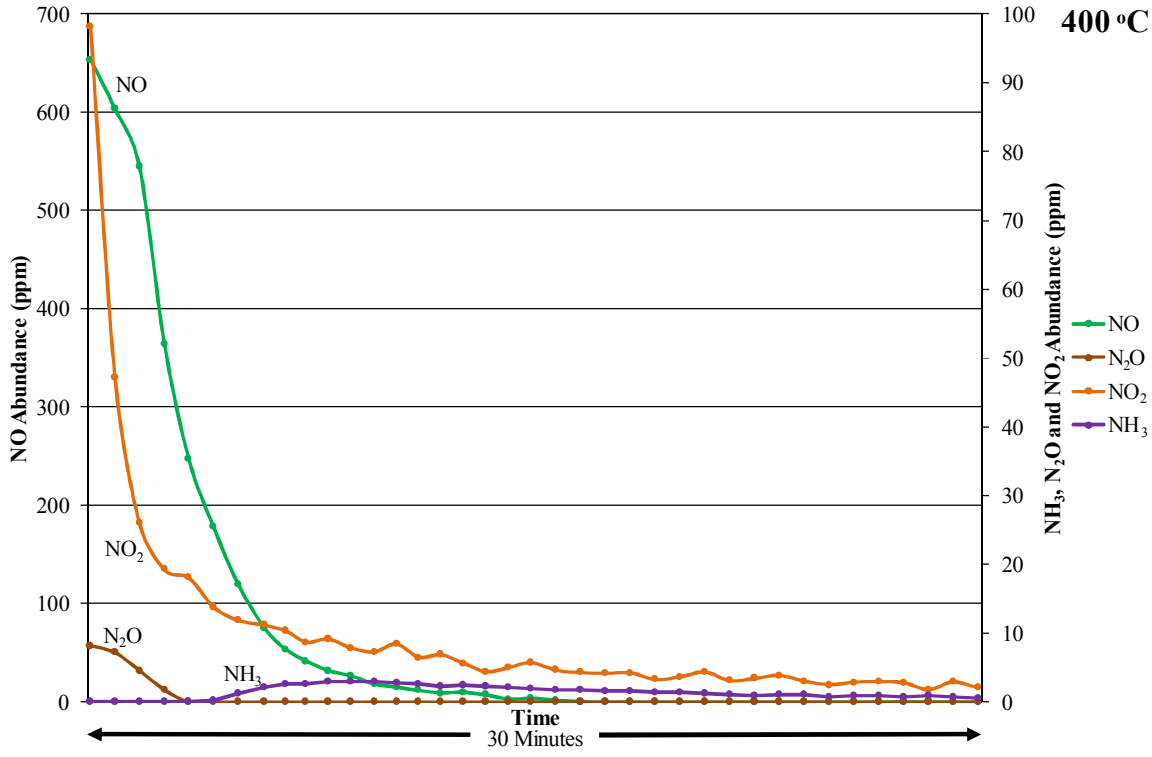

Figure 4.18 Trace species observed during the rich phase of H_2–NSR over $Ba/Ag/Al_2O_3$ at under 'Lean vs Rich 1' conditions 400 °C. Rich conditions: 2500 ppm H_2, balance N_2. Note the primary x–axis denotes NO concentration only.

4.4.1.1.3.3 $K/Ag/Al_2O_3$

$K/Ag/Al_2O_3$ was explored as a potential novel H_2–NSR catalyst. The catalysts had an average silver loading of 2.1 wt%, an average potassium loading of 16.0 wt% and an average γ–Al_2O_3 loading of 24.3 wt% with respect to the complete catalyst system. Preparation details can be found in Section 4.1.

The overall measured abundances of both main and trace reactant species formed during H_2–NSR investigations over the $K/Ag/Al_2O_3$ catalyst under 'Lean vs Rich 1' conditions are shown in Figure 4.19. In addition, the species formed during the lean phase only are presented in Figure 4.20 and similarly during the rich phase only in Figure 4.21 (main species) and Figure 4.22 (trace species).

When considering the overall (Figure 4.19) and lean phase (Figure 4.20) plots, it is apparent that the $K/Ag/Al_2O_3$ catalyst demonstrates significantly different behaviour to those catalysts previously investigated:

- 'Breakthrough' of NO is observed only after an initial dip in concentration (a phenomena not observed with any other catalyst) and reaches a maximum abundance of 413 ppm.
- Evolution of N_2O (15.5 min) gradually increases to 52 ppm by the end of the period. N_2O formation has not been observed during the lean phase of any other catalyst investigation in this project with the exception of the K/Al_2O_3 study. Thus it may be assumed that reaction of NO with surface K–species are responsible for its evolution.
- No formation of NO_2 observed throughout the lean phase.
- NO_x^{Outlet} increases throughout the lean phase though does not approach the NO^{Inlet} and demonstrates a maximum calculated value of only 514 ppm.
- **72.3 %** of the supplied NO is stored, the greatest fraction yet observed in this study.
- Significant evolution of H_2O (1026 ppm) decreasing to 0 ppm after 27 min.

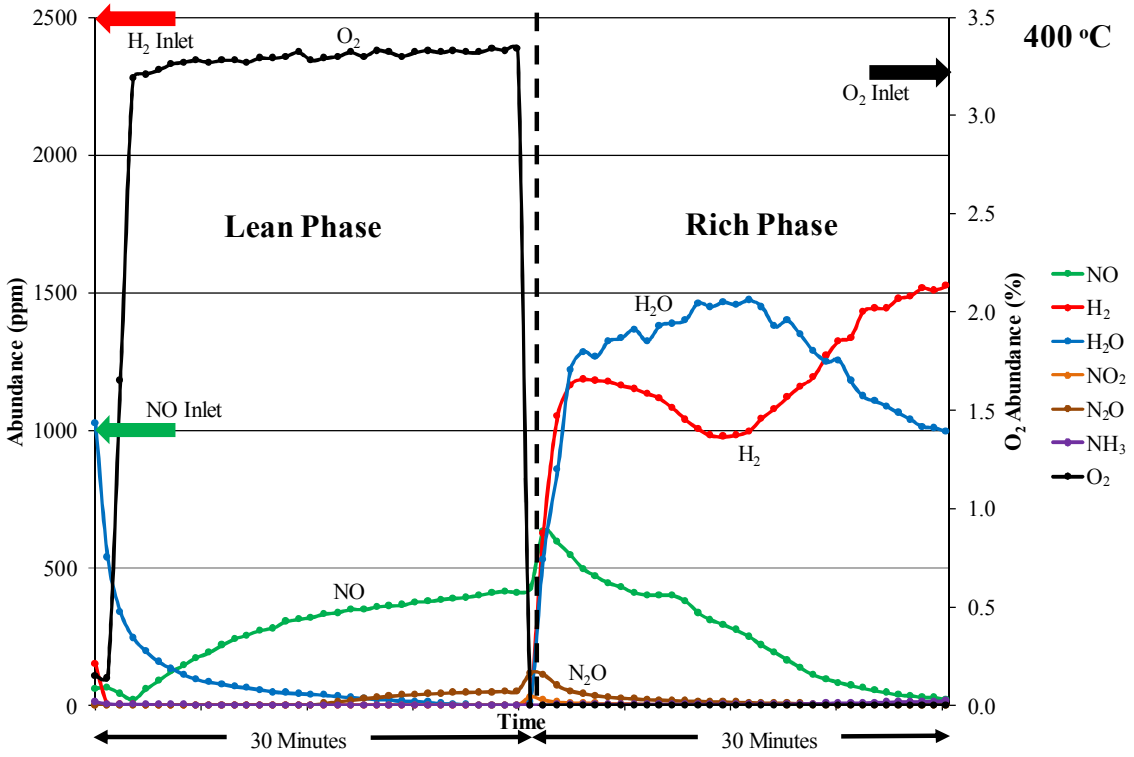

Figure 4.19 H_2–NSR over $K/Ag/Al_2O_3$ under 'Lean vs Rich 1' conditions at 400 °C. Lean conditions: 1000 ppm NO, 3.2 % O_2, balance N_2. Rich conditions: 2500 ppm H_2, balance N_2. Note that the secondary y–axis denotes O_2 abundance only.

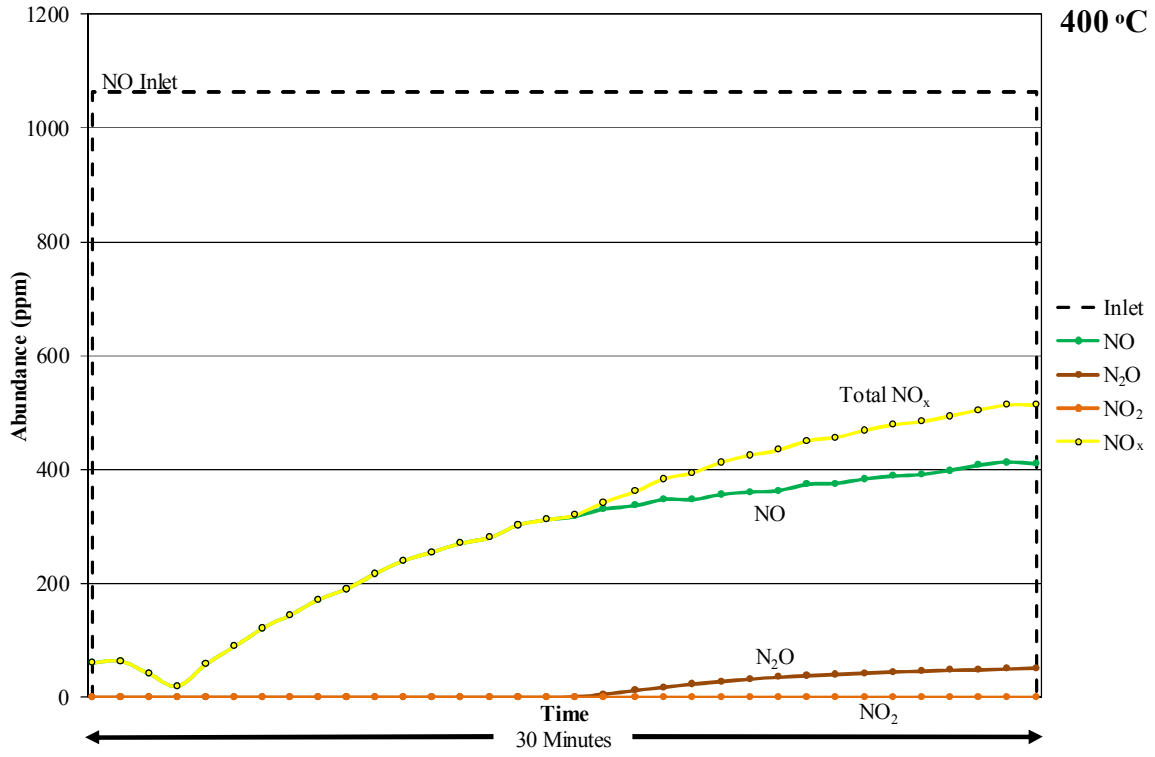

Figure 4.20 Species observed during the lean phase of H_2–NSR over $K/Ag/Al_2O_3$ under 'Lean vs Rich 1' conditions at 400 °C. Lean conditions: 1000 ppm NO, 3.2 % O_2, balance N_2.

On switching to the rich phase (Figure 4.21 and Figure 4.22):

- Immediate H_2 and H_2O breakthrough;
  - Follow a similar trend for the first 3.5 min, after which H_2 concentration equals 1163 ppm and H_2O concentration equals 1219 ppm.
- Beyond this stage however;
  - H_2 concentration decreases to a local minima of 975 ppm after 14 min, and
  - H_2O concentration increases to 1473 ppm at the same point.
- After which, for the final 16 min of the period;
  - H_2 concentration increases as H_2O concentration decreases, reaching final measured values of 1522 ppm (H_2) and 1003 ppm (H_2O).

Considering the trace species it is clear that whilst there was indication of substantial NO_x storage during the lean phase, it is not translated into successful reduction:

- Evolution of NO peaks at 630 ppm after switching (100 s) and gradually decreases to 19 ppm.
- Immediate formation of N_2O and NO_2 (117 ppm and 31 ppm respectively) decreases to 0 ppm as the phase progresses.
- Breakthrough of 1 ppm NH_3 (165 s) increases to 14 ppm.

It is not clear what has caused the shape of the plotted H_2 and H_2O abundances, although perhaps it is related to the NO abundance; there is a step in the NO trace which coincides with the start of the apparent minima and maxima experienced by the H_2 and H_2O respectively. Although it may be suggested that the NO is loosely adsorbed to the surface of the catalyst and is merely desorbed after switching to the rich phase, perhaps the NO is re–formed through the reaction of H_2 with the nitrates and nitrites, in a similar fashion to Equation 4.5 detailed previously:

$$Ba(NO_3)_2 + 3H_2 \rightarrow BaO + 2NO + 3H_2O \qquad (4.5)$$

$$Ba(NO_2)_2 + H_2 \rightarrow BaO + 2NO + H_2O \qquad (4.9)$$

Thus should the H_2 be reacting with both $Ba(NO_2)_2$ and $Ba(NO_3)_2$ to form NO, or indeed one type of species is found in differing environments, it may be envisaged that reaction with one species/environment is favoured over reaction with the other. Consequently, differing rates of reaction may explain both the step in the NO evolution profile and maxima/minima traces displayed by the H_2 and H_2O abundances.

Despite the significant evolution of NO observed during the rich phase, the calculated amount of stored NO_x which is converted to N_2 is **59.8 %**. Coupled with the previously described storage of **72.3 %** of the supplied NO during the lean phase, this catalyst outperforms both the 'standard' NSR catalyst and the additional novel silver catalyst previously detailed when investigated under the same reaction conditions.

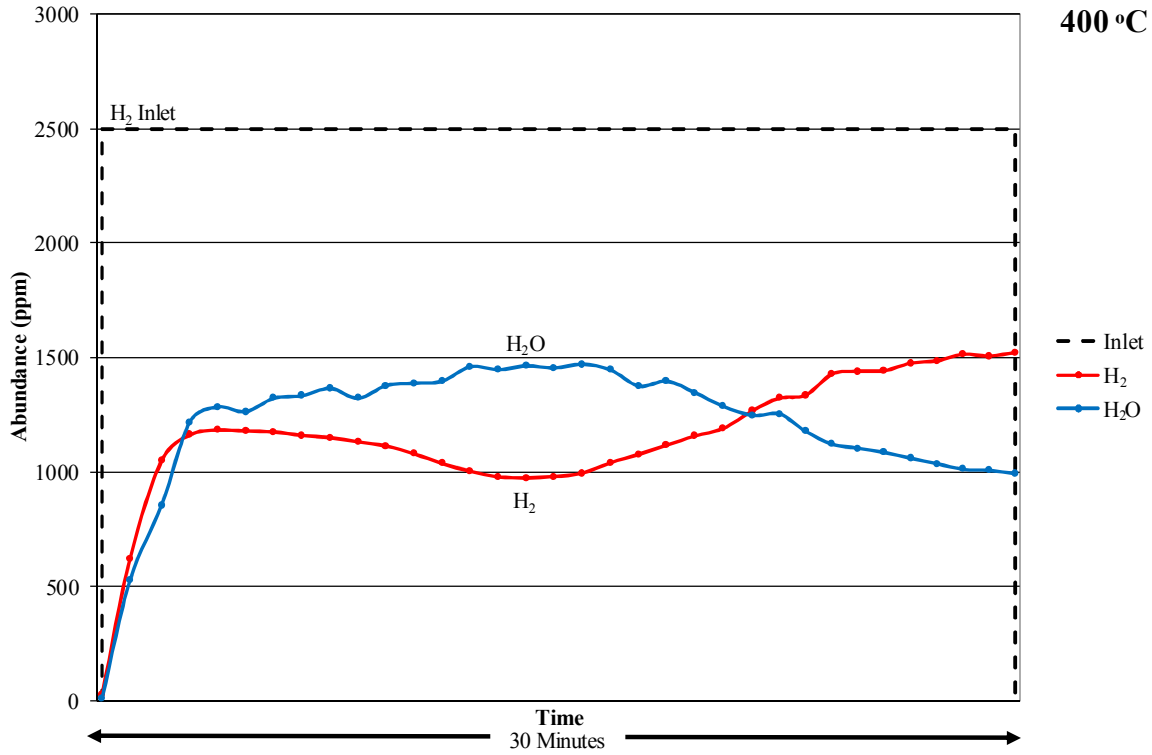

Figure 4.21 Main species observed during the rich phase of H_2–NSR over $K/Ag/Al_2O_3$ under 'Lean vs Rich 1' conditions at 400 °C. Rich conditions: 2500 ppm H_2, balance N_2.

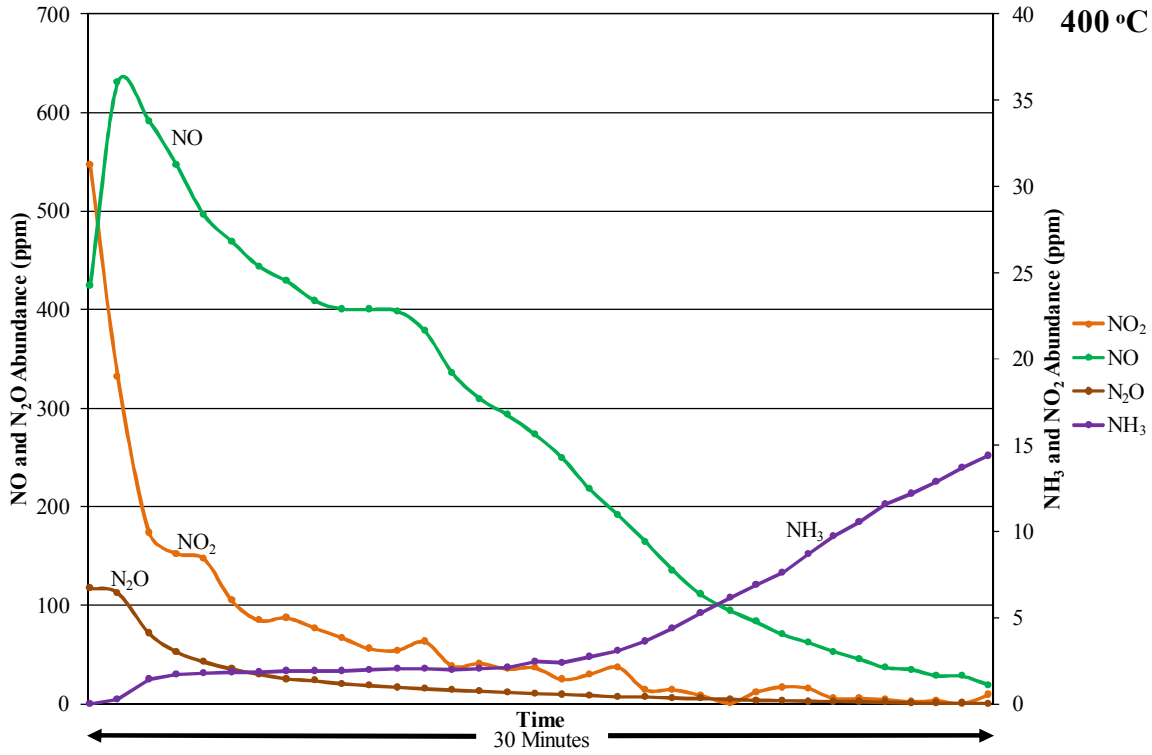

Figure 4.22 Trace species observed during the rich phase of H_2–NSR over $K/Ag/Al_2O_3$ at under 'Lean vs Rich 1' conditions 400 °C. Rich conditions: 2500 ppm H_2, balance N_2. Note the primary x–axis denotes NO and N_2O concentration only.

4.4.1.2 Lean vs Rich 2

It may be found that the presence of O_2 is necessary to reduce the stored NO_x species and that it plays a role in the reaction, much like the desired H_2–SCR reactions discussed in Chapter 3.

The reactor was loaded with three monolith pieces. The temperature was increased to 400 ^oC at 10 ^oC min^{-1} under N_2 at a flow rate of ~330 cm^3 min^{-1}. The temperature was maintained whilst the following flow rates and compositions were approximately set using the reactor bypass (Table 4.9). The inlet conditions were unaltered for the duration of each NSR experiment and alternatively cycled, for periods of 30 min each, until repeatable measurements between consecutive cycles were observed; it is for this reason that pre–treatment was deemed unnecessary.

Table 4.9 Approximate gas mixture flow rates and ultimate inlet compositions utilised during final H_2–NSR 'Lean vs Rich 2' investigations.

Sequence	Gas Mixture	Flow Rate (dm^3 h^{-1})	Flow Rate (cm^3 min^{-1})	Composition
Lean	4000 ppm NO/N_2	8.24	137	1000 ppm NO 3.2 % O_2 balance N_2
	N_2	19.88	331	
	Air	5.06	84	
	Total	33.18	553	
Rich 2	8000 ppm H_2/N_2	11.13	185	2500 ppm H_2 2.9 % O_2 balance N_2
	N_2	19.88	331	
	Air	5.06	84	
	Total	36.06	600	

4.4.1.2.1 Storage Components

4.4.1.2.1.1 Ba/Al_2O_3

The investigated samples had an average barium loading of 3.6 wt% and an average γ–Al_2O_3 loading of 28.5 wt% with respect to the complete catalyst system. Preparation details can be found in Section 4.1.

In terms of lean phase performance, the Ba/Al_2O_3 catalyst demonstrated almost identical behaviour when compared to the results of the Lean vs Rich 1 conditions experiment:

- Initial NO_2 formation (62 ppm) which levels out to 20 ppm.
- However, no N_2O formation observed.

This is not necessarily surprising as the lean inlet conditions are consistent between the procedures, although it does suggest that the rich phase, now with the inclusion of O_2, in this instance does not produce a vastly different catalyst surface or the surface species which would impact on the lean phase reactions.

On switching to the rich period, the catalyst again demonstrates a similar performance to that observed in the Lean vs Rich 1 experiment above; although in this instance there was no formation of N_2O, the NO_2 formation remains consistent (initial formation of 10 ppm which gradually decreases over the course of the rich period). Perhaps the presence of O_2 suppresses N_2O formation. There is significantly greater conversion of H_2 and formation of H_2O in comparison to the Lean vs Rich 1 experiment; 54.2 % and 1339 ppm respectively assuming steady state at the end of the rich phase. In the absence of the formation of any other trace species it may be assumed that the H_2 is reacting with some of the O_2 present to produce the greater levels of H_2O measured. Again there is also some apparent desorption of NO; 88 ppm which gradually decreases over the rich period, albeit at a faster rate than observed in the Lean vs Rich 1 experiment above.

4.4.1.2.1.2 K/Al_2O_3

The investigated samples had an average potassium loading of 19.2 wt% and an average γ–Al_2O_3 loading of 23.9 wt% with respect to the complete catalyst system. Preparation details can be found in Section 4.1.

Once more, a similar performance during the lean phase is observed; NO and O_2 consumption (no formation of NO_2) and formation of N_2O only after 600 s of the period. However in this instance the N_2O concentration gradually increases until an outlet value of only 5 ppm is reached. Again, given that the inlet conditions are similar this suggests that the presence of both H_2 and O_2 during the rich phase subsequently influences the reactions of the lean phase.

Switching to the rich phase there is no formation of N_2O observed although formation of NO_2 follows the same shape as above; initial formation of 7 ppm which decreases to 0 ppm as the rich phase progresses. There is also some apparent desorption of NO (96 ppm) which gradually decreases to 46 ppm over the course of the period.

Interestingly the presence of O_2 does not increase H_2 consumption and formation of H_2O during the rich phase. In fact, conversion of H_2 drops to less than 1 % by the end of the rich phase and formation of H_2O gradually decreases to 92 ppm from a highest concentration of 115 ppm.

4.4.1.2.2 Complete Catalyst Systems

4.4.1.2.2.1 $Ba/Pt/Al_2O_3$

The catalysts had an average platinum loading of 0.2 wt%, an average barium loading of 4.7 wt% and an average γ–Al_2O_3 loading of 28.2 wt% with respect to the complete catalyst system. Preparation details can be found in Section 4.1.

The overall measured abundances of both main and trace reactant species formed during H_2–NSR investigations over the $Ba/Pt/Al_2O_3$ catalyst under 'Lean vs Rich 2' conditions are shown in Figure 4.23. In addition, the species formed during the lean phase only are presented in Figure 4.24 and similarly during the rich phase only in Figure 4.25 (main species) and Figure 4.26 (trace species).

The behaviour of the catalyst during the lean phase (Figure 4.24) closely resembles that of the 'Rich vs Lean 1' investigation.

- Breakthrough of both NO and NO_2 is observed and their concentration continues to increase.
- Slight suggestion that the NO_x^{Outlet} level continues to approach the NO^{Inlet} as the period progresses.
- The amount of NO_x stored on the catalyst, is **23.1 %** of the NO supplied during the lean phase.
    - Slight increase (4.3 %) on the proportion of NO_x stored during the 'Lean vs Rich 1' investigation (18.8 %) with respect to the total NO_x stored.

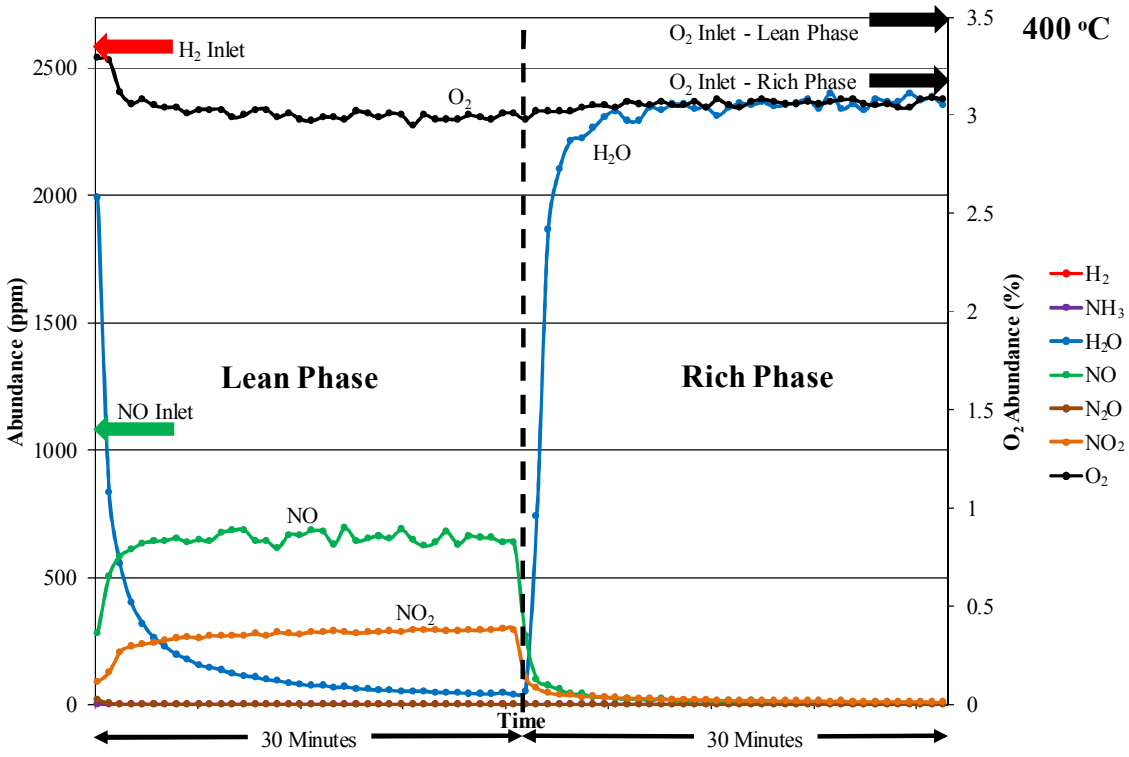

Figure 4.23 H_2–NSR over $Ba/Pt/Al_2O_3$ under 'Lean vs Rich 2' conditions at 400 °C. Lean conditions: 1000 ppm NO, 3.2 % O_2, balance N_2. Rich conditions: 2500 ppm H_2, 2.9 % O_2, balance N_2. Note that the secondary y–axis denotes O_2 abundance only.

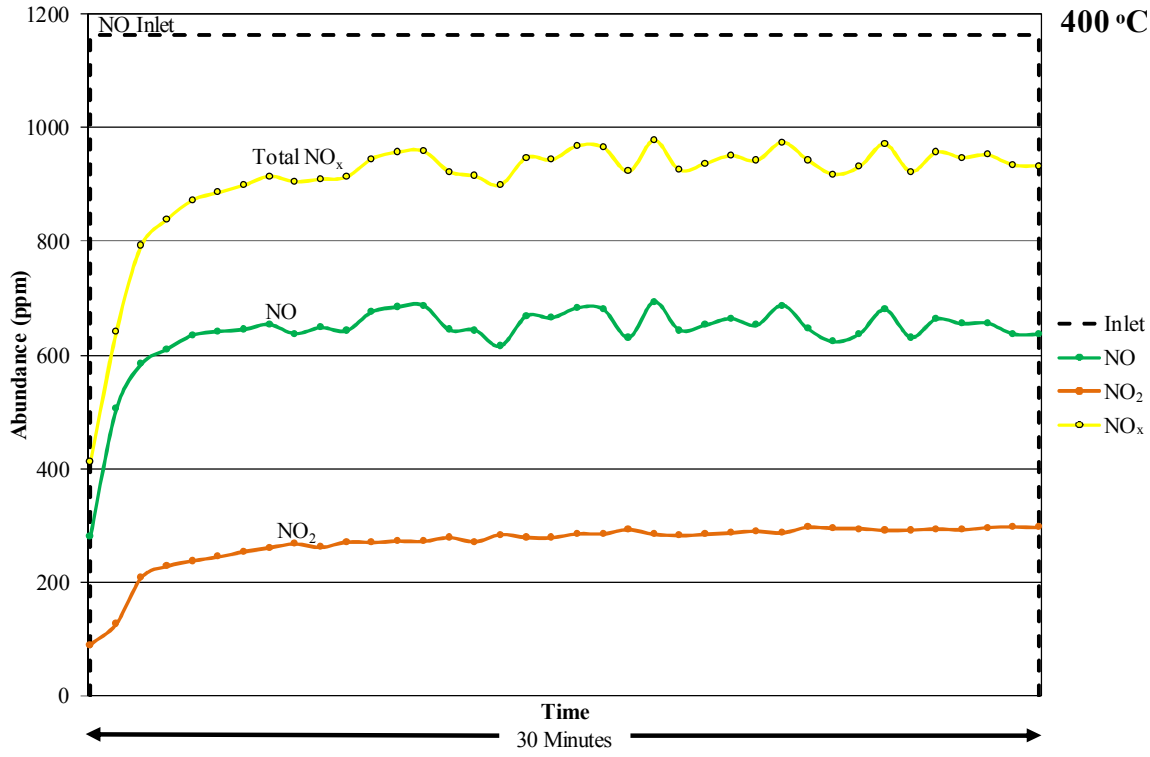

Figure 4.24 Species observed during the lean phase of H_2–NSR over $Ba/Pt/Al_2O_3$ under 'Lean vs Rich 2' conditions at 400 °C. Lean conditions: 1000 ppm NO, 3.2 % O_2, balance N_2.

In terms of the rich phase (Figure 4.25 and Figure 4.26):

- Instant formation of H_2O observed, reaching a maximum of 2353 ppm.
- Complete conversion of H_2 throughout the entire period.
- Apparent evolution of NO (273 ppm decreasing to 0 ppm) and NO_2 (108 ppm decreasing to 11 ppm).
- No evidence of N_2O or NH_3 formation.
- Calculated amount of stored NO_x which is converted to N_2 is **82.3 %**, a significant increase on the results of the 'Lean vs Rich 1' conditions investigation (56.8 %).

It appears that the presence of O_2 in the rich phase plays several important roles in the catalyst reactions of both the lean and rich phases.

During the lean phase:

- A greater proportion of NO is stored on the catalyst surface.

During the rich phase:

- Excess H_2 is consumed to form H_2O.
- The formation of NH_3 or N_2O is supressed or indeed they are reacted further to form the observed species.
- In addition, the formation of NO is greatly reduced and although the formation of NO_2 is slightly increased, the overall conversion of stored NO_x to N_2 is greatly increased.

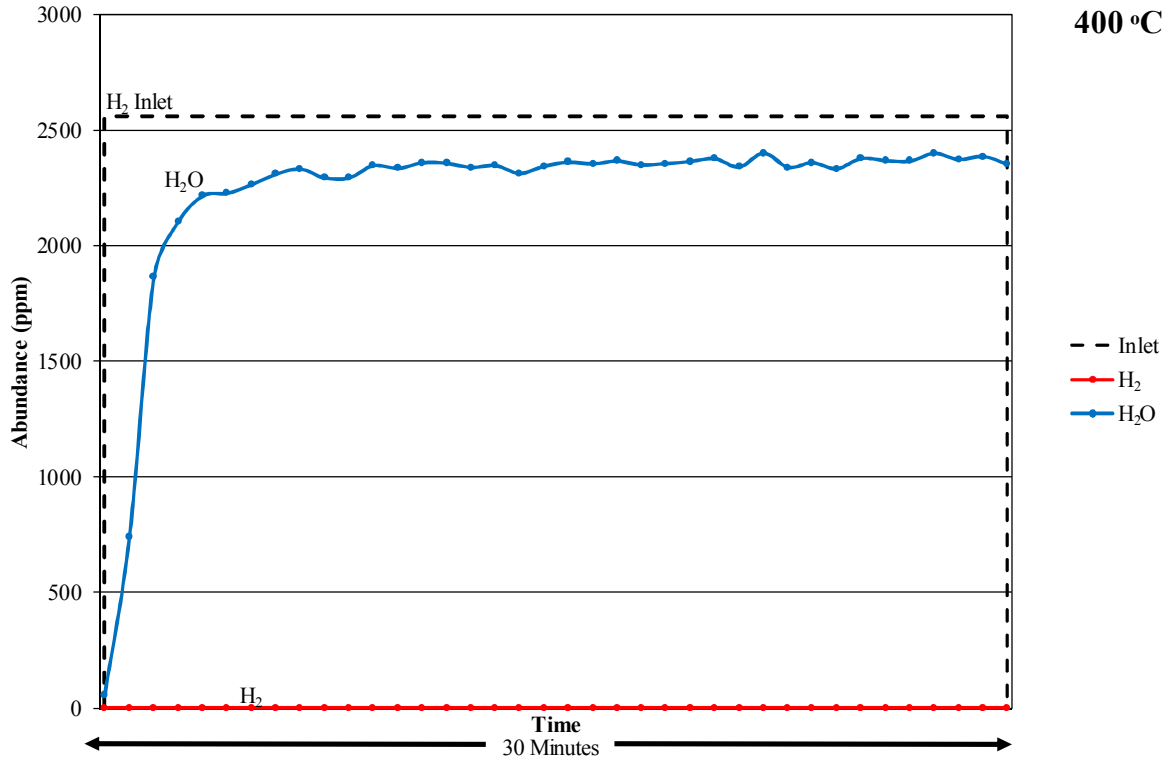

Figure 4.25 Main species observed during the rich phase of H_2–NSR over $Ba/Pt/Al_2O_3$ under 'Lean vs Rich 2' conditions at 400 °C. Rich conditions: 2500 ppm H_2, 2.9 % O_2, balance N_2.

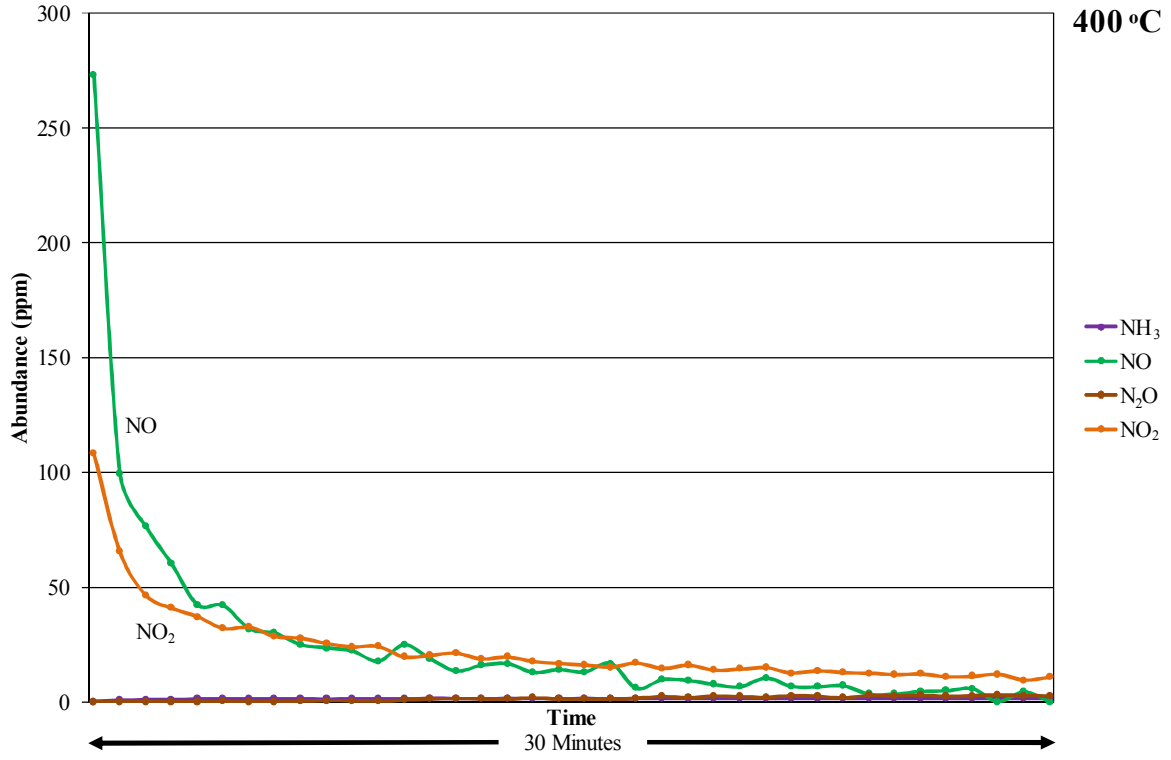

Figure 4.26 Trace species observed during the rich phase of H_2–NSR over $Ba/Pt/Al_2O_3$ under 'Lean vs Rich 2' conditions at 400 °C. Rich conditions: 2500 ppm H_2, 2.9 % O_2, balance N_2.

4.4.1.2.2.2 $Ba/Ag/Al_2O_3$

The catalysts had an average silver loading of 1.8 wt%, an average barium loading of 5.0 wt% and an average γ–Al_2O_3 loading of 27.6 wt% with respect to the complete catalyst system. Preparation details can be found in Section 4.1.

The overall measured abundances of both main and trace reactant species formed during H_2–NSR investigations over the $Ba/Ag/Al_2O_3$ catalyst under 'Lean vs Rich 2' conditions are shown in Figure 4.27. In addition, the species formed during the lean phase only are presented in Figure 4.28 and similarly during the rich phase only in Figure 4.29 (main species) and Figure 4.30 (trace species).

Unsurprisingly, the behaviour of the $Ba/Ag/Al_2O_3$ catalyst during the lean phase (Figure 4.28) closely resembles that of the 'Rich vs Lean 1' investigation.

- Breakthrough of both NO and NO_2 is observed and as their concentration continues to increase the NO_x^{Outlet} continues to approach the NO^{Inlet}.
- Significant initial formation of H_2O (2151 ppm) which sharply decreases to 13 ppm.

However, in this instance the area apparent between the NO_x^{Outlet} and NO^{Inlet} plots (representing the amount of NO_x stored on the catalyst) appears greater. This difference may be accounted for by the relative concentrations of NO_2 formed. Considering the values presented in Table 4.10; if the last values of the lean periods under each respective overall reaction condition are taken, on each occasion the NO conversion reaches a similar level (~31 %). However, the conversion to NO_2 greatly differs.

Although the specific experimental conditions for each lean period remain the same, it appears that the conditions of the rich phase are again influencing the NO_x storage capacity of the catalyst. On the occasion when only H_2 is present in the rich period, the conversion of NO to NO_2 reaches over 95 % by the end of the lean phase. Contrast this to the conversion of NO to NO_2 when the rich mixture includes both H_2 and O_2 (65 %) and the impact of O_2 is clear. Thus under the 'Lean vs Rich 2' conditions it appears that NO_x storage occurs throughout the entire lean phase (in a similar manner to the behaviour of the $Ba/Pt/Al_2O_3$ catalyst) and indeed the calculated NO_x^{Outlet} level suggests as much.

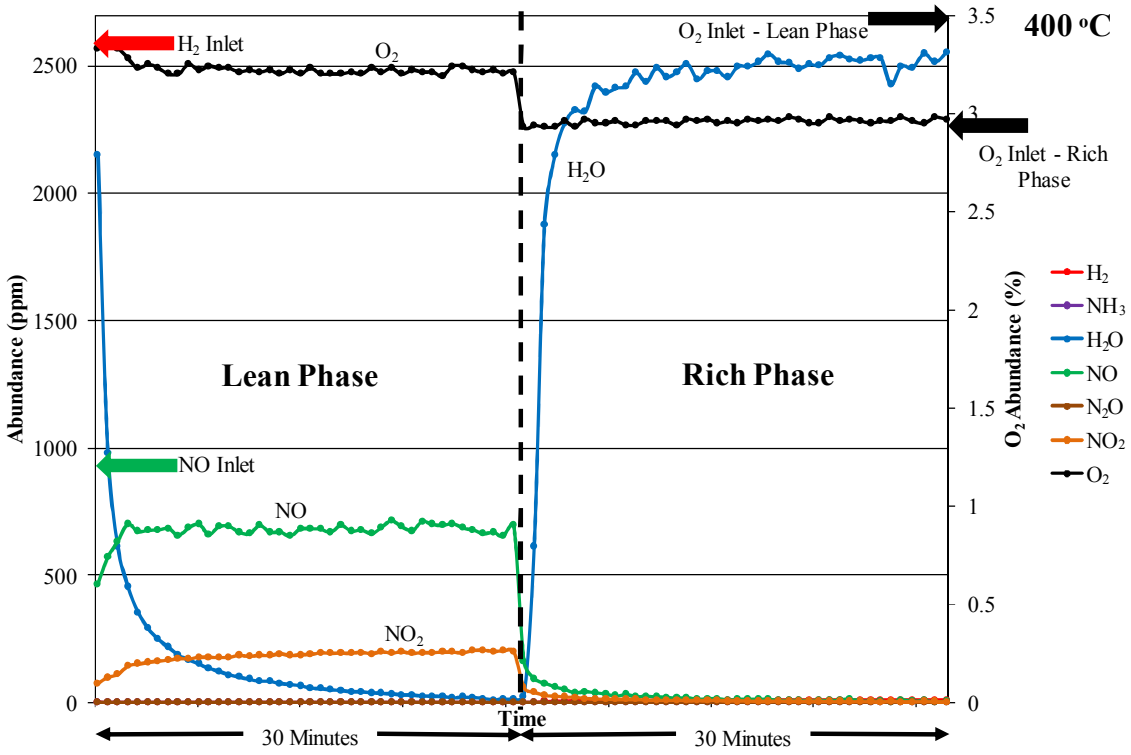

Figure 4.27 H_2–NSR over $Ba/Ag/Al_2O_3$ under 'Lean vs Rich 2' conditions at 400 °C. Lean conditions: 1000 ppm NO, 3.2 % O_2, balance N_2. Rich conditions: 2500 ppm H_2, 2.9 % O_2, balance N_2. Note that the secondary y–axis denotes O_2 abundance only.

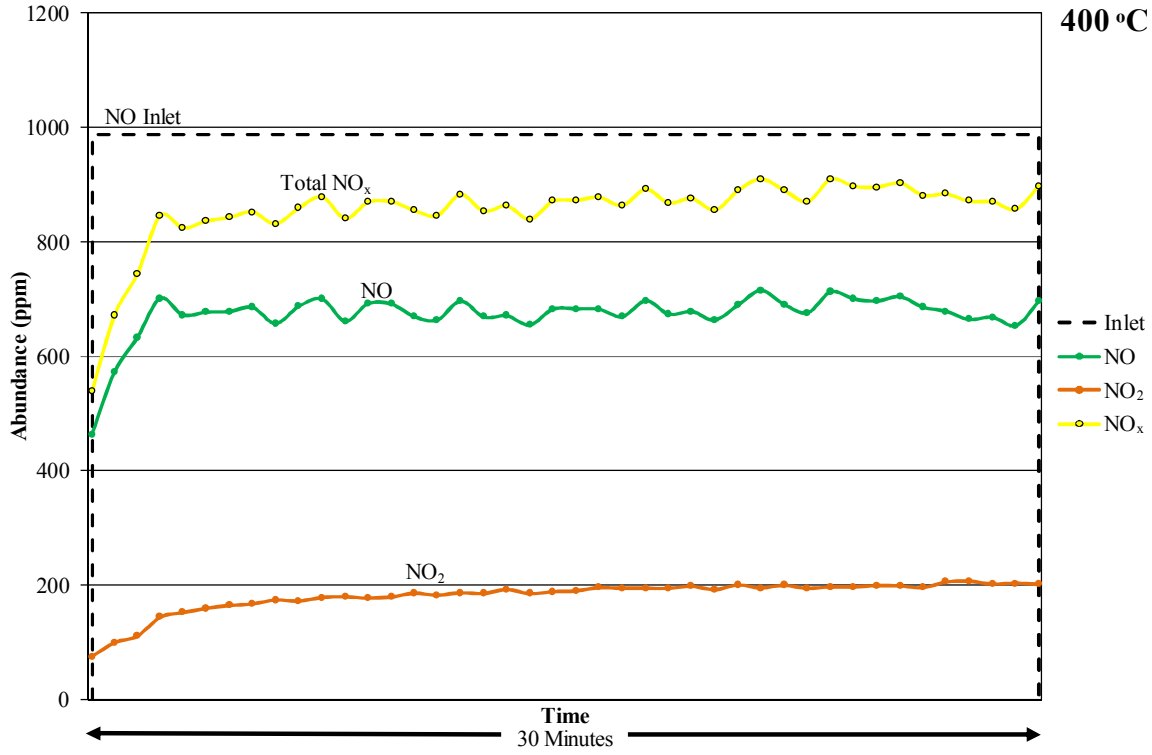

Figure 4.28 Species observed during the lean phase of H_2–NSR over $Ba/Ag/Al_2O_3$ under 'Lean vs Rich 2' conditions at 400 °C. Lean conditions: 1000 ppm NO, 3.2 % O_2, balance N_2.

Table 4.10 Conversion of NO and selectivity NO_2 over $Ba/Ag/Al_2O_3$ observed during the lean phases of the different overall reaction conditions.

Conditions	Conversion of NO (%)	Selectivity to NO_2 (%)
Lean vs Rich 1	30.7	95.2
Lean vs Rich 2	31.1	65.7

As a result, it is calculated that **14.7 %** of the supplied NO is stored on the catalyst during the lean phase, an increase of 4.2 % (with respect to the total NO_x stored) when compared with the 'Lean vs Rich 1' investigation over the same catalyst. In terms of the rich phase (Figure 4.29 and Figure 4.30), once again the $Ba/Ag/Al_2O_3$ performance closely resembles that of the $Ba/Pt/Al_2O_3$ catalyst:

- Immediate formation of H_2O is observed and a maximum measured concentration of 2553 ppm is measured at the end of the period (which incidentally closely matches the concentration of the H_2 inlet).
- Complete conversion of H_2 throughout the entire period.
- Evolution of NO (161 ppm decreasing to 6 ppm) and NO_2 (59 ppm dropping to 3 ppm).
- No evidence of N_2O or NH_3 formation.
- Calculated amount of stored NO_x which is converted to N_2 is **77.4 %**, a substantial increase on the results of the 'Lean vs Rich 1' conditions investigation (5.6 %).

The conclusions regarding O_2 presence in the 'rich' phase made in Section 4.4.1.2.2.1 are also applicable here:

- Excess H_2 is consumed to form H_2O.
- The formation of NO is greatly reduced whilst the formation of NO_2 is slightly increased.
- The formation of NH_3 or N_2O is supressed or indeed they are reacted further to form the observed species.

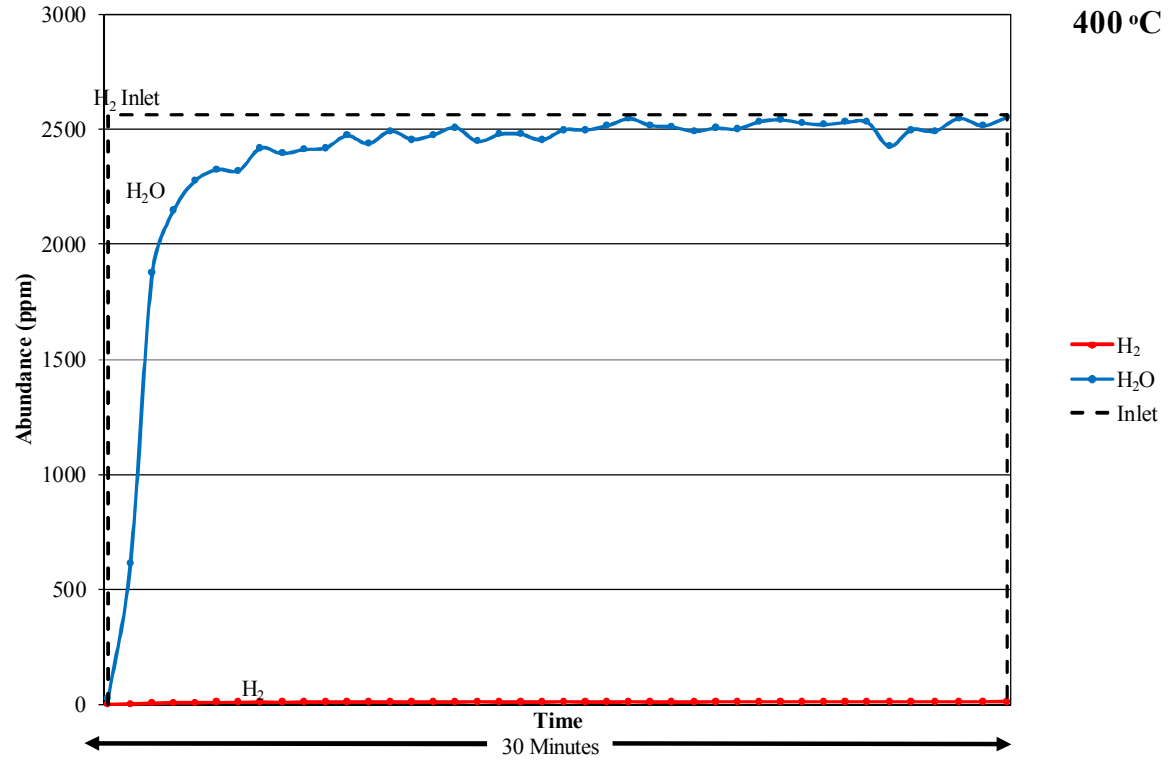

Figure 4.29 Main species observed during the rich phase of H_2–NSR over $Ba/Ag/Al_2O_3$ under 'Lean vs Rich 2' conditions at 400 °C. Rich conditions: 2500 ppm H_2, 2.9 % O_2, balance N_2.

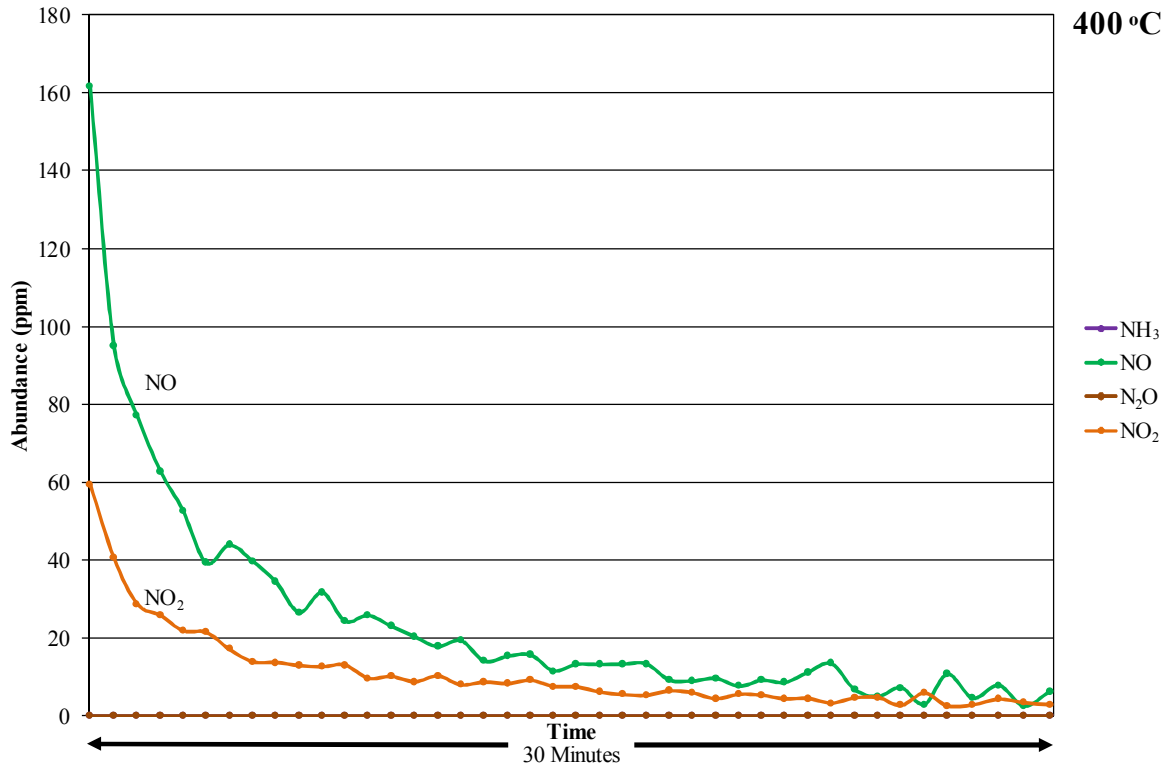

Figure 4.30 Trace species observed during the rich phase of H_2–NSR over $Ba/Ag/Al_2O_3$ at under 'Lean vs Rich 2' conditions 400 °C. Rich conditions: 2500 ppm H_2, 2.9 % O_2, balance N_2.

4.4.1.2.2.3 $K/Ag/Al_2O_3$

The catalysts had an average silver loading of 2.1 wt%, an average potassium loading of 16.0 wt% and an average γ–Al_2O_3 loading of 24.3 wt% with respect to the complete catalyst system. Preparation details can be found in Section 4.1.

The overall measured abundances of both main and trace reactant species formed during H_2–NSR investigations over the $K/Ag/Al_2O_3$ catalyst under 'Lean vs Rich 2' conditions are shown in Figure 4.31. In addition, the species formed during the lean phase only are presented in Figure 4.32 and similarly during the rich phase only in Figure 4.33 (main species) and Figure 4.34 (trace species).

The performance of the $K/Ag/Al_2O_3$ catalyst during the lean phase (Figure 4.32) after the catalyst has been subject to a number of 'Lean vs Rich 2' cycles, is slightly different to the performance observed as a result of the catalyst being subject to a number of 'Lean vs Rich 1' cycles:

- Although there is an initial decrease in the measured outlet NO concentration before a gradual increase is observed, the eventual NO level reached (795 ppm) is significantly greater than detected in the previous investigation.

- Breakthrough of NO_2 occurs after 150 s and N_2O after 250 s, which reach levels of 57 ppm and 19 ppm respectively.

- NO_x^{Outlet} approaches the NO^{Inlet} as the period progresses, reaching 85.8 % of the inlet concentration by the end of the phase and resulting in **22.9 %** of the supplied NO being stored on the catalyst during the lean phase. This compares favourably with the performance observed for the 'standard' $Ba/Pt/Al_2O_3$ catalyst (23.1 %) investigated under the same conditions.

- Significant initial abundance of H_2O (759 ppm) which sharply decreases to 0 ppm after 19.5 min.

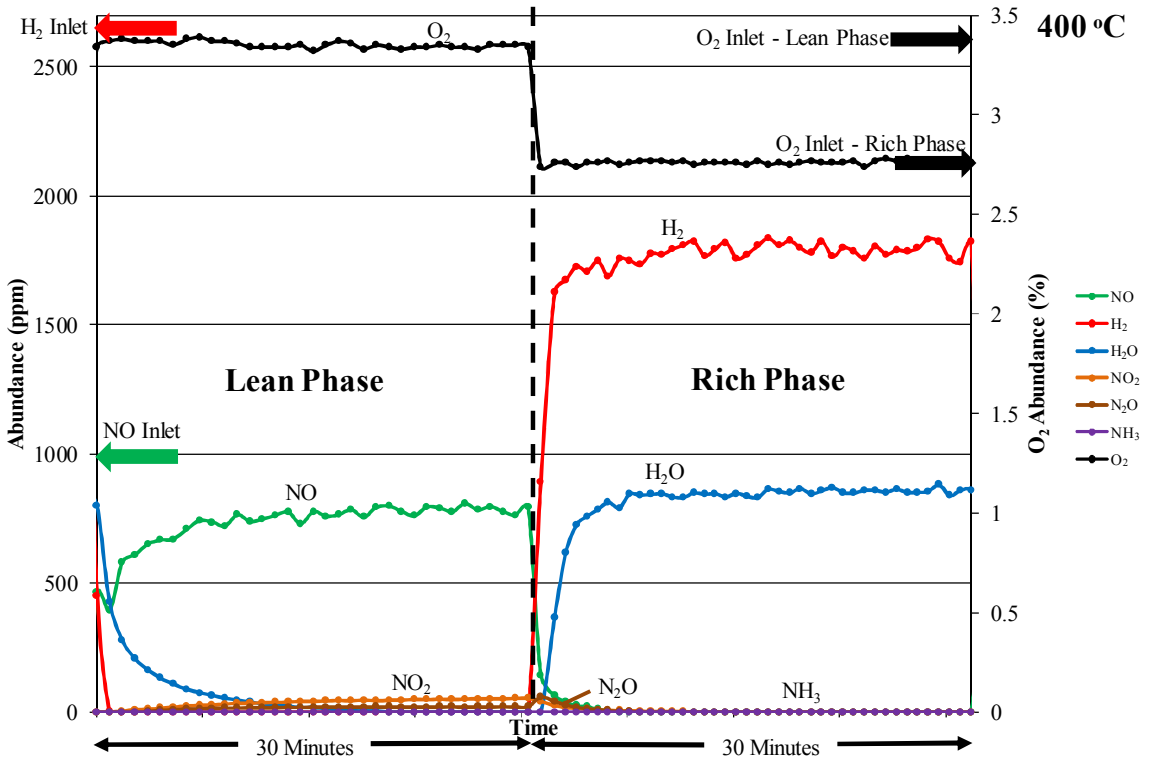

Figure 4.31 H_2–NSR over $K/Ag/Al_2O_3$ under 'Lean vs Rich 2' conditions at 400 °C. Lean conditions: 1000 ppm NO, 3.2 % O_2, balance N_2. Rich conditions: 2500 ppm H_2, 2.9 % O_2, balance N_2. Note that the secondary y–axis denotes O_2 abundance only.

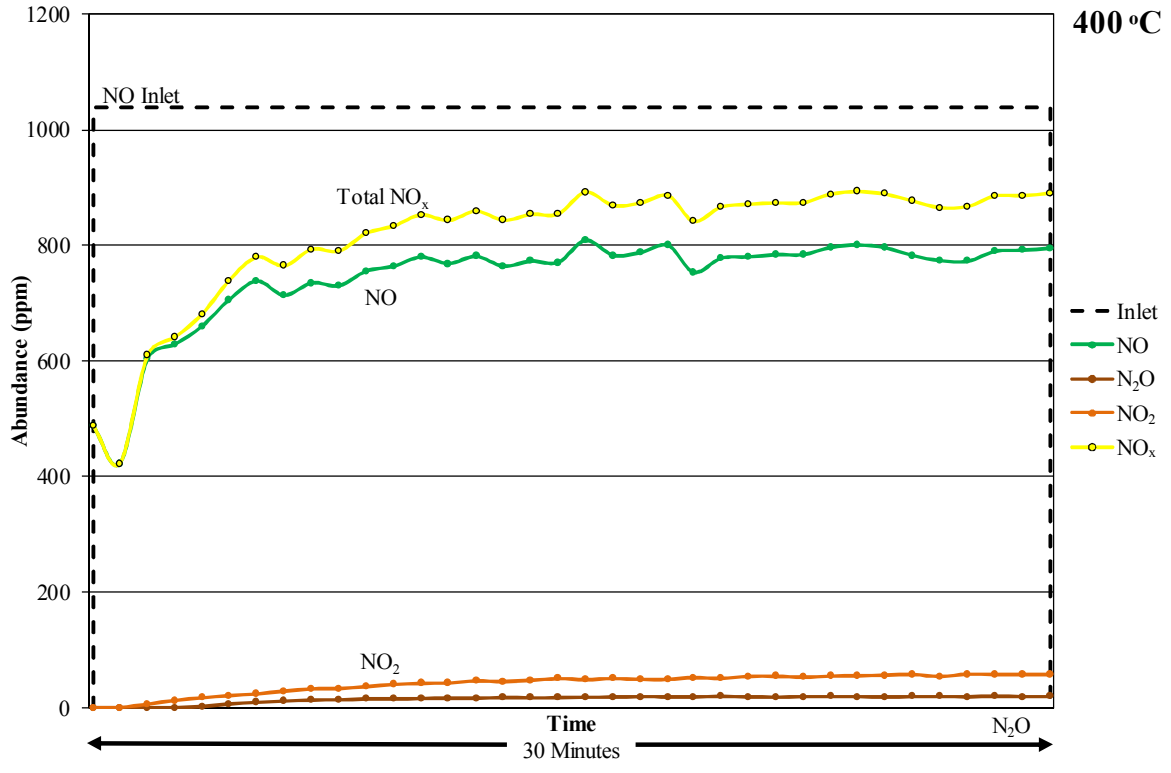

Figure 4.32 Species observed during the lean phase of H_2–NSR over $K/Ag/Al_2O_3$ under 'Lean vs Rich 2' conditions at 400 °C. Lean conditions: 1000 ppm NO, 3.2 % O_2, balance N_2.

On switching to the rich phase:

- H_2 and H_2O breakthrough are again both observed immediately and reach values of 1799 ppm and 817 ppm at the end of the phase respectively.
- Initial evolution of NO (138 ppm), N_2O (60 ppm) and NO_2 (47 ppm) which quickly fall to 0 ppm after 360 s, 450 s and 750 s respectively.
- No evidence of NH_3 formation.
- Calculated amount of stored NO_x converted to N_2 equals **92.0 %**; this is the greatest proportion of conversion to N_2 identified throughout this study, improving upon the performance of the $Ba/Pt/Al_2O_3$ catalyst explored under the same conditions by 9.7 % with respect to the total amount of stored NO_x converted to N_2.

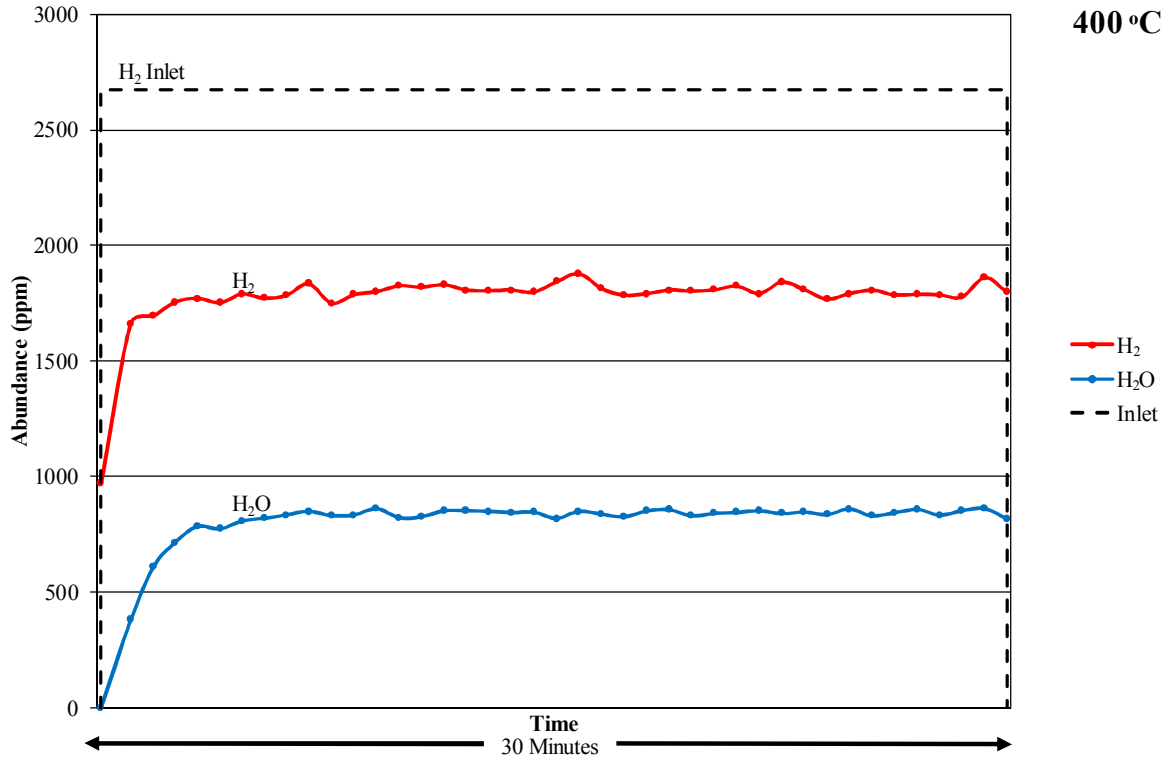

Figure 4.33 Main species observed during the rich phase of H_2–NSR over $K/Ag/Al_2O_3$ under 'Lean vs Rich 2' conditions at 400 °C. Rich conditions: 2500 ppm H_2, 2.9 % O_2, balance N_2.

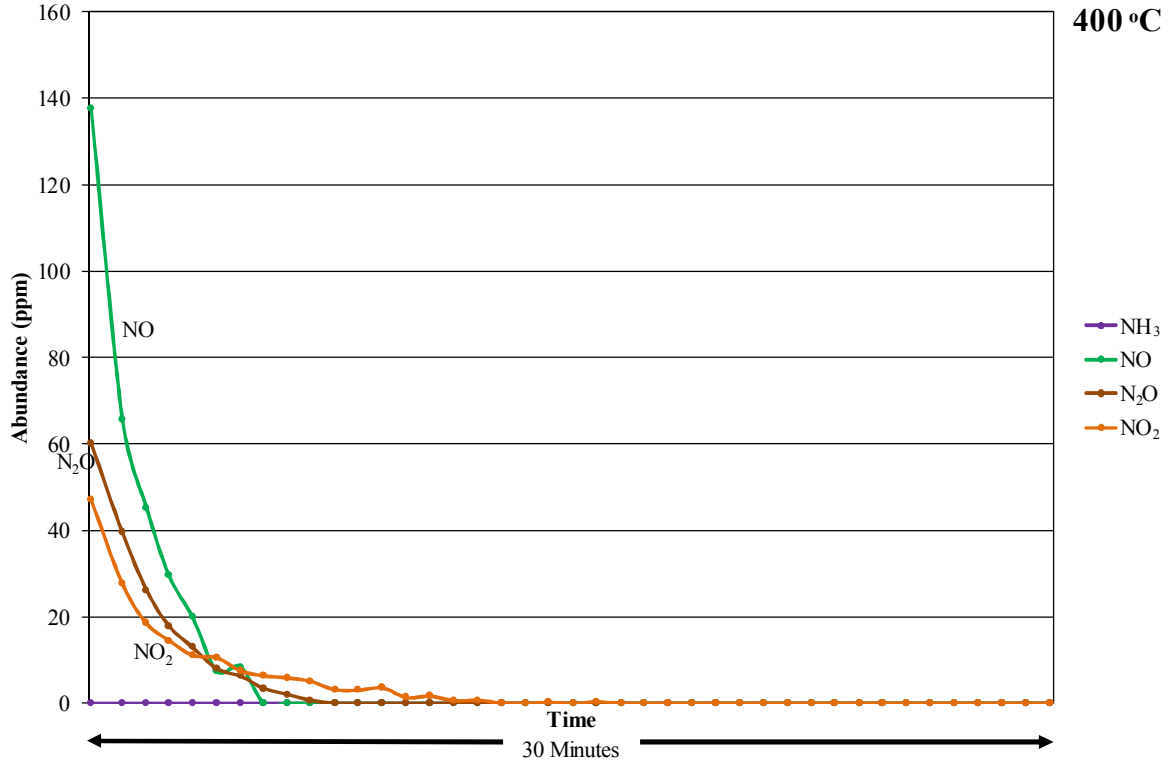

Figure 4.34 Trace species observed during the rich phase of H_2–NSR over $K/Ag/Al_2O_3$ at under 'Lean vs Rich 2' conditions 400 °C. Rich conditions: 2500 ppm H_2, 2.9 % O_2, balance N_2.

4.4.1.3 NSR Conclusions

Although the obtained traces have been discussed in detail throughout presentation of the results, a number of overall conclusions can be made with regards to the NSR reaction investigations when considering the complete data sets.

These conclusions relate to the summary information detailed in Table 4.11:

- In general, the novel silver catalysts demonstrate comparable performance to the 'standard' $Ba/Pt/Al_2O_3$ system.
- The addition of O_2 to the 'rich' phase of the NSR cycle increased both the amount of stored NO_x reduced to N_2 and the amount of NO_x subsequently stored during the lean phase, on all but one occasion (the amount of NO_x stored over the $K/Ag/Al_2O_3$ catalyst decreased after introduction of O_2).
- Addition of O_2 to the 'rich' phase of the NSR cycle also suppresses N_2O and NH_3 formation during this phase, often in their entirety.
- The $K/Ag/Al_2O_3$ catalyst demonstrates improved stored NO_x reduction capacity (92 %), in tandem with a similar NO_x storage capacity (22.9 %) with respect to the 'standard' $Ba/Ag/Al_2O_3$ catalyst (82.3 % and 23.1 % respectively). Whilst this data has not been normalised for catalyst loading, due to the vast difference in cost between platinum and silver, these results suggest a viable alternative.

Table 4.11 Summary table detailing the NO_x storage performance, and subsequent reduction of the stored NO_x species under both NSR reaction conditions.

Catalyst	Reaction Conditions	% Supplied NO stored	% Stored NO Reduced to N_2
$Ba/Pt/Al_2O_3$	Lean vs Rich 1	18.8	56.8
	Lean vs Rich 2	23.1	82.3
$Ba/Ag/Al_2O_3$	Lean vs Rich 1	10.5	5.6
	Lean vs Rich 2	14.7	77.4
$K/Ag/Al_2O_3$	Lean vs Rich 1	72.3	59.8
	Lean vs Rich 2	22.9	92.0

4.4.2 TPD/TPSR

TPD and TPSR measurements were carried out in order to investigate the catalysts abilities to adsorb different reactant species and identify any evidence of surface reactions at particular temperatures. Specifically these investigations may give information as to how the nitrates/nitrates formed in the storage phase are subsequently decomposed when subject to temperature. As described in Mudiyanselage *et al.* (2012), some possible pathways for thermal decomposition of nitrites are:

$$Ba(NO_2)_2 \rightarrow NO_2 + NO + BaO \quad (4.10)$$

$$2Ba(NO_2)_2 \rightarrow 4NO + O_2 + 2BaO \quad (4.11)$$

$$Ba(NO_2)_2 \rightarrow 2NO + BaO_2 \quad (4.12)$$

$$BaO_2 \rightarrow O_2 + 2BaO \quad (4.13)$$

$$3Ba(NO_2)_2 \rightarrow 4NO + Ba(NO_3)_2 + 2BaO \quad (4.14)$$

Likewise, some possible pathways for thermal decomposition of nitrates are:

$$Ba(NO_3)_2 \rightarrow 2NO_2 + BaO_2 \quad (4.15)$$

$$2Ba(NO_3)_2 \rightarrow 4NO_2 + O_2 + 2BaO \quad (4.16)$$

$$2Ba(NO_3)_2 \rightarrow 4NO + 3O_2 + 2BaO \quad (4.17)$$

$$Ba(NO_3)_2 \rightarrow 2NO + O_2 + BaO_2 \quad (4.18)$$

$$Ba(NO_3)_2 \rightarrow NO_2 + NO + O_2 + BaO \quad (4.19)$$

Note that there is no proposed formation of N_2O in the above reactions although from the preliminary experiments its formation has been observed.

4.4.2.1 NO–TPD

The reactor was loaded with three monolith pieces of the catalyst under investigation. The reactor temperature was increased to 500 ^{o}C at a rate of 10 ^{o}C min^{-1} under a flow of N_2 at 300 cm^3 min^{-1}. Then 8000 ppm H_2 in N_2 was introduced at 300 cm^3 min^{-1} for 30 min, before the reactor was flushed with N_2 at 330 cm^3 min^{-1} for 15 min. The catalysts were then subject to 10 % O_2 at 600 cm^3 min^{-1} for 15 min before being cooled down in N_2 at 330 cm^3 min^{-1} to 150 ^{o}C. 1000 ppm NO in N_2 was then introduced at 400 cm^3 min^{-1} for 30 min. Finally the reactor was flushed with N_2 at 300 cm^3 min^{-1} for 15 min to remove any residual NO and the temperature increased to 700 ^{o}C at a rate of 10 ^{o}C min^{-1}. The desorbed species were subsequently measured. Although it is recognised that typically both NO and O_2 would be present in the reaction mixture, and that the combination would produce the desired stored NO_x species, the presence of O_2 is also responsible for undesired side reactions. Thus it is anticipated that by pre–treating the catalysts in O_2 the necessary surface O–species will be created and react with the NO supplied during the adsorption step.

4.4.2.1.1 $Ba/Pt/Al_2O_3$

The catalysts had an average platinum loading of 0.2 wt%, an average barium loading of 4.7 wt% and an average γ–Al_2O_3 loading of 28.2 wt% with respect to the complete catalyst system. Preparation details can be found in Section 4.1.

Following the NO–TPD procedure in Section 4.4.2.1 the desorbed species were measured and the traces are displayed in Figure 4.35. Although as discussed in Section 4.4.2.1 the adsorption step occurs in the absence of O_2, it appears that formation of N–species still takes place. This gives some indication of catalyst affinity for NO and the surface reactions occurring, and justifies the experimental method. It should be noted that the adsorption of NO occurs in minimal quantities; only 4.5 % of the supplied NO was adsorbed during the adsorption step in this particular experiment.

Loosely bound NO dominates the evolved surface NO_x species and is released on heating from 193 – 598 °C. It reaches a maximum of 73 ppm from 193 – 518 °C although levels reach 1118 ppm at 578 °C. In addition, slight N_2O formation (1 – 2 ppm) occurs at temperatures of 204 °C above, although a gradual increase occurs from 498 °C and formation reaches 174 ppm at 697 °C. There is some evidence of slight NO_2 formation ($\leq$7 ppm) at lower temperatures (175 – 361 °C) however, more significant formation occurs from 558 °C and reaches 12 ppm at 696 °C.

According to Pohanish (2008); $Ba(NO_3)_2$ decomposes at 210 °C and then melts at 590 °C. This may explain the presence of NO_2 and N_2O at the lower temperatures and may also contribute to the NO levels at these temperatures. As temperatures increase, more N_2O is released as melting occurs.

Table 4.12 Proportion of the N–containing species desorbed during NO–TPD over $Ba/Pt/Al_2O_3$.

Species	% of desorption products
NO	39.4
N_2O	55.9
NO_2	4.7

Table 3.19 details the selectivity in terms of the observed N–species which evolved during NO–TPD over $Ba/Pt/Al_2O_3$. It is apparent that the majority of the adsorbed NO is converted to N_2O, whilst the majority of the remainder remains as NO and there is minimal formation of NO_2. However, when considering the mass balance; in terms of NO adsorption and N–containing species desorption, it is apparent that the abundance of the evolved N–species account for 390 % of the adsorbed NO. Although pre–treatment steps were taken in order to remove all surface species from the catalysts, it appears that conditions were not appropriate in order to achieve this. The catalysts had been subject to NSR investigations prior to TPD studies and it appears that surface N–species during such trials were not removed until higher temperatures i.e. >500 °C were reached. Thus the results presented in Table 3.19 and Figure 4.35 are presented for an indication only.

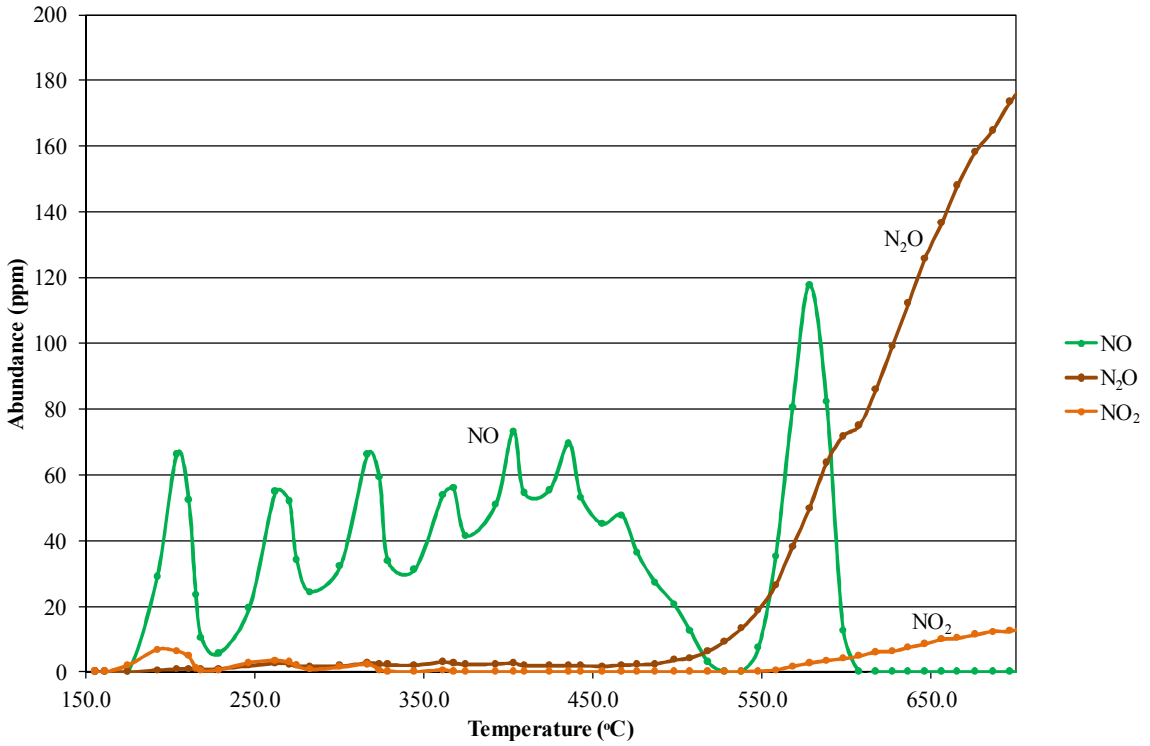

Figure 4.35 Desorbed N–species observed during NO–TPD over $Ba/Pt/Al_2O_3$ with an adsorption temperature of 150 °C.

4.4.2.1.2 $Ba/Ag/Al_2O_3$

The catalysts had an average silver loading of 1.8 wt%, an average barium loading of 5.0 wt% and an average γ–Al_2O_3 loading of 27.6 wt% with respect to the complete catalyst system. Preparation details can be found in Section 4.1.

Following the NO–TPD procedure in Section 4.4.1.3 the desorbed species were measured and are displayed in Figure 4.36. In an effort to aid explanation of the above results, the detailed procedure was repeated; without the NO adsorption step and without both the H_2 pre–treatment and NO adsorption steps although these results are not presented here.

The observed results follow a similar pattern to those obtained for the $Ba/Pt/Al_2O_3$ catalyst system:

- Loosely bound NO dominates the evolved surface NO_x species and is released on heating from 183 – 548 °C reaching a maximum of 50 ppm at 356 °C.
- Slight N_2O formation (1 – 4 ppm) occurs at temperatures of 194 – 515°C. Above these temperatures more significant evolution is witnessed; 15 ppm at 690 °C.
- Slight NO_2 formation (≤3 ppm) at lower temperatures (202 – 406 °C).

The decomposition and melting of $Ba(NO_3)_2$ at 210 °C and then 590 °C has already been discussed in Section 4.4.2.1.1. Given the nature of the measurements observed here, this explanation may be equally applied to the obtained results of this catalyst system.

In terms of the distribution of the observed N–species desorption products, a summary is presented in Table 4.13. In this case, the majority of the desorption products are NO (71.3 %) whilst almost a quarter are N_2O (24.7 %) and only 4.0 % of the products are NO_2.

Table 4.13 Proportion of the N–containing species desorbed during NO–TPD over $Ba/Pt/Al_2O_3$.

Species	% of desorption products
NO	71.3
N_2O	24.7
NO_2	4.0

This suggests that only adsorption of NO, and not further reaction is favoured. Again the overall measured levels of N–species are very low in comparison to the total supplied concentration of NO and indeed there is a calculated NO uptake of only 5.91 % during the adsorption step, although this is an improvement on the adsorption levels observed for NO–TPD and H_2–TPSR of the $Ba/Pt/Al_2O_3$ system.

However, the total abundance of desorption products accounts for 89.7 % of the apparent adsorbed NO. This value is in closer agreement than the corresponding value for the $Ba/Pt/Al_2O_3$ system (390 %) and given that the evolved N_2O concentration appears to still be rising at 700 °C, it could be envisaged that N_2O abundance may also account for the remaining 10.3 %.

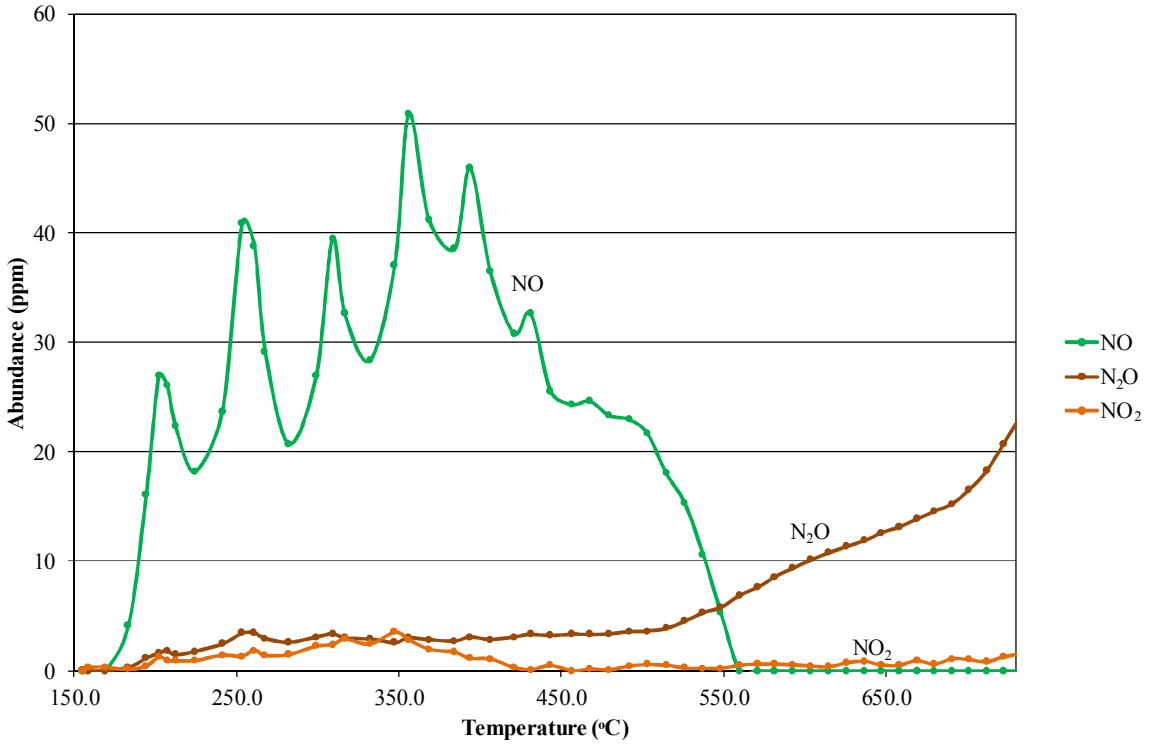

Figure 4.36 Desorbed N–species observed during NO–TPD over $Ba/Ag/Al_2O_3$ with an adsorption temperature of 150 °C.

4.4.2.1.3 $K/Ag/Al_2O_3$

The catalysts had an average silver loading of 2.1 wt%, an average potassium loading of 16.0 wt% and an average γ–Al_2O_3 loading of 24.3 wt% with respect to the complete catalyst system. Preparation details can be found in Section 4.1.

Following the NO–TPD procedure in Section 4.4.1.3 the desorbed species were measured and are displayed in Figure 4.37. Once again the performance of the $K/Ag/Al_2O_3$ catalyst demonstrates significantly different behaviour to those catalysts previously investigated:

- No N–species are observed at temperatures lower than 350 °C.
- At 359 °C, initial N_2O formation is observed and this rapidly increases to 112 ppm at 472 °C and then 490 ppm at 698 °C.
- Formation of NO_2 occurs at 398°C and gradually increases to 41 ppm at 698 °C.
- NO is released between 574 °C and 689 °C, peaking at 346 ppm at 654 °C.

This formation amounts to the relevant proportions detailed in Table 4.14; there is considerable preference towards forming N_2O over only adsorption of NO or formation of N_2O.

Although NO adsorption now reaches 9.59 % with respect to the total amount of NO supplied, the significant evolution of N–species (in particular N_2O and NO) results in the abundance of the total desorption products equalling 488 % of apparent adsorption. Again it is not clear the cause of this substantial mismatch, although it appears that pre–treatment process proved inadequate, and significant levels of N–species, in particular N_2O, were already present on the surface of the catalyst prior to analysis.

Table 4.14 Proportion of the N–containing species desorbed during NO–TPD over $K/Ag/Al_2O_3$.

Species	% of desorption products
NO	26.6
N_2O	67.6
NO_2	5.8

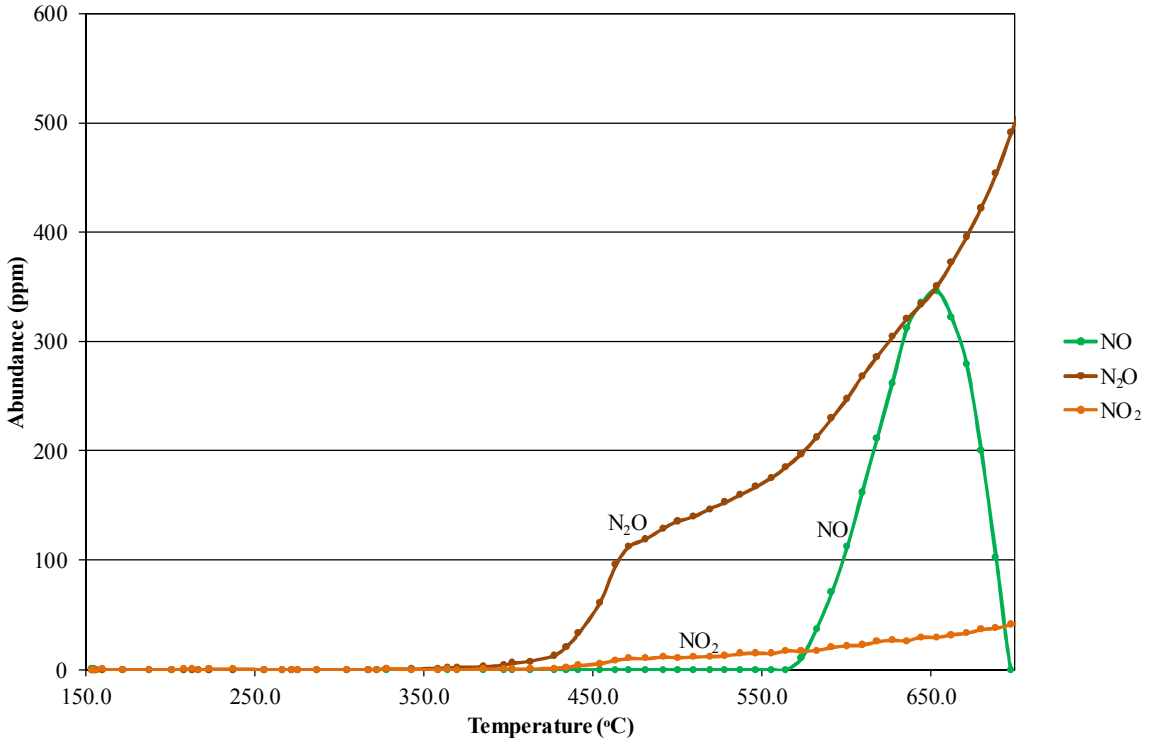

Figure 4.37 Desorbed N–species observed during NO–TPD over $K/Ag/Al_2O_3$ with an adsorption temperature of 150 °C.

4.4.2.2 H_2–TPSR

The reactor was loaded with three monolith pieces of the catalyst under investigation. The reactor temperature was increased to 500 ^oC at a rate of 10 ^oC min^{-1} under a flow of N_2 at 300 mL min^{-1}. Then 8000 ppm H_2 in N_2 was introduced at 300 cm^3 min^{-1} for 30 min, before the reactor was flushed with N_2 at 330 cm^3 min^{-1} for 15 min. The catalysts were then subject to 10 % O_2 at 600 cm^3 min^{-1} for 15 min before being cooled down in N_2 at 330 cm^3 min^{-1} to 150 ^oC. 1000 ppm NO in N_2 was then introduced at 400 cm^3 min^{-1} for 30 min. The reactor was then flushed with N_2 at 300 cm^3 min^{-1} for 15 min to remove any residual NO. Finally, 2000 ppm H_2 in N_2 at a flow rate of 400 cm^3 min^{-1} was introduced and the temperature increased to 700 ^oC at a rate of 10 ^oC min^{-1}. The desorbed species were subsequently measured.

4.4.2.2.1 $Ba/Pt/Al_2O_3$

The catalysts had an average platinum loading of 0.2 wt%, an average barium loading of 4.7 wt% and an average γ–Al_2O_3 loading of 28.2 wt% with respect to the complete catalyst system. Preparation details can be found in Section 4.1.

H_2–TPSR was conducted following the procedure detailed in Section 4.4.2.2. The results are displayed in Figure 4.38 and should be compared to the results of the NO–TPD investigation presented in Figure 4.35:

- The presence of H_2 during desorption appears to suppress the formation of NO, or indeed the NO is reacted with the H_2 to form H_2O; there is no evolved NO observed throughout the entire temperature range.

- Whilst N_2O formation was significant in NO–TPD studies (forming around 204 ^oC and reaching 174 ppm at 697 ^oC), there is very little formation observed during the TPSR investigation. However, slight formation (1 – 2 ppm) occurs at temperatures as low as 208 ^oC before gradually increasing to a peak of 18 ppm at 585 ^oC.

- There was no considerable NO_2 formation observed throughout.

Once more, formation of N_2O appears to be the favoured process, with no NO and only minimal NO_2 observed (Table 4.15).

Assuming the absence of any surface N–species prior to catalyst investigation, and by considering the mass balance in terms of NO adsorption and N–containing species desorption; the desorbed species account for 56.7 % of the apparent adsorbed NO. Thus 43.3 % of apparent adsorbed NO is reduced throughout the desorption period. Incidentally, only 3.22 % of the supplied NO was adsorbed on to the catalyst during the adsorption step.

In terms of H_2 and H_2O abundance: breakthrough of H_2 is apparent on introducing the reaction mixture at 150 °C. However, evolution of H_2O (and indeed any other species) is not apparent until 208 °C. H_2O formation generally increases to a local maximum of 612 ppm at 271 °C, before it drops to 280 ppm at 394 °C and gradually increases to 712 at 700 °C. H_2 abundance reaches a peak of 1758 ppm at 230 °C and maintains a somewhat steady concentration until 417 °C after which is gradually decreases (as H_2O abundance increases) to a final value of 1139 ppm at 700 °C. In addition to reaction with N–species, it may be assumed that H_2 is also combining with surface O–species to form H_2O, particularly at higher temperatures (>400 °C).

Table 4.15 Proportion of the N–containing species desorbed during H_2–TPSR over $Ba/Pt/Al_2O_3$.

Species	% of desorption products
NO	0.0
N_2O	98.9
NO_2	1.1

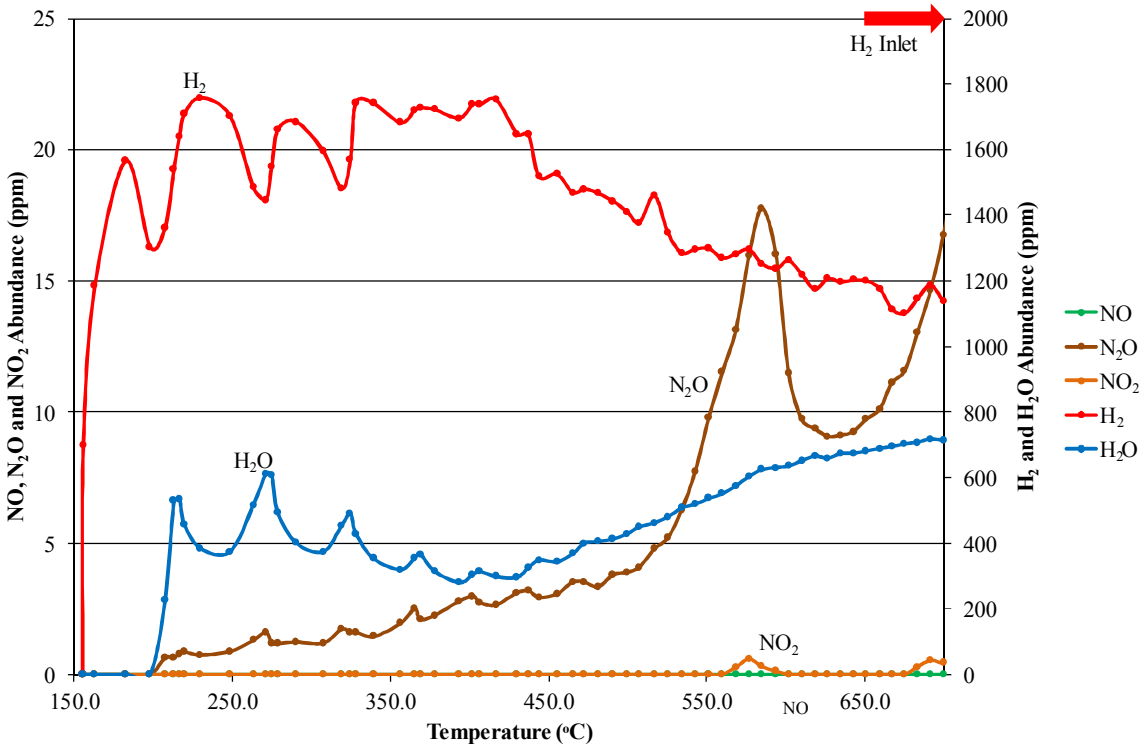

Figure 4.38 Desorbed N–species observed during H_2–TPSR over $Ba/Pt/Al_2O_3$ with an adsorption temperature of 150 °C. Note that the secondary y–axis denotes H_2 and H_2O abundance only.

4.4.2.2.2 $Ba/Ag/Al_2O_3$

The catalysts had an average silver loading of 1.8 wt%, an average barium loading of 5.0 wt% and an average γ–Al_2O_3 loading of 27.6 wt% with respect to the complete catalyst system. Preparation details can be found in Section 4.1.

H_2–TPSR was conducted following the procedure detailed in Section 4.4.2.2. The results are displayed in Figure 4.39 and should be compared to the results of the NO–TPD investigation presented in Figure 4.36. As can be seen, the results match quite closely with that of the NO–TPD experiment over the same catalyst system:

- NO is released at lower temperatures, and in similar abundance (maximum of 62 ppm at 298 °C) to the NO–TPD experiment, although the temperature range in which it is released is narrower (156 – 415 °C).
- There is some impact on NO_2 concentration which is now only evident in very small amounts (≤1 ppm) and predominantly in the 569 – 687 °C temperature range.
- The N_2O levels are not greatly affected by the presence of H_2; slight formation (1 – 4 ppm) occurs at temperatures of 166 – 446 °C beyond which a gradual increase in evolution is observed and reaches a maximum of 14 ppm at 698 °C.
- H_2 abundance after introduction falls steadily to 1219 ppm at 698 °C.
- H_2O breakthrough occurs at 209 °C and after an initial sharp increase to 291 ppm at 258 °C there is then a gentler increase to 707 ppm at 698 °C.

In this instance, 7.10 % of the supplied NO was adsorbed on to the catalyst during the adsorption step, again an increase on the maximum relative NO adsorption observed. Once again assuming the absence of any surface N–species prior to catalyst investigation, the desorbed species account for 72.3 % of the apparent adsorbed NO. Thus 27.7 % of apparent adsorbed NO is reduced throughout the desorption period. In addition, on comparison to the NO–TPD results (89.7 % of adsorbed NO was subsequently desorbed) it may be presumed that at least 17.4 % of the stored N–species were reduced to N_2 during TPSR.

Although the results suggest there is some reduction of N–species occurring throughout TPSR, from the obtained results the reaction is not clear. Perhaps there is some reduction of NO at higher temperatures (425 – 548 °C), thus accounting for the narrower temperature range of NO detection.

In terms of the proportion of each N–species evolved during TPSR, the results are presented in Table 4.16. They match very closely the results of the NO–TPD investigation (Table 4.13) suggesting that only adsorption of NO, and not further reaction, is favoured.

Table 4.16 Proportion of the N–containing species desorbed during H_2–TPSR over $Ba/Ag/Al_2O_3$.

Species	% of desorption products
NO	72.7
N_2O	25.8
NO_2	1.5

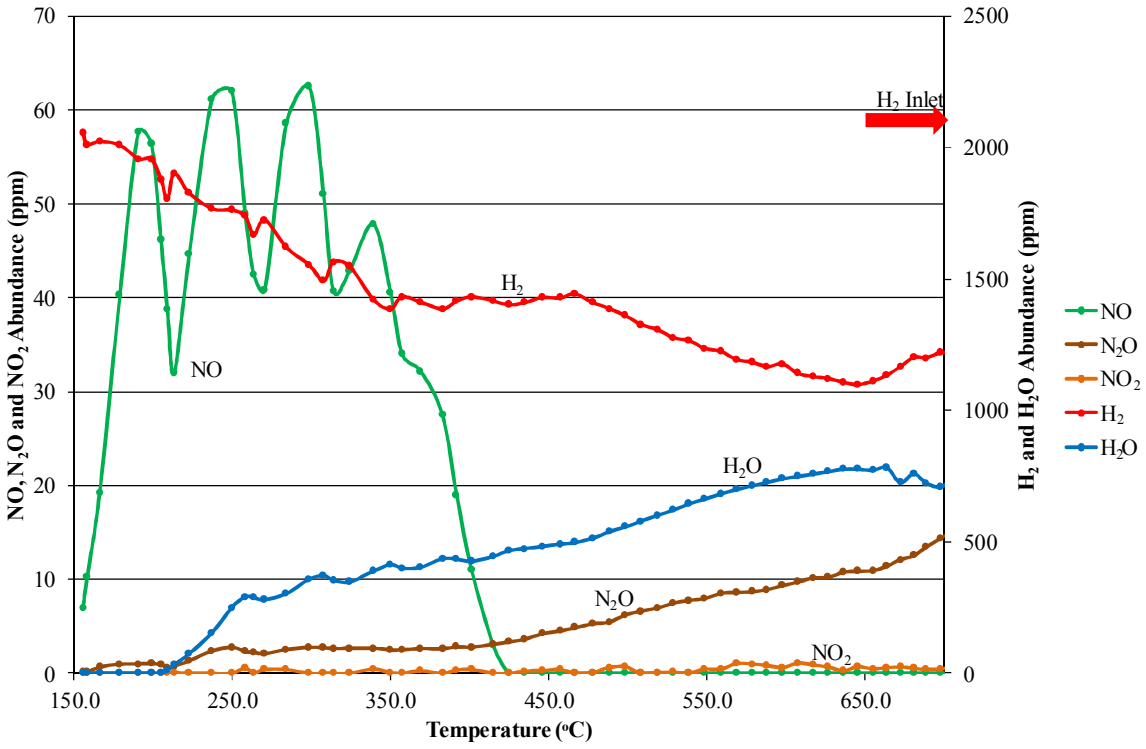

Figure 4.39 Desorbed N–species observed during H_2–TPSR over $Ba/Ag/Al_2O_3$ with an adsorption temperature of 150 °C. Note that the secondary y–axis denotes H_2 and H_2O abundance only.

4.4.2.2.3 $K/Ag/Al_2O_3$

The catalysts had an average silver loading of 2.1 wt%, an average potassium loading of 16.0 wt% and an average γ–Al_2O_3 loading of 24.3 wt% with respect to the complete catalyst system. Preparation details can be found in Section 4.1.

TPSR was conducted following the procedure detailed in Section 4.4.2.2. The results are displayed in Figure 4.40 and should be compared to the results of the NO–TPD investigation presented in Figure 4.37.

Similar results to those obtained during NO–TPD are observed:

- The presence of H_2 has little effect on the shape of the N_2O and NO_2 desorption curves, although their concentrations are relatively less.
    - N_2O formation is observed at 322 °C, rising rapidly to 75 ppm at 506 °C and then gradually increasing to 222 ppm at 699 °C.
    - Formation of NO_2 first occurs at 407 °C and gradually increases to 14 ppm at 699 °C. NO is only released between 202 °C and 279 °C, peaking at 11 ppm at 270 °C.
- H_2 abundance steadily drops as temperature increases although, as H_2O breakthrough occurs at 279 °C, the H_2 concentration also increases.
- Somewhat steady values of ~1600 ppm (H_2) and ~650 ppm (H_2O) are then observed before consumption of H_2 (and formation of H_2O increased) at a temperature of 465 °C.
- Final abundances at 699 °C for H_2 and H_2O reach 810 and 986 ppm respectively.

This results in an obvious switch in terms of the proportions of each N–species observed during desorption (Table 4.17). N_2O accounts for 92.4 % of the desorbed N–species whilst NO_2 and NO account for 5.7 % and 1.9 % respectively.

A drop in the relative adsorption of NO, to 7.1 %, is observed in this investigation although there is also a drop in the total abundance of desorption products; albeit to 252 % of the apparent total NO adsorption. This may suggest there is some reduction occurring, and indeed the near absence of NO, and vastly reduced concentrations of N_2O and NO_2 (with respect to their concentrations during NO–TPD) support this.

Table 4.17 Proportion of the N–containing species desorbed during H_2–TPSR over $Ba/Ag/Al_2O_3$.

Species	% of desorption products
NO	1.9
N_2O	92.4
NO_2	5.7

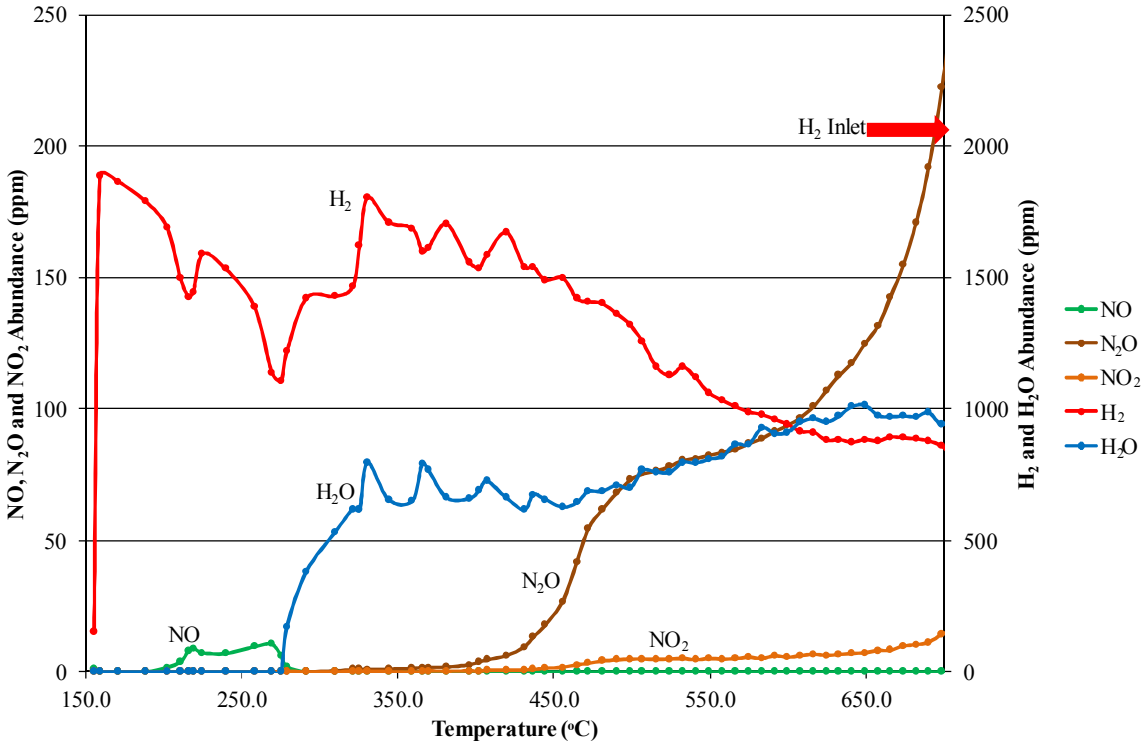

Figure 4.40 Desorbed N–species observed during H_2–TPSR over $K/Ag/Al_2O_3$ with an adsorption temperature of 150 °C. Note that the secondary y–axis denotes H_2 and H_2O abundance only.

4.4.2.3 H_2–TPD

The reactor was loaded with three monolith pieces of the catalyst under investigation. The reactor temperature was increased to 500 ^oC at a rate of 10 ^oC min^{-1} under a flow of N_2 at 300 cm^3 min^{-1} and then cooled to 200 ^oC, the adsorption temperature. 2000 ppm H_2 in N_2 was introduced at 440 cm^3 min^{-1} for 5 min, before the reactor was flushed with N_2 at 330 cm^3 min^{-1} for 5 min. The temperature was then increased to 500 ^oC at a rate of 5 ^oC min^{-1} and then 700 ^oC at a rate of 10 ^oC min^{-1} and the desorbed species were subsequently measured. The slower temperature ramp rate to 500 ^oC was in an effort to identify desorbed species.

With reference to the preliminary TPD experiments, the adsorption temperature was increased to 200 ^oC in order to increase the catalysts' affinity for H_2 and also investigate the materials at conditions more closely related to the application. Ideally a range of different adsorption temperatures would be explored although this was not conducted in this investigation.

However, although the preliminary investigated H_2–TPD procedure did provide some evidence of H_2 affinity for the $Ba/Pt/Al_2O_3$ catalysts, and the adsorption temperature was increased as a result, in a similar fashion to the SCR catalysts there was no apparent desorption observed for any the catalyst materials investigated in this Section and as a result, there will be no presentation of H_2–TPD results here.

4.4.2.4 TPD/TPSR Conclusions

Although the obtained traces have been discussed in detail throughout presentation of the results, a number of overall conclusions can be made with regards to both the TPD and TPSR reaction investigations when considering the complete data sets.

These conclusions relate to the summary information detailed in Table 4.18 and Table 4.19:

- $K/Ag/Al_2O_3$ demonstrates the greatest affinity for NO at an adsorption temperature of 150 °C, followed by $Ba/Ag/Al_2O_3$ and then $Ba/Pt/Al_2O_3$. However, adsorption levels appear low in comparison to supplied amounts, 3.2 – 9.6 %, and the mass balances are not always successfully realised.

- The presence of H_2 (during TPSR) significantly reduces the relative amount of desorbed N–species observed – this suggests reaction with the H_2 to form N_2 and H_2O.

- The breakdown in proportion of N–species is similar for both $Ba/Pt/Al_2O_3$ and $K/Ag/Al_2O_3$ catalysts during both NO–TPD and H_2–TPSR. During NO–TPD formation of N_2O is preferred over NO adsorption and the formation of NO_2. On introduction of H_2 during TPSR, selectivity to N_2O is increased and approaches 100 %.

- The $Ba/Ag/Al_2O_3$ catalyst demonstrates a similar breakdown in proportion of N–species for both NO–TPD and H_2–TPSR investigations; preference of NO adsorption, followed by N_2O formation and then NO_2 formation.

Table 4.18 Summary table detailing the relative measured amounts of NO adsorbed and subsequently desorbed during NO–TPD and H_2–TPSR investigations.

Catalyst	NO–TPD		H_2–TPSR	
	Relative amount of NO adsorbed (%)	Relative amount of N–species desorbed (%)	Relative amount of NO adsorbed (%)	Relative amount of N–species desorbed (%)
$Ba/Pt/Al_2O_3$	4.5	390	3.2	56.7
$Ba/Ag/Al_2O_3$	5.9	89.7	7.1	72.3
$K/Ag/Al_2O_3$	9.6	488	7.1	252

Table 4.19 Summary table detailing the relative proportion of each N–species desorbed during NO–TPD and H_2–TPSR investigations.

Catalyst	NO–TPD Proportion (%)			H_2–TPSR Proportion (%)		
	NO	N_2O	NO_2	NO	N_2O	NO_2
$Ba/Pt/Al_2O_3$	39.4	55.9	4.7	0	98.9	1.1
$Ba/Ag/Al_2O_3$	71.3	24.7	4.0	72.7	25.8	1.5
$K/Ag/Al_2O_3$	26.6	67.6	5.8	1.9	92.4	5.7

4.4.3 Key Conclusions

In light of the results obtained for the explored materials in NSR, TPD and TPSR investigations, a number of key conclusions can be drawn:

- The developed methods for preparation of the investigated catalysts proved successful.
- The constructed experimental set–up was successfully operated, enabling provision of the alternating lean and rich conditions necessary for NSR investigations.
- The catalyst systems were robust, demonstrating repeatable performance after multiple experimental runs during both preliminary and final investigations.
- The observed $Ba/Pt/Al_2O_3$ catalyst performance agreed well with results reported in the literature for similar systems.
- The novel silver catalysts demonstrate comparable and in some cases improved performance relative to the prepared 'standard' catalyst, highlighting their suitability for the explored processes.

In terms of the observed mechanisms of storage and reduction, and identified species during TPD/TPSR investigations:

- The $Ba/Ag/Al_2O_3$ catalyst appeared to facilitate storage and reduction of NO in the same manner as the $Ba/Pt/Al_2O_3$ system.
- However, there were a number of apparent differences observed in the performance of the $K/Ag/Al_2O_3$ catalyst (and studied K/Al_2O_3 system):
  - Throughout NSR, TPD and TPSR investigations these systems produced considerably less (if any) NO_2 when compared to other catalysts.
  - The most abundant trace species observed throughout the investigations was N_2O, in greater quantities than produced in the alternative systems.
  - In addition, during the rich period of 'Lean vs Rich 1' NSR investigations the measured H_2 and H_2O abundance exhibited fluctuating traces, perhaps suggesting a number of different reduction mechanisms occurring concurrently.
- The $K/Ag/Al_2O_3$ system demonstrated a similar breakdown of measured N–species, in both TPD and TPSR studies, as the $Ba/Pt/Al_2O_3$ catalyst.

REFERENCES

Abdulhamid, H., Fridell, E., et al. (2004). Influence of the Type of Reducing Agent (H_2, CO, C_3H_6 and C_3H_8) on the Reduction of Stored NO_x in a Pt/BaO/Al_2O_3 Model Catalyst. Topics in Catalysis, Vol. 30–31, pp. 161–168.

Cant, N. W. and Patterson, M. J. (2002). The Storage of Nitrogen Oxides on Alumina–supported Barium Oxide. Catalysis Today, Vol. 73, No. 3–4, pp. 271–278.

Castoldi, L., Lietti, L., et al. (2010). The NO_x Storage–reduction on Pt–K/Al_2O_3 Lean NO_x Trap Catalyst. Journal of Catalysis, Vol. 276, No. 2, pp. 335–350.

Cumaranatunge, L., Mulla, S. S., et al. (2007). Ammonia is a Hydrogen Carrier in the Regeneration of Pt/BaO/Al_2O_3 NO_x Traps with H_2. Journal of Catalysis, Vol. 246, No. 1, pp. 29–34.

Doronkin, D. E., Fogel, S., et al. (2012). Study of the "Fast SCR" – like Mechanism of H_2–assisted SCR of NO_x with Ammonia over Ag/Al_2O_3. Applied Catalysis B: Environmental, Vol. 113–114, No. 0, pp. 228–236.

Han, P. H., Lee, Y. K., et al. (2001). NO_x Storage and Reduction Catalysts for Automotive Lean–burn Engines: Effect of Parameters and Storage Materials on NO_x Conversion. Topics in Catalysis, Vol. 16, No. 1–4, pp. 165–170.

Klinghoffer, A. A., Cerro, R. L., et al. (1998). Catalytic Wet Oxidation of Acetic Acid Using Platinum on Alumina Monolith Catalyst. Catalysis Today, Vol. 40, No. 1, pp. 59–71.

Lietti, L., Forzatti, P., et al. (2001). NO_x Storage Reduction over Pt–Ba/γ–Al_2O_3 Catalyst. Journal of Catalysis, Vol. 204, No. 1, pp. 175–191.

Mudiyanselage, K. and Szanyi, J. (2012). NO_2 Uptake Under Practically Relevant Conditions on BaO/Pt(111). Catalysis Today, Vol. 181, No. 1, pp. 116–123.

Nova, I., Lietti, L., et al. (2006). New Insights in the NO_x Reduction Mechanism with H_2 over Pt–Ba/γ–Al_2O_3 Lean NO_x Trap Catalysts Under Near–isothermal Conditions. Journal of Catalysis, Vol. 239, No. 1, pp. 244–254.

Pohanish, R. P. (2008). Sittig's Handbook of Toxic and Hazardous Chemicals and Carcinogens (5th Edition). William Andrew Publishing. p. 303.

Roy, S. and Baiker, A. (2009). NO_x Storage–Reduction Catalysis: From Mechanism and Materials Properties to Storage–Reduction Performance. Chemical reviews, Vol. 109, No. 9, pp. 4054–4091.

Sakamoto, Y., Matsunaga, S., et al. (2012). Effect of Precious Metals and NO_x Storage Materials on Hydrogen Reduction of Stored NO_x on Millisecond Time Scale. Appl. Catal., A, Vol. 445–446, pp. 133–142.

CHAPTER 5

Conclusions and Recommendations for Future Work

The use of hydrogen as a reducing agent in the treatment of NO_x creates more sustainable and efficient processes with less waste, compared to the current industrial standard NH_3/urea systems. It also removes the dependence on significant quantities of additional, toxic materials which in themselves are manufactured from finite natural resources and contribute to global warming and climate change through their production. Through investigating the viability of this NO_x treatment approach, the work described in this thesis may be considered to have three main aspects:

- Design, construction and commission of the experimental rig and the various methods used to explore catalyst performance.
- Development of an analytical technique to enable accurate measurement of the products of the investigated H_2–deNO_x reactions.
- Preparation of catalytic materials and subsequent testing in a number of different processes, utilising the apparatus and techniques described above.

5.1 Conclusions

5.1.1 Viability Study

To the best of the author's knowledge this thesis represents the first viability study of its type. Whilst H_2 as a reducing agent for NO has previously been explored in the literature, it is typically with a view to treating stationary diesel engines and using on–site reformers to provide a source of H_2. Thus, separating H_2 from the syngas produced from a biomass gasification process to treat the exhaust emissions of the subsequent gas engine represents a novel approach.

5.1.2 Source of H_2

Through the gas analysis conducted at Refgas Ltd it has been shown that the composition of clean syngas produced through the gasification of wood waste consisted of between 10 – 17 % H_2, depending on the conditions in the gasifier. The confirmation of the presence of H_2 in significant quantities validates the approach of this work; the necessary concentrations of H_2 required (which would be separated from the produced syngas) for a $deNO_x$ application, would not significantly affect the composition of the syngas provided to the gas engine.

5.1.3 General Experimental Set–up

The constructed apparatus provided great flexibility in terms of the type of $deNO_x$ (or characterisation) processes, reaction gas compositions and reaction temperature ranges which could be explored. In addition, information on the potential temperature differences over the catalyst bed could be gleaned. This was a significant achievement and one which future researchers may build upon.

The successful combination of the constructed experimental set–up, developed analysis technique and experimental procedure validated the complete approach through close agreement of obtained results, and the literature, for the relevant catalyst systems.

5.1.4 QMS Analytical Technique

A method was developed to calibrate a QMS to enable on–line, real time measurements of eight potential $deNO_x$ reaction species. The QMS is a powerful analysis tool and this was not a trivial task; to the best of the author's knowledge, such an approach has not previously been reported. Particular care was required to separate the overlapping contributions of NH_3 and H_2O, as well as the overlapping contributions of NO, O_2, N_2O and NO_2. In addition, the measurement of H_2 and total N_2 concentration was also possible through the analytical method developed.

5.1.5 H_2–SCR Experimental Investigations

In these experiments the ability of the catalysts to directly reduce NO using H_2 in the presence and absence of O_2 was explored. For a reaction system for NO_x control as illustrated in Figure 5.1, two catalyst systems supported on cordierite substrate honeycomb monolith structures were prepared and explored in the 50 to 450 ◦C temperature range.

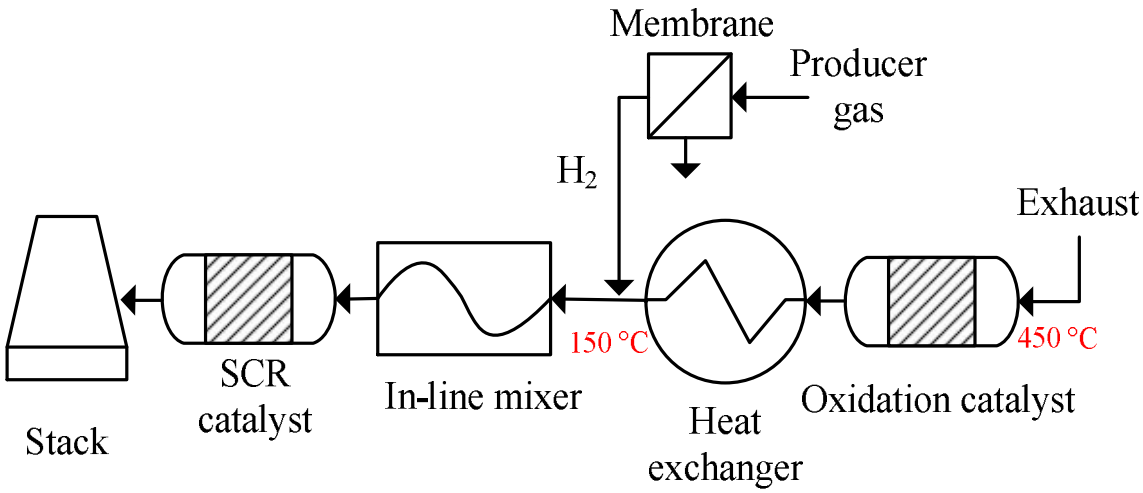

Figure 5.1 Proposed H_2–SCR NO_x removal system.

a) Pt/Al_2O_3 (0.8/29.4 wt%): performance at 50 °C appears to be the most suitable temperature for direct NO_x reduction to N_2 using H_2 (87.6 % NO conversion), although there are also significant levels of N_2O formed (66.6 % selectivity to N_2 formation). At higher temperatures, NO conversion drops (22.8 – 86.9 %) and formation of NO_2 dominates (59.3 % at 350 °C).

b) Ag/Al_2O_3 (2.3/28.9 wt%): this catalyst demonstrated poor SCR performance, especially at lower temperatures (≤ 250 °C). At higher temperatures some NO conversion was observed (21.3 % at 350 °C, 17.7 % at 450 °C) although this was accompanied by significant formation of NO_2 and thus the selectivities to N_2 formation were poor (39.9 % at 350 °C, 40.1 % at 450 °C). It appears that Ag/Al_2O_3 is not suitable for the reduction of NO_x using H_2.

5.1.6 H_2–NSR Experimental Investigations

In these experiments the ability of the catalysts to first store NO during a 'lean' period and then subsequently reduce the stored NO_x species using H_2 during a 'rich' period were explored. The impact of the presence and absence of O_2 in the 'rich' period was also investigated. For a reaction system for NO_x control as illustrated in Figure 5.2, three catalyst systems (two novel materials) supported on cordierite substrate honeycomb monolith structures were prepared and explored. The catalysts were tested under two separate sets of NSR reaction conditions at a temperature of 400 °C. The addition of O_2 to the 'rich' phase had a substantial impact on the NSR cycle as it increased both the apparent amount of stored NO_x reduced to N_2, and also the amount of NO_x subsequently stored during the following lean phase.

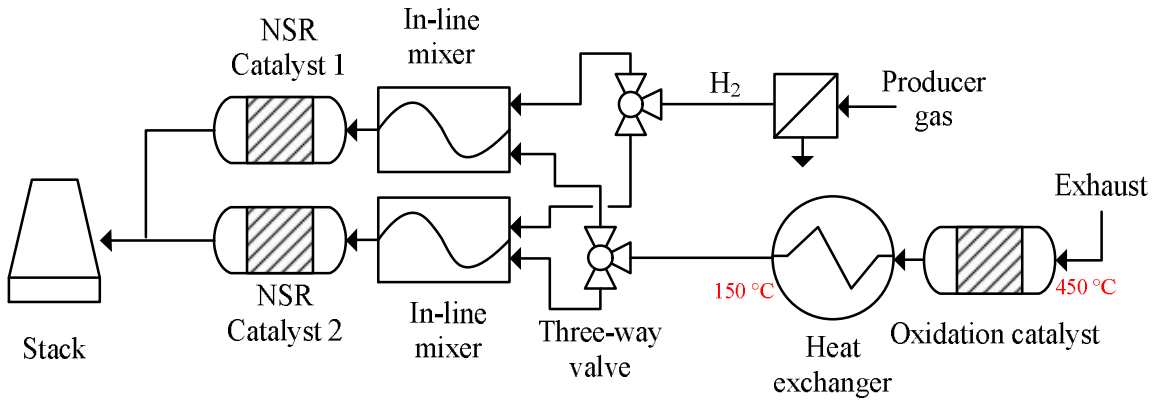

Figure 5.2 Proposed H_2–NSR NO_x removal system.

a) $Ba/Pt/Al_2O_3$ (4.7/0.2/28.2 wt%): this catalyst stored 18.8 % of the supplied NO and subsequently reduced 56.8 % of the stored NO_x species to N_2 when O_2 was only present in the lean phase. When O_2 was introduced to both phases the catalyst stored 23.1 % and reduced 82.3 % of those stored species to N_2.

b) $Ba/Ag/Al_2O_3$ (5.0/1.8/27.6 wt%): this system demonstrated poorer performance with

   i. O_2 present only in the lean phase: 10.5 % of NO stored and 5.6 % of that subsequently reduced to N_2; but somewhat comparable performance when;

   ii. O_2 was present in both phases: 14.7 % NO stored and 77.4 % subsequently reduced to N_2.

c) $K/Ag/Al_2O_3$ (16.0/2.1/24.3 wt%): this system demonstrated improved performance both when

   i. O_2 was present only in the lean phase: 72.3 % of NO stored and 59.8 % of that subsequently reduced to N_2; and when,

   ii. O_2 was present in both phases: 22.9 % NO stored and 92.0 % subsequently reduced to N_2.

Various engineering approaches can be envisaged to incorporate this process in the end application; a hybrid technique utilising a dual catalyst bed (Figure 5.2) would enable the separate exhaust and H_2 streams to be alternatively supplied creating the desired lean and rich periods. Incorporating lean/rich cycling of the gas engine could also produce the desired storage and reduction cycles.

Although the performance data for the catalysts has not been normalised (e.g. for number of active sites) the initial observed performance of the $K/Ag/Al_2O_3$ system is encouraging and seems well suited to the explored process. The improved NO storage capacity may be explained through the greater weight loading of the storage component, and whilst the weight loading of the noble metal component is an almost tenfold increase with respect to the 'standard' $Ba/Pt/Al_2O_3$ system, the relative cost of these components ensures the novel catalyst is a financially viable alternative; an important aspect to consider when developing catalysts for industrial applications. Indeed, the prepared silver catalysts appear to be a good example of the type of necessary developments of more cheap, effective and selective catalysts described in Forzatti (2001).

5.2 Recommendations

Due to the broad, interconnected research activities undertaken throughout this project, and necessary groundwork required e.g. building a rig and constructing an analytical method; there is great scope to drive this work further and build on the promising initial results. A number of suggestions for potential future work are described below:

5.2.1 Experimental Investigations

As a result of the promising performances displayed by the silver catalysts and the economic advantages their use offers; catalyst and process development should be conducted through optimisation of catalyst preparation procedures and exploration of various reaction conditions. Improved catalyst performance may be achieved by varying:

- Catalyst component loading.
- NSR reaction temperature.
- SCR/NSR reaction gas mixture composition e.g. O_2 concentration or H_2:NO ratio.
- SCR/NSR reaction gas mixture flow rate.
- TPD/TPSR adsorption temperature.

Various aspects of traditional heterogeneous catalysis are acknowledged here due to their importance and relevance to the final application, but were not explored throughout this project:

- Consideration of potential catalyst poisons i.e. CO, CO_2, SO_2.
- Catalyst ageing or sintering.

5.2.2 QMS Analytical Technique

Use of an inert carrier gas i.e. He or Ar, in deNO_x investigations would enable the unequivocal identification of N_2 formation and provide another indicator of catalyst performance.

Although the acquisition time proved adequate to follow the experiments conducted within this project, improved resolution may aid in the identification of the reaction mechanisms involved with release and reduction of stored NO_x species in particular. In addition, *in–situ* surface species analysis techniques such as those applied by Chansai *et al.* (2011) would assist in this process.

REFERENCES

Chansai, S., Burch, R., et al. (2011). The use of Short Time–On–Stream *In Situ* Spectroscopic Transient Kinetic Isotope Techniques to Investigate the Mechanism of Hydrocarbon Selective Catalytic Reduction (HC–SCR) of NO_x at Low Temperatures. Journal of Catalysis, Vol. 281, No. 1, pp. 98–105.

Forzatti, P. (2001). Present Status and Perspectives in De–NO_x SCR Catalysis. Applied Catalysis A: General, Vol. 222, No. 1–2, pp. 221–236.

Appendix I – Gas Analysis: Design and Construction of an Analytical Method Using an Online Mass Spectrometer

A Quadrupole Mass Spectrometer (QMS) was employed to conduct online measurements of the products of the deNO_x and other related reactions. In order to accurately interpret the data recorded by the QMS it was necessary to conduct a detailed calibration of the equipment under operating conditions using a variety of gas mixture compositions. This was a complicated task due to the potential presence of many species with clashing signals in the reaction mixture i.e. NO, NO_2, N_2O as well as the potential for the presence of trace quantities of these species.

The magnitude of this task was highlighted by the fact that although a basic training course was undertaken (provided by Hiden Analytical Limited), and a previous research group member had extensive experience of using the QMS in a similar application (Le (2012)), it still took over eleven months of continual development and iteration to reach the methodology described within this chapter. The nature of the changes undertaken will not be described in detail here, although select issues encountered throughout the process will be highlighted.

A1.1 Introduction

It has already been identified that whilst QMS's have previously been utilised for analysis of deNO_x reactions (Chapter 2), it is often in combination with other analysis techniques; there did not appear to be a single item of equipment used to identify all the potential species of the reaction. The benefits of using a single technique to provide on–line gas analysis of deNO_x reactions were also highlighted. It is proposed that by developing a thorough understanding of the operation of a QMS, an analytical method for accurate identification of the key reaction species could be produced. To the best of the author's knowledge, such a study does not exist.

The typical composition of a mass spectrometer as described by Patnaik (2004), and also in the accompanying schematic (Figure A1.1), consists of (1) inlet sample system, (2) ion source, (3) ion acceleration system, (4) mass (ion) analyzer, (5) ion–collection system, usually an electron multiplier detector, (6) data–handling system, and (7) vacuum system connected to components (1) through (5). Then to provide a collision–free path for ions once they are formed, the pressure in the spectrometer must be less than 10^{-6} torr.

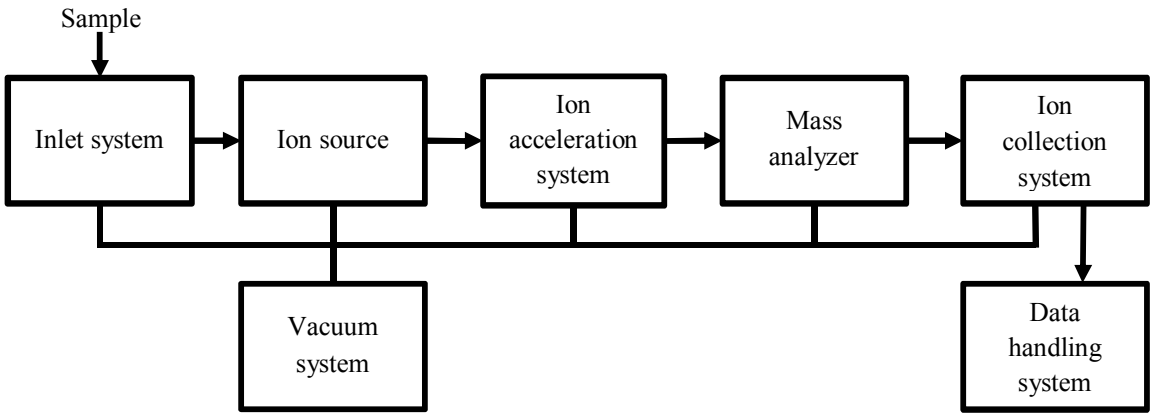

Figure A1.1 Schematic detailing the composition of a MS, recreated from Shugar (1990).

A1.2 The Quadrupole Mass Spectrometer

In this project, a Hiden HPR–20 QIC (Quartz Inert Capillary) gas analysis system (Figure A1.2) was utilised along with Hiden's MASsoft software for QMS control and data analysis.

Figure A1.2 Photograph of Hiden HPR–20 gas analysis system.

A schematic drawing of a typical Hiden HPR–20 QIC system is displayed in Figure A1.3, where the main components of the system have also been labelled.

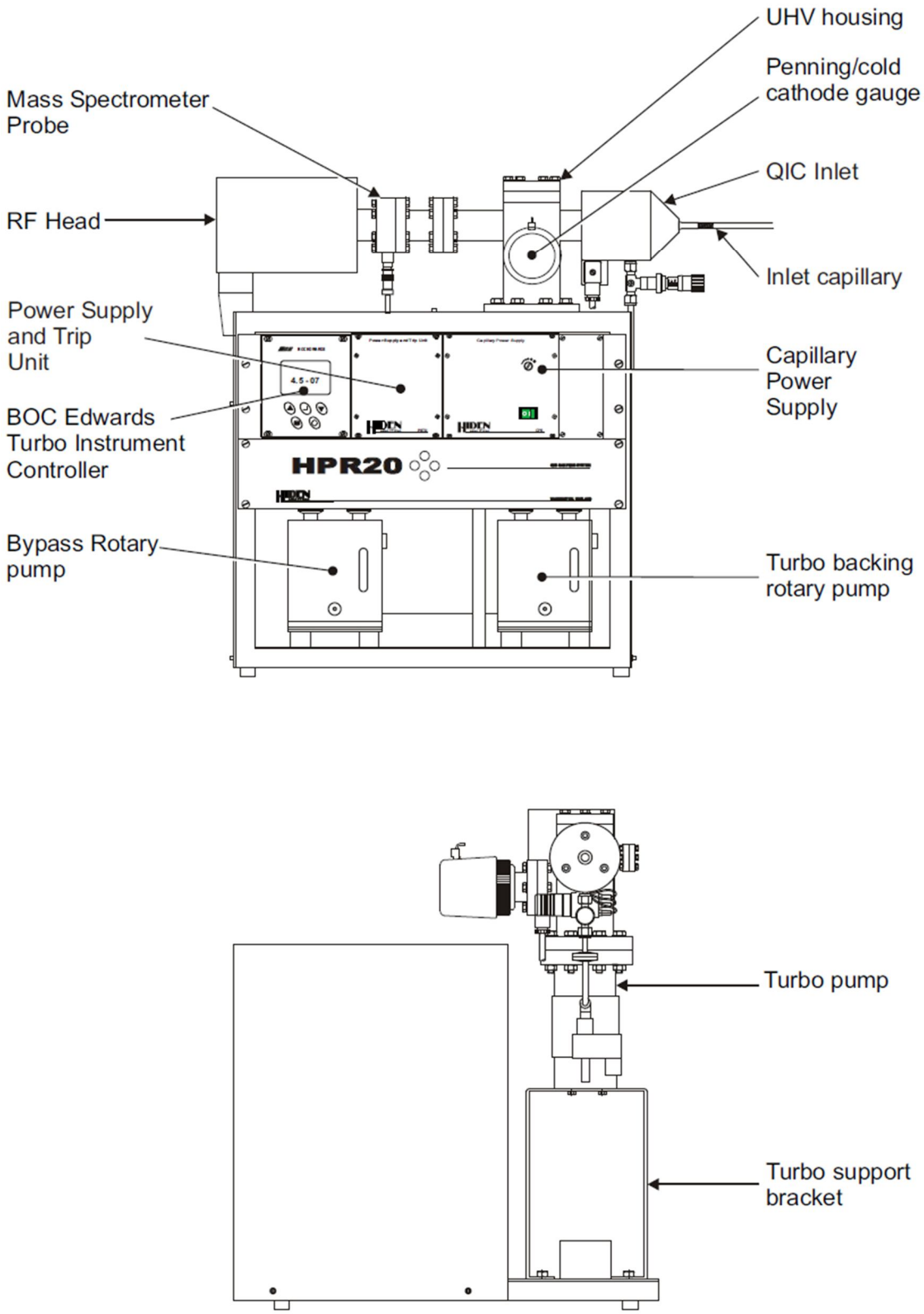

Figure A1.3 HPR–20 QIC benchtop gas analysis system (Hiden Analytical Ltd (2009)).

The role of the most important of the components identified in Figure A1.1 and Figure A1.3 will be briefly explained below. Note that a thorough description of the intricate working details of the QMS will not be included in this report.

A1.2.1 Inlet

The MS inlet is responsible for continuous sampling directly from the exhaust of the experimental set–up through connection with the QIC. Hassell (2003) describes the importance of an MS inlet, stating that these inlets must transition the sample from the higher pressure of the sample line to the vacuum required for the mass spectral analysis, yet this transition must occur without affecting the concentrations of the analytes of interest.

The specifications of the QIC inlet system (Figure A1.4) used in the Hiden HPR–20 QMS are described by Hiden Analytical Ltd (2009):

QIC capillary inlet with:

- 2 metre heated capillary with heater supply, operating up to 200 ^{o}C;
- Replaceable inert quartz capillary liner;
- Direct ionisation source inlet with replaceable platinum orifice leak;
- Variable bypass control valve and rotary bypass pump;
- Inlet particulate filter with replaceable element.

Hiden Analytical Ltd (2010) then expands on some of these individual components and their associated roles within achieving accurate gas sampling. They state that:

a) The QIC provides a dynamic method of sampling reactive or condensable gases and vapours by a mass spectrometer.

b) The inlet employs two pressure reduction stages to reduce sample pressure to an acceptably low level for operation of the mass spectrometer ion source.

c) In the first stage, sample gas is drawn down the silica capillary by the action of the sample bypass pumping line. The sample gas exits the capillary at low pressure and high velocity. This flow impinges on a platinum orifice which provides the second stage pressure reduction directly into the mass spectrometer ion source.

d) The distance from the capillary exit to the orifice, and from the orifice to the ion source, is very short, typically 4 mm and 12 mm respectively. This provides maximum free transmission of sample gas directly to the ion source with minimum surface interaction or memory effects.

e) Condensation of vapours, or adsorption of active sample gas species, is minimised by continuous heating of the inlet capillary, orifice and sample bypass regions. The silica capillary is resistively heated by passing an electric current through the stainless steel capillary sheath which surrounds its entire length. The capillary electrical connections are configured to ensure that the sampling end connection remains at ground potential.

f) The orifice and sample bypass regions are heated by an integral cartridge heater. A bimetallic disk–type thermal cutout provides over–temperature protection to these regions. The capillary and cartridge heater current is controlled by a Capillary Temperature Controller.

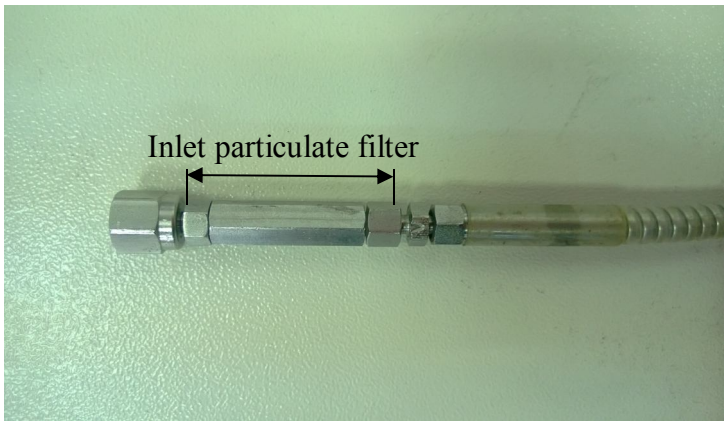

Figure A1.4 Photograph of the QIC.

A1.2.2 Ionization

The ion source within an MS is responsible for ionizing the sampled species prior to separation by the analyser. There are various ionization techniques of which Electron Ionization (EI), where the sampled species interact with high energy electrons, is the most popular. Watson *et al.* (2007) provide the following details on the use of EI in identifying unknown species:

a) In mass spectrometry, electron ionization (EI) produces molecular ions from gas–phase analytes. These molecular ions then fragment in a reproducible way, which results in a "fingerprint" of the analyte.

b) Because of the uniqueness of these "chemical fingerprints", commercially available libraries containing hundreds of thousands of standard EI mass spectra can be used to facilitate identification of unknown compounds.

The compound library within the MASoft software contains fragment patterns for 72 of the most commonly analysed gas phase species. The use of this information within this thesis is discussed in greater detail in Section A1.3.3.1.

There are also various ways to produce the high energy electrons required to ionize the gas samples. Watson *et al.* (2007) discuss a typical technique for producing high energy electrons, stating that the source of electrons in nearly all EI mass spectrometers (regardless of the type of *m/z* analyzer) is a thin ribbon or filament of metal that is heated electrically to incandescence, or to a temperature at which it emits free electrons.

The oxide–coated iridium filaments from the Hiden HPR–20 QMS used within this project are displayed in Figure A1.5. In this case, two filaments are fitted to the Mass Spectrometer ionisation source so that when one fails the other filament may be used.

Different species also exhibit different fragmentation patterns depending on the energy of the interacting electrons. In some cases this property may be used to separate complex mixtures, as described by Hiden Analytical Ltd (2012a), and this approach was adopted within this project and is discussed in more detail in Section A1.3.4.1.

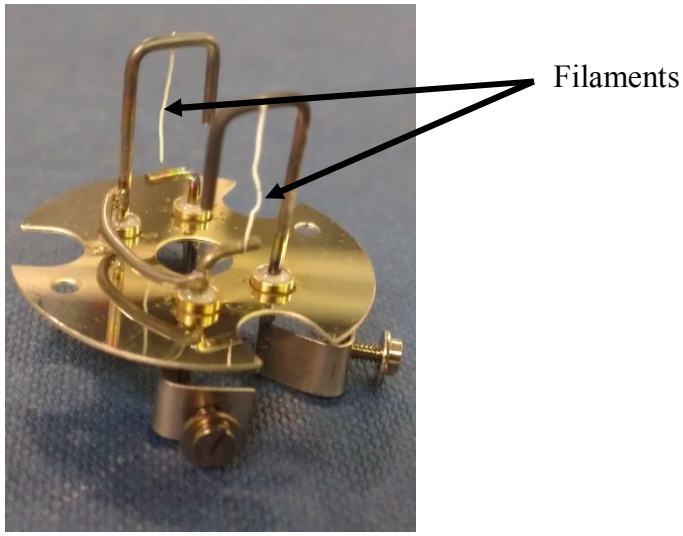

Figure A1.5 Photograph of oxide–coated iridium filaments from Hiden HPR–20 QMS.

A1.2.3 Mass Analyzer

The produced ions now require separation and as already mentioned in Chapter 2 this is achieved using their mass to charge ratios, *m/z*. As a result, multiply ionized species need to be accounted for. Due to the varying methods of ionization, different types of analyser also exist. The Hiden HPR–20 QMS used for this project utilises a quadrupole analyser and Hiden Analytical Ltd (2009) details the composition of the analyser system:

> Quadrupole mass spectrometer comprising:
>
> - Quadrupole probe with:
>   - 200 amu mass range capability;
>   - Dual Faraday/Electron Multiplier detectors.
> - RF (Radio Frequency) Head with:
>   - RF generator and pre–amplifier electronics.
> - RC (Radio Communication) Interface unit with:
>   - Microcomputer controlled data acquisition system;
>   - Power supply electronics;
>   - Variable supplies for Probe lenses;
>   - RS232, RS422 and Ethernet LAN serial communications interfaces.

Hassell (2003) describes the principles and operation of a quadrupole analyser as follows: These consist of four parallel rods with the ends arranged in a square pattern. The rods at opposite corners of the square are electrically connected. An rf signal is applied to one set, and an equivalent but inverted rf signal is applied to the opposite set. Likewise, opposing positive and negative DC offset voltages are applied to the rod sets. This combination creates a resonance condition that permits particles with a specific *m/z* to travel down the length of the rods, while all other *m/z* particles are annihilated by collision with one of the rods or some other surface.

A1.2.4 Detectors

Hoffmann *et al.* (2007) describe the process through which a detector is utilised within a MS, stating that the ions pass through the mass analyser and are then detected and transformed into a usable signal by a detector. Detectors are able to generate from the incident ions an electric current that is proportional to their abundance.

Hassell (2003) describe the various detectors which may be found within an MS, stating that:

a) Most process analyzers utilise either a Faraday cup or a secondary electron multiplier (SEM) for detection.

b) The Faraday cup is the simpler and more rugged and stable of the two, but is generally useful for detection of species at higher concentrations (100 ppm to 100 %).

c) The SEM is much more sensitive, capable of measurements in the ppb range.

Hassell (2003) states that often a single MS will be configured with both the Faraday cup and the SEM detectors and indeed the Hiden HPR–20 QMS utilised in this project contained both.

A1.2.5 Vacuum System

As is shown in Figure A1.1, the ion source, mass analyser and ion collection system (detector) are all connected into a vacuum system. This is necessary for the operation of the MS, as discussed by Hassell (2003), who stated that:

a) This vacuum must be sufficient (i.e. the mean free path must be sufficiently long) to prevent collisions between particles prior to analysis.

b) A roughing pump is first used to provide vacuum for the sample inlet, as well as to provide the backing pumping for the turbomolecular pump, which provides the vacuum needed (between 10^{-5} and 10^{-7} torr) for the ion source and mass filter.

The specifications for the Hiden HPR–20 vacuum system are described in Hiden Analytical Ltd (2009) and consist of:

HPR–20 QIC ultra high vacuum (UHV) housing with:

- Conflat flange type ports for turbo pump, Probe, Penning gauge and inlet.

Vacuum pumping system comprising:

- 60 litre per second turbomolecular pump with controller;
- Rotary backing pump;
- Automatic vent valve with vent delay;
- Cold cathode (Penning) gauge providing protection interlock.

A1.2.6 Analysis

The electrical signals from the detector are then converted to a digital signal which can then be processed and interpreted by a relevant software program. Hiden Analytical Ltd (2009) specifies the capabilities of the computer software provided with the Hiden HPR–20 gas analysis system:

MASsoft PC software including:

a. Full suite of data display modes;
b. Quantitative analysis software with percentage, PPM and PPB data output;
c. Comprehensive data export facilities.

The software is installed on a PC which is also used for MS control through altering various parameters (these parameters are discussed in Section A1.3.2). Conversion of the signals between MS and PC is accomplished by the RC interface.

A1.2.7 Operating Parameters

A summary of the main operating parameters of the HPR–20 QIC gas analysis system is presented in Table A1.1.

Table A1.1 Operating parameters of the Hiden HPR–20 QIC gas analysis system (data collected from Hiden Analytical Ltd (2009)).

Component	Parameter	Description
Inlet	Inlet type	2 m quartz inert capillary
	Inlet temperature	up to 200 °C
	Sampling pressure	0.1 – 2 bar (absolute)
Ionization	Electron ionization	4 to 150 eV (in 0.1 eV increments)
	Filaments	Oxide–coated iridium filaments
Mass analyser	Quadrupole mass range	200 amu
Detectors	Quadrupole detectors	Faraday and Electron Multiplier Detectors
	Fragmentation pattern library	72 compounds

A1.3 Development of Calibration Method

A1.3.1 Experimental Set–up

The typical set–up utilised throughout calibration of the QMS is presented in Figure A1.6(A). A detailed description of the apparatus is presented in Chapter 3. The calibration gases were supplied, through flexible stainless steel hoses, to variable area flowmeters where the flow rate could be varied e.g. 30 to 300 cm^3 min^{-1}. In addition, an oil bubbler filled with water (Figure A1.6) was placed in an ice bath and one of the calibration gases directed through it to provide a known concentration of H_2O to the calibration mixture. The use of the flowmeters enabled calibration mixtures containing all species of interest to be delivered directly to the QMS through stainless steel tubing. It was verified that complete mixing occurred within the tubing and thus additional apparatus to aid mixing was not included in the calibration set–up. The flowmeters also required calibration for use with the relevant calibration gas mixtures, the procedure for flowmeter calibration is described in Chapter 3. The calibration gases utilised throughout the calibration method were supplied from BOC, Bristol, UK and consisted of:

- 2070 ppm H_2 in N_2
- 2020 ppm NO, 458 ppm NO_2 in N_2
- 500 ppm NO_2 in N_2
- 9.2 % O_2 in N_2
- 512 ppm NH_3 in N_2
- 483 ppm N_2O in N_2
- 'Zero' N_2

Calibration gases were supplied adhering to BOC's β standard which specifies an accuracy of ± 2 % with respect to the certification and, from conversation with a BOC employee, a H_2O content of no greater than 5 ppm in each cylinder. In addition, 'Zero' refers to the purity of the gases which in this instance is 99.998 % and thus there is a total impurity concentration of 20 ppm.

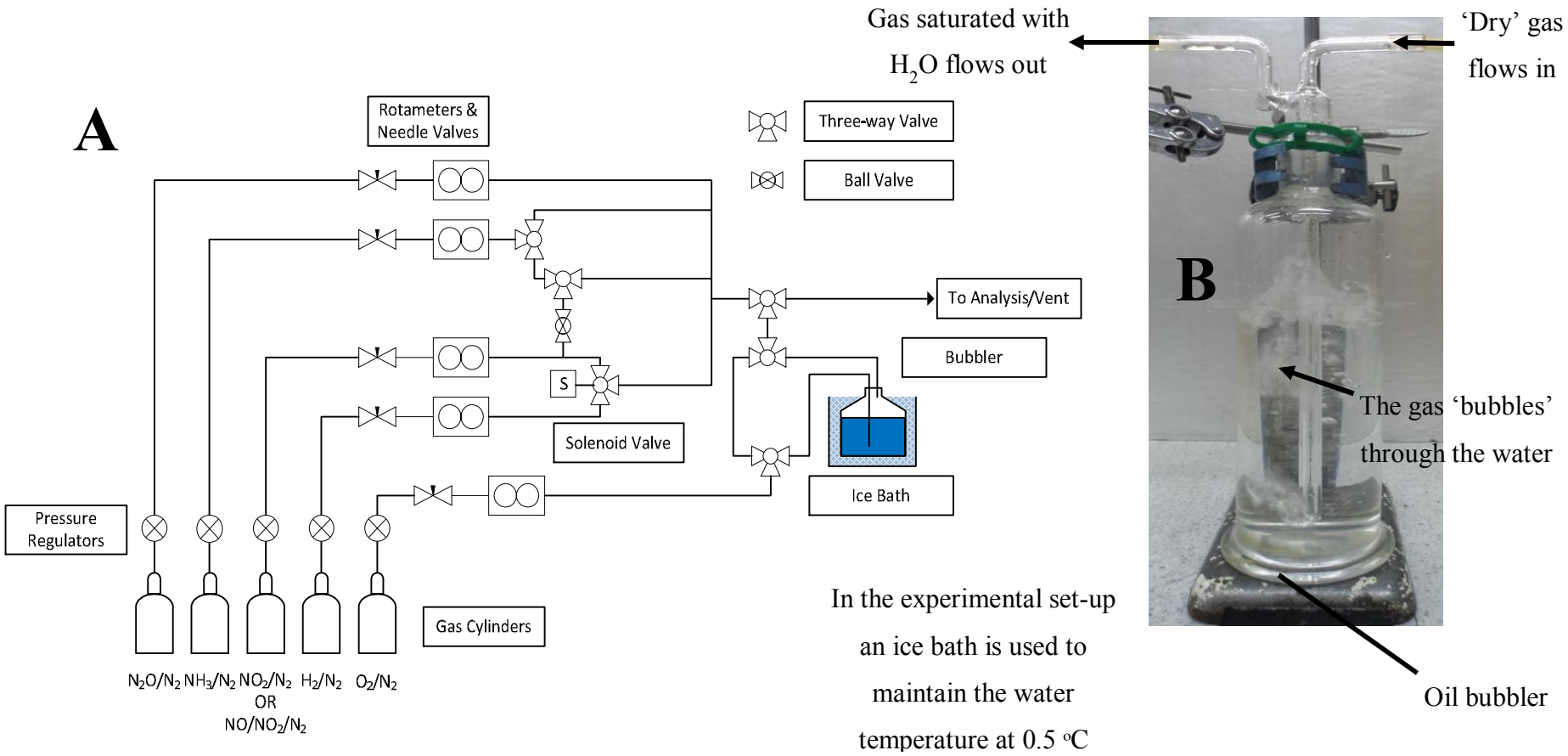

Figure A1.6 (A) Schematic of experimental set–up used for calibration of the QMS. (B) Photograph of oil bubbler used in calibration of the QMS to deliver H_2O.

A1.3.2 Setting of Operating Parameters

Setting of appropriate QMS operating parameters formed a large part of the calibration method. As concluded in Chapter 2, a QMS has not been utilised within a $deNO_x$ application for the detection of both NH_3 and H_2O simultaneously and this was identified as a key issue to enable distinction between this work and other studies. This is a notoriously difficult problem to address as the fragment pattern of both species includes significant contributions at *m/z* ratios of 17 and 18. Note that whilst a variety of different types of experiment were conducted within this project e.g. SCR, TPD, TPSR, and each involved an individual calibration procedure, the procedure explained here concerns calibration for the 'complete' $deNO_x$ mixture including the following species: H_2, NH_3, H_2O, N_2, NO, O_2, N_2O and NO_2.

A1.3.2.1 Vacuum Pressure

As already discussed in Section A1.2.5, the vacuum pressure plays a very important role in the operation of the MS and thus any change in pressure can have a detrimental effect on the measurement accuracy. This is consistent with findings in related studies (Turner *et al.* (2004)) and thus the pressure was closely monitored throughout both calibration and $deNO_x$ experiments; if the pressure was found to have drifted it was altered to the correct value by using the sample by–pass control valve. The base pressure used throughout this project was typically 1.8×10^{-6} torr.

A1.3.2.2 Detector Selection

The choice of detector depends on the concentration of the species being measured at particular *m/z* ratios. As discussed in Section A1.2.4, the SEM detector offers greater resolution than the Faraday cup (up to ppb level depending on operating conditions). In terms of detectable pressure ranges, the SEM detector can detect gases within a range of 1 x 10^{-7} to 1 x 10^{-13} torr whilst the Faraday cup operates within a range of 1 x 10^{-5} to 1 x 10^{-10} torr. In this project it was found to be necessary to use a combination of both detectors to measure the range of concentrations of different species under investigation. This had a significant impact on the subsequent operation of the QMS throughout both calibration and deNO_x experiments; the voltage supplied to the SEM detector required calibration with respect to the Faraday cup such that both detectors gave equivalent signals (this is discussed further in Section A1.3.2.5). Additionally, as the method required switching between the two detectors, the acquisition time was increased.

A1.3.2.3 Electron Energy, eV

Although this is typically set at 70 eV (Hiden Analytical Ltd (2007)), which is suitable to both singly and doubly ionize most species, the electron energy was altered within this project to combat the aforementioned problem of separating the contributions of both NH_3 and H_2O at *m/z* ratios of 17 and 18. Hiden Analytical Ltd (2012a) recently utilised the technique of 'soft ionisation' to successfully separate the two species:

> "…minimal ionisation of water occurs below 15 eV. Above this level, ionisation of H_2O to H_2O^+ occurs. It can be seen that at 18 eV the only ionisation products (m/z 18) detectable when sampling water is H_2O^+. Ionisation of H_2O to OH^+ does not occur until around 20 eV. Therefore, this difference in ionisation energy can be used to separate OH^+ and NH_3^+ if the ionisation threshold of NH_3 to NH_3^+ is below this level. Theoretically, the ionisation to NH_3^+ occurs at around 11 eV"

Adopting this approach, how the various fragment patterns of both NH_3 and H_2O altered through variation of the electron energy was investigated. Ideally an electron energy which produced no contribution from H_2O at *m/z* 17 and no contribution from NH_3 at *m/z* 18 would have been identified and, acting upon the results reported by Hiden Analytical Ltd (2012a), a range of *m/z* ratios from 12 to 20 were investigated. Unfortunately this could not be achieved as unexplained secondary ionization products from H_2O were witnessed at lower electron energies, where there was no fragmentation from NH_3. As a result a compromise was reached with the fragmentation patterns of the two species presented in Table A1.2. These patterns were achieved using individual gas mixtures consisting of 512 ppm NH_3 in N_2 and ~6380 ppm H_2O, 9.8 % O_2 in N_2 (see humidity calculation, Section A1.3.3.3). Due to the nature of the method of introducing moisture to the calibration mixture, the levels present were increased with respect to what could realistically be expected during $deNO_x$ experiments, whilst the levels of NH_3 present were of the order of magnitude expected. As a result, it was decided that during $deNO_x$ experiments, the contribution of H_2O at *m/z* 17 would be negligible if any NH_3 was present, and thus the electron energy was set at 18 eV.

Table A1.2 Fragmentation of NH_3 and H_2O at *m/z* ratios of 17 and 18 with an electron energy of 18 eV.

Species	*m/z*	
	17	18
NH_3 (& N_2)	100.00 %	18.05 %
H_2O (& O_2, N_2)	0.15 %	100.00 %

A1.3.2.4 Electron Emission Current, µA

The electron emission current is directly related to the magnitude of the signal detected by the detector. Due to the alteration of the electron energy, the emission current required reducing to prevent damaging the filament through excessive current demands. As can be seen from Figure A1.7 (presented in Hiden Analytical Ltd (2007)) for a given electron energy there is a recommended emission current. After consultation with a Hiden engineer, an electron emission of 180 µA was deemed acceptable, although in Figure A1.7 it lies just outside the recommended operating region for an electron energy of 18 eV.

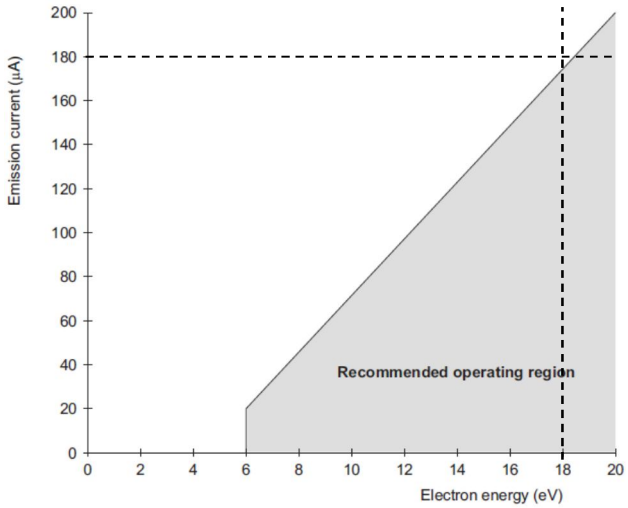

Figure A1.7 Graph depicting emission current – minimum electron energy characteristic for 0 to 20 eV. From Hiden Analytical Ltd (2007)

A1.3.2.5 SEM Detector Voltage

As already alluded to, the use of both the Faraday cup and SEM detectors required additional calibration to ensure the SEM detector gave an equivalent signal to that of the Faraday detector. This in turn increases the sensitivity when measuring trace levels of gases. Calibration of the SEM detector was achieved by detecting a species at a single mass and directly comparing the intensity of the signals from each detector (Figure A1.8). The SEM detector voltage was then manually altered until the peaks were the same height.

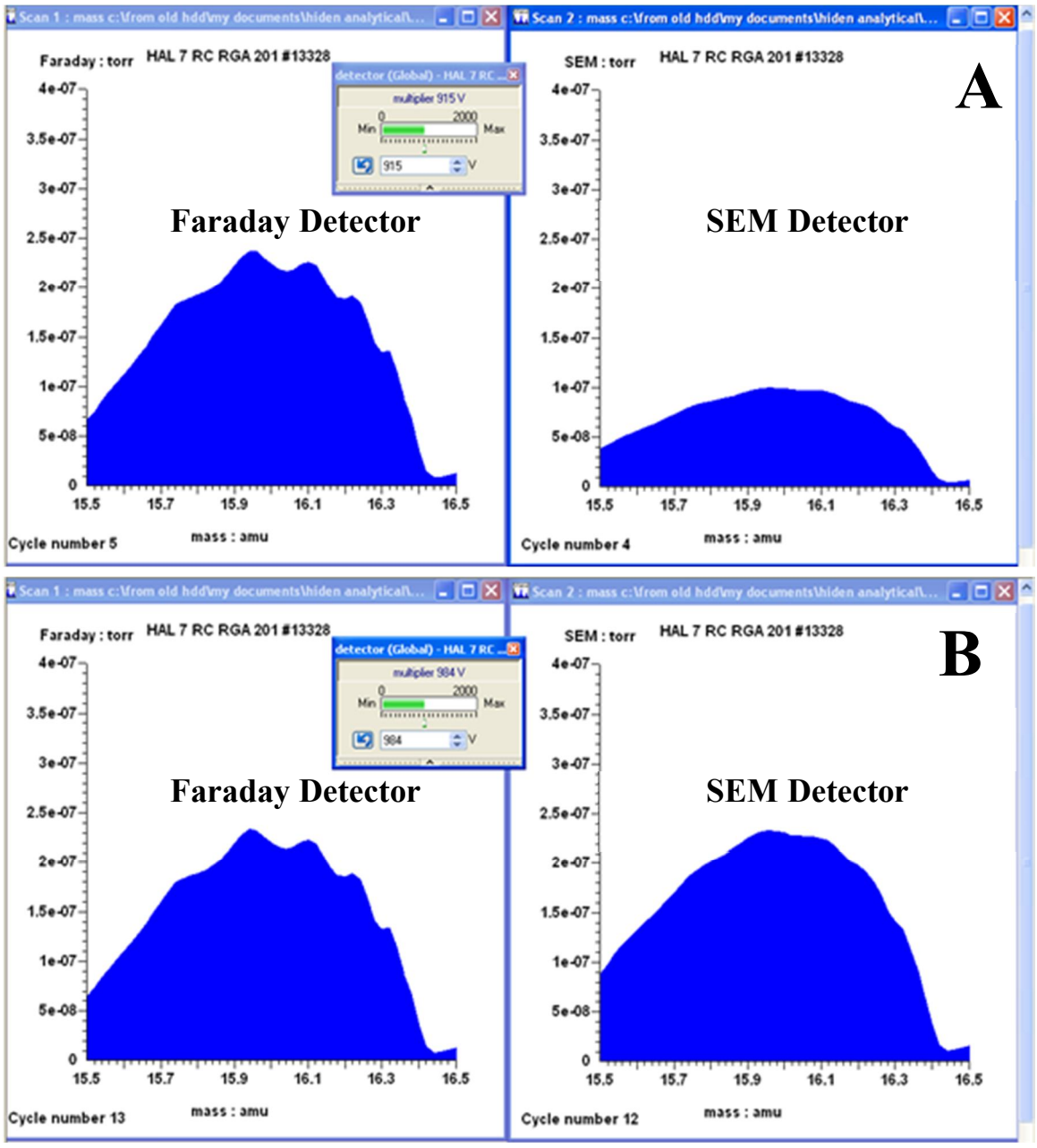

Figure A1.8 Detected abundance of O_2 at *m/z* 16 using both SEM and Faraday detectors (A) before calibration at 915 V and (B) after calibration at 984 V.

A1.3.2.6 Summary and General Procedure

A summary of the QMS operating parameters is presented in Table A1.3. It is important to note that although once calibrated the QMS demonstrates excellent repeatability; due to natural 'drift' of the QMS as the filament degrades, it is necessary to re–calibrate at regular intervals (typically every 3 months). As a result, the parameters presented here only represent the outcome of one particular QMS calibration process (and the subsequent experimental investigations), and were not necessarily utilised in all deNO_x experiments (for which further calibration processes would have been completed).

The relatively low electron energy and electron emission, in addition to utilising both the Faraday and SEM detectors, resulted in an acquisition time of 42 s for a 'full' deNO_x mixture.

In terms of operating procedure, after initial start–up the QMS was left running in order to achieve the base vacuum pressure, and adjusted as necessary throughout the calibration procedure, to maintain a constant value. It was also generally necessary to warm up the filament prior to use in both calibration and experimental investigation; depending on the operation parameters this may take 2 h (at e.g. 70 eV) or overnight (at e.g. 18 eV).

Table A1.3 QMS parameters used during calibration and deNO_x experiments.

Parameter	Setting
Base pressure	1.8×10^{-6} Torr
Electron energy	18 eV
Electron emission	180 μA
SEM detector voltage	995 V
Acquisition time	42 s

A1.3.3 Challenges

Although suitable operating parameters had been identified, further issues were encountered throughout the construction of a robust calibration method.

A1.3.3.1 Fragmentation

Whilst using a QMS, a major task when identifying the composition of an unknown gas mixture is the separation of the relevant contributions of two or more species at a particular *m/z* ratio. Hoffmann *et al.* (2007) discuss the issues which arise due to overlapping fragmentation patterns, stating that:

a) The most common interferences are the spectral interferences, also called isobaric interferences. They are due to overlapping peaks which can mask the analyte of interest and can give erroneous results.

b) Such interferences may occur from ions of other elements within the sample matrix, elemental combination, oxide formation, doubly charged ions, and so on.

In the gas mixture of interest this is particularly evident:

- NO, O_2, N_2O and NO_2 all contribute at a *m/z* of 30.
- NH_3 and H_2O both contribute at *m/z* ratios of 17 and 18.

Whilst these particular issues have been addressed before (Hiden Analytical Ltd (2012a) and Hiden Analytical Ltd (2012b)), and as mentioned previously vast databases of compound fragment patterns exist; each QMS system is unique in the exact measurements it conducts. Indeed different species also behave differently in the presence of others, and may provide differing fragment patterns under different conditions. Thus whilst the library fragment patterns may give an indication of the species 'fingerprint', the requirement to calibrate the QMS for each gas mixture is highlighted.

Under the specified operating parameters, it is important to identify specific *m/z* ratios which can be attributed to a particular species. If this is not possible then it is imperative to be able to calculate the relative contributions of overlapping species at a particular *m/z*.

An indication of the fragment patterns of each species of interest (at the defined operating parameters) can be observed in Table A1.4. Note that the green highlighted *m/z* ratio for each species indicates its use as the 'main peak' for that species, from which its contribution at other *m/z* ratios may be calculated (Sections A1.3.4.1 and A1.3.4.3). Although the highlighted peaks here represent the 'ion–molecule' peak and it may be expected that these peaks would demonstrate the most intensive signal for a particular species, this is not always the case, as is highlighted in Section A1.3.4.3.

Table A1.4 Matrix detailing contributions from the species of interest at different masses under the derived operating parameters.

Species	*m/z*							
	2	17	18	28	30	32	44	46
H_2	X							
NH_3		X	X					
H_2O			X					
N_2				X				
NO					X			
O_2					X	X		
N_2O					X		X	
NO_2					X	X	X	X

A1.3.3.2 Method of Calibration

There are a number of approaches which may be made to calibrate a QMS for a particular gas mixture, namely the 'external standard' and 'internal standard' methods. Hoffmann *et al.* (2007) provide the following description of the use of the 'external standard' method:

a) This consists of preparing a synthetic sample containing a known quantity of the molecule to be measured (M_{ste}), then introducing a precise volume of this solution into the spectrometer and recording the intensity of the response signal (I_{ste}).

b) Then, without any modification of the analytical conditions, an equal volume of the solution containing the molecule to be quantified (M_x) is introduce into the spectrometer and the intensity of its response signal (I_x) is measured.

c) There is a proportionality between the response intensities and the quantities as long as the response signal intensity remains linear with respect to the concentration and as long as the signal intensity is zero at zero concentration.

Although the response between intensity and concentration is typically linear when utilising a chemical ionization method (the ionization technique in this project), a heavy reliance is placed upon maintaining the operating conditions of the QMS. As even slight adjustments to the operating parameters will affect the measurements this method is considered to have poor repeatability.

The alternative, 'internal standard' method can avoid the errors associated with the 'external standard' method. In this case, instead of relying on absolute intensities and assuming a linear relationship with the concentration of the species of interest (external method'), the reliance is on measurement of a ratio between the intensity of the species of interest and a reference compound. This approach forms the basis of the calibration method discussed here.

A1.3.3.3 Introduction of Moisture to the Calibration Mixture

In order to build the most accurate calibration method for a complete reaction mixture it is necessary to produce a calibration gas mixture containing all the potential species. Assuming that, as advised by a BOC representative the supplied calibration gases contained no H_2O (or certainly < 5 ppm H_2O in each cylinder), it was thus necessary to identify a technique to accurately deliver a known H_2O concentration to the QMS.

A method was devised using a standard oil bubbler, filled with H_2O, through which one of the calibration gases flowed (Figure A1.6(B)). By cooling the H_2O to 0.5 ^oC, saturation of the flowing gas stream could achieved with a minimised H_2O concentration of 6380 ppm. A further challenge emerged in addition to the use of the bubbler: it was found that some of the reactant species readily dissolve in the water, and thus only particular calibration gas mixtures could be used to 'bubble through' the H_2O.

A1.3.4 Methodology

The following sections described the steps to be taken in developing a method for the accurate analysis of a gas mixture of unknown composition.

A1.3.4.1 *M/z* Ratios and Species Overlap

Utilising the information presented in Table A1.4, the initial step was to identify, with consideration to the operating parameters, the *m/z* ratios of interest and any potential overlaps. This was achieved by scanning the range of *m/z* ratios with each species individually, at relevant concentrations, and identifying peaks of significant intensity.

As a result the abundance of H_2, NH_3, N_2 and NO_2 were derived from the signals at *m/z* 2, *m/z* 17, *m/z* 28, and *m/z* 46 respectively. Under the operating parameters determined in Section A1.2.7, and specifically the electron energy chosen to distinguish between NH_3 and H_2O in Section A1.3.2.3, it can be assumed the following species are the only found to contribute at these masses:

$$
\begin{aligned}
P_{H_2} &= P_{m/z\,2} \\
P_{NH_3} &= P_{m/z\,17} \\
P_{N_2} &= P_{m/z\,28} \\
P_{NO_2} &= P_{m/z\,46}
\end{aligned}
\tag{A1.1}
$$

P_{i} is the corrected partial pressure of component i and $P_{\mathrm{m/z\ j}}$ is the raw partial pressure recorded by the QMS at peak *m/z* j, respectively.

From Table A1.4 it can be seen there is significant overlap between various combinations of NO, O_2, N_2O and NO_2. As a result:

- the partial pressure of H_2O at *m/z* 18 was corrected for NH_3 overlap,
- the partial pressure of O_2 at *m/z* 32 was corrected for NO_2 overlap,
- the partial pressure of N_2O at *m/z* 44 was corrected for NO_2 overlap, and
- the partial pressure of NO at *m/z* 30 was corrected for O_2, N_2O and NO_2 overlap.

The following equations were utilised to calculate the contribution of each species at their associated 'main' peak:

$$P_{H_2O} = P_{m/z\,18} - \left(P_{NH_3} \times C_{NH_3\,18}\right) \tag{A1.2}$$

$$P_{O_2} = P_{m/z\,32} - \left(P_{NO_2} \times C_{NO_2\,32}\right) \tag{A1.3}$$

$$P_{N_2O} = P_{m/z\,44} - \left(P_{NO_2} \times C_{NO_2\,44}\right) \tag{A1.4}$$

$$P_{NO} = P_{m/z\,30} - \left(P_{O_2} \times C_{O_2 30}\right) - \left(P_{N_2O} \times C_{N_2O\,30}\right) - \left(P_{NO_2} \times C_{NO_2 30}\right) \tag{A1.5}$$

$C_{\mathrm{i\ j}}$ is the ratio of the partial pressure of component i at peak *m/z* j, $P_{\mathrm{i\ j}}$, to that of component i at its main peak, P_i (equation A1.6).

$$C_{i\,j} = \frac{P_{i\,j}}{P_i} \tag{A1.6}$$

Note that these ratios are highly dependent on the operating parameters and presence of other species in the gas mixture and as such are also carefully determined (Section A1.3.4.3) for use in the calibration method.

The concentration of each species was calculated as follows (Equation A1.7A1.7):

$$x_i = \frac{(P_i/RS_i)}{\sum_i (P_i/RS_i)} \qquad \text{(A1.7)}$$

x_i is the concentration and RS_i is the relative sensitivity, RS value (Section A1.3.4.3), of component i.

A1.3.4.2 Background levels

It is necessary to identify the 'base' level or background readings of each *m/z* ratio of interest as over time the operation of the QMS alters e.g. through poisoning of the filament erroneous readings at particular *m/z* ratios may occur. This is particularly important when dealing with trace levels as slight differences in signal intensity can translate to significant errors in subsequent abundance calculations.

Background readings (Table A1.1) were obtained by flowing 'zero' nitrogen through the QMS and analysing the *m/z* ratios of interest. It was assumed there were no residual impurities within the system and the gas was supplied until the signals stabilised (2 – 3 h).

Table A1.1 Example of background readings obtained at relevant *m/z* ratios using 'zero' nitrogen.

m/z	Background Reading (torr)
2	3.2×10^{-11}
17	1.53×10^{-11}
18	7.35×10^{-11}
30	5.41×10^{-11}
32	6.07×10^{-11}
44	8.68×10^{-12}
46	3.48×10^{-14}

Note the reading at *m/z* 46 is outside the operating limits of the both Faraday and SEM detectors (Section A1.3.2.2) and thus can be considered 'noise' within the system. However, the remaining *m/z* ratios exhibit significant intensities, particularly if trace species are to be considered with this method (and the associated parameters). These readings will be utilised through subtraction from the raw measurements obtained during calibration of experimental runs, before the necessary calculations are applied.

In addition it is possible to periodically 'clean' the filaments through use of a highly reducing atmosphere (i.e. H_2) in a process known as "bake–out". Although this technique was not applied here it may aid the reduction of the intensity of measured background levels.

A1.3.4.3 Relative Sensitivity Values, RS

Building upon the 'internal standard method' described in Section A1.3.3.2, the final step in the development of the calibration process is to obtain an RS value for each species in the calibration mixture. An RS value accounts for the variation in sensitivity the QMS demonstrates for different species (once again each QMS exhibits unique behaviour under varying operating conditions).

This is achieved by successfully separating the contributions of each species at each *m/z* ratio and relating the intensity of the individual 'main peaks' to that of the species in highest concentration within the mixture (Table A1.2 and Table A1.3). Note that separation of the overlapping species contributions is not a trivial task and required 'building' the gas mixture species by species. Although as already discussed, the addition of a species to a mixture *may* impact on the fragmentation of the other species; if the added species also contributes at the same *m/z* ratios (as those already present) then separation can only be achieved by assuming there is no impact on the fragmentation of the species in the original mixture.

Table A1.2 Measured fragment pattern of NH_3.

Species	Relative Signal Intensity (%) *m/z*	
	17	18
NH_3	100	9.17

Table A1.3 Measured fragment patterns of O_2 and the various NO_x species.

Species	Relative Signal Intensity (%) *m/z*			
	30	32	44	46
O_2	0.62	100	–	–
N_2O	26.95	–	100	–
NO_2	2275	19545	224	100

These RS values then represent the relationship between the two species at the particular concentrations supplied to the QMS. For this reason it is necessary to try and produce a gas mixture which is representative of what would be produced during experimental investigations. Obviously this necessitates speculation in terms of catalyst performance etc. However some flexibility is seen and RS values can demonstrate accuracy over a range of concentrations.

In this study, as N_2 is the carrier gas it is found in great excess and is assigned an RS value of 1. The RS values of the remaining species are then calculated with respect to the N_2 concentration. In an effort to deliver a robust experimental method capable of identifying each species of interest over a (realistic) range of concentrations, a number of different gas mixtures (Table A1.4), with varying concentrations of each species, were delivered to the QMS and the RS values for each component recorded and averaged. These mixtures were delivered within the constraints of the experimental apparatus (i.e. flow ranges of the flowmeters) and in addition, RS values for selected species in the absence of the complete gas mixture were also obtained with a view to the additional experiments to be completed e.g. NO–TPD, H_2–TPSR etc.

Although it was assumed there was no H_2O present in the calibration system (in the absence of using the bubbler), in reality this was not the case (even allowing for the presence of potential background levels, Section A1.3.4.2). It is suggested that condensation within the steel tubing or 'wet' gases may be responsible for the measured signals. In any case the concentration of H_2O provided through the bubbler was far greater than that expected in the experimental investigations. Thus the H_2O RS value was obtained utilising the set–up described in Section A1.3.3.3 but the RS values of the remaining species were obtained in the absence of additionally provided H_2O.

Table A1.4 Various gas mixtures used to obtain RS values.

Mixture	Abundance						
	NO (ppm)	NO_2 (ppm)	H_2 (ppm)	O_2 (%)	NH_3 (ppm)	N_2O (ppm)	N_2(%)
1	1312	297	189	0.64	55	40	99.17
2	175	40	1370	0.62	53	39	99.21
3	188	43	198	5.64	57	42	94.31
4	116	26	122	0.41	402	26	99.52
5	165	37	173	0.58	50	326	99.34
6	421	95	431	1.92	96	91	97.97
7	165	37	422	2.82	104	99	97.10
8	152	35	160	3.47	144	91	96.48

The obtained RS values for each mixture were obtained and analysed and most species demonstrated consistency through the entire range of investigated concentrations. However, some species exhibited a wider range of obtained RS values and these were typically the species for which calculation of overlap from other species was required i.e. NO, N_2O. In other instances there were distinct patterns between the concentration of the species and the obtained RS values and in these cases some discretion was demonstrated when calculating an overall RS value from those obtained with the most appropriate species concentration.

The accuracy of the chosen RS values was analysed by introducing a mixture of known composition and comparing the specified abundances with those produced by the QMS. An example of the RS values obtained and used for the complete species mixture is presented in Table A1.5.

Table A1.5 Example of the RS values for the species in the complete gas mixture obtained on completion of the calibration process.

Species	H_2	NH_3	H_2O	NO	O_2	N_2O	NO_2
RS Value	1.76	9.30	3.62	4.37	1.72	4.44	0.30

A1.4 Conclusions

Although not a trivial task, the QMS has been calibrated to measure a complete mixture of all potential deNO_x species. Whilst there are certainly some limitations to the ranges in which particular species can be identified, the calibration was attempted in such a way as to avoid such issues. Good repeatability in performance is observed although recalibration should be conducted after a period of 2–3 months. It should also be noted that if, during experimental trials, it appears a mixture containing species within ranges out with those used for calibration is formed; recalibration involving a relevant mixture may be conducted to obtain a more accurate RS value and the experimental trial repeated.

Although the QMS is a powerful piece of equipment, there are some drawbacks to its use in this application:

- Throughout development of the calibration method it was identified that setting and maintaining the operating parameters was very important to the accuracy of the measurements.

- In order to make accurate measurements it needs to be 'trained' in what to measure. This in turn requires predictions as to what may occur in the experimental trials. Further assumptions were also made throughout the calibration process.

- Although the QMS provides on–line, real time measurements, due to the operating parameters the sample acquisition time is relatively long (42 seconds). Although this is deemed an adequate response for the processes which are investigated here, it may be too slow for other applications in which case a compromise between accuracy and response time must be made.

The procedure discussed here is the results of many studies and iterations and continual development of the method will occur in a bid to improve the accuracy and robustness of the overall method.

REFERENCES

Hassell, C. (2003). Process Mass Spectrometry. In Handbook of Spectroscopy. G. Gauglitz and T. Vo–Dinh, Eds., Vol. 2, Wiley–VCH, pp. 316–335.

Hoffmann, E. d. and Vincent, S. (2007). Mass Spectrometry: Principles and Applications. Third Edition, J. Wiley & Sons Ltd.

Hiden Analytical Ltd (2009) HPR–20 QIC Gas Analysis System Manual. Document: HA–085–092, Issue D.

Klinghoffer, A. A., Cerro, R. L., et al. (1998). Catalytic Wet Oxidation of Acetic Acid Using Platinum on Alumina Monolith Catalyst. Catalysis Today, Vol. 40, No. 1, pp. 59–71.

Le, C. D. (2012). Gasification of Biomass: An Investigation of Key Challenges to Advance Acceptance of the Technology. PhD Thesis, Department of Chemical Engineering, University of Bath, Bath.

Hiden Analytical Ltd (2012a) NH_3 Detection in H_2O Vapour. Document: Application Note 288

Hiden Analytical Ltd (2012b) NO_x Detection. Document: Application Note 289

Patnaik, P. (2004). Dean's Analytical Chemistry Handbook. 2nd Edition, McGraw–Hill.

Hiden Analytical Ltd (2010) QIC Fast Sampling Capillary Inlet User Manual. Document: HA–085–027, Issue G.

Hiden Analytical Ltd (2007) RC RGA Analyser Operator’s Manual. Document: HA–085–005, Issue N.

Shugar, G. J. (1990). The Chemist's Ready Reference Handbook. McGraw–Hill.

Turner, P., Taylor, S., et al. (2004). Calibration Effects During Natural Gas Analysis Using a Quadrupole Mass Spectrometer. TrAC Trends in Analytical Chemistry, Vol. 23, No. 4, pp. 281–287.

Watson, J. T. and Sparkman, O. D. (2007). Introduction to Mass Spectrometry Instrumentation, Applications and Strategies for Data Interpretation. Wiley. p. 317.

Appendix II – Examples of Detailed Catalyst Preparation Procedures

A **Experiment Number**: DM 016 **Experiment Description**: Pt Coating

Chemical	Molecular Weight (g)	Density	Amount Used	Mols	Equivalents
$H_2PtCl_6 \cdot 6H_2O$	517.90	–	5.3 g	0.010	1
H_2O	18	1 g/ml	194.7 g	10.81	1056

Experimental Procedure

Following the procedure described in Klinghoffer *et al.* (1998), a 1 wt% Pt Solution was prepared.

15/05 18 x Al_2O_3 monoliths (box 6, A1→C6)

6 x Ba/Al_2O_3 monoliths (box 3, D1→D6)

6 x K/Al_2O_3 monoliths (box 5, B1→B6)

were submerged in the solution for a total of 10 mins, during which the monoliths were turned over once.

Once removed from the solution the monoliths were placed in a ceramic dish and dried for 2 h at 120 °C before they were calcined at 500 °C overnight (15 h, 15/05→16/05).

Klinghoffer, A. A., Cerro, R. L., et al. (1998). Catalytic Wet Oxidation of Acetic Acid Using Platinum on Alumina Monolith Catalyst. Catalysis Today, Vol. 40, No. 1, pp. 59–71.

B **Experiment Number**: DM 012 **Experiment Description**: Ag Coating

Chemical	Molecular Weight (g)	Density	Amount Used	Mols	Equivalents
$AgNO_3$	169.87	–	6.3 g	0.037	1
H_2O	18	1 g/ml	200 g	11.11	300

Experimental Procedure

$AgNO_3$ (6.3 g) was dissolved in H_2O (200 g) in order to produce a solution of ~2 wt% silver.

08/05 18 x JM Al_2O_3 monoliths (box 4, A1→C6) were submerged in the solution for 2 h.

Once removed from the solution the monoliths were placed in a ceramic dish and dried overnight (19 h, 08/05 → 09/05) at room temperature before they were calcined at 550 °C for 4 h (09/05).

C **Experiment Number**: DM 017 **Experiment Description**: Ba Coating

Chemical	Molecular Weight (g)	Density	Amount Used	Mols	Equivalents
$Ba(NO_3)_2$	261.34	–	10 g	0.038	1
H_2O	18	1 g/ml	100 ml	5.55	145

Experimental Procedure

The solution prepared in DM 013 was used again (details can be found in the table above).

16/05 6 x Pt/Al2O3 monoliths (box 6, B1→B6)

6 x Ag/Al2O3 monoliths (box 4, B1→B6)

were submerged in the solution for 30 mins.

Once removed from the solution the monoliths were placed in a ceramic dish and dried at 120 °C overnight (18 h, 16/05→17/05) before they were calcined at 550 °C for 4 h (17/05)

D **Experiment Number**: DM 014 **Experiment Description**: K Coating

Chemical	Molecular Weight (g)	Density	Amount Used	Mols	Equivalents
K(acac)	98.14	–	34.35 g	0.35	1
H_2O	18	1 g/ml	100 ml	5.55	15.9

Experimental Procedure

K(acac) (34.35 g) was dissolved in H_2O (100 ml) in order to produce a solution of concentration = 3.5 mols/L.

10/5 18 x JM Al_2O_3 monoliths (box 5, A1→C6) were submerged in the solution for 30 mins.

Once removed from the solution the monoliths were placed in a ceramic dish and dried at 120 °C overnight (19 h, 10/5→11/5) before they were calcined at 500 °C for 4 h (11/5).
